Атомная энергия

Number 5, 1956

The Soviet Journal of

ATOMIC ENERGY

IN ENGLISH TRANSLATION

CONSULTANTS BUREAU, INC.

227 WEST 17TH STREET, NEW YORK 11, N. Y. ALGONQUIN 5-0713

CONTENTS

Price per article: $ 12.50.
Address orders to: CONSULTANTS BUREAU, INC., 227 West 17th Street, New York 11, N. Y.

ATOMNAYA ENERGIYA

Academy of Sciences of the USSR

Number 5, 1956

The Soviet Journal

of

ATOMIC ENERGY

IN ENGLISH TRANSLATION

CONSULTANTS BUREAU, INC.
227 West 17th Street
New York 11, N. Y.

Printed in the United States

Annual Subscription $ 75.00
Single Issue 20.00

EXTRACTION OF HIGH-ENERGY PARTICLE BEAMS THROUGH THE YOKE OF THE SYNCHROCYCLOTRON MAGNET

A. E. Ignatenko, V. V. Krivitsky, A. I. Mukhin, B. Pontecorvo, A. A. Reut * and K. I. Tarakanov

A method of obtaining collimated beams of high-energy particles (in particular, pions) is described; this method makes use of the yoke of the synchrocyclotron magnet as the main shield against the direct radiation of the accelerator. The collimators, which are set into channels drilled in the yoke of the magnet, make it possible to obtain beams of pions with energies up to 400 Mev.

INTRODUCTION

It is well known that in carrying out research at the phaseotron (synchrocyclotron), it is necessary that the detection apparatus being used in the experiments be shielded against the direct and scattered radiation of the accelerator. For this purpose generally a special expensive shield of steel or concrete, several meters in thickness, is required. It is natural, in this connection, to raise the question of using for such a shield the yoke of the synchrocyclotron magnet which, in high-energy accelerators, is of rather large thickness (2.7 m for the synchrocyclotron of the Institute of Nuclear Problems, Academy of Sciences of the USSR).

The present report describes a method, first used in the summer of 1953, for obtaining collimated beams of pions which is based on the use of the yoke of the magnet as the main shield against the direct radiation of the accelerator.

In addition to its economic advantage, the use of the yoke as a shield makes it possible to increase considerably the working area available for research. At the six-meter synchrocyclotron of the Institute of Nuclear Problems, Academy of Sciences of the USSR, for example, research on the properties of the meson is carried out on beams which are extracted not only through the yoke but also through a specially designed "main" concrete shield. However, the main concrete shield of the machine is located relatively far from the accelerator chamber, and hence the meson beams extracted through the yoke are more intense than those which pass through the main shield.

Extraction of Pion Beams Through the Yoke of the Synchrocylotron Magnet

The extraction of monoenergetic pion beams through the yoke is accomplished by means of the scheme shown in the figure. After being produced at the target, located inside the accelerator chamber, by bombardment with 680-Mev protons, the mesons are energy analyzed by the fringing field of the synchrocyclotron, and pass into one of the three channels drilled in the magnet yoke. Passing through the collimators located in the channels, the mesons enter a chamber which contains the experimental apparatus ("the meson laboratory"). Here the pions are deflected through an angle of 30° by means of a supplementary magnet and then enter the apparatus.

By means of a special mechanism the deflecting magnet can be aligned with the axis of any one of the three collimators.

* Deceased.

The most important factor in the extraction of mesons by this method is the choice of direction for the collimators. Since each collimator must be set in the yoke, and drilling holes in the yoke imposes a severe technical problem, it is necessary to choose the direction in such a way as to obtain monochromatic mesons whose energy, over a rather wide range, is determined by the position of the meson target.

To choose the directions of the collimators, studies were made of possible pion trajectories, using a method which involves the use of current-carrying wires under tension [1,2]. In all these experiments the wire tension (a copper wire 0.09 mm in diameter) was 50 g.

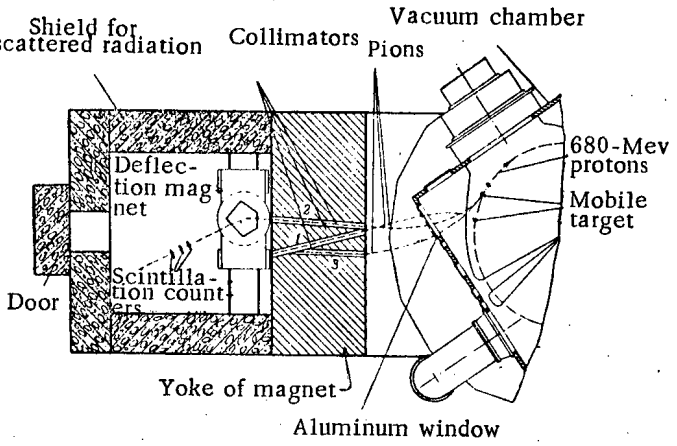

Scheme for extracting pion beams.

As a result of these studies three collimator-directions (1, 2, 3 in the figure) were chosen; these were designed to yield energies of, respectively, 150-250 Mev, 250-350 Mev, and 350-400 Mev.

In each actual case the energy is uniquely determined by the position of the target inside the dee of the accelerator. The target can be shifted within certain limits with respect to both azimuth and radius. It is sometimes necessary to move the target by remote control while the machine is in operation. Hence, the target is connected with a traversing mechanism through a quartz insulator.*

The direction of collimator 2 was chosen in such a way that its axis passes through the center of the accelerator chamber (that is, at an angle of 90° with respect to the direction of proton incidence on the target). This allows the possibility of research on the neutral radiation produced when the target is bombarded by protons of various energies and also permits studies of the possibility of the production of Λ^0-particles by protons with energies of 680 Mev [3].

Drilling holes for the collimators in the yoke required a great deal of time, and carrying out this task after the machine was in operation would have meant the loss of operating time of the accelerator. For this reason, it was decided to drill the channels even before obtaining proton beams with energies of 680 Mev.

Drilling holes for the extraction of maximum-energy mesons in this way entailed a certain risk, since the operating radius and the intensity of the magnetic field are, in general, not known with sufficient accuracy before a machine is put in operation.

The direction and ejection point for the pion beam in the magnet yoke was determined by the measurements with the wire. Since the horizontal boring machine could not be set up on the inside because of lack of room, it was necessary to use a theodolite to locate the direction of the collimator on the other side of the yoke.

*The remote control mechanism for the target was developed by M. P. Balandin and V. I. Sidorov.

Since the magnetic field intensity inside the collimator aperture was 1,600 gauss, it was necessary to provide an effective shield against the magnetic field. The properties of various magnetic shields were investigated in separate experiments. On the basis of these experiments, the collimators were made in the form of multilayered cylindrical magnetic shields of steel and brass (220-180 mm brass; 180-156 mm steel; 156-130 mm brass; 130-114 mm steel; 114-90 mm brass; 90-80 mm steel). Under these conditions the intensity of the magnetic field in the collimators, which had an internal diameter of 80 mm, was approximately 1 gauss, corresponding to a reduction of the field by more than a factor of one thousand.

Pion Beams

The energy and intensity of the pion beams was determined in the "meson laboratory" at the deflection magnet. The meson intensity was measured by a telescope consisting of three scintillation counters connected in coincidence. The orientation of the telescope was determined by means of the small current-carrying conductor. The pion energy was determined from range measurements in copper. It was shown by an analysis of the absorption curves and by controlled magnetic measurements that the energy inhomogeneity of the beams was not greater than $\pm$ 2 Mev.

Collimator 1 was designed to obtain both positive pions (emitted at an angle $\geq 150°$ with respect to the proton beam) [4], as well as negative pions (emitted at an angle of 30°). Hence, the intensity of the pion beams passing through this collimator was comparatively small.

Collimators 2 and 3 were used only for negative pion beams [5]. As is well known, the intensity of extracted beams of high-energy positive pions, produced in an internal target, is extremely small [6]; hence, it was found more advantageous to obtain positive pions at the main shield of the synchrocyclotron, using the extracted proton beam.

The intensities of the pion beams of various energies in the "meson laboratory" at the deflection magnet are shown in Table 1.

The data presented in Table 1, however, do not give a complete spectrum of the emitted mesons.

TABLE 1

Collimator No.	π^--mesons (Be target, 1 cm)		π^+-mesons (Cu target, 1 cm)	
	Energy Mev	Intensity	Energy Mev	Intensity
1	140	200	160—180	7
1	200	50	200—230	1—2
1	230	30	245	0.5
2	300	200		
2	340	80		
3	370	18		
3	400	4		

Scattered Radiation

It has already been noted that the shielding against the direct radiation of the machine is provided by the yoke itself. Shielding against the scattered radiation of the accelerator is provided by concrete walls and a concrete ceiling 1 m in thickness.

In Table 2 are shown the results of measurements of the "background" in the "meson laboratory", that is, the intensity of radiation aside from that of the pions.

The data of Table 2 indicate that it would be desirable to increase the thickness of the side walls and the ceiling of the meson laboratory; the thickness of the chief shield – the yoke – is completely adequate.

At this point, we should like to introduce the results of certain experiments which, in our opinion, may be useful in solving a number of shielding problems in connection with the scattered radiation which is found in the operating enclosure of high energy accelerators (we are concerned here with accelerators of several hundred Mev, located above ground).

TABLE 2

Type of Radiation	Detection Instrument	Intensity
Total radiation	Air-filled ionization chamber	1 mc/sec
γ-rays	Geiger counter with copper walls	~10 counts (sec/cm^2 surface of counter
Thermal neutrons	Emulsions with high lithium content	≤ 500 cm^{-2} sec^{-1}
Fast neutrons (E >> 50 Mev)	Bismuth fission chamber	<< 10 cm^{-2} sec^{-1}
Fast neutrons (E > 50 Mev)	Emulsions (by stars)	2 ÷ 4 cm^{-2} sec^{-1}

*These data were kindly furnished by I. B. Sokolov, Physics Institute of the Academy of Sciences of the USSR.

The efficiency of the concrete shield for scattered radiation was investigated with several detectors (a proportional counter, an ionization chamber and a scintillation counter). The detectors were located at a distance of 2.5 m from the magnet yoke (in approximately the same place in which the detection apparatus is installed). It was found that a concrete shield (density 2.4 g/cm^3) 1 m thick, completely inclosing the detectors served to reduce the scattered radiation by approximately a factor of 40.

SUMMARY

The utilization of the yoke of the synchrocyclotron magnet as the chief shield against direct radiation is completely satisfactory. For charged particles the use of the yoke presents some serious shortcomings associated with the six apertures and the necessity for magnetic shielding of the collimator. These inconveniences, however, do not apply in the collimation of beams of neutral particles and γ-rays.

The use of the yoke as a shield is especially attractive in the case of accelerators which are located above ground, since it is not necessary to furnish additional shielding against the scattered radiation. We should also point out that when the yoke is used as a shield it is always possible to carry on simultaneous operations with various types of beams. For instance, it is possible to obtain simultaneously from one target a neutron beam through the yoke and meson beams in the other directions.

In conclusion, we wish to express our gratitude to A. V. Chestnoi and B. I. Zamolodchikov for valuable advice, to K. A. Baicher and S. I. Zhigoman for drilling the holes in the magnet yoke, and to P. T. Pavlov for the construction of the collimators which were installed in the yoke.

LITERATURE CITED

[1] J. J. Thomson, Phil. Mag. 13, 561 (1907).

[2] M. F. Kozodaev and A. A. Tyapkin, Report of the Inst. Nuc. Probs. (Acad. Sci. USSR, 1952).

[3] M. P. Balandin, B. D. Balashov, V. A. Zhukov, B. Pontecorvo and G. I. Selivanov, J. Exptl.-Theoret. Phys. (USSR) 29, 265 (1955).

[4] A. E. Ignatenko, A. I. Mukhin, E. B. Ozerov and B. Pontecorvo, J. Exptl.-Theoret. Phys. 30, 7 (1956).

[5] A. E. Ignatenko, A. I. Mukhin, E. B. Ozerov, and B. Pontecorvo, Proc. Acad. Sci. USSR 103, 45 (1955); 103, 395 (1955); N. A. Mitin and E. L. Grigoryev, Proc. Acad. Sci. USSR 103, 219 (1955); L. S. Dulkova, T. A.

Romanova, I. B. Sokolova, L. V. Sukhov, K. D. Tolstov and M. G. Shafranova, Proc. Acad. Sci. USSR 107, 1 (1956); S. M. Korenchenko and V. A. Zinov, Proceedings of the All-Union Conference on the Physics of High-Energy Particles (Moscow, 1956).

[6] H. L. Anderson, J. Marshall, L. Kornblith, Jr., L. Schwartz and R. Miller, Rev. Sci. Instr. 23, 707 (1952).

Received June 14, 1956

RELATIVISTIC STABILIZED ELECTRON BEAM*

G. I. Budker

The physical principles underlying the formation of a relativistic stabilized electron beam are presented and questions connected with the stability of such a configuration are discussed.

1. Introduction

In ordinary accelerators the requirement that curl **H** and div **E** vanish in the region of particle motion imposes rather strict limitations on the fields which can be used for acceleration. The removal of this requirement opens new possibilities for building accelerators with extremely strong focusing in which the initial ion ejection is also easier. Thus, for example, it would be possible to accelerate particles in an axially-symmetric magnetic field which increases sharply with radius. In this case both the radial and vertical focusing may prove to be many times greater than that which obtains in ordinary accelerators, including those in which alternate-gradient focusing is employed.

It may be feasible to create such fields by means of a so-called closed stabilized electron beam.

By stabilized electron beam we mean an intense beam of relativistic electrons, the charge of which is completely or partially compensated by ions and which has certain definite properties.

Because of magnetic attraction, the repulsive force between two electrons which move parallel to each other is reduced by a factor γ_0^2 compared with the repulsion between electrons at rest, where $\gamma_0 = \left(1 - \frac{v^2}{c^2}\right)^{-1/2}$ is the relativistic factor. Hence, the presence of even a comparatively small number of ions in an intense relativistic electron beam leads to a situation in which the Coulomb repulsion force vanishes and is replaced by strong attractive force.

Strong magnetic self-focusing causes characteristic electromagnetic radiation which tends to damp out the transverse electron oscillations. If certain other conditions are also satisfied, this effect causes the beam to contract into a thin thread-like structure with enormous electric and magnetic fields at the surface and which is apparently a stable and long-lived configuration.

Since the time typically required for the establishment of a stable configuration (contraction) is of the order of several seconds or more, the electrons traverse enormous distances, and a rectilinear stabilized beam could only be produced in a distance of cosmic dimensions. Under terrestrial laboratory conditions only a closed stabilized beam can be considered. For this reason, the beam must be located in a magnetic field of definite configuration, the direction of which is perpendicular to the plane containing the electron-current loop, as in the betatron.

In contrast with a betatron, however, in the present case the inherent magnetic field at the surface of the beam is much larger than the external magnetic field.

Such a beam is essentially a well-defined, long-lived configuration of electrons and ions which are held together chiefly by the inherent electric and magnetic fields. The failure of many attempts at creating a stabilized classical system, held together only by inherent electromagnetic fields, is well known. Although a rigorous proof of the instability of such a system has never been given, at the present time there is little doubt of the impossibility

* Presented at the C.E.R.N. symposium (Geneva) on high-energy accelerators and meson physics (June, 1956).

of realizing a stable configuration of this type. A closed stabilized electron beam is not an isolated system inasmuch as it is under the influence of external fields. These fields, which are sufficient for providing stability in the system, are many times smaller than the inherent fields of the beam.

The configuration of the inherent beam field is such that the region inside the beam lends itself to the acceleration of ions. The ions being accelerated are constrained in the orbit and focused by the inherent magnetic and electric field of the beam. If the inherent field is large, one may hopefully expect to obtain very high energy particles with a relatively small accelerator and a small magnetic field, used to constrain the beam to the equilibrium radius; strong focusing and the possibility of using part of the ions which compensate the electron charge for acceleration, may make it feasible to obtain intense beams of accelerated particles, limited only by the power which is available for acceleration.

In the present paper the physical principles which underlie the formation of a stabilized beam are considered and the results of theoretical studies are presented without details or mathematical calculations.

In the near future it is expected that some work by G. I. Budker and S. T. Belyaev on the theory of a relativistic plasma, which has direct bearing on the problem considered here, will be published along with a description of some of the experimental work. The idea that a stabilized electron beam would be possible was advanced by the author in 1952. The basic calculations were carried out in 1953 and experimental work was started in 1954.

The concept of magnetic self-focusing in weak relativistic beams was first advanced by Bennett in 1934 [1]. Recently a second paper by this same author has appeared [2]. Bennett, however, does not consider the radiation produced by the transverse oscillations and it is the existence of this radiation which determines the basic properties of a stabilized electron beam.

2. Equilibrium State

Conditions for mechanical equilibrium. We consider an infinite linear beam of moving electrons the charge of which is partially neutralized by ions. The equilibrium conditions are most obvious if each gas (electron and ion) is considered in the coordinate system in which it is at rest.

If n_1 and n_2 are the electron density and the ion density in the laboratory coordinate system, in which the ions are at rest, n_1' and n_2' are the same densities in the coordinate system, in which the electrons are at rest (electron system), and v_0 is the directed electron velocity, then from the condition that the current $j_i = (nv_x; nv_y; nv_z; inc)$, a four vector, we must have:

$$\left.\begin{aligned} n_1^2 v_0^2 - n_1^2 c^2 &= -n_1'^2 c^2, \\ -n_2^2 c^2 &= n_2'^2 v_0^2 - n_2'^2 c^2 \end{aligned}\right\} \tag{1}$$

where

$$n_1' = \frac{1}{\gamma_0} n_1; \qquad n_2' = \gamma_0 n_2. \tag{2}$$

We introduce two dimensionless quantities ν_1 and ν_2 which will appear frequently in the following*:

$$\left.\begin{aligned} \nu_1 &= r_0 \cdot 2\pi \int_0^r n_1(r)\, r\, dr, \\ \nu_2 &= r_0 \cdot 2\pi \int_0^r n_2(r)\, r\, dr, \end{aligned}\right\} \tag{3}$$

* We may note than when ν_1 and ν_2 equal unity these values correspond to a beam in which there are $3.6 \cdot 10^{12}$ particles per cm, and this in turn corresponds to electron currents (for velocities close to that of light) of approximately 17,000 amp.

where $r_0 = e^2/mc^2$ is the classical electron radius ($r_0 = 2.8 \cdot 10^{-13}$ cm).

From (2) it follows that if the following condition is satisfied:

$$1 \geqslant \frac{\nu_2}{\nu_1} \gg \frac{1}{\gamma_0^2} \tag{4}$$

then in the laboratory coordinate system the beam is negatively charged while in the electron system it is charged positively. This means, that in the present case an equilibrium state is possible for the electron gas as well as the ion gas. The electrons and the ions are each in a potential well and cannot escape unless the transverse energy becomes equal to the depth of the potential well.

If the inequality in (4) is strong on both sides, the depth of both potential wells is of the order

$$W_2 \approx (\nu_1 - \nu_2)\, mc^2 \approx \nu_1 mc^2; \quad W_1' \approx \gamma_0 \nu_2 mc^2. \tag{5}$$

We shall be interested in beams in which ν is of order unity. In this case the electron gas and the ion gas may be at extremely high temperatures.

The radial density distribution is obtained by solving the self-consistent problem of the motion of particles in fields which are created by the particles themselves. Disregarding the fact that the electron gas is not in thermodynamic equilibrium at the edge of the beam, some idea of the density distribution in the beam may be obtained by assuming that, in its own coordinate system, each gas is in thermodynamic equilibrium at the temperature T_2 and T_1'.

Then, using Maxwell's equation $\operatorname{div} \mathbf{E} = 4\pi\rho$ in conjunction with the Boltzmann distribution, we have the following equations for the density distribution

$$\left.\begin{aligned}
&\frac{1}{r}\frac{d}{dr}\left(r\frac{dU_1'}{dr}\right) = \\
&\qquad = 4\pi e\left\{\gamma_0 n_2^0 e^{-\frac{eU_2}{T_2}} - n_1^{0\prime} e^{\frac{eU_1'}{T_1'}}\right\}, \\
&\frac{1}{r}\frac{d}{dr}\left(r\frac{dU_2}{dr}\right) = \\
&\qquad = -4\pi e\left\{\gamma_0 n_1^{0\prime} e^{\frac{eU_1'}{T_1'}} - n_2^0 e^{-\frac{eU_2}{T_2}}\right\}, \\
&\qquad n_1'(r) = n_1^0 e^{\frac{eU_1'(r)}{T'}}; \\
&\qquad n_2(r) = n_2^0 e^{-\frac{eU_2(r)}{T_2}},
\end{aligned}\right\} \tag{6}$$

where n^0 is the density at the axis of the beam.

In the particular case for which the beam is uncharged ($n_2 = n_1$; $T_2 = 0$) a solution is obtained which agrees with the results of [1]:

$$n(r) = \frac{n^0}{\left(1 + \frac{r^2}{r^{*2}}\right)^2}, \tag{7}$$

where

$$r^{*2} = \frac{2T_1'}{\pi e^2 \gamma_0^2 \beta_0^2 n_1^{0\prime}}.$$

It is apparent from (7) that such a self-focused beam is a rather sharply defined configuration and that it is meaningful to introduce a beam radius r^*.

The external magnetic field required to produce a closed circular beam is found to be

$$H = \gamma_0\beta_0 \frac{e}{Rr_0}(1+\gamma_0\nu_2) \times \left(1 + \frac{\nu_1}{\gamma_0} \ln\frac{8R}{r^*} + \frac{\nu_1-\nu_2}{\gamma_0} \ln\frac{8R}{r^*}\right) \tag{8}$$

where R is the radius of the loop formed by the electron current.

The situation being described here differs from that in a betatron in two ways: the increase in the rest mass per unit length of beam due to the high transverse electron energy which occurs as a result of the strong magnetic focusing and the presence of the inherent electric and magnetic fields. The corrections associated with the inherent fields can be neglected since they contain the factor γ_0 in the denominator. In the case which is of interest here, the change in the effective mass (the factor $1 + \gamma_0\nu_2$) is important and, as will be shown later, raises the value of the required magnetic field by a factor of 3 as compared with that in a betatron.

Collisions. In their motion, the electrons are scattered on ions and in this process energy associated with the longitudinal motion is converted to energy associated with transverse motion. As is well known, in Coulomb interactions the most important contribution is that of multiple scattering, in which an electron is scattered through a small angle in each collision. It is most convenient to treat the problem in the electron coordinate system.

As seen in this system, the fast ions travel through the electron gas which is at rest, and, to some extent, tend to heat the gas and drag it along.

We now find the energy and momentum which are imparted to the electrons by the ions, as seen in the electron coordinate system. First, we consider the case of a non-relativistic electron temperature in which the electron velocity may be neglected as compared with the ion velocity. In each collision there is transferred an amount of energy and momentum*

$$\Delta E = \gamma_0^2\beta_0^2 mc^2 \frac{\vartheta^2}{2},$$

$$\Delta p = \frac{1}{v_0}\Delta E.$$

Multiplying these expressions by the ion density, the ion velocity and the cross section for deflection of a particle through an angle ϑ in the center-of-mass system

$$\sigma(\vartheta) = \frac{8\pi r_0^2}{\gamma^2\beta^4}\frac{1}{\vartheta^3},$$

and integrating over all angles, we obtain:

$$\frac{dp'}{dt'} = \frac{1}{v_0}\frac{dE'}{dt'} = \frac{\gamma_0 4\pi r_0^2 L n_2 mc^2}{\beta_0^2}, \tag{9}$$

where $L = \ln \gamma_0 \beta_0^2 \frac{r^*}{r_0}$ is the Coulomb logarithm term.

To calculate the momentum and energy transfers for relativistic temperatures, we consider a group of electrons moving in a given direction. In accordance with the foregoing, considering these particles in the coordinate

* See [3], Equation (12.3). In the present case $\gamma_0 m \ll M$, $\vartheta \ll 1$.

system (designated by double primes) in which they are at rest, and taking the x-axis along the relative motion of the ions, the vector giving the rate of change of momentum $\frac{dpl}{ds}$ has the following form:

$$\frac{dp_e}{ds'} = 4\pi r_0^2 Lmc\left(\frac{n_2''}{\beta_2''};\ 0;\ 0;\ \frac{in_2''}{\beta''}\right).$$

Two vectors are available in the formation of this vector: the electron-velocity vector U_k and the ion-current density vector J_k which have the following components in the coordinate system which has been chosen

$$U_k = (0;\ 0;\ 0;\ i); \qquad \frac{1}{c} J_k = (n_2''\beta'';\ 0;\ 0;\ in_2'').$$

Whence it is obvious that

$$\frac{dp_e}{ds} = 4\pi r_0^2 mL \frac{(U_k J_k)^2}{[J_k^2 + (U_k J_k)^2]^{3/2}} [U_l J_k^2 - J_l (U_k J_k)] \tag{10}$$

Substituting the values of U_k and J_k in the electron coordinate system and assuming that, in this system, the electron velocity is distributed uniformly over angle, by simple integration we obtain

$$\frac{\overline{dp'}}{dt'} = \frac{1}{\beta_0 c} \frac{dE'}{dt'} = \frac{4\pi r_0^2 \gamma_0 L n_2 mc^2}{\beta_0^2 \tilde{\gamma}}, \tag{11}$$

where $\tilde{\gamma}$ is the average value of a quantity given by

$$\frac{1}{\tilde{\gamma}} = \overline{\frac{1}{\gamma}\left(1 + \frac{1}{\gamma_0^2} - \frac{1}{2\beta\gamma_0^2} \ln \frac{1+\beta}{1-\beta}\right)}. \tag{12}$$

The averaging is carried out over the absolute values of the electron velocities (β, γ) in the electron coordinate system. At large values of γ_0, $\frac{1}{\tilde{\gamma}} = \overline{\frac{1}{\gamma}}$ and in accordance with (5)

$$\tilde{\gamma} \approx 1 + \gamma_0 v_2. \tag{13}$$

Equation (11) agrees completely with the results obtained in [4] in which the transfer of energy and momentum was found by solving the relativistic Boltzmann equation.

Radiation of electromagnetic waves. At sufficiently high currents, because of the increased focusing forces a new phenomenon makes its appearance: namely, the radiation of electromagnetic waves associated with the transverse electron oscillations. Under certain conditions this radiation becomes all-important and consumes practically all the energy supplied to the beam. Substituting the value $E \approx H \approx 2\pi e n_2' r$* in the expression for the radiation associated with a relativistic particle moving in an electric and magnetic field*

$$J_{ave} = \frac{2}{3} r_0^2 c \frac{\overline{\left\{ + \frac{1}{c} \mathbf{vH} \right\}^2 - \frac{1}{c^2} (\mathbf{vE})^2}}{1 - \frac{v^2}{c^2}}, \tag{14}$$

we obtain a quantity of order

$$J' \approx \gamma_0 v_2 (1 + \gamma_0 v_2)^2 4\pi r_0^2 \gamma_0 n_2 cmc^2, \tag{15}$$

* See [3], Equation (72.4).

where J' is the average amount of energy radiated by the electrons in the electron coordinate system.

The spectral composition of this radiation in the electron coordinate system can be estimated in the following way. In the cases for which the radiation is important, the electrons are at relativistic temperatures. Consequently, the frequency of the oscillations is given by

$$\omega_0 \approx \frac{c}{r^*} . \tag{16}$$

It has been shown by L. A. Artsimovich and Yu. A. Pomeranchuk [5] that, in contrast with a nonrelativistic particle, which emits at the frequency of its oscillations, a relativistic particle moving in a circle radiates a quasi-continuous spectrum, the maximum of which lies in the frequency region $\omega' = \gamma^3 \omega_0$; the intensity falls off exponentially at considerably larger values of ω'. It may be assumed that this same result holds, at least qualitatively, if the trajectory is not exactly circular. Thus, from (13) and (16), in the electron coordinate system the radiation spectrum has a maximum at

$$\omega' = (1 + \gamma v_2)^3 \frac{c}{r^*} . \tag{17}$$

Assuming that the radiation is symmetric in the electron system, after some transformation we find the distribution for the radiated energy as a function of angle and frequency in the laboratory coordinate system:

$$\frac{dW}{d\Omega} d\omega\, d\Omega = \frac{1}{4\pi} \frac{W'[\gamma_0 \omega (1 - \beta_0 \cos\vartheta)]}{\gamma_0 (1 - \beta_0 \cos\vartheta)} d\Omega\, d\omega, \tag{18}$$

where $W'(\omega')$ is the spectral distribution of the radiation in the electron coordinate system $\int W' d\omega = J'$. Integrating over frequency, we obtain the radiation distribution over angle

$$\frac{dJ}{d\Omega} d\vartheta\, d\varphi = \frac{J'}{4\pi\gamma_0^2} \frac{\sin\vartheta}{(1 - \beta_0 \cos\vartheta)^2} d\vartheta\, d\varphi. \tag{19}$$

For $\gamma_0 \gg 1$ the small angles are most important. Expanding $\cos\vartheta$ about unity, we obtain

$$\frac{dJ}{d\vartheta} d\vartheta = J' \frac{2\gamma_0^2 \vartheta\, d\vartheta}{(1 + \gamma_0^2 \vartheta^2)^2} . \tag{20}$$

The radiation is distributed over a small angle $\vartheta \sim \frac{1}{\gamma_0}$ along the line of motion, and for large values of ϑ falls off as $\frac{1}{(\gamma_0 \vartheta)^3}$. Integrating over all angles, we find $J = J'$.

In the laboratory coordinate system this radiation carries away momentum

$$\frac{dp}{dt} = \frac{v_0}{c^2} J.$$

The spectral distribution of the radiation in the laboratory system is a function of angle. In the important region $\vartheta < \frac{1}{\gamma_0}$,

$$\frac{dW(\omega)}{d\Omega} \approx \frac{1}{2\pi} \gamma_0 W'\left(\frac{\omega}{2\gamma_0}\right). \tag{21}$$

In the laboratory system, the radiation maximum occurs at a frequency which is $2\gamma_0$ times greater than that in the electron system, in complete agreement with the expression for the relativistic Doppler effect

$$\omega_{max} = 2\gamma_0\omega'_{max} = 2\gamma_0(1+\gamma_0\nu_2)^3\frac{c}{r^*}. \qquad (22)$$

It is interesting to note that by varying the parameters within reasonable limits, it is possible to shift this maximum from the millimeter-wave region to the visible region beyond.

Equilibrium state. If the directed velocity of the electrons is to remain constant, it is necessary to apply to the beam a longitudinal electric field (for a closed beam this is an induced circular electric field). For a given number of particles in the beam and with a given electric field, an equilibrium state is set up in the beam in which the momentum acquired from the field by the electrons is lost as a consequence of collisions with ions, while the energy acquired from the field is lost by radiation. In this state of the system the directed electron velocity and the radius of the cross section of the beam (γ_0 and r^*) are established as definite functions of the external parameters (E and ν_2). Converting to the electron coordinate system the energy acquired by electrons from ions, the energy carried away by radiation, and the momentum acquired by the electrons due to the effect of the electric field eE_{long}, we find from (11) and (15), the following equilibrium conditions:

$$\left.\begin{aligned}\gamma_0 &= \frac{\varkappa}{\nu_2},\\ r^* &= \sqrt{\frac{4\varkappa L}{1+\varkappa}}\sqrt{\frac{e}{E_{long}}},\end{aligned}\right\} \qquad (23)$$

where κ is a root of the equation $\kappa(1+\kappa)^3 = L$ (for $L = 35$, $\kappa \approx 1.7$). At first sight, it is surprising to find that the electron energy is independent of the electric field and that the beam radius is independent of the number of particles. It would seem that a greater electric field should be associated with a higher electron energy. As a matter of fact, if the electric field is increased the electrons start to be accelerated. However, with an increase of electron energy the radiation increases and the beam is compressed. In the more dense beam the friction forces become greater than the force of the electric field and the electron velocity falls off until it assumes approximately the equilibrium value. In accordance with Equation (23) the radius of the beam is now smaller. For an uncharged beam ($\nu_1 = \nu_2$), Equation (23), substituting the numerical coefficients, assumes the form

$$\left.\begin{aligned}i_{el} &= \frac{2.9\cdot10^4}{\gamma_0}(a),\\ r^* &= \frac{3.6\cdot10^{-3}\,(\text{cm})}{E^{1/2}(\text{v/cm})},\end{aligned}\right.$$

where i_{el} is the electron current.

Thus, a typical equilibrium state may obtain for an electron energy of 15 Mev if the electron current is ~ 1000 amp. It is apparent from these considerations that in betatrons the currents are far from the equilibrium values. For an electric field intensity of one volt (per centimeter) (this corresponds to an induced voltage of 600 v, corresponding to a complete circuit of the electric field for a closed beam of radius of about 1 meter) the radius of the cross section the beam, in accordance with (23), is $4 \cdot 10^{-2}$ mm. At a current of 1000 amp the magnetic field at the surface of the beam is 50,000 gauss while the external magnetic field required to constrain electrons with an energy of 15 Mev at a radius of 1 m is 1350 gauss, as seen from (8).

Lifetime. The time associated with the establishment of the equilibrium state is determined by multiple scattering and for ($\gamma_0 \gg 1$):

$$t \approx \frac{\gamma_0 r^{*2}}{4Lcr_0}. \qquad (24)$$

Multiple scattering does not cause the ejection of a particle from the beam because of the radiation damping effect. The ejection of particles from the beam is caused by a single scattering event through some large angle such that the amplitude of the transverse oscillation becomes greater than the width of the chamber. The lifetime, due to this process, is

$$t \approx \left(1 + 2 \ln \frac{r_{cham}}{r^*}\right) \frac{\gamma_0 r^{*2}}{2cr_0}, \qquad (25)$$

where r_{cham} is the transverse dimension of the chamber; this quantity is much greater than the time required to establish the equilibrium state. The time during the course of which the required induced electric field in one direction can be maintained is

$$t = \gamma_0 \frac{(1+\varkappa)^2}{4\varkappa L} \frac{r^{*2}}{r_0 c} \frac{\Delta B}{2H},$$

where ΔB is the change in the magnetic flux, producing the induced field, as averaged over the area of the loop and H is the magnetic field required to constrain the electrons in the orbit.* In practice (ΔB equals 30,000 gauss; from $-15{,}000$ to $+15{,}000$) this time exceeds the time associated with scattering at a large angle and does not limit the lifetime of the beam.

3. Stability Problems

One of the most important problems is the question of beam stability. The instability of a "pinched" current in a plasma with respect to all kinds of oscillations is well known. In particular, closed high-current ring discharges have been investigated. These have a number of instabilities. On the other hand, the electron beam in a betatron is absolutely stable.

Since ν (ν_1 and ν_2) is a dimensionless combination of the number of particles in the beam, the velocity of light and the charge and mass of the electron, and its value in a betatron may be much smaller than unity, and much larger than unity in a ring discharge, it is reasonable to expect that the intensity of a beam for which $\nu \approx 1$ (for $\gamma_0 >> 1$) should represent the transition from stability to instability. As a matter of fact, calculations which have been made indicate that stable equilibrium of the beam is to be expected at relativistic velocities and $\nu < 1$ and unstable equilibrium for nonrelativistic velocities and $\nu >> 1$.

The question of stability must be treated extremely carefully since no final theoretical solution to the stability problem is available in the present case. A rigorous proof of the stability of a system can be found only in those cases in which use is made of thermodynamic laws or conservation laws, or in isolated simple cases when one can speak of the motion of individual particles, as in ordinary accelerators. In systems such as the stabilized beam, which are essentially systems with an infinite number of degrees of freedom, the problem of stability must be considered with respect to a definite kind of perturbation, the risk of production of which follows from physical considerations. In practice, the stability, as a rule, cannot be analyzed beyond a first (linear) approximation. Hence the theoretical results are never rigorous and can only furnish the experimenter with more or less assurance that the stability of the beam in which he is interested may be realized for values of the parameters which are of practical interest.

The stability of a beam has been considered with respect to different types of perturbation; of these, in the present paper, because of space limitations only three are considered.

a) Stability with respect to deviations of the directed electron velocity from equilibrium values. The directed electron velocity in the beam remains constant because the longitudinal electric field is compensated by the force of friction. This equilibrium will be stable only if the friction characteristic is positive, that is, the friction force increases with velocity. In the opposite case (a negative characteristic) a small increase in the velocity is sufficient to reduce the value of the friction force below the electric-field force and the particle starts to accelerate – then the friction force becomes still smaller. If the velocity of the particle falls below the equilibrium value, the particle is slowed down continuously.

Since the cross section for Coulomb scattering falls off with velocity both for nonrelativistic and relativistic velocities, at first glance it would appear that the equilibrium between the electric field and the friction force should be unstable.

In actual fact, however, from Equation (11) it follows that in the electron system the force with which the electrons are carried by ions depends on velocity as γ_0/β_0^2 (for small values of ν the variation of $\tilde{\gamma}$ with velocity can be neglected). A typical curve for this force is shown in Fig. 1.

* The well-known betatron condition 2:1 does not apply in the present case. Hence, as a rule, $\frac{\Delta B}{2H} \neq 1$.

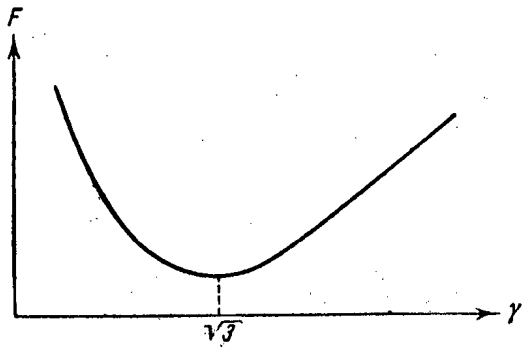

Fig. 1.

It follows from this curve that for $\gamma_0 > \sqrt{3}$ the friction characteristic becomes positive and stable equilibrium between the friction force and the force of the electric field becomes possible.

From the point of view of an observer in the laboratory system the contradiction between this statement and the well-known fact that the Coulomb cross section falls off with velocity can be explained in the following manner. The electromagnetic radiation which damps the energy of the transverse electron oscillations also carries away momentum in the laboratory coordinate system since it is directed in the direction of motion of the electron. This radiation friction force increases with velocity in the relativistic region. The left-hand part of the curve in Fig. 1 represents the Coulomb friction with respect to ions and falls off with velocity. The right-hand part is the radiation friction, which increases with velocity. We may recall that in deriving Equation (11) we did not take account of radiation in the electron coordinate system (since it does not carry away momentum here). The positive friction characteristic in the laboratory system is obtained as a result of the stationary condition. Any other effect which damps out the energy of transverse electron oscillations in the electron system must, from the condition of relativistic invariance, give rise, in the laboratory system, to a friction force with the same dependence on velocity. Furthermore, stable equilibrium will obtain even in the case in which there is no attenuation of the transverse electron oscillations of electrons moving in a given potential well and scattered by ions. In this case the process is not stationary. In a non-stationary process the condition that the mean velocity remain constant is not the same as the condition that the mean momentum remain constant because the rest mass μ per unit beam volume increases with time as the random velocities increase.

The equilibrium condition (that is, constant mean velocity) has the form

$$\mu \frac{dv}{dt} = eE - F_{\text{dis}} - v \frac{d\mu}{dt}.$$

The last term $\left(v \frac{d\mu}{dt}\right)$ (once again from the condition of relativistic invariance) must have the same velocity dependence as the radiation friction in the stationary state.

b) Stability with respect to the excitation of plasma waves and the separation of the beam into separate bunches. It is well known that when a beam of electrons passes through a plasma, characteristic plasma oscillations are excited and the beam is space-modulated and loses considerably more energy than is to be expected from a theory which considers only the Coulomb pair interactions.

As a preliminary step a simpler problem was solved – the nonselfconsistent problem of longitudinal oscillations of the beam; it is assumed that the beam radius does not change during the time of oscillations. This simplified treatment makes it possible to explain a number of interesting properties which serve to distinguish a beam from an infinite plasma in which, among other things, the problem of oscillations is generally solved under the same assumptions. After this step, it was possible to solve the complete problem of self-consistent oscillations of a beam in terms of the longitudinal coordinate z and the cylindrical radius r. After extremely lengthy calculations, in certain cases the same dispersion relation was obtained as in the simplified problem.*

The simplified problem amounts to a solution of the two kinetic equations together with Maxwell's equations:

$$\left.\begin{aligned} \frac{\partial f_1}{\partial t} + v \frac{\partial f_1}{\partial x} - e\mathbf{E} \frac{\partial f_1}{\partial p} = 0, \\ \frac{\partial f_2}{\partial t} + v \frac{\partial f_2}{\partial x} + e\mathbf{E} \frac{\partial f_2}{\partial p} = 0, \end{aligned}\right\} \quad (26)$$

*It is proposed to publish this solution in the near future.

$$\left.\begin{aligned} \nabla^2\varphi - \frac{1}{c^2}\frac{\partial^2\varphi}{\partial t^2} &= -4\pi\int (f_1 - f_2)\,dp, \\ \nabla^2\mathbf{A} - \frac{1}{c^2}\frac{\partial^2\mathbf{A}}{\partial t^2} &= -\frac{4\pi}{c}\int (f_1 v_1 - f_2 v_2)\,dp, \\ \mathbf{E} &= -\frac{\partial\varphi}{\partial x} - \frac{1}{c}\frac{\partial\mathbf{A}}{\partial t}, \end{aligned}\right\} \quad (26)$$

where $f_1(x, t, p)$ and $f_2(x, t, p)$ are the electron and ion distribution functions in phase-space which, in accordance with our assumption, will be considered functions of $p = p_x$ and $\underline{x}$ up to a certain value $r = r^*$ and zero for larger values of $\underline{r}$.

$\mathbf{A}(x, t, r)$ and $\varphi(x, t, r)$ are the electromagnetic potentials, which also depend on $\underline{r}$. In this formulation of the problem collisions are not considered. Under certain limiting conditions, if the thermal velocities are neglected as compared with the directed velocity, the following dispersion equation is obtained:

$$\frac{4\nu_1}{\gamma_0^3}\frac{1}{(\beta_\Phi - \beta_0)^2} + \frac{4m\nu_2}{M}\frac{1}{\beta_\Phi^2} = \frac{\psi^2[(1-\beta_\Phi^2)^{1/2} kr^*] + (1-\beta_\Phi^2)\,k^2 r^{*2}}{1-\beta_\Phi^2}, \quad (27)$$

where $\beta_\Phi = \frac{\omega}{ck}$, ω is the frequency and $\underline{k}$ the propagation vector of the wave; $\beta_0 = \frac{v_0}{c}$; v_0 is the electron velocity.

$\psi(x)$ is a solution of the equation

$$\psi\frac{J_1(\psi)}{J_0(\psi)} = -x\frac{K_1(x)}{K_0(x)},$$

where $J_1(x)$, $J_0(x)$ and $K_1(x)$, $K_0(x)$ are Bessel functions. In two limiting cases the equation is simplified

$$kr^* \gg (1-\beta_\Phi^2)^{-1/2}; \qquad kr^* \ll (1-\beta_\Phi^2)^{-1/2}.$$

For short waves $\lambda \ll (1-\beta_\Phi^2)^{1/2} r^*$ the equation becomes

$$\frac{4\nu_1}{\beta_0^2\gamma_0^3 k^2 r^{*2}}\frac{1}{(1-x)^2} + \frac{4m\nu_2}{M\beta_0^2 k^2 r^{*2}}\frac{1}{x^2} = 1, \quad (28)$$

where $x = \frac{\beta_\Phi}{\beta_0} = \frac{\omega}{kv_0}$.

For small values of the coefficients of the terms containing the unknown $\frac{1}{(1-x)^2}$ and $\frac{1}{x^2}$ the roots are real and it is easy to show that the values of ω obtained coincide with the Langmuir frequency in an ion and electron gas in the appropriate coordinate system.

At certain values of the coefficients complex roots appear, that is, oscillations start. The stability criterion

$$\left[\frac{4\nu_1}{\gamma_0^3\beta_0^2}\right]^{1/3} + \left[\frac{4m\nu_2}{M\beta_0^2}\right]^{1/3} = \left(\frac{r^*}{\lambda}\right)^{2/3} \quad (29)$$

determines the wavelength $\lambda = \lambda_{crit}$ at which oscillations start.

Thus it is apparent that in this approximation there will always be waves of sufficient length that oscillations, to which the beam is unstable, appear. It is also necessary, however, that this wavelength satisfy the relation: $\lambda \ll (1-\beta_\varphi)^{1/2} r^*$. This fact imposes definite requirements on the parameters:

$$\frac{4\nu_1}{\gamma_0^3\beta_0^2}\left\{1-\beta_0^2\frac{\left(\gamma_0^3\frac{m}{M}\frac{\nu_2}{\nu_1}\right)^{2/3}}{\left[1+\left(\gamma_0^3\frac{m}{M}\frac{\nu_2}{\nu_1}\right)^{1/3}\right]^2}\right\}\times \times\left\{1+\left(\gamma_0^3\frac{m}{M}\frac{\nu_2}{\nu_1}\right)^{1/3}\right\}^3\gg 1. \tag{30}$$

In the case which is of most interest

$$\gamma_0^3\frac{m}{M}\frac{\nu_2}{\nu_1}\ll 1$$

this condition assumes the form

$$\frac{4\nu_1}{\gamma_0^3\beta_0^2}\gg 1. \tag{31}$$

This means that for currents

$$i\gg 4\cdot 10^3\gamma_0^3\beta_0^2 a$$

short waves will be excited in the beam. At smaller currents the beam is stable to the excitation of short waves. The stability with respect to long waves must be considered separately. For this purpose, we now consider the second limiting case $\lambda \gg (1-\beta_\Phi^2)^{1/2} r^*$. Equation (27) now assumes the form

$$\frac{2\nu_1 L}{\gamma_0^3\beta_0^2}\frac{1}{(1-x)^2}+\frac{2m\nu_2 L}{M\beta_0^2}\frac{1}{x^2}=\frac{1}{1-\beta_0^2x^2}, \tag{32}$$

where $L = \ln(kr^*\sqrt{1-\beta_\Phi^2})$.

In this case, the phase velocity is independent of wavelength if the weak dependence on L is not considered. In this case, the equation can again have complex roots, indicating the excitation of oscillations. However, now the oscillations appear at definite values of the parameters, regardless of the wavelength.

Equation (32) can be investigated easily. We obtain the following instability criteria:

$$\left.\begin{aligned}&\nu>\frac{\gamma_0^3\beta_0^2}{2L}, && \text{if} \quad \left(\gamma_0\frac{m}{M}\right)^{1/3}\ll\frac{2}{\gamma_0-1},\\ &\nu>\frac{1}{8L}\sqrt{\frac{M}{m}}\gamma_0^{3/2}; && \text{if} \quad \gamma_0\gg\left(\frac{M}{4m}\right)^{1/3}.\end{aligned}\right\} \tag{33}$$

Thus it follows that at nonrelativistic velocities instability sets in at very small values of the current, while at relativistic velocities it sets in at currents which exceed tens of thousands of amperes.

The results which have been obtained can be easily understood if one considers a bounded plasma column through which particles pass. In the short-wave case the plasma may be considered infinite. In an infinite plasma the frequency is independent of the propagation vector. As a matter of fact, if one charge is deflected from the

others in a plane, they will oscillate, acting like a plane condenser with an external field equal to zero. This means that the perturbation is not propagated, that is, the group velocity of the waves is zero. The phase velocity then increases linearly with wavelength. However, if the wavelength becomes larger than the cross section of the beam, the field produced by the deflection of some of the charges is different from zero both between the charges as well as outside. This means that the group velocity is different from zero and, as is shown by calculations, the phase velocity is almost independent of the wavelength. The phase velocity curve is given in Fig. 2.

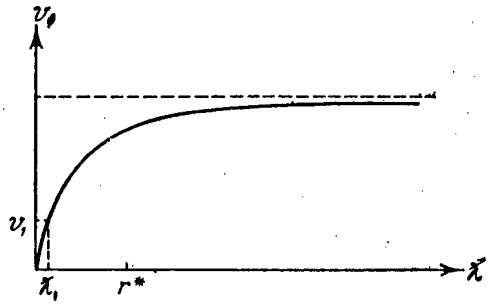

Fig. 2

If the velocity of the particles is smaller than the maximum phase velocity, then there will always be a wavelength λ_1, such that $v_1 = v_\Phi$. In this case, however, there is a characteristic braking resonance of the particles, and waves arise which are similar to those which are excited in a traveling-wave tube. If the particle velocity is greater than the limiting phase velocity, such waves are not found and oscillations are not excited. Assuming roughly that the curve reaches a plateau at $\lambda \approx r^*$, and substituting for this value the usual expression for the Langmuir frequency $\omega^2 = \frac{4\pi e^2 n_1}{m}$, we obtain a qualitative stability criterion.

$$v_\Phi^2 = \omega^2\lambda^2 = \omega^2 r^{*2} = 4\nu_1 c^2 < v_0^2$$

or

$$\nu_1 \ll \frac{\beta_0^2}{4}, \qquad (34)$$

which coincides with that obtained above. For relativistic particles this implies very high currents, which are quite sufficient for the formation of a stabilized beam with large electric and magnetic fields.

c) Stability of the beam with respect to transverse bending. As is well known, the electron beam in a betatron is stable with respect to transverse bending. This stability arises as a result of the fact that the external transverse focusing forces are much greater than the defocusing forces which may appear at the bend.

On the other hand, it is well known that a current passing through a plasma is unstable with respect to bends if the current is pinched and separates itself from the wall. This instability is explained by the fact that the thread-like current configuration gives rise to a magnetic field such that its effect on the current is to cause further bending.

The inherent field of a stabilized electron beam is much stronger than the guiding field. Hence, at least for sufficiently short waves, the inherent magnetic field which causes bending may be greater than the external focusing field.

There is still one more mechanism which leads to instability of the thread in a plasma current. The origin of this instability is the following. Assume that the beam is bent. Then those electrons in the plasma which are strongly bound to the thin thread will experience a centrifugal force. It is easily seen that this hydrodynamic force is directed in such a way as to increase the bending of the current thread. It is not difficult to calculate this force and compare it with the electrodynamic force. It is found that

$$\frac{F_{hydro}}{F_{el\text{-}dy}} = \frac{\gamma_0}{\nu \ln \frac{8R}{r^*}}$$

For currents in a plasma this ratio is much smaller than unity (at rather high currents for which the defocusing force becomes appreciable) and this means it is always valid to neglect the hydrodynamic defocusing forces as compared with the electrodynamic forces.

In a stabilized beam this ratio is of the order unity or larger, that is, the hydrodynamic effects are important. A stabilized beam, however, differs from a plasma in that the conditions for quasineutrality are not present. At bends in the ion thread, the electrons do not move in a curved path at all, and generally speaking, do not necessarily

give rise to a hydrodynamic defocusing force. Furthermore, the existence of the high velocities in the electron leads to hydrodynamic stiffness of the beam with respect to bends, at least for short waves.

Unfortunately, at the present time a calculation of the internal motion of the particle and the particle distribution over the cross section of the beam has not been given.

In view of the importance of this question to the over-all problem, we have attempted to elucidate a number of important features, confining ourselves to a model of the beam in which each of the gases (the electron and ion) is a uniform system – a flexible thread under tension. If one thread is deflected from the other, forces of attraction appear which are proportional to this deflection and equal (for unit length of thread) $F = 2\pi e^2 n_1 n_2 r^{*2} z$.

Assuming, as a first approximation, that the longitudinal motion is unchanged we obtain an equation for transverse motion of the electron and ion threads

$$\left.\begin{aligned} \pi r^{*2} n_1 \gamma_0 m \frac{d^2 z_1}{dt^2} &= -2\pi e^2 n_1 n_2 r^{*2}(z_1 - z_2) + \\ &\quad + F_{1\,\text{ext}} + F_{1\,\text{el-dyn}} \\ \pi r^{*2} n_2 M \frac{d^2 z_2}{dt^2} &= -2\pi e^2 n_1 n_2 r^{*2}(z_2 - z_1) + \\ &\quad + F_{2\,\text{ext}} + F_{2\,\text{el-dyn}} \end{aligned}\right\} \tag{35}$$

where z_1 and z_2 are the deflections of the electrons and ions; F_{ext} are the external forces (e.g., the focusing forces of the external magnetic field); $F_{el\text{-}dyn}$ are the inherent electrodynamic forces of the thread, approximately equal to $F_{el\text{-}dyn} \sim \pi r^{*2} n_1 \gamma_0 mc^2 k^2 z \ln kr^*$. The hydrodynamic forces appear in the left side of the equation.

The equations obtained above can be rewritten in the following form:

$$\left.\begin{aligned} \ddot{z}_1 &= -\Omega^2(z_1 - z_2) + \lambda_1 z_1, \\ \ddot{z}_2 &= -\xi\Omega^2(z_2 - z_1) + \xi\lambda_2 z_2, \end{aligned}\right\} \tag{36}$$

where $\Omega = \sqrt{\frac{2\pi e^2 n_2}{\gamma_0 m}}$ is the oscillation frequency of the electrons in the ion field; $\xi = \frac{\gamma_0 m \nu_1}{M \nu_2}$ is the ratio of the transverse mass of the electron thread to the transverse mass of the ion thread; λ_1 and λ_2 are the sums of the elasticity coefficients for the external and electrodynamic forces divided by $\gamma_0 \pi r^{*2} m n_1$.

We will assume that $v_1 = v_0$; $v_2 = 0$; $\lambda_1 = \lambda$; $\lambda_2 = 0$, and assume a solution of the form $e^{i(kx-\omega t)}$. The dependence of ω on $\underline{k}$ is given by the following characteristic equation:

$$\begin{aligned} \omega^4 - 2kv\omega^3 - [\Omega^2(1+\xi) - \lambda - k^2v^2]\omega^2 + \\ + 2kv\xi\Omega^2\omega - \xi\Omega^2(k^2v^2 + \lambda) = 0. \end{aligned} \tag{37}$$

Investigation of this equation leads to the result that the stabilized electron beam, in an equilibrium state, is stable with respect to bending at least for wavelengths up to

$$\lambda \leqslant \frac{\gamma_0\beta_0}{\sqrt{2\varkappa}} r^*, \quad \text{where } \varkappa = 1.7. \tag{38}$$

At longer wavelengths the excitation of hydrodynamic oscillations starts.

Thus the existence of high velocities for the electrons leads to a situation in which the electrodynamic forces do not produce bending; further weak (as compared with the ordinary plasma) interactions between electrons and ions implies the absence of hydrodynamic bending at small wavelengths.

Bending at large wavelengths can probably be suppressed by eddy currents in the chamber walls, by a specially designed external focusing system or other schemes.

LITERATURE CITED

[1] W. H. Bennett, Phys. Rev. 45, 890 (1934).

[2] W. H. Bennett, Phys. Rev. 98, 1584 (1955).

[3] L. D. Landau and E. M. Lifshits, Theory of Fields (1948).

[4] S. T. Belyaev and G. I. Budker, Proc. Acad. Sci. USSR 107, 807 (1956).

[5] L. A. Artsimovich and Yu. Ya. Pomeranchuk, J. Exptl.-Theoret. Phys. 16, 379 (1946).

Received August 11, 1956

ALTERNATING-GRADIENT FOCUSING IN LINEAR ACCELERATORS*

A. D. Vlasov

A linear theory for alternating-gradient ("strong") focusing in linear ion accelerators is presented.

In linear accelerators designed for use with protons or other heavy particles, as is well known, it is not possible to achieve motion which is stable simultaneously against radial oscillation and longitudinal (phase) oscillations if special measures are not taken in focusing the beam.

The use of such focusing methods as a longitudinal magnetic field, as applied to heavy particles, implies field strengths of tens of thousands of gauss. The use of focusing grids or diaphragms means the loss of a considerable number of particles and, in many cases, is impossible because of the excessive heating of the grids or diaphragms.

There are definite advantages to be gained, as compared with other known methods, in the use of alternating-gradient ("strong") focusing in which use is made of a periodic alternation of focusing and defocusing sections in the accelerator. In linear ion accelerators this scheme means that focusing can be accomplished by both transverse magnetic and transverse electrostatic fields (lens focusing), as well as the high frequency accelerating field itself (alternating-phase focusing).

Lens focusing is accomplished by means of quadrupole magnetic or electrostatic lenses with pole pieces (electrodes) which are hyperbolic in cross section and which provide a constant-gradient field

$$\frac{\partial B_y}{\partial X} = \frac{\partial B_x}{\partial Y}, \qquad \frac{\partial E_x}{\partial X} = -\frac{\partial E_y}{\partial Y}$$

along the X- and Y-axes (we assume a rectangular coordinate system, the Z-axis of which coincides with the accelerator axis). A lens which causes focusing in the XZ plane acts as a defocusing lens in the YZ plane and vice versa.

Alternating-phase focusing is accomplished by periodically changing the sign of the equilibrium phase.

Alternating-gradient focusing has several disadvantages, most of which are related to the tolerances on the accelerating fields and the beam currents and the stringent requirements on the dimensions and operating parameters of the acceleration-focusing system.

The theory of alternating-gradient focusing in linear accelerators has been developed a great deal since the publication of the original paper by Courant, Livingston and Snyder [1] and Blewett [2]. Of the foreign work the most important papers are those of Teng [3], Smith and Gluckstern [4], and an earlier work by Bell [5]. There have also been reported a number of unpublished investigations.

The present paper is a brief description of work carried out by the author in 1953-1955 [6,7]. Questions such as alternating-phase focusing, tolerances, the defocusing effect of space charge, etc. are not treated in this paper, and will be considered elsewhere.

*Presented at the All-Union Conference on the Physics of High Energy Particles, May 18, 1956.

1. Basic Equations. Amplitude of Oscillations Within a Structural Period

In the linear approximation, the radial motion of a particle with mass $m = \frac{m_0}{\sqrt{1-\beta^2}}$, velocity $v = \beta c$, and phase φ is described in the XZ plane by the equation

$$\frac{d}{dt}\left(m\frac{dX}{dt}\right) = F(Z, \varphi)\cdot X.$$

The gradient associated with the radial forces consists of the gradient produced by the lenses plus the gradient due to the defocusing forces of the accelerating field

$$F(Z, \varphi) = evB'\cdot f + \frac{\pi e E_m (1-\beta^2)}{\beta\lambda}\sin\varphi\cdot g.$$

Here e is the charge of the particle; E_m is the amplitude of the accelerating wave; λ is the wavelength; g is a function of the longitudinal coordinate which, on the average, is equal to unity; f is an alternating-sign function of the longitudinal coordinate; B' is the calculated value of the gradient of the magnetic field in the lens; in electrostatic focusing lenses vB' is to be replaced by E'.

Assuming that the velocity v and the structural period 2L change slowly, and introducing the dimensionless coordinates x and s

$$X = \sqrt{(mvL)_0}\sqrt{\frac{L}{mv}}\cdot x, \qquad dZ = L\,ds, \tag{1}$$

we have the equation*

$$\frac{d^2x}{ds^2} - [\Lambda^2\cdot f(s) + A\sin\varphi\cdot g(s)]\cdot x = 0, \tag{2}$$

where

$$A = \frac{\pi e E_m (1-\beta^2)^2 L^2}{m_0 c^2 \beta\lambda^3}, \qquad \Lambda^2 = \frac{eB'L^2}{mv} \tag{3}$$

The subscript "0" refers to the initial values of the quantity.

In the case of an accelerator with a drift tube ($L \sim v$) the "kinematic" factor $\sqrt{\frac{L}{mv}}$ in (1) is constant in the non-relativistic approximation. For an accelerator consisting of uniform evenly-spaced resonators and for free oscillations in a cyclical accelerator (L = const), this factor is inversely proportional to the square root of the momentum mv.

Because of the periodicity of the accelerator-focusing system the coefficient in Equation (2) as well as the functions f, g, $F(Z, \varphi)$ are approximately periodic.

The values x and x' at the output and input of a structural period are related by the linear expression:

*The quantity L, which changes discontinuously, will, for the purposes of this analysis, be replaced by a function which is only slightly different and which is continuous and has a continuous derivative.

$$\begin{bmatrix} x_{out} \\ x'_{out} \end{bmatrix} = \begin{bmatrix} a_{11} & a_{12} \\ a_{21} & a_{22} \end{bmatrix} \cdot \begin{bmatrix} x_{in} \\ x'_{in} \end{bmatrix}$$

Because there is no first derivative in Equation (2) the determinants of the four elements of the matrix being considered here are equal to unity. We introduce the notation

$$\cos\mu = \frac{a_{11}+a_{22}}{2}, \qquad \nu = \frac{a_{12}}{\sin\mu}, \qquad \xi = \frac{a_{22}-a_{11}}{2a_{12}}$$

The motion described by Equation (2) is stable for the condition $-1 < \cos\mu < 1$ and can be given, within the limit of a structural period $2n \leq s \leq 2n+2$, (as well as the case of a periodic coefficient for x and any s) in the form

$$x = C_1 e^{\frac{i\mu s}{2}} \varphi_1(s) + C_2 e^{-\frac{i\mu s}{2}} \varphi_2(s) = \sqrt{4C_1C_2\varphi_1(s)\varphi_2(s)}\sin\left[\frac{\mu s}{2} + \Phi(s)\right], \tag{4}$$

where φ_1, φ_2 and Φ are periodic functions with period 2 and n is a whole number (the number of the period if the enumeration is started with 0). The functions $w_1(s) = e^{\frac{i\mu s}{2}} \varphi_1(s)$ and $w_2(s) = e^{\frac{-i\mu s}{2}} \varphi_2(s)$ satisfy the initial conditions $w_{1,2}(2n) = 1$, $w'_{1,2}(2n) = \xi \pm \frac{1}{\nu}$, in which $w_1(s)w'_2(s) - w'_1(s) \times w_2(s) = \text{const} = \frac{2}{i\nu}$. Determining the constants C_1 and C_2 through x, and x', carrying out the analogous operation in the YZ plane and denoting the quantities here by a line over the symbols, we obtain:

$$\left.\begin{aligned} 4C_1C_2 &= \\ &= \nu^2[w'_1w'_2 \cdot x^2 + w_1w_2 \cdot (x')^2 - (w_1w_2)' xx'], \\ 4\bar{C}_1\bar{C}_2 &= \\ &= \bar{\nu}^2[\bar{w}'_1\bar{w}'_2 \cdot y^2 + \bar{w}_1\bar{w}_2 \cdot (y')^2 - (\bar{w}_1\bar{w}_2)' yy'] . \end{aligned}\right\} \tag{5}$$

It can be shown that the products $w_1w_2 = \varphi_1\varphi_2$ and $\bar{w}_1\bar{w}_2 = \bar{\varphi}_1\bar{\varphi}_2$ are positive and for the equation being considered (2), have maxima at approximately the center of the focusing sections and minima at the center of the defocusing sections. The coefficients $(w_1w_2)'$ and $(\bar{w}_1\bar{w}_2)'$ become zero at these points. The products $w'_1w'_2$ and $\bar{w}'_1\bar{w}'_2$ are positive and take on minimum values approximately in the center of both the focusing and defocusing sections. Hence, it is convenient to choose the injection point at the center of a section which focuses, say in the XZ plane. Of the six coefficients, five assume minimum values and one assumes a maximum (w_1w_2) which is only slightly larger than the value at the edge of a section.*

We now modify the initial part of this analysis for use with a center section, which focuses in the XZ plane. The matrix a_{ij} then becomes approximately symmetric ($a_{11} \approx a_{22}$).

In what follows, it will be assumed that a period includes one focusing and one defocusing section and consists of two mutually symmetric halves. The structures in the XZ and YZ planes differ only by a shift of a half period $a_{11} = a_{22} = \bar{a}_{11} = \bar{a}_{22}$,

$$(\varphi_1\varphi_2)_{max} = \varphi_1(2n)\varphi_2(2n) = 1,$$
$$(\bar{\varphi}_1\bar{\varphi}_2)_{max} = \bar{\varphi}_1(2n+1)\bar{\varphi}_2(2n+1) = \gamma^2.$$

*The convenience of shortening the first lens was indicated, starting from qualitative considerations, by I. L. Zelmanov in 1953.

The quantity γ_2 is equal to the ratio of the Wronskians

$$\gamma^2 = \frac{\nu}{\bar{\nu}} = \frac{a_{12}}{\bar{a}_{12}} = \frac{b_{22}}{b_{11}}.$$

Here the b_{ij} are the elements of the matrix of the first half period. From (4) and (5) we have

$$\left.\begin{aligned} x^2_{\max} &= [x(2n)]^2_{\max} = [x(2n)]^2 + [\nu x'(2n)]^2, \\ y^2_{\max} &= \gamma^2 [y(2n)]^2_{\max} = \\ &= [\gamma y(2n)]^2 + \left[\frac{\nu y'(2n)}{\gamma}\right]^2. \end{aligned}\right\} \qquad (6)$$

Whence for n = 0, if it is undesirable to take different requirements for the XZ plane and the YZ plane we have:

$$R_0^2 \geqslant (\gamma r)_0^2 + (\nu L\alpha)_0^2,$$

where 2R is the diameter of the apparatus; 2r and 2 α are the diameter and angle-of-spread of the injected beam.

2. Region of Stability. Possibilities for Alternating-Gradient Focusing.

We now consider the simplest type of period, one in which we have an idealized accelerator with non-attenuated travelling waves and lenses characterized by linear gradients (f = $\pm$ 1, g = 1, φ = const). Equation (2) becomes

$$\frac{d^2x}{ds^2} + [\pm \Lambda^2 - A \sin\varphi]\, x = 0. \qquad (7)$$

The matrices associated with the focusing and defocusing half-periods assume the form

$$\begin{bmatrix} \cos\psi_1 & \frac{1}{\psi_1}\sin\psi_1 \\ -\psi_1 \sin\psi_1 & \cos\psi_1 \end{bmatrix}, \quad \begin{bmatrix} \operatorname{ch}\psi_2 & \frac{1}{\psi_2}\operatorname{sh}\psi_2 \\ \psi_2 \operatorname{sh}\psi_2 & \operatorname{ch}\psi_2 \end{bmatrix},$$

where $\psi^2_{1,2} = \Lambda^2 \mp A \sin\varphi$. The computation of the a_{ij}, ν, and γ is comparatively simple in this case:

$$\begin{aligned} a_{11} = a_{22} = \cos\mu &= \cos\psi_1 \operatorname{ch}\psi_2 + \\ &+ \frac{\psi_2^2 - \psi_1^2}{2\psi_1\psi_2} \sin\psi_1 \operatorname{sh}\psi_2, \\ a_{12} = \frac{1}{\psi_1}\Big[&\sin\psi_1 \operatorname{ch}\psi_2 - \frac{\psi_2^2 - \psi_1^2}{2\psi_1\psi_2}\cos\psi_1 \operatorname{sh}\psi_2 + \\ &+ \frac{\psi_2^2 + \psi_1^2}{2\psi_1\psi_2}\operatorname{sh}\psi_2\Big], \\ a_{21} = \psi_1\Big[&-\sin\psi_1 \operatorname{ch}\psi_2 + \frac{\psi_2^2 - \psi_1^2}{2\psi_1\psi_2}\cos\psi_1 \operatorname{sh}\psi_2 + \\ &+ \frac{\psi_2^2 + \psi_1^2}{2\psi_1\psi_2}\operatorname{sh}\psi_2\Big]. \end{aligned}$$

The boundaries of the stability region $\cos\mu = \pm 1$ coincide with the equation $\psi_1 \tan\frac{\psi_1}{2} = \psi_2 \left(\operatorname{th}\frac{\psi_2}{2}\right)^{\pm 1}$. The region of stability in terms of the coordinates ψ_2^2 and $-\psi_1^2$ are given in Fig. 2 of [1] (the region between

two curves which intersect at the right side of the figure). In considering a linear accelerator, it is more convenient to present the region of stability in terms of the coordinates $A \sin \varphi = \frac{\psi_2^2 - \psi_1^2}{2} \Lambda = \sqrt{\frac{\psi_2^2 + \psi_1^2}{2}}$ (see figure). It is convenient to plot the family of curves ν = const, γ = const in this same plane.

Because the amplitude of oscillations increases with an increase of ν and γ, and also because of the undesirability of stringent requirements on the gradient in the lenses, the amplitudes of the accelerating fields and the phase of the particle (which can, during a phase oscillation, change over wide limits), it is not practical to use the upper part of the region of stability ($\Lambda > 1.7$). This situation imposes a limitation on the value of A in (3), that is, on the magnitude of the accelerating field for a given β, L and λ. Because of the lower requirements on A with a reduction in Λ, the operating point should be chosen in the center part of the region of stability ($\Lambda = 1.4 - 1.6$).

Reducing the alternation period for the lenses makes it possible to increase the accelerating field, but at the same time requires a higher lens gradient. In an accelerator with drift tubes ($L \sim \beta$, $\beta^2 \ll 1$) the required accelerating field is proportional to β, the lens gradient $B' \sim 1/\beta$, E' = const (for Λ = const). For example, in a proton accelerator with an energy of 10 Mev ($\beta = 0.146$), $\Lambda = 1.6$, $A_{max} = 0.3$, $\lambda = 2$ m and $L = 2\beta\lambda$, we have $B' = 340$ gauss/cm ($E' = 15$ kv/cm^2) and $E_m \leq 1.6$ Mev/m $\left(\frac{E_m}{\beta} \leq 11 \text{ Mev/m}\right)$. At low energies the efficiency of alternating-gradient focusing is reduced to the point at which it becomes expedient to use other methods (grid focusing).

The change-over from ions with a certain $\frac{m_0}{e}$ to ions with another $\frac{m_0}{e}$ can be realized without changing the accelerating system (that is, if the original β is maintained); if the original equilibrium phase φ_s and the original Λ are to be maintained, it is necessary that the accelerating field and the lens gradient be changed in proportion to $\frac{m_0}{e}$. In this case A remains the same. The original values of E_m and $B'(E')$ can be maintained only in those cases for which the associated variables φ_s, A, and Λ remain within the required limits.

If the values of E_m and φ_s are maintained in going over to other ions, then it is necessary that β be changed; consequently, a change of the accelerating system is required in which A and Λ or $B'(E')$ are modified.

3. Calculation of the Matrices for Complicated Periodic Structures

In many cases, in dealing with a complicated periodic structure, it is possible to carry out the calculation as in the simple case described above. We present a simplified method for calculating, for example, an accelerator with drift tubes and a period which covers 2N tubes (for N focusing lenses there are N defocusing lenses; $L = N\beta\lambda$).

Employing the usual simplifications, the matrices associated with the focusing lenses, the defocusing lenses, and the gaps between lenses (including the accelerating space) assume the form:

$$\begin{bmatrix} \cos\frac{\Lambda(1-\alpha)}{N} & \frac{1}{\Lambda}\sin\frac{\Lambda(1-\alpha)}{N} \\ -\Lambda\sin\frac{\Lambda(1-\alpha)}{N} & \cos\frac{\Lambda(1-\alpha)}{N} \end{bmatrix},$$

$$\begin{bmatrix} \operatorname{ch}\frac{\Lambda(1-\alpha)}{N} & \frac{1}{\Lambda}\operatorname{sh}\frac{\Lambda(1-\alpha)}{N} \\ \Lambda\operatorname{sh}\frac{\Lambda(1-\alpha)}{N} & \operatorname{ch}\frac{\Lambda(1-\alpha)}{N} \end{bmatrix},$$

$$\begin{bmatrix} 1+\frac{\alpha A\sin\varphi}{2N^2} & \left(1+\frac{\alpha A\sin\varphi}{4N^2}\right)\frac{\alpha}{N} \\ \frac{A\sin\varphi}{N} & 1+\frac{\alpha A\sin\varphi}{2N^2} \end{bmatrix},$$

where α is the fraction of a period occupied by the gap between lenses.

We divide the period into elements, each of which consists of the second half of the gap between the lenses, the lens and the first half of the following gap. The matrices for the focusing and defocusing elements can be written in the form

$$\begin{bmatrix} \cos\frac{\psi_1}{N} & \frac{1}{k_1}\sin\frac{\psi_1}{N} \\ -k_1\sin\frac{\psi_1}{N} & \cos\frac{\psi_1}{N} \end{bmatrix}, \quad \begin{bmatrix} \operatorname{ch}\frac{\psi_2}{N} & \frac{1}{k_2}\operatorname{sh}\frac{\psi_2}{N} \\ k_2\operatorname{sh}\frac{\psi_2}{N} & \operatorname{ch}\frac{\psi_2}{N} \end{bmatrix} \tag{8}$$

where

$$\left.\begin{aligned} \cos\frac{\psi_1}{N} &= \left(1+\frac{\alpha A\sin\varphi}{2N^2}\right)\cos\frac{\Lambda(1-\alpha)}{N}+ \\ &+\left[\frac{A\sin\varphi}{2\Lambda N}-\left(1+\frac{\alpha A\sin\varphi}{4N^2}\right)\frac{\alpha\Lambda}{2N}\right]\sin\frac{\Lambda(1-\alpha)}{N}, \\ \operatorname{ch}\frac{\psi_2}{N} &= \left(1+\frac{\alpha A\sin\varphi}{2N^2}\right)\operatorname{ch}\frac{\Lambda(1-\alpha)}{N}+ \\ &+\left[\frac{A\sin\varphi}{2\Lambda N}+\left(1+\frac{\alpha A\sin\varphi}{4N^2}\right)\frac{\alpha\Lambda}{2N}\right]\operatorname{sh}\frac{\Lambda(1-\alpha)}{N}. \end{aligned}\right\} \tag{9}$$

The matrices in (8) may be considered as the matrices of a more simple period, described by Equation (7). The focusing lengths and the defocusing lengths of the equivalent half periods are $\frac{\psi_1}{k_1}$ and $\frac{\psi_2}{k_2}$ and are different from unity. Strictly speaking, a further transformation of the equivalent period to the simplest form is required. Practically, however, the differences $\frac{\psi_1}{k_1}$ and $\frac{\psi_2}{k_2}$ do not exceed several percent and their sum differs still less from two. Hence, direct use can be made of all the results of Section 2 (see figure), computing ψ_1 and ψ_2 from Equation (9) and obtaining

$$\Lambda_{\text{equiv}} \approx \sqrt{\frac{\psi_2^2+\psi_1^2}{2}}$$

$$(A\sin\varphi)_{\text{equiv}} \approx \frac{\psi_2^2-\psi_1^2}{2}$$

The accuracy of this calculation increases with increasing N. If account is taken of the small values of the coefficients for the sine terms in (9) and the small departure of the coefficients of the cosine term from unity, it is possible to make use of the simpler expressions (which also yields a better approximation):

$$\Lambda_{\text{equiv}} \approx \Lambda\left(1-\frac{\alpha}{2}\right)$$

$$A_{\text{equiv}} \approx A\left(1-\frac{\alpha}{2}\right)$$

4. Change of Parameters from Period to Period. Effect of Phase Oscillations

Because of the increase in the particle energy, changes of the parameters of the accelerator-focusing system along the accelerator and changes in the phase oscillations of the particles, the matrices of the structural periods also change from period to period. The matrix of a period, which in the general case will be non-symmetric, can be given in the form of a product

$$\begin{bmatrix} a_{11} & a_{12} \\ a_{21} & a_{22} \end{bmatrix} = \begin{bmatrix} 1 & 0 \\ \xi & 1 \end{bmatrix}\cdot\begin{bmatrix} \cos\mu & \nu\sin\mu \\ -\frac{1}{\nu}\sin\mu & \cos\mu \end{bmatrix}\cdot\begin{bmatrix} 1 & 0 \\ -\xi & 1 \end{bmatrix}$$

considered as the matrix of a certain equivalent section, described by the equation

$$\frac{d^2U}{dQ^2} + k^2U = 0 \tag{10}$$

and of length $\Delta Q = \mu\nu$, in which, within the section $k^2 = \frac{1}{\nu^2} = \text{const}$, and at the input and output of the section $k^2 = \pm \xi \cdot \delta(Q_{i,o})$. The gradient $k^2 = \frac{1}{\nu^2}$ characterizes the focusing properties of the period and the pair of δ-functions the asymmetry of the period. For $a_{11} = a_{22}$ this pair vanishes.

The values of U and U' at the ends of these equivalent sections are equal to the values of x and x' at the ends of the corresponding periods. The sequence of equivalent sections forms a system which is equivalent to the accelerator-focusing system of the accelerator.

If the matrices are constant ($a_{ij} = \text{const}$) the δ-functions at the junctions of the equivalent sections cancel each other and in Equation (10) $k^2 = \frac{1}{\nu^2} = \text{const}$. Consequently, the amplitude $[x(2n)]_{max} = U_{max}$ is constant.

For matrices which change slowly from period to period the δ-functions at the junctions of the sections almost completely cancel each other and $k^2 \approx 1/\nu^2$. Hence

$$[x(2n)]_{\max} = U_{\max} \sim \sqrt{\nu},$$

if there is no parametric resonance between the changes of the a_{ij} and the radial oscillations.*

In the case in which there is an arbitrarily fast variation of the matrix, we have $\nu = \nu_{mean} \cdot \nu_{\sim}$, where ν_{mean} is a slowly varying "mean" component and $\nu_{\sim}$ is a factor which oscillates discontinuously about unity. Carrying out a transformation of the variables $U = \sqrt{\nu_{mean}}\,u$ and $dQ = \nu_{mean}\,dq$, as in (1) we have the equation

$$\frac{d^2u}{dq^2} + k^2\nu_{cp}^2 \cdot u = 0. \tag{11}$$

Assume that the matrices are symmetric; then $k^2\nu^2_{mean} = \frac{1}{\nu_{\sim}^2}$. The square of the amplitude $u^2_{max} = u^2 + (u')^2\nu_{\sim}^2$ becomes larger by an increment $(u')^2 \cdot \Delta(\nu_{\sim}^2)$ at the moment in which $\nu_{\sim}$ changes. If, at this time $u' = 0$, then u_{max} is not changed. If $(u')^2 = (u')^2_{max}$ $(u = 0)$, then u_{max} is changed in proportion to $\nu_{\sim}$. Thus, as a function of the phase of the radial oscillations at a junction of the periods, the relative change in the amplitude of the radial oscillations at the junction is given by

$$\eta_n = \left(\frac{\nu_{\sim n}}{\nu_{\sim n-1}}\right)^{\chi_n}, \qquad 0 \leqslant \chi \leqslant 1. \tag{12}$$

For non-symmetric matrices η_m becomes more complicated. However, if the asymmetry of the matrices is small, the quantity η_m remains approximately within the same limits.

Returning to the original coordinates (1) and taking account of (6) we obtain

$$X_{\max} = \sqrt{\frac{L/m\nu}{(L/m\nu)_0}}\sqrt{\frac{\nu_{mean}}{\nu_{0\,mean}}}\prod_{i=1}^{n}\eta_i \times \sqrt{X_0^2 + \left(\nu L\frac{dX}{dZ}\right)_0^2},$$

$$Y_{\max} = \gamma_n\sqrt{\frac{L/m\nu}{(L/m\nu)_0}}\sqrt{\frac{\nu_{mean}}{\nu_{0\,mean}}}\prod_{i=1}^{n}\eta_i \times \sqrt{Y_0^2 + \left(\frac{\nu L}{\gamma^2}\frac{dY}{dZ}\right)_0^2}.$$

*This result, but without the calculation of the parametric resonances, was obtained by E. L. Burshtein and L. S. Solovyev [8].

In the case for which η_m for all n assumes the maximum possible value, there is a pronounced parametric resonance and the amplitude of the oscillations increases; for an asymmetry in the matrices which is not too large, this increase is by a factor of approximately $\frac{\nu_- \max}{\nu_- \min}$ per cycle of change of a_{ij}.

During the phase oscillations $\frac{\mu_- \max}{\mu_- \min}$ may reach a value of 1.2 (for $\Lambda = 1.6$). It is practically impossible to avoid a resonance between the phase and radial oscillations, since the corresponding resonance curves, expressed for small phase oscillations by the equation

$$\frac{T_{\text{phase}}}{T_{\text{rad}}} = \frac{\mu}{\sqrt{8A\sin\varphi}} = \frac{m}{2},$$

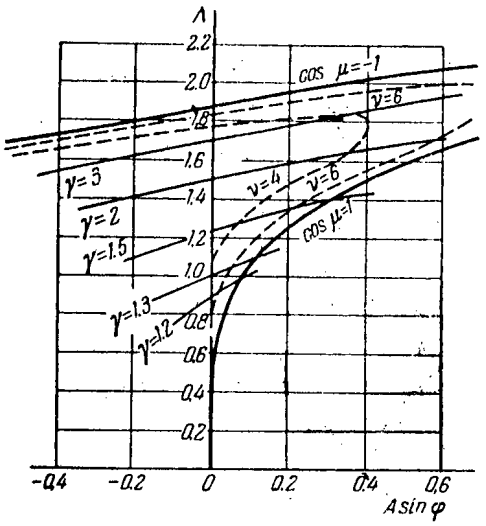

Stability region for alternating-gradient focusing.

(m is a whole number), are densely distributed in the part of the region of stability which is used for operation (center). However, because of the small total number of phase excursions (of the order of ten in accelerators of many hundreds of millions of electron volts), the damping of these oscillations is proportional to the particle acceleration and in the absence of any pronounced resonances, the growth of the amplitude of the radial oscillation, due to the effect of the phase oscillation, never exceeds several tens of percent (and occurs chiefly at small particle energies).

Using Equation (12) it is also possible to calculate changes in the amplitude of the oscillations at the junctions of different-parameter sections of an accelerator.

LITERATURE CITED

[1] E. D. Courant, M. S. Livingston and H. S. Snyder, Phys. Rev. 88, 1190-1196 (1952). A translation appears in Problems of Contemporary Physics, 11, 169-179 (1954).

[2] J. P. Blewett, Phys. Rev. 88, 1197-1199 (1952).

[3] L. C. Teng, Rev. Sci. Instr. 25, 264-268 (1954).

[4] L. Smith, R. L. Gluckstern, Rev. Sci. Instr. 26, 220-228 (1955). A translation appears in Problems of Contemporary Physics 4, 138-154 (1956).

[5] J. S. Bell, AERE T/R, 1072, Harwell (1952).

[6] A. D. Vlasov and N. I. Kotova, Report No. 182, R.A.L. Acad. Sci. USSR (1954).

[7] A. D. Vlasov, Report No. 197, 210 R.A.L. Acad. Sci. USSR (1955).

[8] E. L. Burshtein and L. S. Solovyev, Proc. Acad. Sci. USSR 109, 721 (1956). (Soviet Physics – "Doklady," 459).

Received March 8, 1956

INVESTIGATION OF A HIGH-CURRENT GASEOUS DISCHARGE IN A LONGITUDINAL MAGNETIC FIELD*

A. L. Bezbatchenko, I. N. Golovin, D. P. Ivanov, V. D. Kirillov, and N. A. Yavlinsky

A gaseous discharge in deuterium at currents reaching 700 kiloamps in longitudinal magnetic fields up to 12,000 gauss has been investigated. The effect of the field on the development of the discharge has been studied and it is shown that there is an increase in the magnetic field within the discharge column. An estimate is made of the conductivity of the plasma and the ionization coefficient.

1. Introduction

In recent years high-current gaseous discharges have attracted a great deal of attention in connection with the search for a means of realizing a controlled thermonuclear reaction. The heating of the plasma by the direct acceleration of ions in the magnetic field produced by the current flowing through the gas itself has been described [1, 2]. In this work it was shown that the "combustible" plasma lasts only briefly because the column of the discharge disintegrates within a short time, whereupon the plasma becomes cooled on coming in contact with the walls.

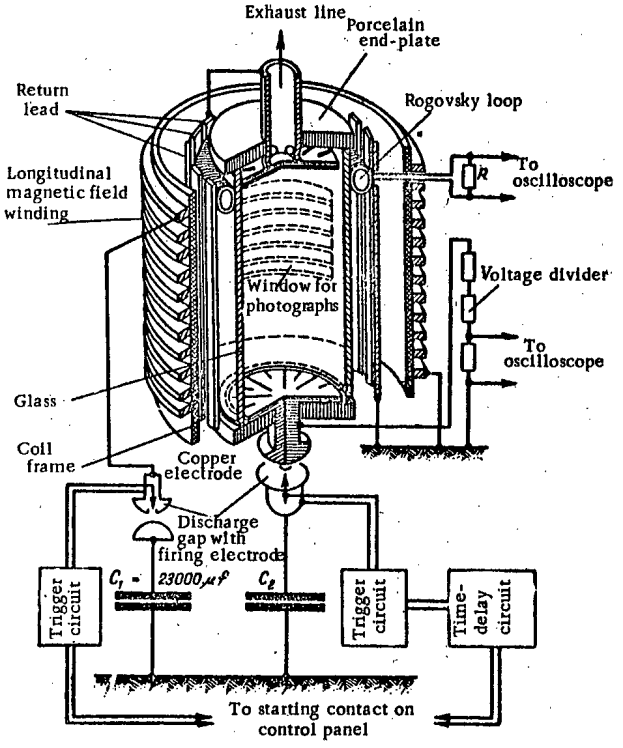

Fig. 1. Diagram of the experimental arrangement.

It seems reasonable that a longitudinal magnetic field should eliminate the plasma instability or, at least, inhibit, to a considerable extent, the disintegration and subsequent cooling of the plasma.

The present paper reports the results of an investigation of a gaseous discharge in deuterium at pressures ranging from 0.05 to 0.4 mm Hg. The development of the discharge was examined in the time during which the current increased from zero to its maximum value. The current strengths reached 700 kiloamps and the intensity of the longitudinal magnetic field was 12,000 gauss. Thus, in this work the intensity of the external longitudinal magnetic field was comparable to the intensity of the field produced by the discharge current itself.

2. Description of the Apparatus

This study of a gaseous discharge was carried out with the pulsed system shown in Fig. 1. The discharge chamber, which was 65-70 cm in length, was fabricated from a glass (or, in certain cases, porcelain) tube 18-20 cm in diameter, and had flat copper electrodes at the end-faces; the chamber

*Presented at a conference at the Karolinska Technical Institutet, Stockholm, September 2, 1956.

was placed in a coil 36 cm in diameter. The coil was wound with gaps between turns to permit observation of the emission from the discharge.

A condenser bank C_1 = 23,000 μf was discharged through the coil by a hemispherical discharge gap; this gave rise to damped oscillations in the circuit at a frequency of 73 cps. The longitudinal magnetic field of the coil was fairly homogeneous in the volume occupied by the discharge chamber, and its intensity in the first half-cycle reached 12,000 gauss for a condenser voltage of 2 kv.

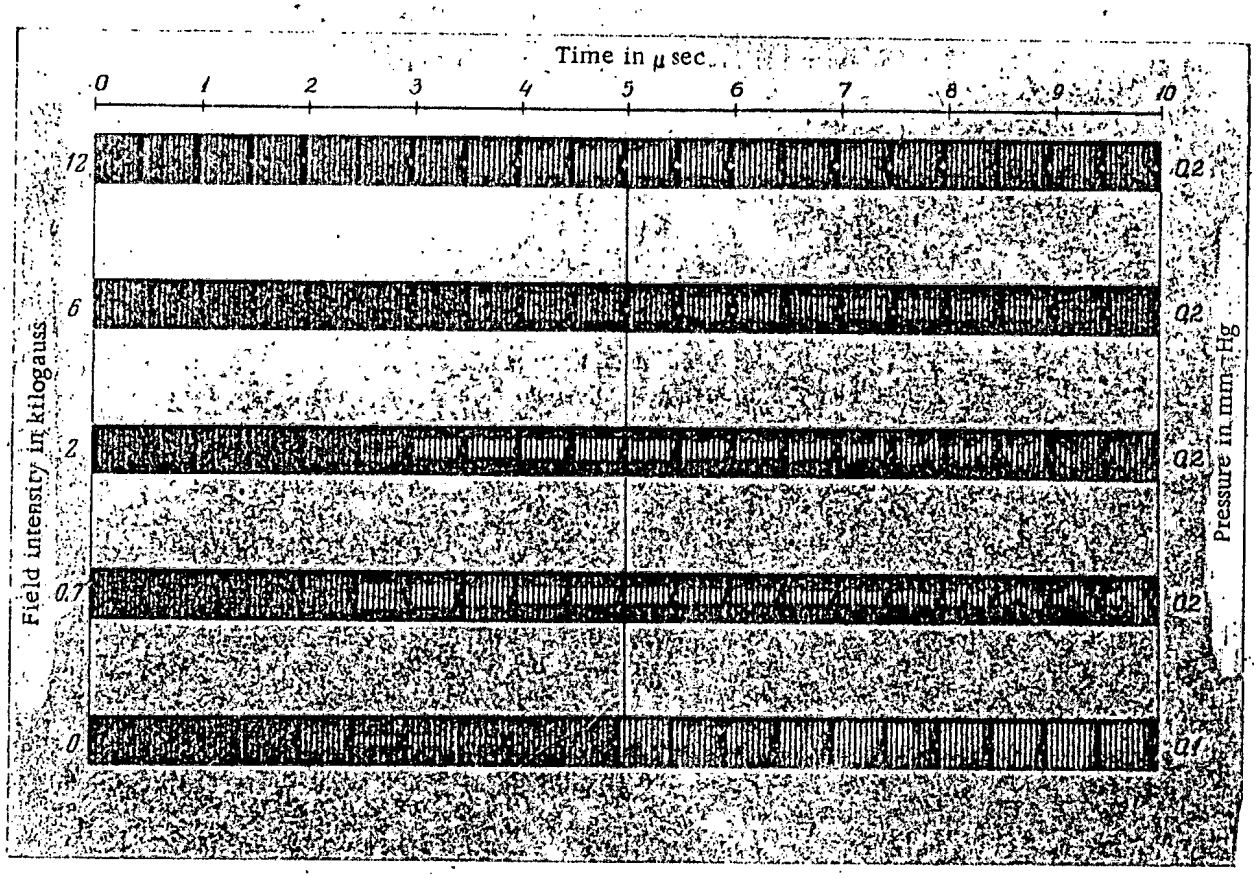

Fig. 2. High-speed cine-photographs of the gaseous discharge. The dark lines across the discharge are caused by the turns of the coil which produces the longitudinal magnetic field.

A second condenser bank C_2 was discharged through the discharge chamber at the instant the magnetic field produced by the coil passed through its maximum value. The oscillation frequency in the circuit consisting of the condenser bank C_2, the current-carrying leads and the discharge chamber was very high so that the longitudinal magnetic field could be considered constant. For the capacities C_2 used in these experiments, 30 μf and 180 μf, the frequency was 43 kc and 17 kc, respectively, while the maximum current through the discharge chamber was 330 kiloamp and 700 kiloamp for a condenser voltage of 40 kv. The hemispherical discharge gaps used with the condenser banks C_1 and C_2 were triggered by thyratron-controlled trigger units. The pulse which triggered bank C_2 was delayed by means of an electronic unit with a variable time delay, with respect to that used to fire C_1.

3. Method of Measurement and Results

In the present work the discharge current, the voltage between the electrodes, the radius of the discharge column, and the average magnetic field therein were measured simultaneously.

The radius of the discharge column was measured by photographing the discharge with a high-speed photo recorder with an exposure rate of $2 \cdot 10^6$ frames/sec. Examples of such photographs are shown in Fig. 2. In Fig. 3 is shown the time-dependence of the radius of the discharge column for different discharge modes. The radius

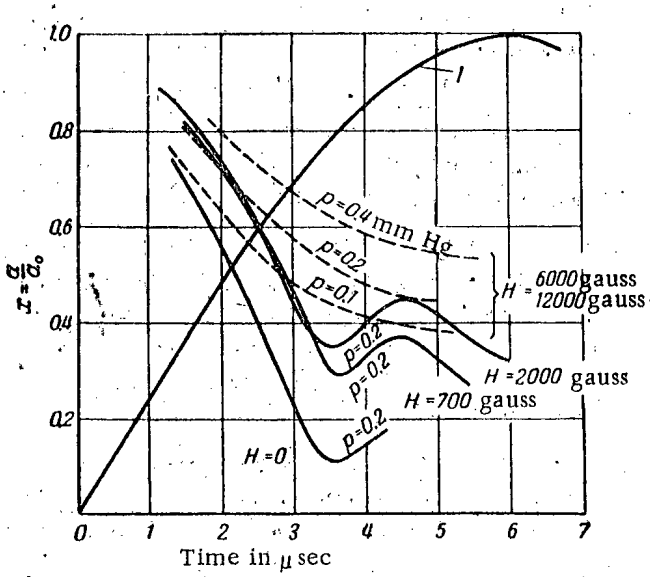

Fig. 3. Time dependence of the radius of the discharge column in deuterium as obtained from high-speed photographs such as those shown in Fig. 2.

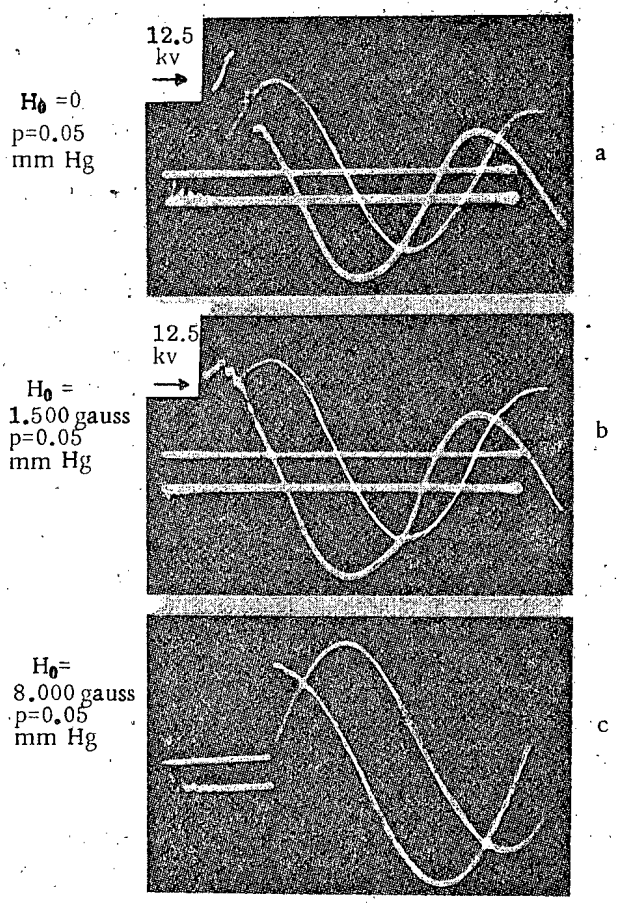

Fig. 4. Oscillograph pictures of the voltage across the electrodes and the discharge current. f = 43 kc; I_{max} = = 250 kiloamp. The lower trace is the voltage and the lines in Fig. a and b indicate the initial electrode voltage.

was determined by measuring the width of the luminous region in the photographs in Fig. 2, starting with the first exposure and ending with the frame in which cylindrical symmetry of the column was lost.

The radius can be determined photographically only 1.5-2 μ sec after the initiation of the discharge because the illumination intensity is small in the early stages. Extrapolation of the curves shown in Fig. 3 to zero indicates that the initial radius of the column a_0 is equal to the inner radius of the discharge chamber. In the following it will be assumed that the radius of the luminous region, measured in this way, is the radius of the region in which current flows. The contraction of the column is inhibited considerably as the intensity of the magnetic field is increased up to 6,000 gauss. Any further increase of the field has only a small effect on the contraction of the column of the gaseous discharge.

It was shown in [1] and [2] that in the absence of a longitudinal magnetic field, the time in which the column of the discharge remains stable is short and depends on the velocity with which the ionized gas moves from the walls of the discharge chamber to the center. We have found that the presence of a longitudinal magnetic field with an intensity of several thousand gauss tends to delay the disintegration of the plasma column.

As a matter of fact, without the external magnetic field, after its first contraction the column executes one-two radial oscillations of very small amplitude; thereafter its boundaries become smeared out quickly and can no longer be distinguished from the general background within the chamber, due to emission from the walls. With a magnetic field, for example, of 700 or 2,000 gauss (see Fig. 3), the column executes a complete radial oscillation and becomes distorted gradually while maintaining its sharp boundaries. After the discharge comes in contact with the walls at one or more points, the wall emission quickly spreads over the entire surface of the discharge chamber. (Silicon lines appear in the emission spectrum of the discharge when it comes in contact with the walls.)

It is apparent from an inspection of Fig. 3 that the average contraction velocity of the column is smaller in the presence of the longitudinal field, for example, at 700 gauss by a factor of 1.3, as compared with the contraction velocity in the absence of the field. At the same time, from Fig. 2 we see that the time in which the column remains sharply defined is increased two-fold.

The discharge current was measured with a Rogovsky loop terminated in a resistance R ($R \ll \omega L$, where ω is the frequency of the discharge

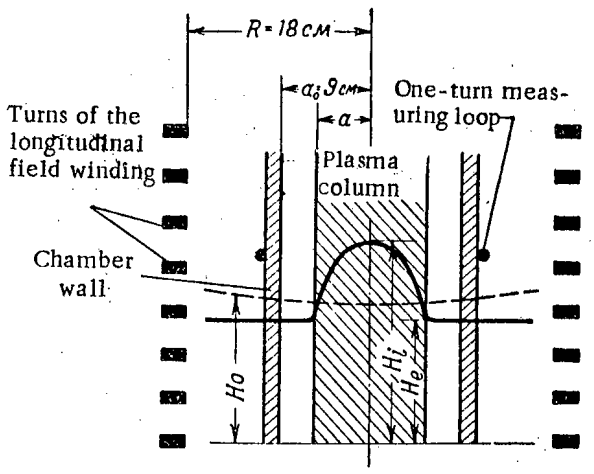

Fig. 5. Redistribution of the longitudinal magnetic field during the discharge.

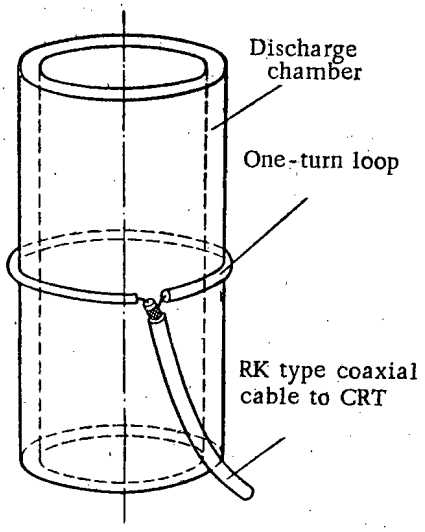

Fig. 6. Arrangement with respect to the chamber of the one-turn loop which measures the redistribution of magnetic field during the discharge.

circuit, L is the loop inductance). The voltage across resistance R is proportional to the current enclosed by the loop and was recorded by one beam of a pulsed two-beam cathode-ray oscilloscope (OK-17).

The sinusoidal time dependence of the current is determined by the circuit since its impedance is greater than that of the discharge column.

Using the low-resistance divider shown in Fig. 1, a fraction of the voltage between the electrodes was applied to the deflection electrodes associated with the second beam in the same oscilloscope. Typical oscilloscope pictures of the current and voltage are shown in Fig. 4.

The spike in the voltage picture for $H_0 = 0$ occurs because the rapid contraction of the discharge column gives rise to an additional inductive component in the voltage across the electrodes $V = 2\frac{\dot{a}}{a}\ell I$, where $\dot{a}$ is the radius of the column, ℓ is the distance between the electrodes, and I is the discharge current. As the magnetic field is increased the contraction of the column is inhibited, the additional inductive component is reduced, and the voltage is described by a smooth cosine function.

In the contraction of the discharge column the magnetic field is carried along by the plasma. The magnetic field inside the column increases but outside is reduced to some extent (Fig. 5). Under these conditions the magnetic flux inside the coil remains constant because the coil which produces the longitudinal magnetic field is virtually short-circuited (at the frequencies of the discharge circuit) by the condenser bank which feeds it. The increment in the magnetic flux inside the one-turn loop, which gives rise to an electromotive-force $\mathcal{E}$, is equal to the decrement of flux outside:

$$\pi a^2 \Delta \overline{H}_i - \pi(\rho^2 - a^2)\Delta H_e = \int_0^t \mathcal{E}\, dt = \pi(b^2 - \rho^2)\Delta H_e, \qquad (3.1)$$

where $\Delta\overline{H}_i = \overline{H}_i - H_0$ is the increase in the field inside the column, averaged over the cross section; $\Delta H_e = H_0 - H_e$ is the reduction in the field outside the column; $\underline{a}$ is the radius of the column; ρ is the radius of the one-turn loop used in the measurement; b is the radius of the coil; t is the time from the initiation of the discharge; H_0 is the longitudinal field applied to the discharge; $\overline{H}_i$ and $\overline{H}_e$ are, respectively, the values of the longitudinal field inside and outside the discharge column.

The measurement of the redistribution of the longitudinal field during the discharge was made with the one-turn loop placed as shown in Fig. 6.

The voltage induced in the loop was applied through a matched coaxial cable directly, or through a resistance divider to the plates of an oscilloscope. The discharge current was recorded simultaneously by the second beam. Typical oscilloscope pictures of the loop voltage are shown in Figs. 7 and 8.

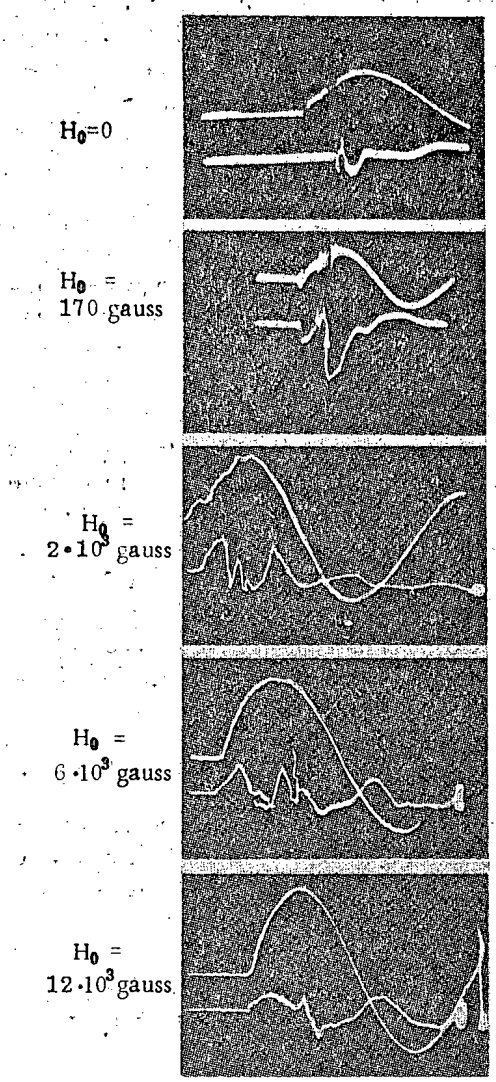

Fig. 7. Oscilloscope pictures of the discharge current and the voltage in the one-turn loop which measures the redistribution of magnetic field during the discharge.
f = 43 kc; p - 0.1 mm Hg; I_{max} = 300 kiloamp. The lower trace shows the voltage in the loop.

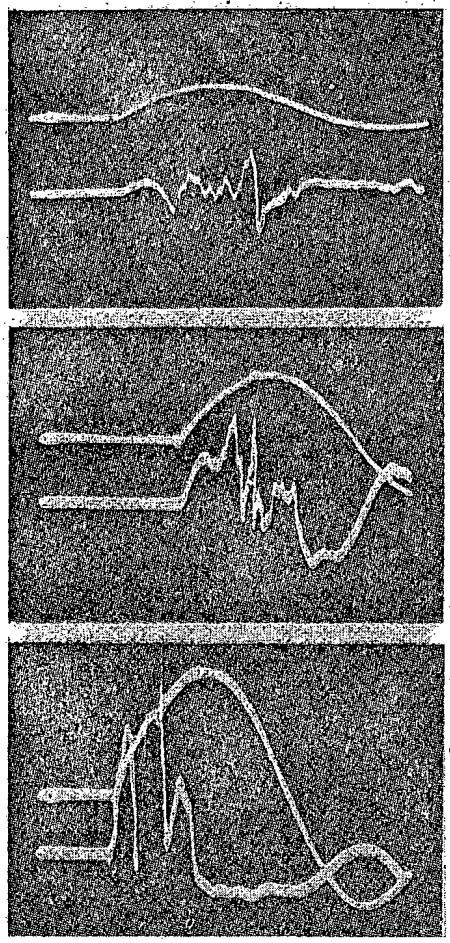

Fig. 8. Oscilloscope pictures of the voltage in the one-turn loop for various values of the maximum current. f = 17 kc; p = 0.1 mm Hg and H_0 = 4000 gauss.

Inspection of the high-speed (Fig. 2) photographs shows that the discharge column retains a truly cylindrical shape for a period of 5-6 μ sec. We see from the oscilloscope pictures (Figs. 7 and 8) that this period corresponds to the smooth curves which indicate the growth of the longitudinal field inside the discharge column for $H_0 \neq 0$ and the absence of an electromotive force in the one-turn loop for $H_0 = 0$.

After 6 μ sec a distortion of the column becomes apparent in the photographs, and in the oscilloscope pictures of the loop voltage one notes uncontrolled oscillations. To determine to what extent the flux of the longitudinal field is entrained by the contracting discharge column, a graphical integration of the loop-voltage curve in the oscilloscope picture was performed in the region for which a, the radius of the column, was known.

As is evident from Equation (3.1), knowing $\int \mathcal{E} dt$, it is possible to determine not only ΔH_e, but also $\Delta \bar{H}_i$ and consequently the flux inside the column ($\Phi_i = \pi a^2 \bar{H}_i$) at any moment of time.

In Fig. 9 the dashed curves show the measured dependence of Φ_i/Φ_0 on time ($\Phi_0 = \pi a_0^2 H_0$). The solid curves were obtained by a calculation based on the assumption that $\bar{H}_i^2 - H_e^2 = H_\varphi^2$, where H_φ is the inherent field produced by the discharge current, at the surface of the discharge column and $\bar{H}_i^2$ is the average value of the longitudinal field. The fact that the curves agree so well indicates that the pressure of the gas is small as compared with the magnetic pressure.

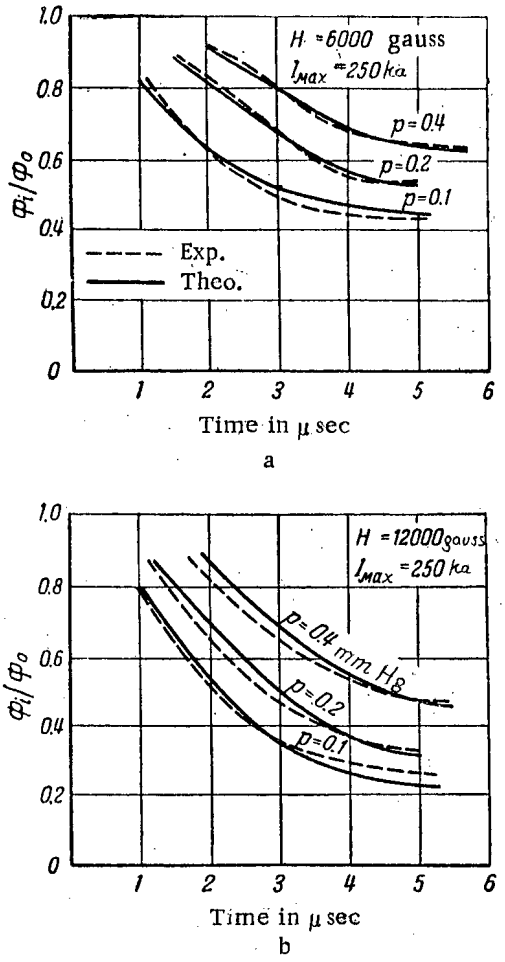

Fig. 9. Time dependence of the ratio of magnetic flux which remains within the column Φ_i to the initial value of the flux $\Phi_0 = \pi a_0^2 H_0$.

The reduction of Φ_i/Φ_0 with decreasing radius is an indication that the plasma conductivity is relatively small during the first three microseconds, since a considerable part of the flux streams out of the column during the contraction process. In the fifth or sixth microsecond, however, as can be seen from Fig. 9, this leakage of the longitudinal field virtually ceases.

To illustrate the extent to which the variation in time of all the quantities measured here depends on the contraction observed in the high-speed photographs, in Fig. 10 we show the time dependence of the radius of the column a, the loop voltage $\mathcal{E}$, the discharge current I and the electrode voltage V. All these pertain to a pressure p = 0.2 mm Hg and H_0 = 2000 gauss. The time at which the voltage in the loop goes through zero corresponds to the instant of the first and maximum contraction of the column. The rate of increase of the discharge current is inhibited at this instant, but the voltage between the electrodes reaches its greatest magnitude. As the column widens, the loop voltage changes sign, the discharge current increases relatively rapidly, and the electrode voltage falls.

4. Radial Motions in the Discharge Column

A complete theoretical description of the state of the plasma during the discharge would be extremely complicated. Hence, we shall carry out here separate analyses of the gas dynamics involved in the contraction of the discharge column and the kinetic processes which occur within it (ionization, scattering, charge exchange, etc.). We now consider the dynamics of the contraction of the plasma column.

It is apparent from the pictures shown in Fig. 2 that for all values of the longitudinal field, in the first five or six microseconds the discharge column is compressed although its length remains the same. The region of the discharge close to the electrodes cannot be seen in the pictures and will not be considered in this paper. Thus, in describing the initial stages it will be assumed that all quantities pertaining to the discharge are functions only of the distance from the axis. We shall also neglect internal dissipation mechanisms, that is, we will assume that the kinetic energy associated with the radial motion is not transferred to other degrees of freedom.

With these assumptions the contraction of the column is given by the equation

$$Mn\alpha\frac{d^2r}{dt^2} = -\frac{d}{dr}(nT) + \frac{1}{c}[\mathbf{j}\,\mathbf{H}] \qquad (4.1)$$

where $\mathbf{j}$ is the current density in the discharge column; M is the mass of an ion, which is equal to the atomic mass; n is the total number of atoms and ions per cm^3 of plasma; T is the temperature of the plasma as a whole. The quantity α refers to the trapping of neutral gas by the contracting plasma. Equation (4.1) describes the motion at an arbitrary point of the plasma inside the discharge column. The time dependence of the radius to the surface of the discharge column a is shown by the high-speed photographs in Fig. 2. In deriving from (4.1) the differential equation which gives the time dependence of a for a given variation of the total current and a given longitudinal field, we shall make the following simplifying assumptions:

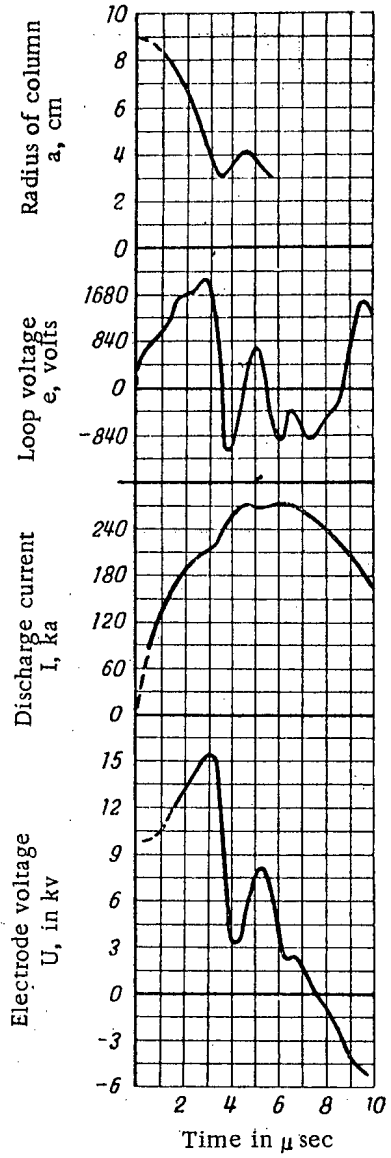

Fig. 10. Time dependence of the radius of the discharge column, the voltage in the one-turn loop, the discharge current and the electrode voltage for a longitudinal field of 2,000 gauss.

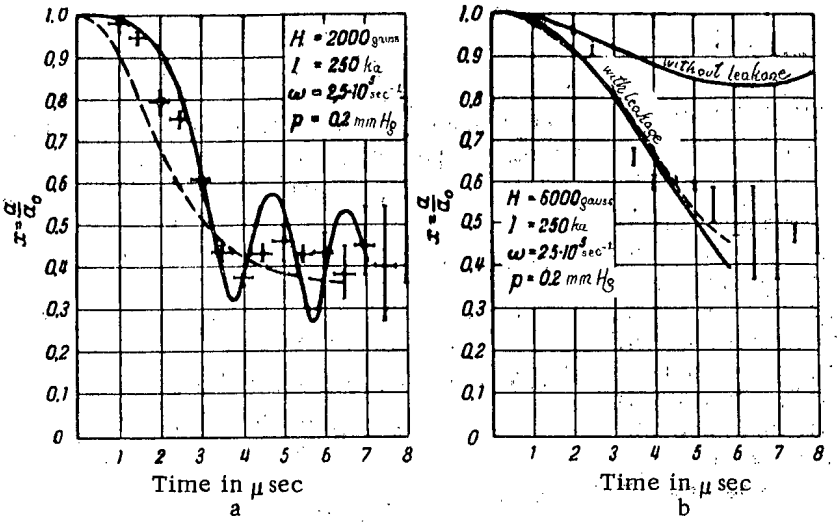

Fig. 11. Time dependence of the radius of the column for a longitudinal field of 2,000 gauss (a) and 6,000 gauss (b).
The solid curves are calculated from Equations (4.2) and (4.5). The dashed curves are obtained by assuming zero mass for the column, that is, the magnetic forces are in equilibrium at the surface of the column $\overline{H_1^2} - H_e^2 = H_\varphi^2$.

1) it will be assumed that the mass of the column which participates in the motion is uniformly distributed over the cross section and remains constant in time;

2) it will be assumed that the velocity, and consequently the acceleration, of points within the column are proportional to the distance from the discharge axis;

3) the pressure nT will be neglected as compared with electrodynamic forces.

The following differential equation for the radial motion in the discharge column (in dimensionless coordinates) is derived in the appendix:

$$\ddot{x}x - \left(\frac{t_{ch}}{t_m}\right)^2 \left[\frac{1}{x^2} - x^2\left(\frac{b_1^2-1}{b_1^2-x^2}\right)^2\right] + \frac{\sin^2 \omega_0 v}{\omega_0^2} = 0. \qquad (4.2)$$

Given the parameters t_{ch} t_m b_1 and ω_0, this equation can be integrated numerically. The results of the integration for two typical cases are given in Fig. 11* (solid line). The results of the measurement of the column radius by high-speed photography are shown in this same figure. For a field H = 2,000 gauss (Fig. 11,a) the calculated curve agrees closely with the experimental points, while for a field of 6,000 gauss (Fig. 11,b) the calculated curve lies far above the experimental points.

The measurements made by means of the one-turn loop (see Section 3) indicate that the flux of the longitudinal field does not remain inside the column, but leaks out of it. A rigorous solution of the problem, taking into account the leakage of flux from the column, would be extremely complicated and is not justified for the relatively poor accuracy of the present measurements and the numerous simplifying assumptions adopted in formulating Equation (4.2). Hence, in analyzing the radial oscillations, we shall take into account the leakage of flux only by introducing a factor $\beta^2(x) < 1$, such that

*The integration was performed on an electronic computer (TsEM-1) by G. A. Mikhailov.

$$\overline{H_i^2} = H_0^2 \frac{\beta^2}{x^4} . \tag{4.3}$$

The curves given in Fig. 9 indicate that for the first six microseconds in fields of 6,000 and 12,000 gauss the flux in the column, with reasonable accuracy, is proportional to the radius, that is

$$\beta^2(x) = x^2. \tag{4.4}$$

Substituting (4.3), (4.4) and (A8) in (A3)*, we obtain an equation for the radial motion of the column which takes into account the leakage of longitudinal field:

$$x\ddot{x} - \left(\frac{t_{ch}}{t_m}\right)^2 \left[\frac{\beta^2}{x^2} - x^2\left(\frac{b_1^2-\beta}{b_1^2-x^2}\right)^2\right] + \frac{\sin^2 \omega_0 \tau}{\omega_0^2} = 0. \tag{4.5}$$

The results of the integration of Equation (4.5) are shown in Fig. 11.

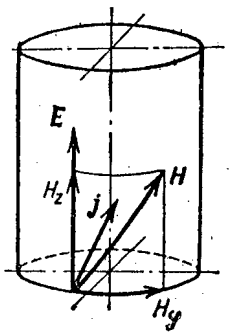

Fig. 12. Current direction in the column for an anisotropic conductivity.

Although the pressure of the gas has not been considered in (4.2) and (4.5), it is apparent that as regards the first four microseconds the experimental points are in satisfactory agreement with the calculated curves. This would seem to indicate that all the important factors pertaining to the contraction process have been taken into account properly. The heating of the plasma is apparently so small as to cause no significant discrepancy between theory and experiment. It is estimated that the mean plasma temperature is less than 15-20 ev.

5. The Conductivity of the Plasma

The increase in the longitudinal magnetic field within the discharge column can be caused by other effects than the increasing field of the contracting plasma. Theoretical analysis shows that if the free-flight-time of an electron depends on its velocity, the equilibrium conductivity of the plasma parallel to the magnetic field is different from that perpendicular to the field. Calculations made on the basis of Coulomb scattering [3] indicate that the conductivity perpendicular to the field is one half the parallel conductivity. In the discharge column the inherent magnetic field combines with the external longitudinal field; as a result, the magnetic force lines assume the form of cylindrical helices. Because the conductivity is anisotropic the current flow is not parallel to the axis but twists as shown in Fig. 12, thus giving rise to a longitudinal component of magnetic field which tends to aid the original field. The magnitude of this effect is a function of the ratio H_φ/H_z. At small values of the longitudinal field $H_z < H_\varphi$ and the effect can become quite important, as has been observed experimentally.

We shall consider this question in somewhat greater detail.

If the column, in shrinking to a small radius, traps all of the longitudinal field which had filled the discharge chamber up to the moment of the discharge, then because the total flux of the longitudinal field in the coil remains constant, the flux which had formerly been outside the discharge chamber is now spread out over almost the entire cross-sectional area of the coil. In this "dilution" of the external field

$$\Delta H_e = H_0 \frac{a_0^2 - a^2}{R^2 - a^2} \approx H_0 \frac{a_0^2}{R^2}, \quad \text{if} \quad a \ll a_0.$$

Hence the integrated electromotive force $\int_0^t \mathcal{E}\, dt$ in the one-turn loop cannot be greater than

$$\pi (R^2 - b^2) \Delta H_e = \pi H_0 (R^2 - b^2) \frac{a_0^2}{R^2} .$$

*The symbol "A" refers to equations in the appendix.

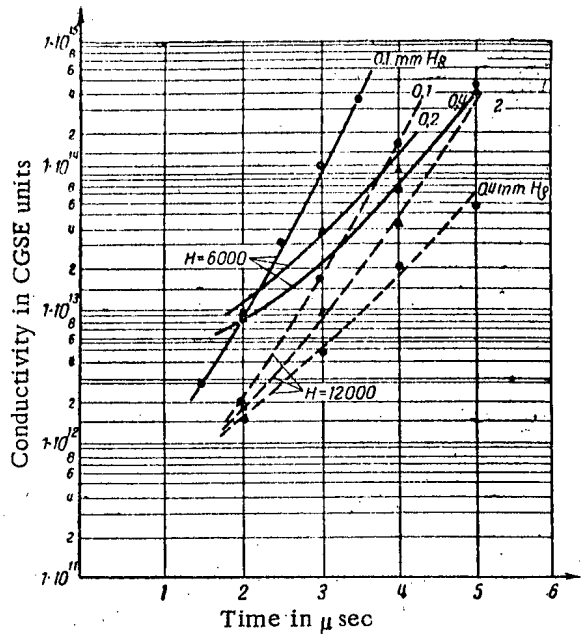

Fig. 13. Conductivity of the plasma as calculated from the measured velocity with which the longitudinal field leaks out of the column. A parabolic distribution of the longitudinal field is assumed inside the column [Equation (5.2)].

If the trapping is not complete the increase of the flux inside the loop and $\int \mathcal{E}\, dt$ will both be smaller.

However, the value of the integral obtained in an experiment with a longitudinal field of 100 gauss is more than twice as big as the value indicated. This means that the flux not only remains inside the column, but that its value increases. The effect which has been observed is far beyond the limits of experimental error. It cannot be attributed to the spiral deformation of the column. Moreover, the distortion of the column is not observed in the first three microseconds. Indeed, the magnitude of the integrated voltage in the loop is larger than that which could be attributed to the trapping of the initially observed field. Hence, it is most probable that the observed increase of the flux of the longitudinal field in the discharge column at small initial fields is produced by the anisotropy in the plasma conductivity due to the magnetic field.

We now estimate the conductivity. Having determined experimentally that the magnetic field leaks out of the contracting column, it is possible to estimate the conductivity of the plasma. To avoid complications in the calculations, we shall limit our conductivity estimate to a plasma in a strong magnetic field (H_0 > 3,000 gauss), neglecting the anisotropy of the conductivity. In this case the rate of change of the longitudinal magnetic flux within the column $d\Phi_i/dt$ is related to the conductivity σ by the relation

$$\frac{d\Phi_i}{dt} = \frac{ac^2}{2\sigma}\left(\frac{\partial H_z}{\partial r}\right)_{r=a}, \tag{5.1}$$

which is derived from Maxwell's equations. In order to calculate the conductivity from Equation (5.1) it is necessary to know not only the velocity with which the field leaks out of the column, but also the distribution of longitudinal field over the cross section.*

For small conductivities, as a first approximation, we shall assume a parabolic distribution of the field inside the column, that is

$$H_i = H_e\left[1 + A\left(1 - \frac{r^2}{a^2}\right)\right]. \tag{5.2}$$

The parameter A is determined easily if the average field inside the column and the field outside are known, since

$$\overline{H}_i = H_e\left(1 + \frac{A}{2}\right).$$

If the magnetic flux contained in a coil of radius R remains constant

$$A = \frac{2R^2(H_0 - H_e)}{a^2 H_e}. \tag{5.3}$$

*V. D. Shafranov has suggested a method for calculating the distribution of the field over the cross section, and participated in the discussion of the results which were obtained.

With this field distribution

$$\left(\frac{\partial H_z}{\partial r}\right)_{r=a} = -\frac{2AH_e}{a}. \tag{5.4}$$

Substituting (5.3) and (5.4) in (5.1) we obtain

$$\sigma = 2c^2 \frac{R^2}{a^2} \frac{H_0 - H_e}{\frac{d\Phi_i}{dt}};$$

$H_0 - H_e$ is measured with the one-turn loop, a by the photographs and $\frac{d\Phi i}{dt}$ is obtained from the curves in Fig. 9. The conductivity calculated by this method for various discharge modes is shown in Fig. 13. For the values of σ which have been obtained, the penetration depth of the current j_φ which supports the longitudinal magnetic flux should be small because of skin effect. Under these conditions the distribution of longitudinal field will tend to become more uniform inside the column and have a greater slope at the edges than is indicated by Equation (5.2). Hence $\left(\frac{\partial H_z}{\partial r}\right)_{r=a}$ and consequently the value of σ will be larger than is indicated by Fig. 13. However, the value of σ, calculated with a correction for skin effect, differs from the value shown in Fig. 13 by less than a factor 2, and that only in the fourth or fifth microsecond, when the determination of σ through the leakage velocity becomes uncertain because of the small contraction velocity of the column.

On the other hand, if the anisotropy of the conductivity is considered, the value of σ which is found is approximately 1.5-2 times smaller. However, even if the current density j_z and the conductivity are considered constant over the cross section of the column then for the entire range of values of σ indicated above, the voltage drop across the longitudinal resistance of the column in the second and third microsecond is considerably greater than the total measured voltage. But because of the phase shift between the voltage and current it is obvious that the real component of the voltage is considerably smaller than the total discharge voltage. Thus the true values of the conductivity are greater than those shown in Fig. 13.

6. Ionization Coefficient

The ionization coefficient can be determined from a knowledge of the plasma conductivity. We shall make use of the well-known conductivity formula

$$\sigma = \frac{e^2 n_e \tau_e}{m} \tag{6.1}$$

where n_e is the number of electrons per cm^3, and τ_e is the free-flight-time for electrons. The electron free-flight-time for collisions with hydrogen molecules and hydrogen atoms is determined by the following expression, which is valid for electron temperature ranging from two to some tens of electron volts:

$$\tau_{ea} = \frac{2.2 \cdot 10^{-10}}{p(1-\eta)}, \tag{6.2}$$

where p is the pressure of the gas expressed in millimeters of mercury, and $\eta = n_e/n_0$ is the ionization coefficient (n_0 is the total number of atoms and ions per cm^3 of the plasma).

We shall use the value $2.2 \cdot 10^{-10}$ in Equation (6.2) since this gives the best agreement with the data of Healey and Reed [4], and with the total interaction cross section for electrons with H_2 molecules from the measurements of Townsend and Ramsauer [5].

The free-flight-time for electrons between Coulomb scattering events on ions differs, depending on whether the directed motion of the electrons is parallel to the magnetic force lines or perpendicular.

If the motion is parallel to the magnetic lines of force, the following formula applies [6]:

$$\frac{1}{\tau_{ei}} = \frac{3\pi^2}{32}\left(\frac{e^2}{kT^0}\right)^2 n_e v \ln\left|\frac{1}{(2\pi n_e)^{1/3}}\frac{kT^0}{e^2}\right|. \qquad (6.3)$$

If the motion is perpendicular to the force lines τ_{ei} is twice as small. In deriving (6.3) the Coulomb forces have been cut off at a Debye length in a plasma whose ion temperature is equal to the electron temperature. If $T_e >> T_i$, then the logarithm term which appears in (6.3) should be replaced by another. For example, if $T_e = 10$ ev and $T_i = \frac{1}{40}$ ev then the logarithm in (6.3) is 1.5 times smaller than that for $T_e = T_i = 10$ ev. Since the ion temperature was not known, in all estimates we have arbitrarily used the value τ_{ei} given by (6.3). For $n_e = 10^{15}$, T = 10 ev, we obtain:

$$\tau_{ei} = 1.3\cdot 10^5 \frac{T^{3/2}}{n_e} = 1.8\cdot 10^{-12}\frac{T^{3/2}}{\eta p}, \qquad (6.4)$$

where T is the temperature in electron volts. The free-flight-time for electrons which appears in (6.1) is related to (6.2) and (6.4) by the expression

$$\frac{1}{\tau_e} = \frac{1}{\tau_{ea}} + \frac{1}{\tau_{ei}} \qquad (6.5)$$

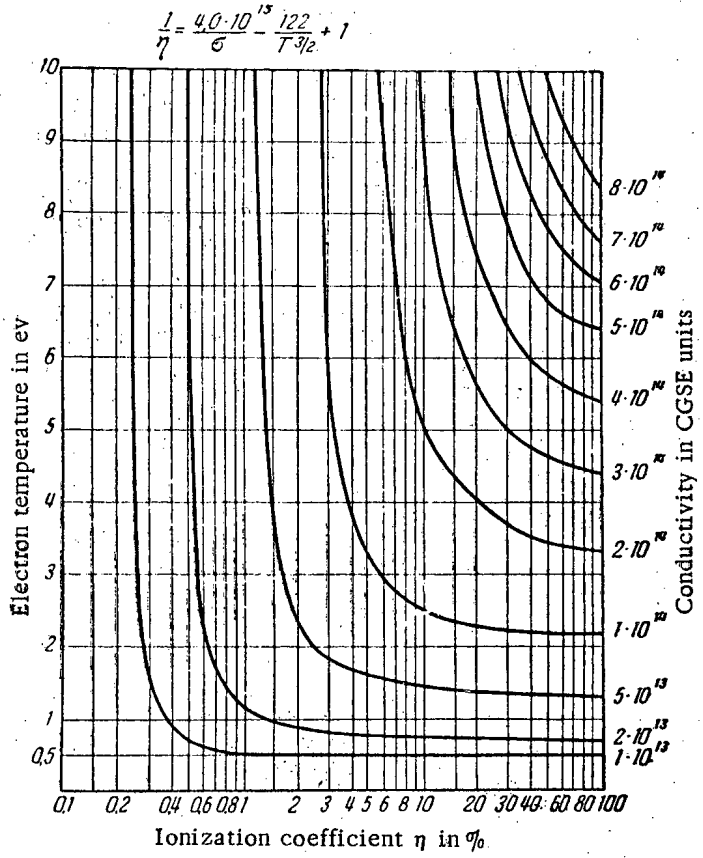

Fig. 14. Relation between the ionization coefficient and the electron temperature for various values of plasma conductivity.

Substituting (6.5), (6.4) and (6.2) in (6.1), we obtain

$$\sigma = \frac{4\cdot 10^{15}}{1/\eta - 1 + \frac{122}{T^{3/2}}}. \qquad (6.6)$$

Thus, a measurement of conductivity only yields a relation between possible values of the ionization coefficient η and the temperature T.

In Fig. 14 are shown curves which relate η and T for different values of σ as calculated from Equation (6.6). In the fourth and fifth microseconds the conductivity reaches a value of $4 \cdot 10^{14}$ cgs units (Fig. 13).

It is apparent from the curves shown in Fig. 14 that even for high electron temperatures the ionization coefficient corresponding to this conductivity is greater than 15%. This is in agreement with the data obtained in [7].

7. Conclusions

The following conclusions have been drawn from the work described in this paper.

1) The longitudinal magnetic field inhibits the contraction of the discharge column due to the inherent field produced by the current. The disintegration of the column occurs later than when $H_0 = 0$. Following the first contraction,

with $H_0 \leq 2000$ gauss, radial oscillations of the column are observed; eventually the column becomes distorted and finally loses well-defined boundaries. Thus the disintegration process with a field present differs considerably from that which obtains in the absence of a field.

2) It is shown that the increase in the intensity of the longitudinal field inside the column of the discharge cannot completely be attributed to the contraction of the column. Apparently part of the effect is explained by the anisotropy in the plasma conductivity produced by the magnetic field.

3) Within the limits of experimental error, the contraction of the column occurs with equilibrium between the pressures of the longitudinal and inherent magnetic fields; this indicates a comparatively low plasma temperature. The plasma temperature is estimated to be less than 15-20 ev.

4) It is estimated from the trapping of the magnetic flux that in the fourth or fifth microsecond the plasma conductivity is $4 \cdot 10^{14}$ cgs units.

5) The ionization coefficient in the column, as estimated from the conductivity, is 15%.

The authors take this opportunity to express their gratitude to L. A. Artsimovich for valuable discussion and interest in this work.

APPENDIX

Discarding the term $-\frac{d}{dr}(nT)$ in (4.1), multiplying the resulting equation by r^2dr and integrating between the limits 0 and a we obtain

$$MN\alpha\ddot{a}=\frac{a^2}{2}[H_\varphi^2-(\overline{H_i^2}-H_e^2)], \tag{A1}$$

where $N = \pi a^2 n$ is the total number of ions and atoms per cm length of the column, $H_\varphi = 2I/ca$ is the field at the surface due to the current I which flows in the column, $\overline{H_i^2}$ is the mean square of the longitudinal field inside the radius a, H_e is the intensity of the longitudinal field at a distance a from the axis.

It is convenient to write (4.2) in terms of the dimensionless variables used in [2]:

$$x=\frac{a}{a_0};\ \tau=\frac{t}{t_{ch}}. \tag{A2}$$

We shall assume that the current varies in accordance with the relation $I = I_0 \sin\omega t$. Under these conditions (A1), in dimensionless variables, assumes the following form

$$\ddot{x}x-\left(\frac{t_{ch}}{t_m}\right)^2\frac{\overline{H^2}-H_e^2}{H_0^2}x^2+\frac{\sin^2\omega_0\tau}{\omega_0^2}=0, \tag{A3}$$

where in addition to the "characteristic time"

$$t_{ch}=\sqrt{\frac{ca_0}{I\omega}}\sqrt{\frac{MN\alpha}{2}}, \tag{A4}$$

which, following [2] determines the time for the contraction of the column in the absence of a longitudinal magnetic field, there appears another time, the "magnetic time"

$$t_m=\frac{\sqrt{2MN\alpha}}{H_0}. \tag{A5}$$

As will be shown later, the magnetic time t_m determines the period of the radial oscillations of the column in the magnetic field. It is convenient to take H_0 equal to the value of the magnetic field applied to the discharge and to take a_0 as the initial radius of the discharge column. The dimensionless frequency in (A3) is determined by the relation

$$\omega_0 = \omega t_{ch} \tag{A6}$$

In order to integrate (A3) it is necessary to know the dependence of $\overline{H_i^2}$ and H_e on the radius of the column.

For high plasma conductivities the magnetic field is "frozen in", the longitudinal field is constant over the cross section of the column, and the flux inside the discharge column does not change in time. Then

$$\overline{H_i^2} = H_i^2 = \frac{H_0^2}{x^4}. \tag{A7}$$

Furthermore, in all the experiments (see Section 3) there is conservation of the flux of the longitudinal field inside the coil of radius b which produces the magnetic field; that is, at any given moment of time

$$H_0 b^2 = H_e (b^2 - a^2) + H_i a^2. \tag{A8}$$

Using (A7) and (A8) and taking $\frac{b}{a_0} = b_1$, we obtain the equation of motion (4.2).

Equation (4.2) was solved for the following initial conditions, $x = 1$, $\dot{x} = 0$ for $t = 0$. Now, let some perturbation cause a departure δ from the configuration x_1, determined by (4.2) for the indicated initial conditions.

Substituting in (4.2) $x = x_1 + \delta$ and neglecting quantities of order δ^2 as compared with unity, and assuming that in the region of oscillations $\ddot{x}_1 \frac{\delta}{x_1} \ll \ddot{\delta}$, we obtain

$$\ddot{\delta} + \left(\frac{t_{ch}}{t_m}\right)^2 P^2 \delta = 0,$$

that is, the radius of the column oscillates about the equilibrium value x_1. The factor P is determined only by the geometry, the radius of the contracted column x_1, and the condition of conservation of flux in the column and in the coil which produces the longitudinal field:

$$P = \sqrt{2\left[\frac{\beta^2}{x_1^4} + \left(\frac{b_1^2 - \beta}{b_1^2 - x_1^2}\right)^2 \left(1 + \frac{2x_1}{b_1^2 - x_1^2}\right)\right]}.$$

Thus the frequency of radial oscillations for the contracted discharge column is

$$\Omega = \frac{P}{t_m} = \frac{PH_0}{\sqrt{2MN\alpha}}. \tag{A9}$$

LITERATURE CITED

[1] L. A. Artsimovich, A. M. Andrianov, O. A. Bazilevskaya, Yu. G. Prokhorov and N. V. Filippov, Atomic Energy 1956, No. 3, 76 (T.p. 367).*

[2] M. A. Leontovich, and S. M. Osovets, Atomic Energy 1956, No. 3, 81 (T.p. 371).*

[3] S. I. Braginsky, private communication.

* T.p. = C. B. Translation pagination.

[4] R. H. Healey and J. W. Reed, The Behavior of Slow Electrons in Gases (1941).

[5] Cf. H. S. W. Massey and E. H. S. Burhop, Electronic and Ionic Impact Phenomena (1952), p. 206.

[6] V. L. Ginzburg, Theory of the Propagation of Radiowaves in the Ionosphere (State Tech. Press, 1949).

[7] S. Yu. Lukyanov, and V. I. Sinitsyn, Atomic Energy 1956, No. 3, 88 (T.p. 379).*

Received September 19, 1956

* T.p. = C. B Translation pagination.

THE STABILITY OF A CYLINDRICAL GASEOUS CONDUCTOR IN A MAGNETIC FIELD*

V. D. Shafranov

Using a hydrodynamic approach, the criteria for stability of an idealized gaseous conductor in an external magnetic field are obtained.

The stability of a cylinder of completely ionized plasma, the pressure of which was in equilibrium with the magnetic forces produced by the current flowing through the cylinder longitudinally, has been investigated [1]. The perturbations which cause the axis of the cylinder to become distorted into a helical shape were analyzed. It was shown that the equilibrium was unstable against these perturbations. In the present paper, as in [1], small vibration theory and the assumption of an idealized conductivity are used in analyzing the stability with respect to arbitrary perturbations when there is a magnetic field directed along the cylinder("longitudinal field"). The stability criteria are investigated.

The basic system of equations consists of the magnetohydrodynamic equations for an idealized conducting medium

$$\left.\begin{aligned} &\frac{d\rho}{dt}+\rho\,\mathrm{div}\,\mathbf{v}=0, \quad \frac{\partial \mathbf{H}}{\partial t}=\mathrm{curl}\,[\mathbf{vH}],\\ &p=\mathrm{const}\,\rho^{\gamma}, \quad \rho\frac{d\mathbf{v}}{dt}=-\nabla p+\frac{1}{c}[\mathbf{jH}]. \end{aligned}\right\} \tag{1}$$

At equilibrium $v = 0$; $\frac{\partial}{\partial t} = 0$, the cylinder is symmetric about the longitudinal axis and in azimuth $\frac{\partial}{\partial z} = \frac{\partial}{\partial \varphi} = 0$. The field components H_z^0 and H_φ^0 are different from zero. We will assume that within the cylinder $H_\varphi^0 = 0$, and H_z^0 is uniform everywhere

$$\left.\begin{aligned} &H^0_{\varphi i}=0; \quad H^0_{\varphi e}(r)=\frac{2I}{cr};\\ &H^0_{zi}=\mathrm{const}; \quad H^0_{ze}=\mathrm{const}. \end{aligned}\right\} \tag{2}$$

(The indices i and e refer respectively to the internal and external fields). Under these conditions the density and pressure are constant over the cross section and we have

$$\begin{aligned} 8\pi p^0 &= H^{02}_{\varphi e}(a)+H^{02}_{ze}-H^{02}_{zi}=\\ &=H^{02}_{\varphi e}(a)\,(1+h_e^2-h_i^2), \end{aligned} \tag{3}$$

* Presented at a conference at the Electronics Laboratory of the Karolinska Technical Institutet, Stockholm, September 2, 1956.

where

$$h_i = \frac{H_{zi}^0}{2I/ca}; \qquad h_e = \frac{H_{ze}^0}{2I/ca}.$$

It is convenient to consider the perturbations in Lagrangian coordinates. Let the particles of the gas undergo a displacement $\boldsymbol{\xi}(r)\, e^{i(kz+m\varphi+\omega t)}$. In the linear approximation (with respect to the perturbation) the correction term for all quantities is proportional to the displacement: $\mathbf{H} = \mathbf{H}^0 + \mathbf{H}^{(1)}(r)\, e^{i(kz+m\varphi+\omega t)}$ and so on. From (1) we obtain, applying these additional terms, the equations

$$\left.\begin{aligned} \rho^{(1)} &= -\rho^0 \operatorname{div}\boldsymbol{\xi}, \qquad \mathbf{H}_i^{(1)} = \operatorname{curl}[\boldsymbol{\xi}\mathbf{H}_i^0], \\ p^{(1)} &= -\gamma p^0 \operatorname{div}\boldsymbol{\xi}, \\ \omega^2\boldsymbol{\xi} + c^2\nabla \operatorname{div}\boldsymbol{\xi} &+ \frac{c_H^2}{H_i^{02}}[\operatorname{curl}\mathbf{H}_i^{(1)}\cdot\mathbf{H}_i^0] = 0; \end{aligned}\right\} \tag{4}$$

$$c^2 = \frac{\gamma p^0}{\rho^0}; \qquad c_H^2 = \frac{H_i^{02}}{4\pi\rho^0}. \tag{5}$$

The equation for $\boldsymbol{\xi}$ has the following solution

$$\left.\begin{aligned} \xi_z &= CI_m(\alpha r); \qquad \xi_\varphi = C\frac{m}{kr}\frac{k^2c^2-\omega^2}{\alpha^2c^2}I_m(\alpha r), \\ \xi_r &= iC\frac{k^2c^2-\omega^2}{k\alpha c^2}\left[\frac{m}{\alpha r}I_m(\alpha r) - I_{m-1}(\alpha r)\right], \end{aligned}\right\} \tag{6}$$

$$\alpha^2 = \frac{\left(k^2-\frac{\omega^2}{c^2}\right)\left(k^2-\frac{\omega^2}{c_H^2}\right)}{k^2-\omega^2\left(\frac{1}{c^2}+\frac{1}{c_H^2}\right)}. \tag{7}$$

In all cases the unit of length is the radius of the cylinder a.

The corrections to the field outside the cylinder are given by the equations $\mathbf{H} = \nabla\psi$, $\Delta\psi = 0$. Taking $\psi = \psi^0 + \psi^{(1)}\, e^{i(kz+m\varphi+\omega t)}$ for $\psi^{(1)}$ we obtain the Bessel equation of the mth order with imaginary argument, the solution of which for $r \to \infty$, is $\psi^{(1)}(r) = \text{const} \cdot K_m(kr)$. The constant of integration is determined from the condition that the normal component of field must be continuous across the surface of the cylinder. By virtue of the idealized conductivity the magnetic field lines within the material remain parallel to the surface. Hence the normal component of the field is zero and the external field is independent of the internal field. We may write the value of the latter at the surface of the perturbed cylinder:

$$\left.\begin{aligned} H_{re}^{(1)} &= i\xi_r(a)\,(mH_{\varphi e}^0 + kH_{ze}^0), \\ H_{\varphi e}^{(1)} &= \frac{\xi_r(a)\, m\,(mH_{\varphi e}^0 + kH_{ze}^0)}{\left[k\frac{K_{m-1}(k)}{K_m(k)} + m\right]}, \\ H_{ze}^{(1)} &= \frac{\xi_r(a)\, k\,(mH_{\varphi e}^0 + kH_{ze}^0)}{\left[k\frac{K_{m-1}(k)}{K_m(k)} + m\right]}. \end{aligned}\right\} \tag{8}$$

The solution for the correction term applies when the eigenvalue ω^2 is completely determined; the sign of ω indicates whether the equilibrium is stable ($\omega^2 > 0$) with respect to a given perturbation, or unstable ($\omega^2 < 0$). This eigenvalue is found from the boundary conditions which appear in the equation of motion. In the present

formulation of the problem this leads to the requirement that the following condition must be satisfied at the surface of the cylinder

$$8\pi p = H_{\varphi e}^2 + H_{ze}^2 - H_{zi}^2. \tag{9}$$

Assuming that

$$H_\varphi^2(a+\xi_r) = H_\varphi^{02}(a) + 2H_\varphi^0(a)\,H_\varphi^{(1)}(a) + \frac{\partial H_\varphi^{02}}{\partial r}\,\xi_r(a)$$

and so on, taking account of (3) and (4) for r = a = 1, we obtain

$$-\gamma p^0 \operatorname{div}\boldsymbol{\xi} = -\frac{\xi_r}{4\pi}\left\{H_{\varphi e}^{02} - \frac{(mH_{\varphi e}^0 + kH_{ze}^0)^2}{k\dfrac{K_{m-1}(k)}{K_m(k)} + m}\right\} + (\operatorname{div}\boldsymbol{\xi} - ik\xi_z)\,\frac{H_{zi}^{02}}{4\pi}. \tag{10}$$

Substituting everywhere the value of $\boldsymbol{\xi}$ from (6) this condition can be written in the form

$$\frac{\gamma}{2}(1 + h_e^2 - h_i^2)\,\frac{\omega^2}{\omega^2 - k^2c^2} = \\ = \left(\frac{I_{m-1}(\alpha)}{\alpha I_m(\alpha)} - \frac{m}{\alpha^2}\right)\left(1 - \frac{(m+kh_e)^2}{k\dfrac{K_{m-1}(k)}{K_m(k)} + m}\right) - h_i^2 \equiv f(\omega^2). \tag{11}$$

Aside from the positive spectrum of solutions $\omega^2 > 0$, corresponding to the acoustic wave and the Alfven wave in the gas in the perturbed cylinder, this solution has one branch of eigenvalues $\omega_m^2(k)$, which become negative for certain cases. If the longitudinal field is zero, then for m = 0 and m = 1 this branch lies completely in the negative region in which for $k \ll 1$

$$\left.\begin{aligned} \omega_0^2 &= -\frac{k^2c^2}{\gamma - 1} \quad (\gamma \neq 1); \\ \omega_0^2 &= -2\sqrt{2}\,k^2c^2 \quad (\gamma = 1); \\ \omega_1^2 &= -\frac{2}{\gamma}\,k^2c^2 \ln\frac{1}{k}. \end{aligned}\right\} \tag{12}$$

For $m \geq 2$ this branch is positive in the region of small and for the value $k = k_m$, determined by the equation $kK_{m-1}/K_m - m^2 + m = 0$, it becomes positive. These values of k_m are as follows: $k_2 = 3$, $k_3 = 8$, $k_4 = 15$, ..., $k_m = m^2$ ($m \gg 1$). In the region of shortwave perturbations the branch $\omega_m^2(k)$, for a given value of m, tends toward one asymptotic value

$$\omega_m^2(k) = -\frac{2}{\gamma}\frac{kc^2}{a} \quad \text{for} \quad k \to \infty. \tag{13}$$

In the presence of a longitudinal field this branch becomes positive at large k. The criterion for stability is obtained from the requirement that the dispersion Equation (11) must not have a solution for $\omega^2 < 0$. For negative values of ω^2 the left-hand side of this equation increases monotonically from $\omega^2 = 0$ to $-\infty$, while the right-hand

side falls off monotonically. Hence there will be no solution for $\omega^2 < 0$, if $f(0) < 0$ or

$$\frac{k^3 h_i^2}{k\frac{I_{m-1}(k)}{I_m(k)} - m} + \frac{(kh_e + m)^2}{k\frac{K_{m-1}(k)}{K_m(k)} + m} > 1. \tag{14}$$

The combinations of factors which appear throughout:

$$\left.\begin{aligned} \varphi_1(k, m) &= k\frac{I_{m-1}(k)}{I_m(k)} - m; \\ \varphi_2(k, m) &= k\frac{K_{m-1}(k)}{K_m(k)} + m \end{aligned}\right\} \tag{15}$$

are independent of the sign of m, whereas the factor $(kh_e + m)^2$ for a given form of the perturbation depends critically on the sign of m/kh_e. In obtaining the criterion for stability it is necessary to take both signs into account. Below, to be definite, we take $k > 0$ and $m > 0$.

Certain cases should be noted in particular:

1) $H_\varphi^0 = 0$. The equilibrium is always stable since (14) becomes

$$\varphi_2 H_{zi}^{02} + \varphi_1 H_{ze}^{02} > 0 \qquad (\varphi_1 > 0,\ \varphi_2 > 0);$$

2) $H_{ze}^0 = h_e = 0$. The criterion for stability for $m = 0$ is $h_i^2 > \frac{I_1^0(k)}{kI_0(k)}$. For $m \geq 2$ a smaller value of h_i is required. The maximum value of the right-hand side of the last inequality is 0.5. Hence, for $H_{zi}^0 > \frac{\sqrt{2}I}{ca}$ the equilibrium is stable with respect to a perturbation with $m \neq 1$. For $m = 1$ the longitudinal field required for stability increases from $k \to 0$ logarithmically. Since $h_i < 1$ (3), the region of stability always occurs for $k > 0.46$;

3) $h_i = H_{zi}^0 = 0$. The condition for stability is $|h_e| > \frac{1}{k}\left(\sqrt{kK_{m-1}/K_m + m} \mp m\right)$, the minus and the plus signs correspond to positive and negative values of m/kh_e respectively. Since $|h_e|$ increases with increasing m, a single external longitudinal field cannot provide stability. Perturbations with a wavelength $\lambda \simeq 2\pi a \frac{|h_e|}{m}$ cannot be stabilized by the field.

In the general case for $h_e \neq 0$ and $h_i \neq 0$ we obtain as the stability criterion $|h_i| > h_0$ where

$$\left.\begin{aligned} h_0 &= \frac{\varepsilon m\varphi_1 + \sqrt{(\varphi_2 + \varepsilon^2\varphi_1 - m^2)\varphi_1\varphi_2}}{k(\varphi_2 + \varepsilon_2\varphi_1)}, \\ \varepsilon &= \left|\frac{h_e}{h_i}\right|. \end{aligned}\right\} \tag{16}$$

The limiting cases are

$$\left.\begin{aligned} h_0 &= \frac{\varepsilon m + \sqrt{(1+\varepsilon^2)m - m^2}}{k(1+\varepsilon^2)} \\ &\qquad (k \ll 1,\ m \neq 0), \\ h_0 &= \frac{\varepsilon m + \sqrt{(1+\varepsilon^2)k - m^2}}{k(1+\varepsilon^2)} \\ &\qquad (k \gg 1). \end{aligned}\right\} \tag{17}$$

The region of stability for longwave perturbations $k < k_m$ for $m \geq 2$ shrinks to zero for $1 + \epsilon \geq m$.

In the curves the region of stability lies between the abscissa axis and the curve $h(k)$.

We may note that the conditions for instability (14) lead to the requirement that the additional force F which appears because of the displacement of the cylinder and acts in the direction of the magnetic field must oppose the displacement. As follows from (10) and (11) this force, for a unit surface, is:

$$F = \xi_r \frac{H_{\varphi e}^2(a)}{4\pi a} \frac{f(0)}{\varphi_1(k)}.$$

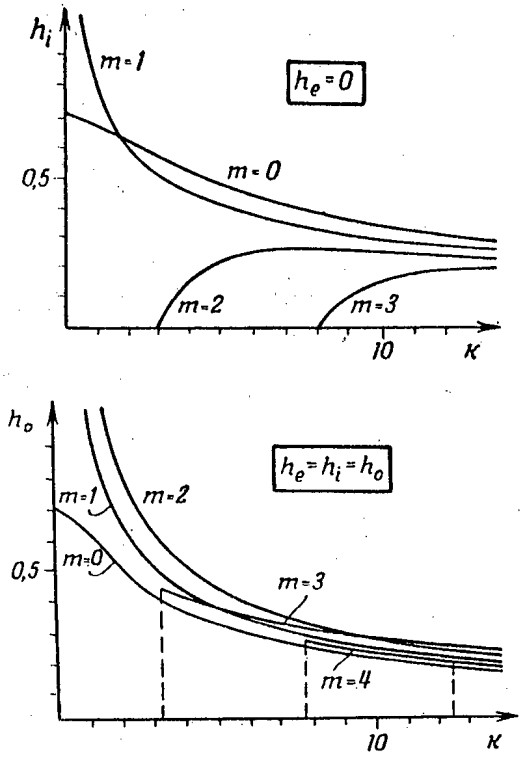

Limits of the stability region at various values of m.

$$h_i = \frac{H_{zi}^0}{2I/ca}; \quad h_0 = \frac{H_{zi}^0}{2I/ca}; \quad k = \frac{2\pi a}{\lambda}.$$

If the gaseous cylinder is placed within a coaxial conducting cylinder of radius b then in (16) we must replace $\varphi_2(k)$ by

$$\frac{[\varphi_2(k) - \chi(kb)\varphi_1(k) I_m(k)/K_m(k)]}{[1 + \chi(kb) I_m(k)/K_m(k)]},$$

where

$$\chi(kb) = \frac{[kbK_{m-1}(kb) + mK_m(kb)]}{[kbI_{m-1}(kb) - mI_m(kb)]}.$$

We shall limit ourselves to a consideration of the effect of a coaxial cylinder for longwave perturbations $kb \ll 1$ for $h_e \neq 0$, $h_i = 0$. If $k = 0$ the force which acts on the cylinder in the direction of the magnetic field is:

$$F = -\frac{I^2\xi_r}{\pi a^3 c^2} \frac{b^{2m}(m-1) + m + 1}{b^{2m} - m} \qquad (m \neq 0);$$

$$F = \frac{I^2\xi_r}{\pi a^3 c^2}\left(1 - \frac{2h_e^2}{b^2 - 1}\right) \qquad (m = 0).$$

The stability criterion is $F/\xi_r < 0$. It is apparent that the magnetic field between the cylinders tends to damp out perturbations with $m = 0, 1$.

In conclusion the author wishes to thank Academician M.A. Leontovich and S.I. Braginsky for valuable advice.

LITERATURE CITED

[1] M. Kruskal and M. Schwarzschild, Proc. Roy. Soc. (London) A 233, 348 (1954).

Received September 19, 1956

NEUTRONS AND NUCLEAR STRUCTURE*

D. J. Hughes

Brookhaven National Laboratory, Upton L.I., U.S.A.

Synopsis

In the past few years slow neutron spectrometers of greatly improved resolving power have been developed at many laboratories throughout the world. During the same period advances in techniques of data analysis have aided in producing the information now available on hundreds of neutron resonances. The manner in which the parameters of these resonances give valuable information on nuclear structure will be described. The experimental findings will be reviewed and particular emphasis paid to their bearing on current theoretical nuclear models. The following aspects will be emphasized. 1) The radiation widths of nuclear energy levels and their relationship to theoretical transition probabilities. 2) The size distributions of neutron widths of levels and recent theoretical treatments of these distributions. 3) The average spacings of levels for different nuclei as well as the apparent non-random distribution of spacings for individual nuclei. 4) The probability of compound nucleus formation, or strength function, compared to recent calculations based on the cloudy crystal nuclear model. 5) Recent determinations of the nuclear radius at high and low neutron energies.

We have heard so much detail about the structure of the nucleus in the last two days of this conference that it seems we may be in danger of losing sight of the nucleus because of the complexity of our methods of studying it. As a result I would like to begin with a few generalizations about nuclear reactions. Professor Bethe began his introductory talk by stating that the subject of the conference was nuclear reactions; however, his entire talk dealt with nuclear structure, energy levels, radii, potentials and so on, rather than with nuclear reactions. It thus was clear that he felt the subject of the conference was the structure of the nucleus and that reactions were means of learning about that structure. The subject of my talk follows the same pattern, for it is concerned only with the nuclear structure that we can infer from nuclear reactions of extremely low energy neutrons, I shall not be concerned as such with the properties of nuclear reactions of slow neutrons, for the properties of these reactions are extremely simple and thoroughly well understood.

You might say that we can learn precious little about nuclei by use of slow neutrons because of the simplicity of the reactions. After all, only zero angular momentum is present, there is no inelastic scattering, angular distributions are completely isotropic, and in short, nothing very complicated happens. However, even though we learn precious little, the little that we learn is precious because it is so definite. In discussing the few, though

* Paper read on July 3, 1956 to the Amsterdam Nuclear Reactions Conference.

definite things that we learn, I shall not consider theory in any detail, for it has already been extensively treated at the conference, practicularly in the talks of Bethe and Weisskopf. I shall limit myself to the problem of the experimental determination of as many nuclear properties as is possible by slow neutron cross sections.

What cross sections are measured with low energy neutrons? The answer is — we measure only resonances and the potential scattering that is observed between resonances. The measurements are made with various types of velocity selectors at many laboratories throughout the world, using pulsed cyclotrons, linear electron accelerators, and betatrons, as well as "fast choppers" located at nuclear reactors. The resonances all have the simple Breit-Wigner single level shape and from these shapes we obtain the so-called resonance parameters. In turn, from the parameters, primarily the radiation and neutron widths, are inferred the facts of nuclear structure.

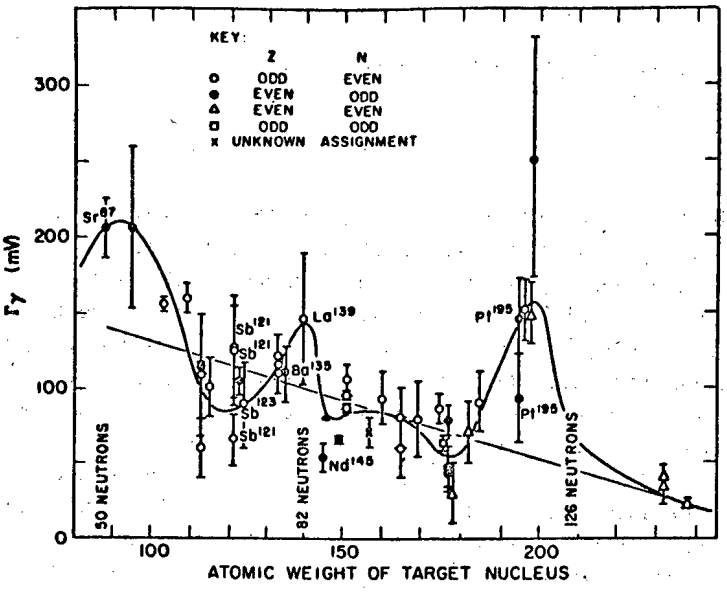

Fig. 1. Radiation widths of individual levels for various nuclides.

The rapidly accumulating information concerning resonance parameters refers both to the internal or inherent properties of nuclei, such as the spacing and radiative probability of levels, as well as external properties, that is, how the nucleus appears to incoming neutrons, in size, transparency, and even shape. The levels that are studied with slow neutrons represent excitation energies of about six Mev, the neutron binding energy. At this energy the disintegration of the compound nucleus is mainly by radiation to many possible states of intermediate energy. The radiation widths of the levels, as well as their spacing, represent the knowledge of the inherent nuclear structure that we gain from slow neutron studies. These properties of the levels are inherent in the sense that they are independent of the way in which the nucleus acquired its excitation energy.

Figure 1 gives the known results on radiation widths of individual levels for various nuclei; the difficulty of the measurements is revealed by the errors and the paucity of results. The first property of the radiation widths to be noted is that they are essentially constant from level to level in a single nucleus. This result is shown much better in some recent measurements at Harwell for silver that will be reported later in the conference by Mr. Rae. The constancy of the radiation widths is related to the many possible final states, that is, exit channels, as discussed already by Bethe. Even from nucleus to nucleus the radiation widths vary only slightly, except for rather large discontinuities that occur at the positions of closed shells, that is, at 50, 82 and 126 neutrons, the "magic numbers". The variations in radiation widths at these positions are in very good agreement with the changes in excitation energy, as given by the neutron binding energy, and in level spacing, that occur at the

closed shells. These variations, as well as those with level spacing and atomic weight for "non-magic" nuclei throughout the periodic table, are consistent with electric dipole radiation, but the absolute magnitude observed experimentally is only about one tenth to one hundredth of that expected theoretically. It is clear that some mechanism must depress dipole radiation by a large factor for complex nuclei.

The method of obtaining the spacing of levels is shown in Figure 2, which gives the number of levels observed as a function of neutron energy for the case of ^{235}U. The linear behavior of the results up to 20 ev is evidence that essentially all of the levels have been found up to this energy, whereas the falling away of the measured number above 20 ev reveals the loss of levels by the increasingly poor resolution at high energy. The slope of the straight line gives the average spacing of levels which in this case is very small, being 1.3 ± 0.1 ev for each spin state, or twice the observed spacing, on the assumption that the two states that are present are equally abundant.

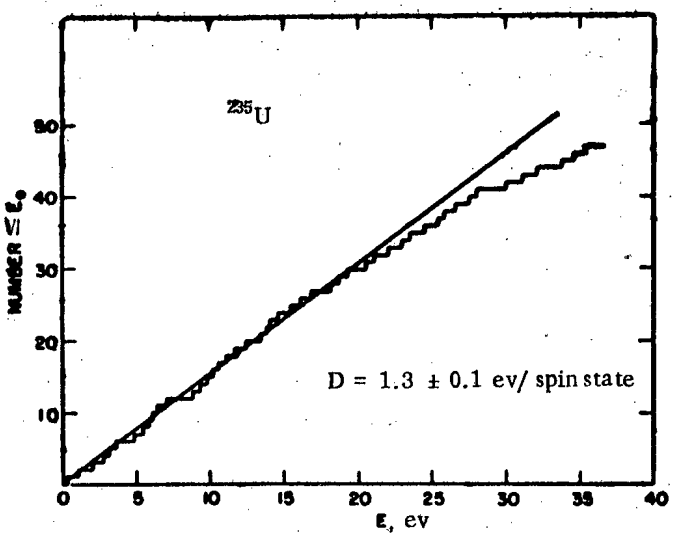

Fig. 2. The number of levels observed in ^{235}U as a function of neutron energy.

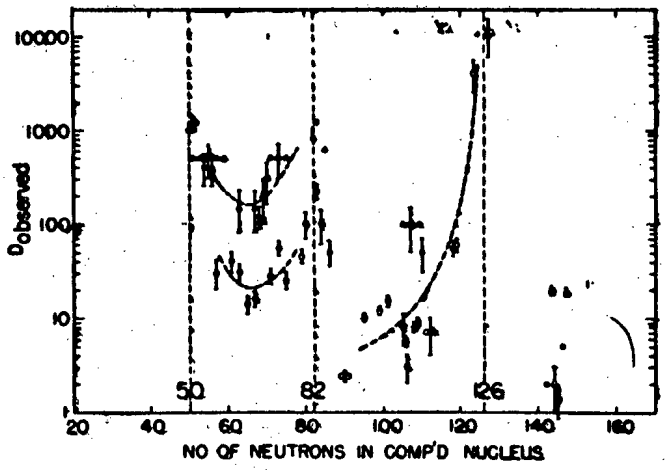

Fig. 3. The observed average level spacing, D, for various nuclides; the discontinuities at closed shells are evident.

The average level spacings thus observed for a number of different nuclides are shown in Figure 3 with different odd-even types of nuclides shown by different symbols. The large discontinuity in level spacings at closed shells is particularly evident, but the data are too sparse as yet to determine definitely the variation of

spacing with even-odd nuclides, binding energy, and nuclear spin. The rapidly improving resolution of velocity selector, however, makes it appear likely that sufficient data will soon be available to establish these variations.

A particularly interesting point has to do with the distribution of level spacings within a single nuclide, that is, whether the levels occur at random or in some regular fashion. The presence of two independent sets of levels in most nuclides $\left(\text{of spins } I+\frac{1}{2} \text{ or } I-\frac{1}{2}, \text{ with I the target nucleus spin}\right)$ confuses the distribution of spacings, making the combined distribution more random in case some regularity exists within each level set. In order to avoid the confusion of the separate sets of levels, studies have been made at Brookhaven for even-even nuclides for which only $J=\frac{1}{2}$ is possible. Figure 4 shows the results that we had obtained some months ago on Th and ^{238}U, which differ greatly from the exponential distribution that would correspond to a random distribution.

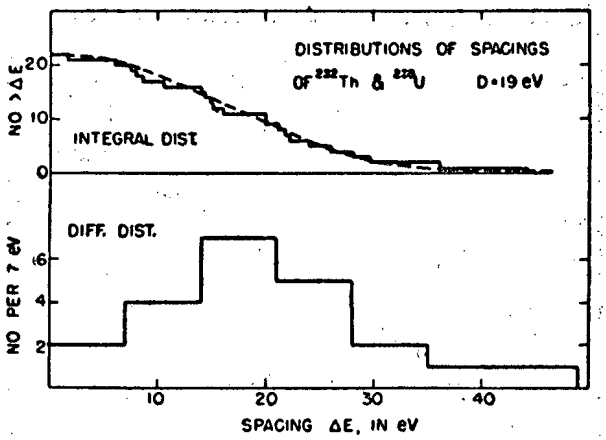

Fig. 4. The distribution of level spacings in the even-even target nuclides ^{232}Th and ^{238}U; both integral and differential distributions are shown.

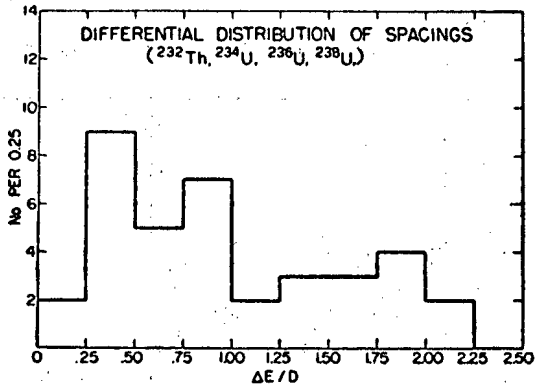

Fig. 5. The differential distribution of the spacings in ^{232}Th, ^{234}U, ^{238}U, and ^{236}U, plotted relative to the average value for each nuclide.

In order to get more data we have recently measured levels in ^{234}U and ^{236}U as well. These new results, combined with the old measurements, appear in Figure 5, where the spacings are plotted in terms of the average value for each nuclide. These more extensive results make the distribution look somewhat less regular than those of Figure 4, but the lack of small spacings still seems to indicate a strong possibility of a "repulsion" of levels. The data of Figure 5 refer only to energy regions in which the resolution was sufficiently good that failure to observe levels was extremely small, hence the departure of the curve for small spacings from exponential can hardly be ascribed to experimental effects. The matter of repulsion of levels is considered in more detail in the paper by Gurevich and Pevsner, to be presented at a later session of the conference.

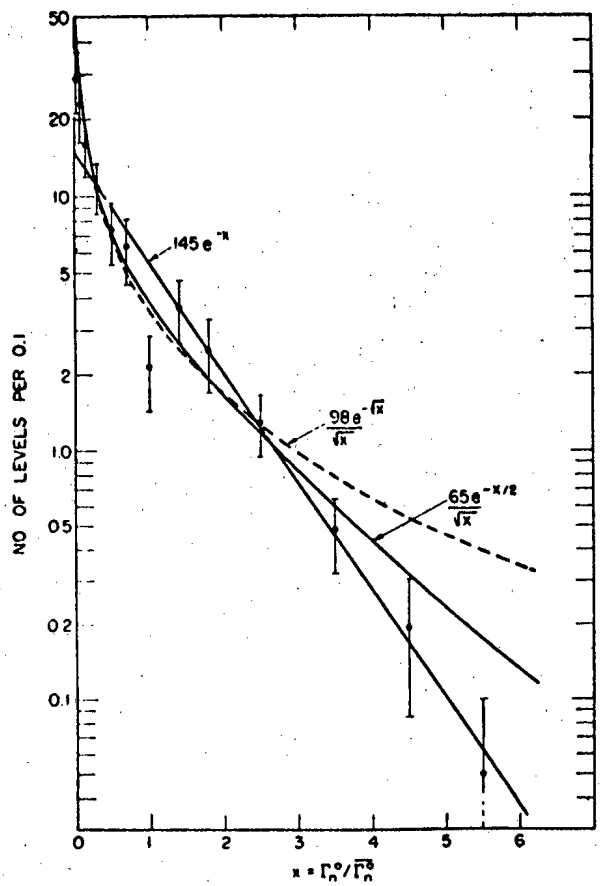

Fig. 6. The combined size distribution of 145 neutron widths, for a number of nuclides, plotted relative to the average value for each nuclide. The solid lines are described in the text; the dashed line is a third suggested distribution.

We now turn from those properties of nuclei that are independent of the method of excitation to the "external" properties, which are of particular interest to recent nuclear models. Here the matters of interest are the neutron widths of levels and the "strength function", or Γ_n^0/D ratio. The neutron width of a level seems at first to be a nuclear property for it gives the disintegration probability of a level by neutron emission. However, division by the average level spacing D removes the specific nuclear part so that the ratio is a property primarily of the penetrability $\underline{p}$ of the nuclear surface. The disintegration probability for the nuclear state per second by neutron emission is of course just $\Gamma_n/\hbar$. The time required for the excitation energy to be concentrated on a single neutron so that the neutron has a chance to emerge from the nucleus, or in other words, the time between collision with the surface, is given by h/D. The product of these quantities, or the probability of emergence per collision, or in other words, the penetrability of the nuclear surface, is given by $2\pi\Gamma_n/D$. Thus the strength function is simply $p/2\pi$ and is not a property of the nuclear energy level system, but of the nuclear surface itself. It is for this reason that the strength function is of particular importance to the cloudy crystal ball and is used to fix some of the parameters in the theory. It is usually evaluated as $\overline{\Gamma}_n^0/D$ where $\overline{\Gamma}_n^0$ is the average value of Γ_n^0, the neutron widths converted to their values at 1 ev.

Before considering the $\overline{\Gamma}_n^0/D$ ratio, however, it is interesting to examine the size distribution of neutron widths that exists within single nuclides. The neutron width is related to the magnitude of the nuclear wave function at the nuclear surface, and the distribution in size of the widths gives information on the variation of the wave function from level to level. The neutron widths, in marked contrast to the radiation widths, show an extremely large variation, as seen in Figure 6, which shows the distribution for many nuclides plotted together in terms of the average value for each nuclide. The distribution is roughly exponential(the straight line in the figure) but closer

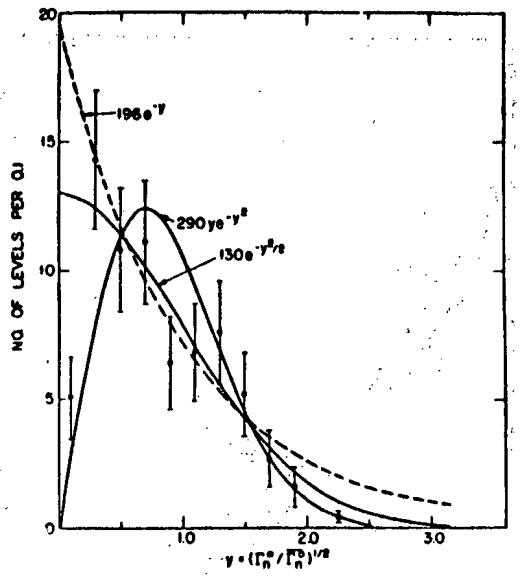

Fig. 7. The results of Fig. 6 plotted against the "reduced width," $\Gamma_n^{1/2}$.

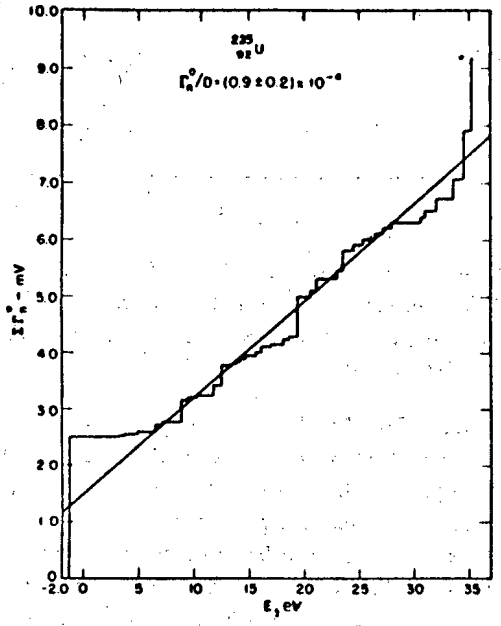

Fig. 8. The integral of the observed neutron widths in ^{235}U as a function of neutron energy; the slope of the straight line gives the "strength function," $\overline{\Gamma}_n^0/D$.

examination reveals an excess of small widths. A distribution law with more physical significance than the empirical exponential has been suggested by Porter and Thomas, and it is shown by the curved line in the figure. In Figure 7 the same distributions are given as a function of $(\Gamma_n^0)^{1/2}$, which is more meaningful physically in terms of the nuclear wave function. In this figure the Porter-Thomas distribution is Gaussian corresponding to the fundamental assumption for the magnitudes of the reduced amplitudes of these authors. Although not obvious in the figure, a statistical analysis of Porter and Thomas shows that their distribution is more likely than the exponential.

The ratio $\overline{\Gamma}_n^0/D$ can be obtained by averaging the parameters observed for individual resonances, and this method is illustrated in Figure 8, which shows the integral of the observed neutron width as a function of neutron energy for ^{235}U. The slope of the straight line gives the strength function but the effect of fluctuations is easily observed. It is also possible to get the strength function by cross section measurements at higher energy because

it is proportional to the average of that part of the cross section curve corresponding to resonances. Even though individual resonances cannot be observed in ^{235}U at 1 kev it is still possible to separate that part of the average cross section representing resonances from that representing potential scattering. The separation is possible because the resonance contribution is proportional to 1/v or to time of flight for a velocity selector measurement, while potential scattering is constant in the region of several kev.

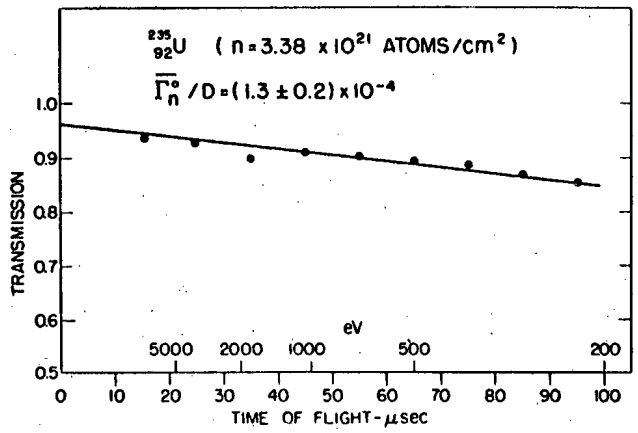

Fig. 9. The method of obtaining the strength function from the average cross section in the kev region; the slope of the straight line is directly proportional to the strength function. The result for ^{235}U agrees well with the method illustrated in Fig. 8.

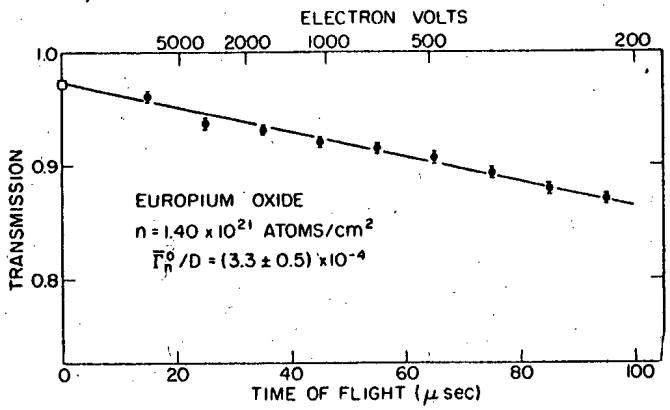

Fig. 10. Determination of the strength function for Eu by the averaging method.

The method is illustrated in Figure 9 for ^{235}U. The slope of the straight line on the transmission plot gives the strength function directly, and the intercept gives the value of the potential scattering, although the latter is not obtained with great accuracy. The method is extremely simple as illustrated by the fact that the cross section averaged over resonances at 1 kev is simply 13.0 $(\overline{\Gamma_n^0}/D) \times 10^4$ barns. The averaging method of obtaining the strength function is illustrated for europium in Figure 10 and in Figure 11 for silver, the slopes of the straight lines in the two cases corresponding to the large strength function for the former, and the very small value for the latter nuclide. A summary of the results obtained at Brookhaven for the $\overline{\Gamma_n^0}/D$ ratio is given in Figure 12, where the open circles refer to the determination from individual resonances and the solid dots to the more recent averaging method. The averaging method is felt to be superior because it is free from the rather serious statistical fluctuations of the previous method.

A matter of great recent interest, which I will pass over briefly because it is the subject of a later session, concerns the size distribution of fission widths. Figure 13 represents the results of a very recent analysis at Brookhaven by Pilcher, Harvey and Hughes, which is now in process of publication. It is obvious that the fission widths behave very much like neutron widths, a fact which is at first rather surprising because the large number of final products in fission seems more like radiation than neutron emission. As we shall learn later in the conference, however, the explanation must be that many different fission products can be produced even though the number of exit channels in fission must be very small, corresponding to the shape of the distribution of Fig. 13.

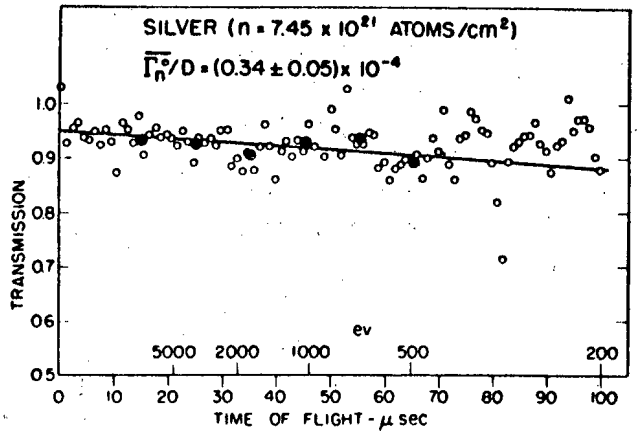

Fig. 11. Determination of the strength function for Ag by the averaging method. The solid dots are averages of the many individual experimental points, shown as open circles.

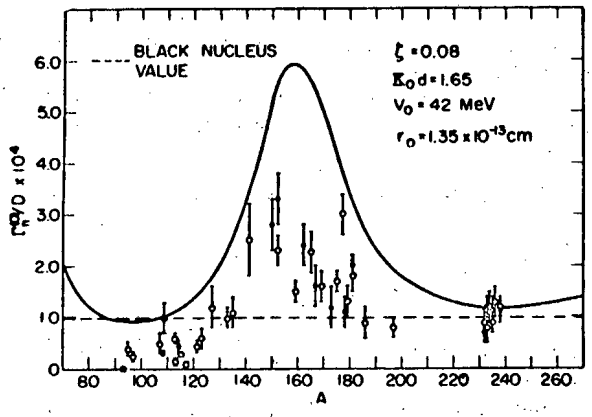

Fig. 12. Brookhaven results for $\overline{\Gamma}_n^0/D$ obtained from individual resonances (open circles) and the averaging method (closed points). The solid line represents a recent calculation based on the "cloudy crystal" nuclear model.

The potential scattering, which is the other item that can be determined accurately with slow neutrons, is of direct interest for nuclear models because it is intimately related to the size, shape and transparency of nuclei. Like the strength function, the potential scattering can be measured not only in the region of a few volts but at higher energies also, where resonances cannot be resolved. At low energies, as shown in Figure 14, the potential scattering is observed between resonances but is affected by the interference of the potential scattering with the resonance scattering, their amplitudes being added coherently. In the figure the cross section is shown as measured (open points) and as corrected by subtraction of the interference effects (solid points) by a computation involving the measured parameters of the nearby levels. The corrected curve is remarkably constant and represents accurately the potential scattering of 10.7b for ^{238}U.

At higher energy, measurement of the cross section for a thick sample gives a value that is almost the same as potential scattering because neutrons of the resonance energies are removed in the first part of the sample and do not affect the results. Small corrections for the residual resonance effects can be made, however. The calculated correction for ^{238}U, for example involves consideration of an average level in ^{238}U at 1 kev (Fig. 15) and the total cross section as affected by Doppler broadening (Fig. 16). The computed transmission curve, based on a potential scattering cross section of 10.7 barns, is given in Fig. 17 compared with the experimental results. The very close correspondence of calculated and measured values shows that the potential scattering in the energy region of several kev agrees within a few percent with that obtained at low energy.

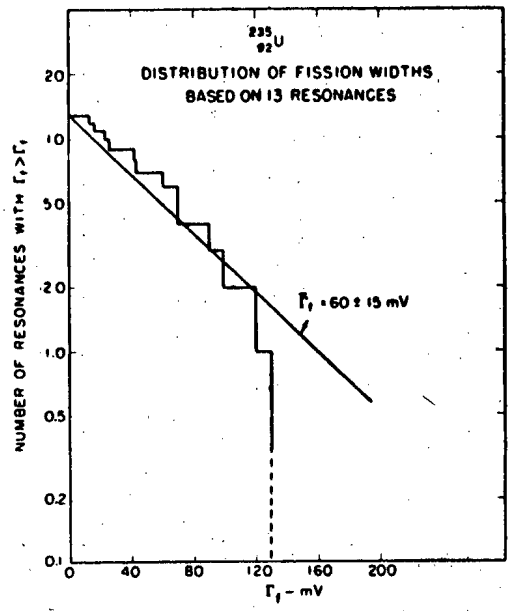

Fig. 13. The size distribution of fission widths in ^{235}U; the wide spread of values indicates a small number of exit channels.

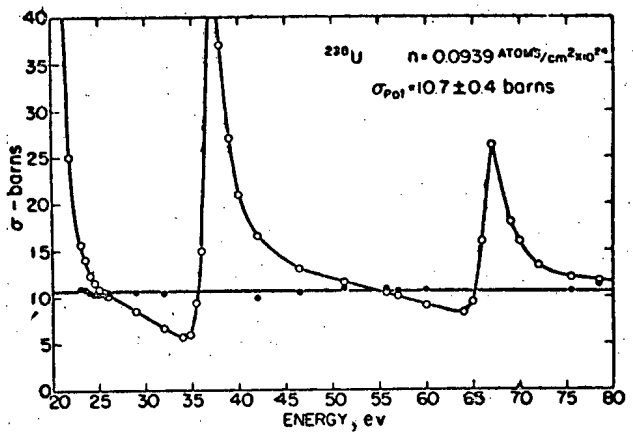

Fig. 14. The measurement of potential scattering by correction of the observed cross section between resonances for the effects of resonance-potential interference.

The question of the relationship of the potential scattering thus determined to the nuclear radius is best discussed in terms of the single particle, or cloudy crystal ball, nuclear model. This comparison is given in Figure 18, which was also shown by Weisskopf this morning but which he did not have time to discuss. The lower part of the figure is the strength function, giving not only the Brookhaven results, but also other measurements, primarily at lower atomic weights. These latter results have large statistical errors because of the small number of levels for the light nuclei within the low energy range. The upper part of the figure gives R', which is the "effective nuclear radius" for potential scattering, as well as the actual nuclear radius R, where R is the distance to the half way point of the nuclear potential well. The potential scattering, σ_p, is given in terms of R' by $\sigma_p = 4\pi(R')^2$.

The measured values for silver, thorium and uranium agree very well with the theoretical curve, and thus not only justify the model but show that R is very close to the value used in the calculation, namely $1.35A^{1/3} \times 10^{-13}$ cm. It will be very valuable to measure potential scattering for nuclei for which R' is appreciably different

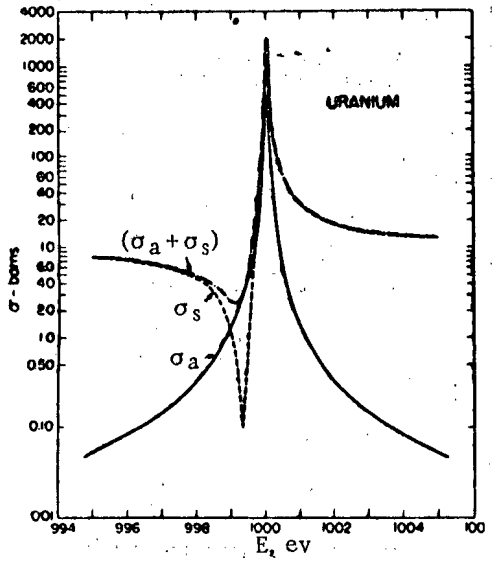

Fig. 15. The cross section for a typical level in ^{238}U at 1 kev, used in correcting a thick sample transmission curve (Fig. 17) for resonance effects.

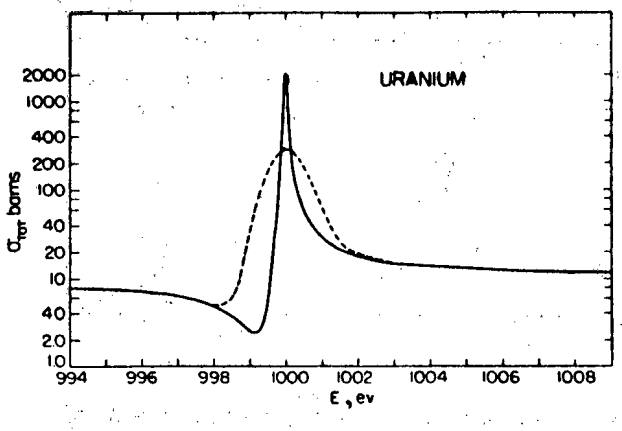

Fig. 16. The total cross section of Fig. 15 as affected by Doppler broadening (dashed line).

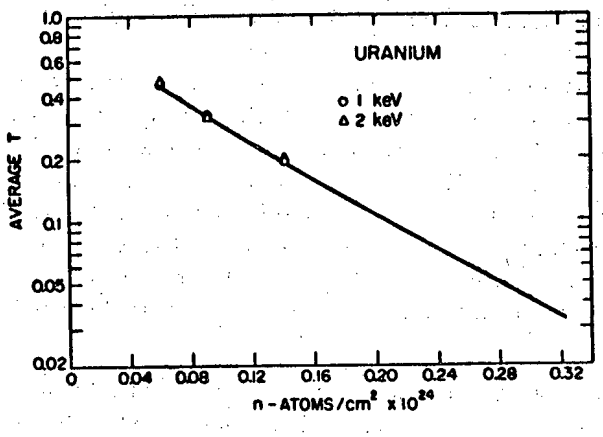

Fig. 17. The computed transmission curve for ^{238}U and the measured points at 1 and 2 kev.

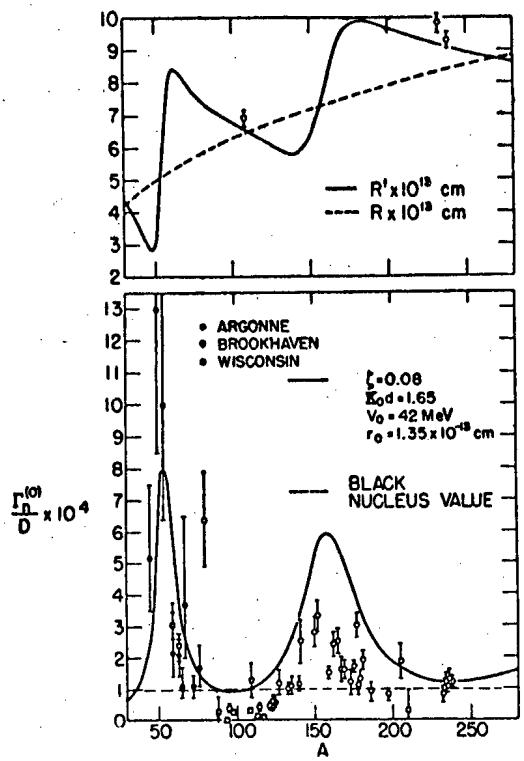

Fig. 18. In the lower section, the theoretical strength function is compared with experimental results. The upper curves are the nuclear radius R and the apparent R', as well as the measurements described for Ag, Th, and ^{238}U.

from R in order to test the nuclear model. The ratio of R' to R is not greatly sensitive to the parameters of the model, however, hence the measurement of potential scattering can be considered to give good values of R, basing the conversion of the measured R' to R on the model. Interpreted in this way, the three points of Fig. 18 give a nuclear radius R, that is, the distance to the half way point of the potential, of $1.38 \times A^{1/3} \times 10^{-13}$ cm. This nuclear radius, which is the so-called nuclear reaction radius, is definitely higher than the electromagnetic radius, and it will be of interest to see if this difference disappears at very high energies, of the order of several Bev. as seems to be indicated by preliminary experiments.

The results that have been obtained with low energy neutrons are sufficient to show the value of the definite quantities, such as strength functions and nuclear radius, that can be obtained from cross sections. Many velocity selectors, of ever-increasing resolving power, are coming into operation at the present time throughout the world. As a result, we may confidently expect that other relationships, which can not be fixed at the present time because of lack of data, will also be accurately determined before many years have passed, and will provide further basic information that will be of great value to future theoretical developments.

Received July 28, 1956

MEASUREMENTS OF THE TOTAL EFFECTIVE CROSS SECTIONS FOR RESONANCE NEUTRONS IN Pd, Os, Ir, Mo, In, I, Ta, Th, U^{238}*

I. A. Radkevich, V. V. Vladimirsky, V. V. Sokolovsky

The results of calculations of the level constants in the elements Pd, Os, Ir, Mo, I, In, Ta, Th, U^{238} are presented; the cross sections for these elements have been published earlier. New measurements for the cross sections in Ir, Th, U^{238} are cited. The measurements were made with a mechanical-chopper spectrometer with a resolution of 0.08 μsec/m in the energy region from 4.5 to 10,000 ev. The integrated and differential curves for the distribution of neutron widths in these elements are plotted.

Analysis of the Results

The neutron energies were measured by a time-of-flight method. A detailed description of the neutron spectrometer has been given [1, 2].

The determination of the level constants from measured transmission curves in samples of different thicknesses has been carried out by the "area" method [3, 4]. In the energy region in which the width of the resolution function R is comparable with the total width of the level Γ, the total width, and consequently the radiative width of the level, can be determined with reasonable accuracy. In the spectrometer being described here this limit was about 50-60 ev. Since the radiative width is a weak function of energy, in determining the neutron widths in the region in which $R \gg \Gamma$, we have used the average values of the radiative widths determined from the levels investigated at low energies.

Using the interference effect [5], from the behavior of the experimental cross-section curve in the region of resonance the neutron width Γ_n can be determined. We write the Breit-Wigner formula in the form

$$\sigma(E) = \left(\frac{E_0}{E}\right)^{1/2} \frac{\sigma_0 \Gamma^2}{4\left[\left(\frac{\Gamma}{2}\right)^2 + (E-E_0)^2\right]} + \frac{\sigma_0 \Gamma \sqrt{\sigma_p}}{2\lambda \sqrt{\pi}(E-E_0)} + \sigma_s \qquad (1)$$

where σ_s is the cross section for potential scattering. In the first term we may set $\left(\frac{E_0}{E}\right)^{1/2} = 1$, and in the second may substitute λ_0 for λ. Taking the difference in the cross sections for the values E_1 and $E_2 = 2E_0 - E_1$ and substituting the numerical constants, we obtain

$$g\Gamma_n = \frac{\sigma_0 \Gamma}{4\pi\lambda_0^2} = 0.31 \sqrt{\frac{E_0}{\sigma_s}} (E_1 - E_2)[\sigma(E_1) - \sigma(E_2)]. \qquad (2)$$

*Presented at the International Conference on Nuclear Reactions in Amsterdam (June 1956).

Since the channel width ΔE increases with increasing energy, $\sigma(E_1)$ is determined for a given channel, while $\sigma(E_2)$ is found by interpolation of the cross section. For the calculations usually 10-20 pairs of points were studied. The statistical error is found from the expression $\Delta = \frac{\Sigma|\Delta_i|}{n}$, where $\Delta_i = \Gamma_{ni} - \frac{\Sigma^n \Gamma_{ni}}{n}$, and n is the number of pairs of points.

The error introduced in the measurements of Γ_n due to the finite resolution of the spectrometer at points far from resonance is small. For the values which were used here $E - E_0 > 5\Delta E$, the correction in the first approximation, as obtained by Equation (1) [6] for all levels, calculated here by the interference effect, was approximately one percent. At points far from resonance the corrections for the Doppler effect were also very small.

TABLE 1

Resonance Parameters in Palladium

№	E_0	$1/n$	A	Γ_γ	$wg\Gamma_n$	$wg\Gamma_n^0$	$w\sigma_0\Gamma$
1	11.68±0.12	50	0.197±0.016		0.03±0.003	0.009±0.0009	6.3±0.5
2	13.05±0.13	50	0.810±0.148	241±73	0.23±0.04	0.06±0.01	43±6
		782	0.0861±0.012				
3	24.8±0.2	50	0.566±0.021	292±200	0.278±0.2	0.05±0.04	
		782	0.05±0.02				25±10
4	32.5±0.5	50	5.81±0.064	180±52	13.67±3.91	2.40±0.70	$\sigma_0\Gamma^2$=200±4 *)
		782	1.572±0.042				
5	55±1	50	0.750±0.15	—	0.85±0.3	0.11±0.04	24±5
6	77.8±2	50	0.52±0.17	—	0.50±0.16	0.06±0.02	17±5
7	89.5±2.4	50	6.97±0.2	—	~110		
		782	2.37±0.16	—	~73	~10	$w\sigma_0\Gamma^2$=780±50
8	148±5	50	1.45±0.38	—	2.66±0.7	0.22±0.06	47±12
9	183±7	50	3.9±0.83	—	8.85±1.88	0.65±0.14	126±27
10	283±15	50	8.95±1.33		50±15	3±1	$w\sigma_0\Gamma^2$=1250±370
		782	2.48±0.8	Γ_{total} = =516±260			
11	355±20	50	2.9±1.75	—	12.8±7.7	0.68±0.4	93.6±56
12	427±27	50	8.16±1.86	—	43±10	2±0.5	—
13	891±80	—	—	—	—	—	—

*This level due to Pd^{108} [9].

The basic contributions to the error in the measurements of Γ_n are due to three factors: the inaccuracy in the determination of the value of E_0, the contribution due to neighboring levels and errors in the measurement of the potential scattering σ_s. The last two sources of error have been estimated by Levin and Hughes [7]. We now consider the error due to the inaccurate determination of E_0. To calculate Γ_n by the interference effect the behavior of the cross section is measured in thick samples. For this reason, position of the resonances is determined very inaccurately. The value of E_0 can be obtained in a more meaningful fashion by measurements in thin samples. In this case the position of the resonance is determined with an accuracy equivalent to the width of one channel ΔE. The error in the difference of the cross section $\Delta\sigma$, due to the error in E_0 is $2(\partial\sigma/\partial E_0)\ \Delta E$. The value of $\partial\sigma/\partial E_0$ can be calculated from the Breit-Wigner formula (1). We shall neglect the first term in (1) as compared with the second (the first term yields a correction which is smaller than the error). In this case we have:

Substituting everywhere, for example, the level parameters for U^{238} at 37 ev and taking $(E - E_0)_{min} = 9\Delta E$, we find $\Delta\sigma = 1$ barn. Thus, the maximum error due to the inaccurate determination of E_0 is no greater than ten percent and as $E - E_0$ increases the error diminishes as $1/E^2$. For average values of $E - E_0$ the error does not exceed 1-2 percent.

To determine the energy above which the weak levels may have an effect, the distribution of resonances was plotted graphically (Fig. 6). The energy is plotted along the abscissa axis and the number of levels with $E_0 < E$ is plotted along the ordinate axis. In the energy region in which it may be reasonably assumed that all the levels are observed, a calculation was made of the mean distance between levels $\bar{D}$ and the ratio $\bar{\Gamma}_n^0/\bar{D}$, where Γ_n^0 is the mean neutron width normalized to 1 ev.

TABLE 2

Resonance Parameters in Osmium

№	E_0	$1/n$	A	Γ_γ	$wg\Gamma_n$	$wg\Gamma_n^0$	$w\sigma_0\Gamma^2$
1	6.73±0.08	102	0.421±0.009	—	0.197±0,025	0.07±0.01	5.8±0.2
2	8.95±0.11	102	0.703±0.01	—	0.745±0,09	0,25±0.03	16±0.45
3	10.3±0.15	102	0.489±0.007		0.31±0,04	0.1±0.012	7.8±0.2
				86±14			
		716	0.143±0.007				
4	12.6±0.2	102	0.237±0.02		0,11±0.02	0,03±0.006	
5	18.8±0.3	102	0.464±0.015	44±10	0.70±0.07	0.17±0.017	7±0.4
		716	0.163±0.012				
6	22±0.4	102	0.753±0.019	62±14	1.86±0.22	0.4±0.05	18.5±0.9
		716	0.300±0,016				
7	27.9±0.6	102	0.889±0.04	—	3.17±0.55	0.6±0.1	25.6±2
8	38.8±1	102	1.34±0.039	Γ_{total} =102±18			
					7.0±1	1.1±0.16	59±4
		716	0.542±0.03				
9	41.2±1	102	0.344±0.033		0.55±0.08	0.09±0.01	
10	44.3±1	102	0.96±0.07		4.8±1.2	0.73±0.18	30±6
11	50.6±1.4	102	1.07±0.06		7.1±1.6	1.0±0.23	37±4
12	55.8±1.8	102	0.941±0.08		5.4±1.5	0.72±0.2	29±5
13	63.1±2	102	1.8±0.08		22±5	2.8±0.6	105±10
14	66.4±2	102	0.77±0.07		3.9±0.9	0.47±0.11	19±4
15	78.2±3	102	6.18±0.1	Γ_{total} =615±224	62±20	7.0±2.3	1240±42
		716	2.3±0.09				
16	89.9±4	102	2.61±0.12	Γ_{total} =167±90	42±17	4.5±1.8	220±20
		716	1.09±0.12				

In the curves showing the distribution of neutron widths (Figs. 7-11), the values of the neutron widths are plotted along the abscissa axis while the number of levels having $g\Gamma_n^0$ greater than the corresponding abscissa are plotted along the ordinate axis. The values of Γ, Γ_γ, Γ_n, and Γ_n^0 given in all tables are in millielectron volts, and σ_0 is in barns.

The area above the resonance transmission curve A is given in electron volts and the reciprocal of the sample thickness $1/n$ is in barns/atom.

Only the statistical errors are shown in the tables.

TABLE 3

Resonance Parameters in Iridium

№	E_0	$1/n$	A	Γ_γ	$wg\Gamma_n$	$wg\Gamma_n^0$	$w\sigma_0\Gamma^2$
1	5,36±0,02	202	0,856±0,007	31±14	3,4±1,3	1,5±0,6	47±1
		1100	0,399±0,006				
2	6,125±0,02	202	0,241±0,005	44±6,9	0,15±0,011	0,06±0,004	—
		1100	0,076±0,004				
3	9,05±0,04	202	0,731±0,02	57,5±8,6	1,84±0,25	0,6±0,08	32±1
		1100	0,335±0,007				
4	9,89±0,05	202	0,187±0,008	—	0,138±0,01	0,04±0,003	—
5	10,4±0,05	202	0,081±0,008	—	0,049±0,0054	0,015±0,0017	—
6	10,8±0,05	73,9	0,046±0,006	—	—	—	$w\sigma_0\Gamma=2,16\pm0,28$
7	11,22±0,06	202	0,016±0,007	—	—	—	$w\sigma_0\Gamma=2,05\pm0,9$
8	18,7±0,12	73,9	0,560±0,018	—	0,805±0,16	0,185±0,03	—
9	19,65±0,12	73,9	0,490±0,013	—	0,608±0,1	0,136±0,02	—
10	24,25±0,20	73,9	2,964±0,038	—	23,8±4,8	4,9±1,0	200±5
11	29,2±0,25	73,9	1,278±0,027	—	6,83±1,4	1,27±0,26	39±1,6
12	30,6±0,26	73,9	0,765±0,037	—	2,37±0,5	0,43±0,1	—
13	35,2±0,26	73,9	0,5±0,04	—	0,875±0,18	0,15±0,03	—
14	39,7±0,36	73,9	0,890±0,18	—	3,87±2,1	0,61±0,33	—
15	41,7±0,40	73,9	3,45±0,17	—	36,8±9	5,6±1,4	280±28
16	50,8±0,50	73,9	4,07±0,1	—	52±17	7,4±2,4	390±20
17	61,2±0,70	73,9	1,96±0,08	—	21,7±4	2,8±0,5	90±7
18	66,3±0,80	73,9	3,54±0,09	—	51±11	6,4±1,2	300±17
19	75,6±1,00	73,9	4,325±0,12	—	69±17	8,0±2,0	430±25
20	93,5±1,40	73,9	7,32±0,6	—	141±38	14,5±4	1250±200

RESULTS

Palladium (Table 1). Two samples of palladium having a thickness $n = 19.7 \cdot 10^{21}$ and $1.28 \cdot 10^{21}$ atom/cm^2 were investigated* [8]. The resolving power in these measurements was 0.18 μsec/m. The levels at 13, 25 and 32 ev were analyzed by the "two-sample area" method. The radiation width obtained from analyzing the resonance at 13 and 32 ev, which was (220 ± 63) mv, was used later in calculating the other levels.

Because natural palladium contains a large number of isotopes, it was possible to determine only the values $wg\Gamma_n$, $w\sigma_0\Gamma$, or $w\sigma_0\Gamma^2$ where w is the unknown relative weight of the isotope to which the given level pertains.

Resonances at 13, 26 and 34 ev have been observed earlier [9]. At present there is no other data on Pd. It is apparent from Fig. 6,A that, starting at approximately 100 ev, a number of levels have been omitted.

A mass spectrometer analysis indicated that the sample had a natural isotopic constituency. No admixture of the rare earths Ka, Na, Pb, and Pt was found.

Osmium (Table 2). An osmium sample with a thickness $n = 9.74 \cdot 10^{21}$ cm^{-2} was investigated with a resolving power of 0.3 μsec/m in the energy region 4.5-10,000 ev. A thin sample with $n = 1.4 \cdot 10^{21}$ cm^{-2} was studied with a resolving power of 0.16 μsec/m from 10 to 10,000 ev.

*In the following the word atom will be omitted in designating the thickness of the sample.

The radiative width Γ_γ was determined for the levels at 10.3 18.8 and 22 ev. The average width for these levels was 67 mv. This value was used in calculating the other levels.

In Table 2 are shown the data for all resonances which were investigated. Levels were also observed at 109, 125, 144, 166 (weak), 208 and 333 ev.

The location of the levels at 6.7, 8.8, 22, 28, and 41 ev is in agreement with the data of Ref. [10]. The value of $\sigma_0\Gamma^2$ given in this reference was determined only to within an order of magnitude and naturally is in agreement with the present data.

Examination of the curve in Fig. 6, B indicates that all the levels above 75 ev were not found.

Analysis of the sample with a mass-spectrometer indicated the presence of only lead (approximately 15 percent) and barium (approximately 2 percent). Neither of these elements has a resonance in the energy region which was investigated. Consequently all the levels which were observed pertain to osmium.

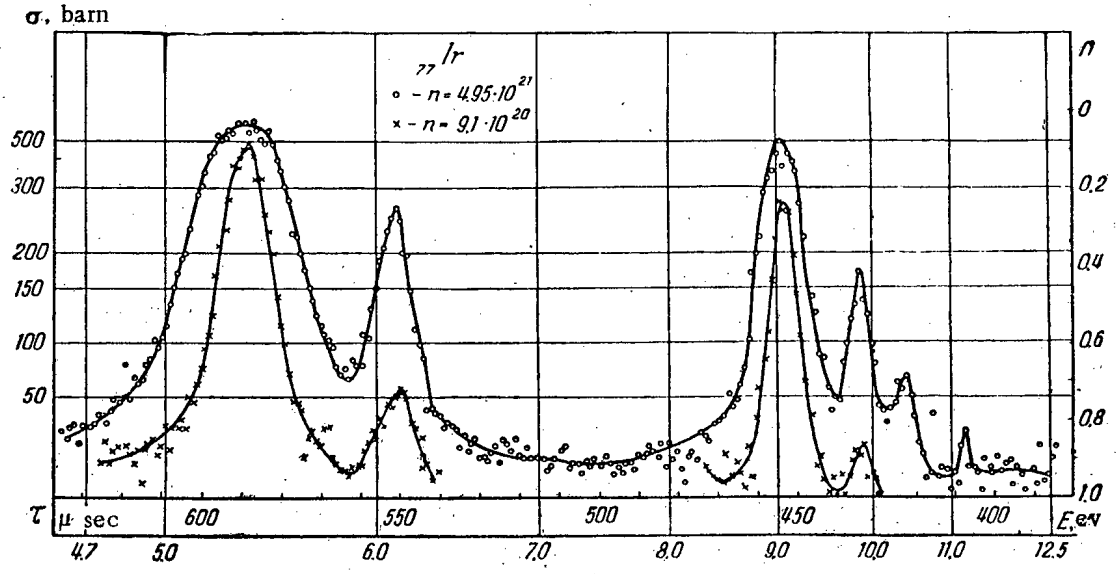

Fig. 1. Energy dependence of the total cross section in iridium. Curves for thick and thin samples are given in the figure. The measurements were performed with a resolution of ~ 0.09 μsec/m.

TABLE 4

Resonance Parameters in Molybdenum

№	E_0	A	Γ_n	Γ_n^0	$\sigma_0\Gamma^2$	Atomic wt. of isotope
1	45±0.5	3.94±0.08	188±30	28±4.5	2200±80	95
2	71.9±1	0.659±0.12	23.6±6	2.8±0.75	100±36	97
3	134±2.5	3.4±0.33	170±55	14.6±4.7	87±28	96

Iridium (Table 3, Fig. 1) Cross section measurements on iridium which were performed by us in the energy region from 2.5 to 10,000 ev indicate [8] that levels which had earlier been considered single [11] are, in fact, comprised of several levels. Many new resonances were found in the region above 10 ev. To carry out more detailed investigations of the level structures below 10 ev, several new measurements with thinner samples and improved resolution, 0.09 μsec/m, were carried out. These measurements indicate that the levels at 6 and 9 ev consist of several resonances with the energy values 5.36 and 6.12 ev for the first and 9.05, 9.89, 10.4, 11.22 for

the second. The radiative width Γ_γ was determined for the first three levels and no significant change was found in going from level to level (and possibly from isotope to isotope).

The existence of two resonances in the region around 6 ev was indicated in [12]. Aside from the measured values of $\sigma_0 \Gamma^2$ given in Ref. [11], at levels of 5.2 and 8.7 ev, the literature contained no data on the level constants. There is also no data on the location of levels above 20 ev. The levels at 0.65 and 1.35 ev which had been observed earlier by us were not considered since the sample was not sufficiently homogeneous.

To determine the ratio $\frac{\overline{\Gamma}_n^0}{\overline{D}}$ use can be made of the expression given in Ref. [13] for a two-isotope element:

$$\frac{\overline{\Gamma}_n^0}{\overline{D}} = \frac{\sum_{i=1}^{m} wg\Gamma_{n_i}^0}{\Delta E},$$

where ΔE is the energy interval in which m levels are found.

Proceeding in this fashion

$$\frac{\overline{\Gamma}_n^0}{\overline{D}} = (0.57 \pm 0.14) \cdot 10^{-4}$$

where the average distance between levels $\overline{D}$ = 10 ev is one isotope and one spin state.

Molybdenum (Table 4). A thick sample of molybdenum of natural isotopic constituency in the form of a metal slab of thickness $n = 1.39 \cdot 10^{22}$ cm^{-2} was investigated in the region from 30 to 1,000 ev, with a resolution of 0.08 μsec/m.

Resonances were observed at 45, 72, 134, 162, 189, 283, 350, 400, 483, 715 and 842 ev. The values of Γ_n and $\sigma_0 \Gamma^2$ were determined in the first three levels and are presented in Table 4.

These data were computed with the use of a value of $\Gamma_\gamma = (260 \pm 80)$ mv, taken from Ref. [14]. The levels were identified from the data in Ref. [14]. In the isotopes Mo^{95} and Mo^{97} the statistical factor was taken as g = 1/2 since the nuclear spin is 5/2, and in the isotope Mo^{96}, g = 1 since the spin is 0. The levels above 134 ev were not computed because of the large statistical errors.

Indium (Table 5). As has already been reported [8], we have investigated the behavior of the cross section in indium in the region from 4.5 to 10,000 ev. In addition to the resonances at 9, 12, 15, and 23 ev, known earlier, a new series of resonances was found; the data is presented in Table 5. Inasmuch as the measurements were made in only one sample of thickness $n = 9.87 \cdot 10^{21}$ cm^{-2}, it is possible, making use of the value $\Gamma_\gamma = (80 \pm 20)$ mv taken from [14], to determine the neutron width Γ_n. Measurements with a mass-spectrometer indicated that the sample being used was of normal isotopic constituency. The identification of the levels was based on recently published work [14].

The present data on the levels in In^{115} are in good agreement with the results obtained [14]. Somewhat poorer agreement was observed in In^{113}. This is explained by the fact that the measurements were made only in a sample of natural indium, in which, as is well known, the 113 isotope is present in a concentration of 4.5 percent. Thus, a number of weak levels could not be found. This situation can be seen in the curve shown in Fig. 6, D. The average distance between levels $\overline{D}_{115}$ = 13 ev if the levels at 1.46 and 3.86 ev are included and the ratio $\overline{\Gamma}_n^0/\overline{D}$ in In^{115} is $(0.26 \pm 0.075) \cdot 10^{-4}$.

In In^{113} it is possible to determine both $\overline{D}$ and $\overline{\Gamma}_n^0/\overline{D}$ averaged over a small interval since a number of weak levels were omitted. In the energy region 14.7-32.3 ev $\overline{D}_{113}$ = 9 ev. For this same level one finds $\overline{\Gamma}_n^0/\overline{D} = (1.82 \pm 0.4) \cdot 10^{-4}$. If account is taken of the levels at 4.71 ev studied by the authors [14] we obtain $\overline{D}_{113}$ = 13 ev and $\overline{\Gamma}_n^0/\overline{D} = (1.0 \pm 0.4) \cdot 10^{-4}$.

In both isotopic species in indium the nuclear spin is 9/2, hence we may take g = 1/2.

TABLE 5

Resonance Parameters in Indium

In^{113}				
№	E_0	A	Γn	Γ_n^0
1	14,67±0.23	0,31±0.017	7,5±0,77	1,95±0.2
2	19.7±0.3	0,074±0.03	—	—
3	21.4±0.4	0,0968±0.019	2,5±0,55	0.54±0.12
4	25.0±0.5	0.270±0.03	9,95±1.5	2,0±0,3
5	32,3±0.7	0.239±0,038	10.2±2.2	1,8±0.4
6	70,0±2.4	0.304±0.095	28.8±10	3,45±1,2

In^{115}					
№	E_0	A	Γn	Γ_n^0	$\sigma_0\Gamma^2$
1	9,00±0.11	0,812±0,009	1,74±0.43	0,58±0.14	22±0.4
2	12.0±0.16	0.152±0,012	0.116±0.01	0.034±0.003	—
3	22.8±0.43	0.526±0,023	1.35±0.19	0.28±0.04	9,8±0,9
4	39.8±1.0	0,75±0.053	4.1±0.79	0.65±0.12	19±2.7
5	47.9±1.3	0.30±0.07	0.975±0.3	0.14±0.04	Two unresolved levels
6	63±2	0,126	—	—	Levels for both isotopes
7	84.2±3	1.015±0.14	13.2±4.5	1.45±0.49	
8	95±4	0.42±0.13	2,22±0,93	0.23±0.095	
9	129±6	0,34±0.28			

TABLE 6

Resonance Parameters in Iodine

№	E_0	A	Γn	Γ_n^0	$\sigma_0\Gamma^2$
1	20,5±0,4	0,720±0,08	1.08±0.24	0.24±0,05	9±2
2	31,4±0.6	2,02±0,21	15±3	2.7±0.54	70±15
3	38,1±0,9	3,0±0.3	36±7	5.8±1.1	155±30
4	46.0±1,2	2.13±0.27	21±6	3.1±0,9	78±20
5	66±2	1.25±0.26	14,5±6.5	1,8±0.8	27±12
6	79,3±3	2,38±0.5	37±16	4,15±1.7	97±40
7	92±4	1,7±0.4	21±11	2.2±1.1	50±25

Iodine-127 (Table 6). The sample was taken in the form of chemically pure iodine with the thickness $n = 18.55 \cdot 10^{21}$ cm^{-2}. The measurements were performed with a resolving power 0.29 μsec/m. The behavior of the cross section and the value of $\sigma_0\Gamma^2$ have been published earlier [8]. In the present work we present the values of Γ_n. In making the calculations it was assumed that $\Gamma_\gamma = 0.1$ ev. The level constants as determined in the present case are in good agreement with the results of [15]. Because of the superior resolution the accuracy of

the measurements of the levels is considerably better than that in the work mentioned. The average distance between levels is $\overline{D}$ = 17 ev in each spin state and the ratio

$$\frac{\overline{\Gamma_n^0}}{\overline{D}} = (1.92 \pm 0.6) \cdot 10^{-4}.$$

Since the spin of the iodine nucleus is 5/2, g is taken as 1/2.

TABLE 7

Resonance Parameters in Tantalum

№	E_0	1/n	A	Γ_γ	Γ_n	Γ_n^0	σ_0	$\sigma_0\Gamma^2$
1	10.2±0.1	100	0.924±0.14	54±10	3.6±0.6	1.15±0.19	12000±4000	27±1
		720	0.385±0.008					
2	13.6±0.14	100	0.417±0.017	36±8	0.944±0.11	0.256±0.03	2400±800	5.5±0.4
		720	0.147±0.011					
3	18.6±0.22	100	0.626±0.018	85±20	0.8±0.1	0.18±0.02	1100±400	
		720	0.187±0.015					
		100	0.451±0.02					
4	20.1±0.23				1.19±0.2	0.26±0.045	1500±700	6.5±0.6
		720	0.137±0.014					
5	22.3±0.3	100	0.181±0.016		0.26±0.035	0.055±0.007	300±40	
6	23.7±0.35	100	0.807±0.020					
				21±8	9±2	1.8±0.4	16000±7000	20±1
		720	0.405±0.019					
7	29.9±0.5	100	0.192±0.036		0.364±0.08	0.066±0.015		
8	35±0.6	100	2.39±0.04		60±11	10±1.9		180±6
		720	1.07±0.03		56±14	9.5±2.4		
	35±0.3	359	1.33±0.03		54±11	9.1±1.9		
9	38.9±0.7	100	2.08±0.4		46±11	7.4±1.8		137±5
		720	0.945±0.03		53±10	8.5±1.6		
	38.7±0.4	359	1.052±0.03		43±10	6.9±1.6		
10	48.5±10.5	359	0.183±0.037		4.1±1	0.6±0.14		
11	51±0.5	359	0.200±0.04		5±1	0.7±0.14		
12	57.4±0.6	359	0.122±0.04		1.6±0.8	0.21±0.10		
13	63.1±1.5	100	0.647±0.11		5.5±2.6	0.71±0.33		
14	76.9±1	359	0.765±0.139		15.2±7.8	17±0.9		
15	83±2.2	100	1.05±0.12		20±7	2.2±0.77		35±8
		720	0.51±0.137		24±13	2.1±0.4		
	83±1.1	359	0.464±0.129		13±6.3	1.43±0.69		
16	98.5±2.8	100	2.44±0.156		99±25	9.9±2.5		190±25
	98.8±1.4	359	1.85±0.152		136±46	13.6±4.6		
17	105±1.5	359	1.27±0.146		82±31	8±3		51±11
18	114.9±1.7	359	1.445±0.223		98±40	9.1±3.7		67±20
19	126.5±2	359	1.215±0.241		81±46	7.2±4.1		47±19
20	135.5±2.3	359	0.97±0.236		57±37	4.9±3		30±15
21	173±3	359	1.25±0.352		98±65	7.4±5		50±28
22	197±4	359	1.13±0.455		88±75	6.3±5		40±32

Tantalum-181(Table 7, Fig. 2). Studies were made in samples of metallic tantalum with thickness $n = 10 \cdot 10^{21}$, $1.39 \cdot 10^{21}$ and $2.79 \cdot 10^{21}$ cm^{-2} [8].

The transmission measurement in the first two samples was performed with a resolution of 0.16 μsec/m while the transmission curve for the third sample was measured in the energy region 35-10,000 ev with a resolution of 0.08 μsec/m.

In the energy region from 10 to 24 ev the calculations of the parameters were performed using the "two-sample" method. The radiative width was determined for the first five levels. The average value, 50 mv, so determined was used in analyzing the other resonances. Since the spin of the tantalum nucleus is 7/2, g was taken as 1/2.

The first resonance levels have been investigated earlier with poorer resolving power [3, 16], and in these measurements the levels near 20, 22 and 24 ev as well as 35 and 39 ev, were virtually impossible to resolve. The location and parameters of the other levels which were found have been indicated [14]. There are only small discrepancies in the individual resonances. The level at 18.6 ev does not appear in the data [14]. It is difficult to attribute this to contamination. It was shown in both mass-spectroscopic and chemical analyses of the sample that there is only 5.7 percent contamination of which approximately one percent was sodium and one percent was potassium. Inasmuch as the dips in the transmission curve were found in two independent measurements in samples of different thickness [8] it is difficult to attribute the level to an instrumental error. The fact that the radiative width is similar to that of nearby resonances is a further indication that the indicated level pertains to tantalum. Although the resolution with which the cross section measurement was carried out was greater in our case than in the work indicated ([12] and Fig. 2) we did not observe the strong level shown in [14] at 36 ev.

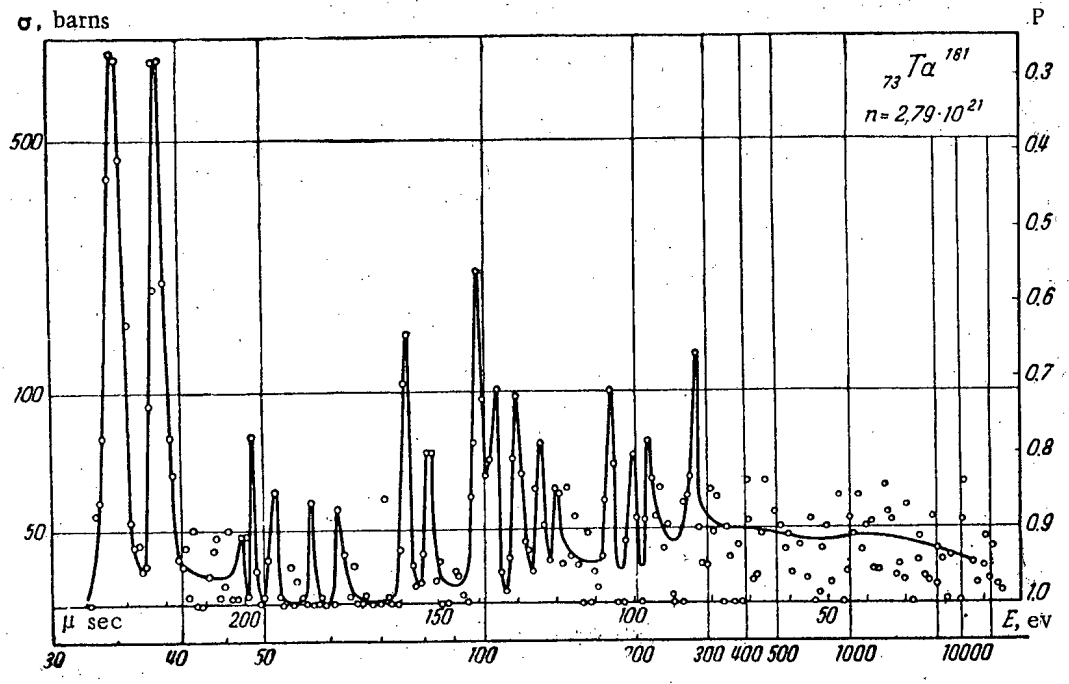

Fig. 2. Energy dependence of the total cross section in tantalum. Resolution ~ 0.08 μsec/m.

The locations of the remaining levels are shown in [14]. Above 126 ev we observe still another series of strong levels at 135, 173, 197, 211 and 279 ev. The parameters for the first three of these levels are given in Table 7. The resonances at 211 and 279 ev were not analyzed because of the large errors.

It is apparent from the curve in Fig. 6,G that the omissions start at 70 ev. The mean distance between levels determined in the energy region 10-63 ev $\overline{D} = 8.8$ ev and the ratio $\overline{\Gamma}_n^0/\overline{D} = (2.17 \pm 0.22) \cdot 10^{-4}$.

Thorium-232 (Tables 8, 9, and Fig. 3). The transmission curves were taken in three thorium samples under the following conditions: a sample of metallic thorium with $n = 3.7 \cdot 10^{22}$ cm^{-2}, at a resolution of 0.08 μsec/m in the energy region from 15 to 200 ev and from 35 to 10,000 ev; a sample of thorium oxide with $n = 2.4 \cdot 10^{21}$ cm^{-2} for the same conditions and thickness [17]; a sample of thorium oxide with $n = 6.85 \cdot 10^{21}$ with a resolution of 0.1 μsec/m in the energy region from 18 to 450 ev.

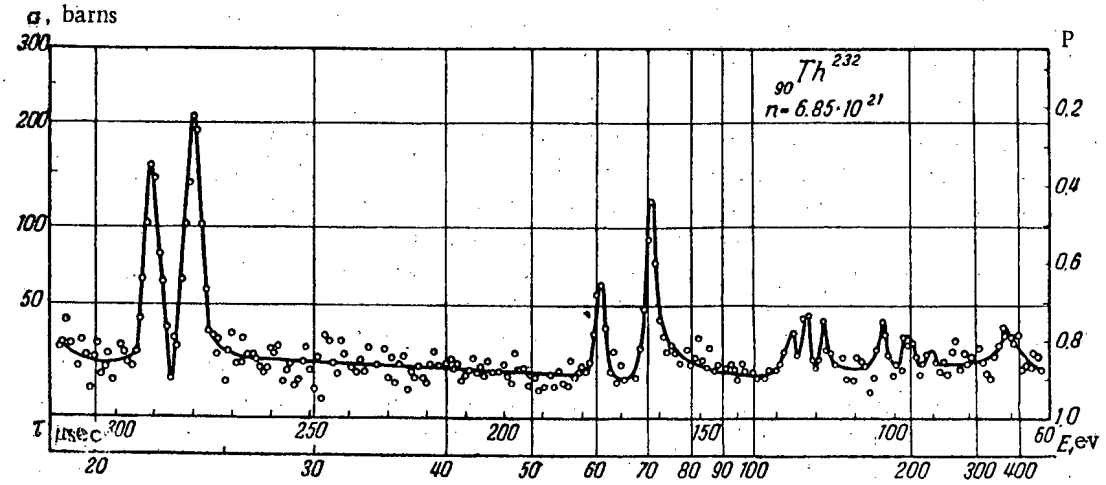

Fig. 3. Energy dependence of the total cross section in thorium. Resolution ~ 0.08 μsec/m.

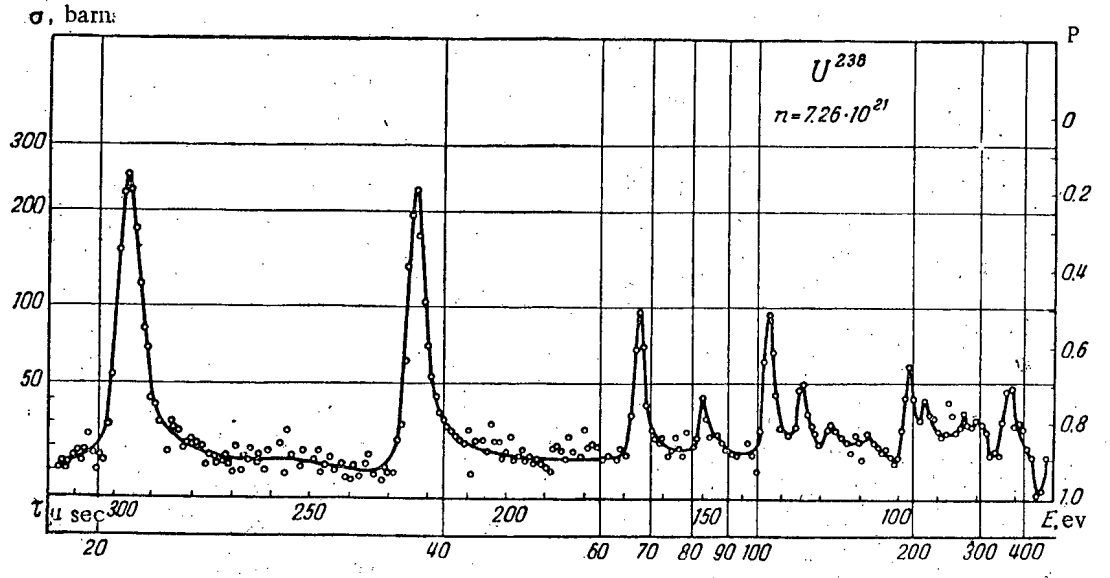

Fig. 4. Energy dependence of the total cross section in U^{238}. Resolution ~ 0.09 μsec/m.

TABLE 8

1/n	Resolution μsec/m	No. of investigated points	Γ_n
27	0.08	12	32 ± 3
27	0.08	12	36 ± 2

The levels in the region 20-130 ev have been observed earlier by other authors [15]. The levels found above 130 ev have been verified [12]. Since thorium is an even-even nucleus the spin is 0 and consequently, g = 1. The radiative width was determined only for the levels at 22 and 23.6 ev. In analyzing the following levels use was made of the value $\bar{\Gamma}_\gamma$ = 25 ± 10 mv.

The parameters for the first eight levels are in good agreement with the data [12] and [16]. The results for the other resonances are in considerably poorer agreement with the data of [12]. This is explained by the fact that in thorium there is a considerable "double" grouping of levels because of which it is difficult to distinguish between two close-lying resonances.

To determine the neutron width for the level at 70 ev by the interference effect, use was made of two separate measurements with thick samples (Table 8).

A comparison of the data presented in Tables 8 and 9 indicates extremely good agreement in spite of a certain distortion introduced by the weak level at 60 ev.

The mean distance between levels $\bar{D}$ was determined in the energy region from 22 to 295 ev and found to be 20 ev. The ratio $\bar{\Gamma}_n^0/\bar{D}$ was calculated from the data on the levels in the region from 22 to 135 ev and was $(1.06 \pm 0.3) \cdot 10^{-4}$.

TABLE 9

Resonance Parameters in Thorium

№	E_0	$1/n$	A	Γ_γ	Γ_n	Γ_n^0	$\sigma_0\Gamma^2$
1	22±0.15	146	0.443±0.014	27.5±11	1.24±0.36	0.27±0.08	4.5±0.3
		413	0.350±0.02				
2	23.6±0.16	27	1.133±0.019	25±8	3.35±0.77	0.7±0.16	12±0.5
		146	0.600±0.01				
		413	0.411±0.02				
3	60±0.7	413	0.46±0.05		6.8±1.9	0.87±0.25	
4	70.7±0.9	27	3.6±0.12		42±10	5.3±1.3	112±7
		146	1.56±0.06		44±13		114±9
		413	1.14±0.07		47±13		
5	115±2	413	0.615±0.1		15±5	1.4±0.5	50±16
6	125±2	27	2.1±0.1		25±10	2.2±0.9	38±4
7	135±2.3	27	1.5±0.12		15±6	1.3±0.5	19±3
8	175±3.4	27	1.52±0.25		35±12		20±6
		146	1.03±0.27		30±18	2.6±0.9	
		413	0.9±0.23		39±20		
9	195±4	27	1.8±0.36		22±7	1.57±0.5	28±11
10	210±4.5	27	0.69±0.2		1.8±1.4	0.12±0.1	4.1±2
11	225±5	27	1.43±0.3		16±9	1±0.6	17.6±7
12	235±5.4	27	1.34±0.30		14±8	0.9±0.5	15±7
13	260±6	27	0.99±0.33		4.5±3	0.28±0.19	8±5
14	270±6.5	27	2.98±0.4		60±12	3.7±0.75	76±20
15	295±7.5	27	1.36±0.34		12±7	0.7±0.4	16±8
16	350±9	27	6.72±1.34		205±50	11±2.8	390±150
		147	3.68±11		250±90	13±4.7	

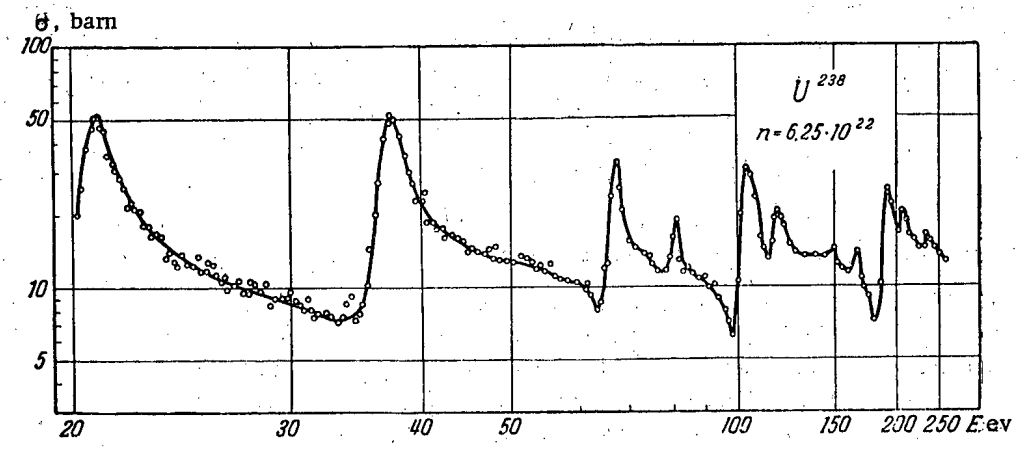

Fig. 5. Total cross section for a thick sample of U^{238}. The measurement was used to calculate the neutron widths from the interference effect.

TABLE 10

1/n	No. of meas.	Energy range, ev	Resolution μ sec/m	Characteristic form
16	3	33—10 000	0.08	Metallic uranium
		18.6—500	0.1	Metallic uranium
		5—110	0.16	Metallic uranium
137	1	18.6—500	0.1	Uranium oxide
429	2	33—10 000	0.08	" "
		5—110	0.16	" "
1880	2	18.6—500	0.1	" "
		4.5—13	0.1	" "
6350	1	4.5—13	0.1	Uranium oxide with lead monoxide
16 370	1	4.5—13	0.1	The same

Uranium-238 (Tables 10, 11, 12 and Figs. 4, 5). A rather detailed investigation of the level constants in uranium was carried out in 1955. The results of the measurements of the cross section were reported briefly [17].

Six uranium samples of different thickness were investigated under the experimental conditions shown in Table 10. A mass-spectrographic analysis indicated that the samples had natural isotopic constituencies. In calculating the resonance parameters the presence of U^{235} in the sample was taken into account.

These results verified some of our earlier data. In addition many new levels were found.

The radiative width, the average value of which is (30 ± 8) mv was determined for the first five levels and was then used in the calculations of the succeeding levels. Since the spin of the uranium nucleus is 0, g = 1.

In addition to determining the parameters by the "area" method, the interference effect between potential and resonance scattering was employed in calculating the neutron width. In the calculations it was assumed that σ_s = 9 barn. The data are presented in Table 12.

A comparison of our results on the radiative width with the results of [5] is given in Table 13.

The location of the resonances is in good agreement with the data [5] and [14]. We also found two weak levels at 135 and 142 ev which were not reported [5] and [14].

The present values of the neutron widths for the first two levels are somewhat smaller than those given in [5] and [14]. It may be noted that since the quantities Γ_n for the resonances at 6.7 and 21 ev were obtained not only from independent measurement but were also calculated from different effects, their relatively good agreement tends to corroborate the validity of the present results. The quantities Γ_n for the level at 120 ev differ by more than the limits of the error in all three reports. Above 300 ev weak levels may be overlooked and the observed strong resonances cannot reliably be assumed to be single. A comparison of the quantity $\sigma_0 \Gamma^2$ obtained in the present paper with the data [5], seems to indicate the consistency of our results at all levels aside from the resonance at 120 ev mentioned above.

The values computed for the radiative widths for the first four levels have been corroborated by the data of [5].

It is of interest to note the considerable reduction of the radiative width with increasing energy. The distance between levels determined by us was $\overline{D}$ = 17 ev for each spin state and the ratio $\overline{\Gamma}_n^0/\overline{D} = (1.5 \pm 0.18) \cdot 10^{-4}$.

CONCLUSIONS

A great deal of data has been accumulated as a result of these measurements (in the present work more than one hundred resonances were investigated) and several general conclusions may be indicated.

1. The radiative widths do not change, to any large extent, from level to level and from isotope to isotope (palladium, iridium, osmium). It was only in uranium and tantalum that the changes were outside the limits of experimental error. The variation in the radiative width in uranium cannot be ascribed to a dependence on spin since the initial nucleus is even-even and consequently has 0 spin. The monotonic reduction of the radiative width for the levels in uranium with increasing energy was also found [5].

TABLE 11

Resonance Parameters in U^{238}

№	E_0	$1/n$	A	Γ_γ	Γ_n	Γ_n^0	σ_0	$\sigma_0\Gamma^2$
1	6.69±0.025	429	0.324±0.005					13.6±0.4
		1880	0.173±0.003	21.15±1.3	1.15±0.04	0.445±0.015	20 000±1800	
		6350	0.087±0.003					
		16734	0.035±0.004					
2	21±0.14	16	2.455±0.4					39.6±5
		138	0.930±0.12	36±3.5	6.35±0.59	1.38±0.128	17 000±2500	
		429	0.585±0.05					
		1880	0.309±0.017					
3	37±0.4	16	4.0±0.15					100±7
		138	1.55±0.05	34±10	22±3.5	3.6±0.58	25 000±8000	
		429	0.896±0.03					
		429						
		1880	0.520±0.03					
4	67.7±0.8	16	2.52±0.11					
		138	1.08±0.08	25.5±12	19.1±4.5	2.3±0.5	14 000±10000	35±5
		1880	0.379±0.07					
5	83±1.1	16	0.93±0.13	21±15	2.7±11	0.3±0.12		—
		138	0.49±0.11					
6	89.5±1.2	16	0.22±0.12		0.09±0.08	0.01±0.008		
7	105±1.4	16	5.14±0.19		54±16			
		138	1.89±0.16		58±16	5±0.5		110±10
		1880	0.527±0.12		43±17			
8	120±2	16	3.88±0.25		40±8	3.7±0.19		76±10
		138	1.27±0.23		36±6			
9	135±2.3	16	0.8±0.23		1.4±1.4	—		
		138	0.38±0.19		2.4±1.9	0.2±0.16		
10	142±2.4	16	0.54±0.21		0.5±0.4	0.04±0.03		
		138	0.183±0.17		0.36±0.4	—		
11	146±2.5	16	1.2±0.23		4±3	0.33±0.26		
12	165±3	16	0.7±0.28		~0.96	0,07		
13	194±3.5	16	7.54±0.38		120±20			290±30
		138	2.53±0.37		118±50	7.4±0.7		
14	202±4	16	5.52±0.4		80±16			155±22
		138	1.75±0.4		69±45	5.3±0.5		
15	240±5	16	4.06±0.47		70±21	4.5±1.3		84±19
16	254±6	16	1.86±0.48		20±11	1,25±0.7		18±9
17	272±7	16	3.5±0.68		62±30			60±23
		138	1.38±0.56		48±36	3.3±0.4		
18	291±8	16	7.32±1.04		147±51			
		138	2.58±0.65		149±90	3.8±1		
19	355±10	16	6.2±1.2		140±90	7.5±4.7		196±77
20	405±12	16	10±1.27		260±80	13±4		510±130

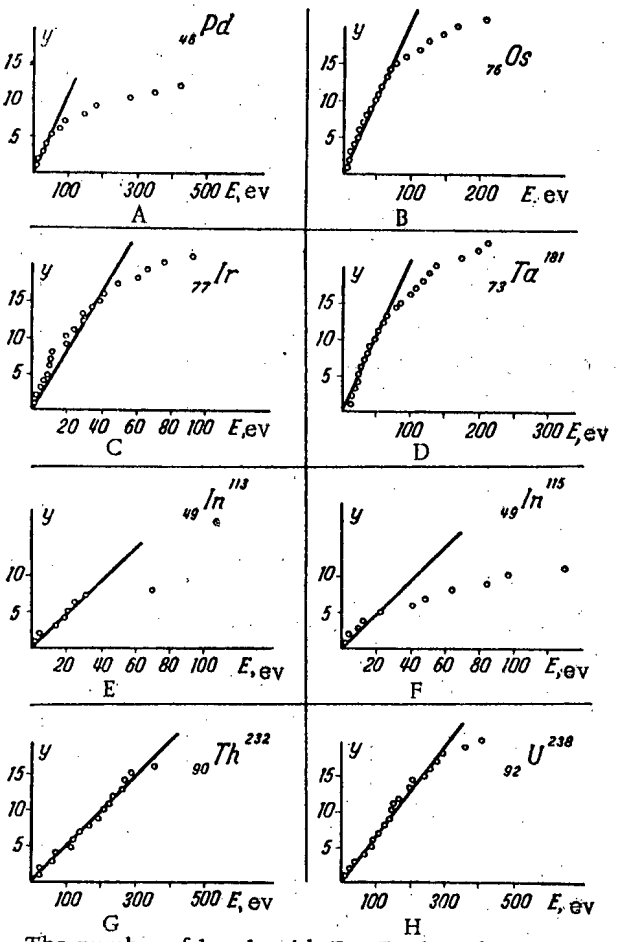

The number of levels with $E_0 < E$ plotted along "y" axis

Fig. 6. Number of levels as a function of energy.

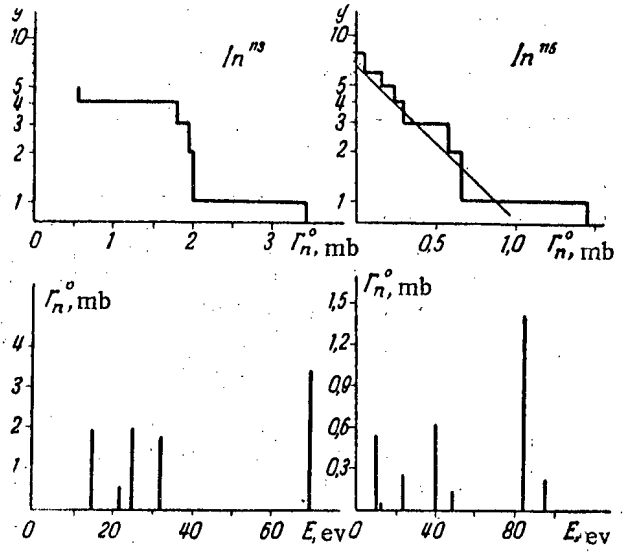

Fig. 7. Distribution of the neutron widths in In^{113} and In^{115}.

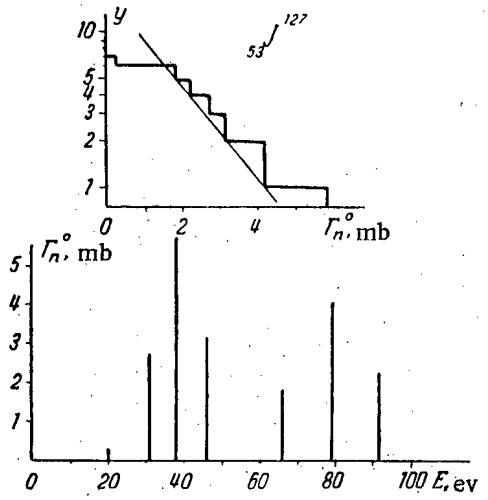

Fig. 8. Distribution of the neutron widths for iodine.

TABLE 12

E_0	1/n	No. of pairs of points	Γ_n	Average
6.7	16	17	1.08±0.15	1.08±0.15
21	16	11	7±0.6	7±0.6
37	16	15	28±2	
	16	16	27±5	27±1
	16	12	25.6±0.4	
67.7	16	7	23±2	
				21±1.5
	16	5	20±1.5	
105	16	3	50±5	50±5

TABLE 13

E_0	$\Gamma\gamma$		
	Our data	Table 6 in [5]	Table 7 in [5]
6.7	21.15±1.3	25±8	26.1±1.5
21	36±3.5	32±20	28.8±2.3
36.8	34±10	45±20	24.9±4.2
67	25±12	—	18.6±27
83	21±15	—	—
103	—	—	15.5±5.4
117	—	—	13.6±4.8

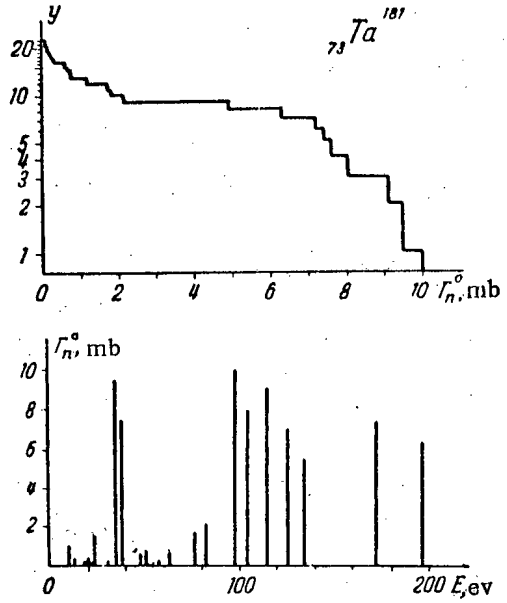

Fig. 9. Distribution of the neutron widths for tantalum.

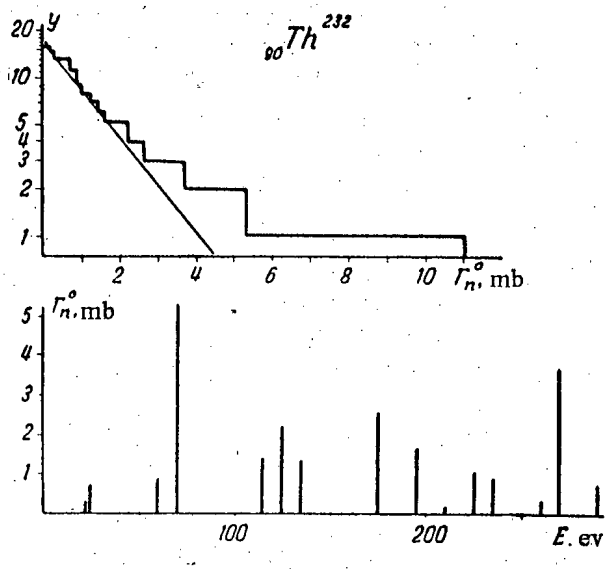

Fig. 10. Distribution of the neutron widths for thorium.

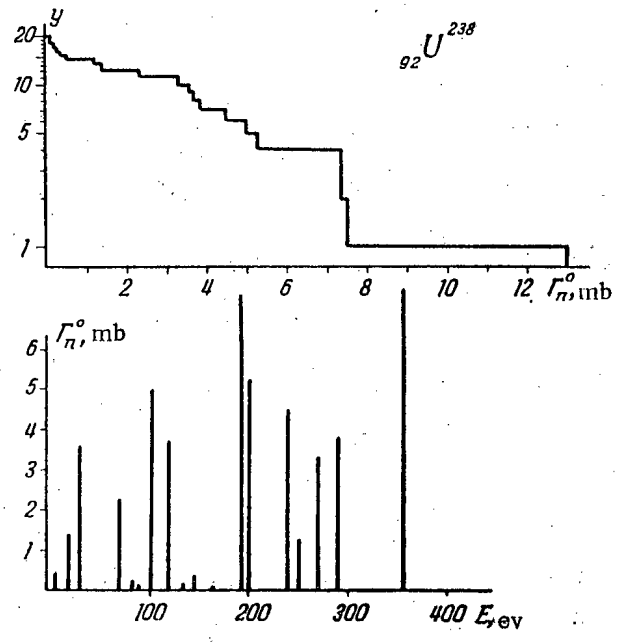

Fig. 11. Distribution of the neutron widths for U^{238}.

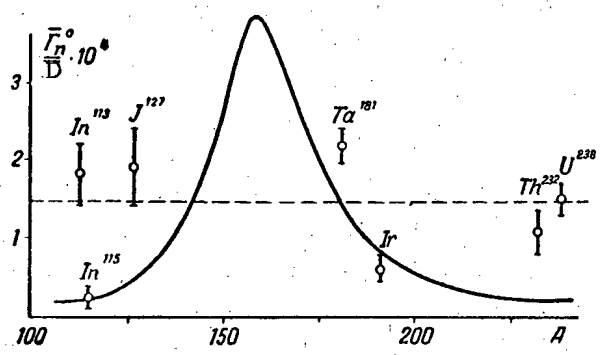

Fig. 12. The dependence of $\frac{\Gamma_n^0}{D}$ on atomic number. The dashes indicate the distribution which agrees with the statistical model for a well depth of 19 Mev. The solid curve corresponds to the "semi-transparent" model of the nucleus with the parameter ζ equal to 0.05.

In tantalum a notable reduction of the radiative width is noted from level to level; this effect reaches a factor of 1.5 even if one excludes the level at 18.6 ev which was not observed [14].

This small difference in widths may be completely explained by dependence of the radiative width on spin. However, the spins of the levels of the compound nucleus have not been measured at the present time.

The average values of the radiative widths for the elements which were investigated are in agreement with the theoretical dependence of Γ_γ on atomic number given in [18].

2. The neutron widths fluctuate over wide limits even in even-even nuclei (uranium, tantalum, thorium) and vary from level to level by a factor of 10^3. This was also noted in [14].

The neutron-width distribution cannot be described by an exponent as was proposed [14]. While it is true that the distribution is close to exponential for certain elements (thorium, iodine) for a number of materials the discrepancy is extremely large (tantalum, uranium).

3. The present measurements indicate that the quantity $\overline{\Gamma_n^0}/\overline{D}$ varies considerably from element to element. The variations of this quantity lie outside the limits given by the simple statistical model as well as the semi-transparent model of the nucleus.

The authors take this opportunity to express their gratitude to U. Chi-Kwa and Suan-Chi-Ling for their assistance in the mathematical analysis of the experimental results, G. M. Kukavadze for the mass-spectrographic analyses of the samples, V. N. Bovinoi and M. P. Anikinoi for providing the chemical analyses and A. I. Ermakov, N. S. Rezvyakov, G. V. Rukolaine and K. A. Trostinoi for help in building the analyzer and in carrying out the measurements.

Received May 4, 1956

LITERATURE CITED

[1] I. A. Radkevich, V. V. Vladimirsky and V. V. Sokolovsky, Experimental Apparatus and Techniques (in press).

[2] V. V. Sokolovsky, V. V. Vladimirsky, and I. A. Radkevich, Experimental Apparatus and Techniques (in press).

[3] E. Melkonian, W. W. Havens, and L. J. Rainwater, Phys. Rev. 92, 702 (1953).

[4] D. J. Hughes, J. Nucl. Energy 1, 237 (1955).

[5] J. E. Lynn, and N. J. Pattenden, "Slow neutron cross sections of the uranium isotopes", Report No. 423, presented by British Delegation to the International Conference on Peaceful Uses of Atomic Energy, 1955.

[6] W. J. Sturm, Phys. Rev. 71, 757 (1947).

[7] J. Levin, and D. Hughes, Phys. Rev. 101, 1328 (1956).

[8] V. V. Vladimirsky, I. A. Radkevich, and V. V. Sokolovsky, "Physical research", Report of the Soviet Delegation to the International Conference on Peaceful Uses of Atomic Energy (Acad. Sci. USSR Press, Moscow, 1955), p. 26.

[9] H. H. Landon, and V. L. Sailor, Phys. Rev. 86, 605 (1952).

[10] C. S. Wu, L. J. Rainwater, and W. W. Havens, Phys. Rev. 71, 174 (1947).

[11] L. J. Rainwater, W. W. Havens, C. S. Wu, and J. R. Dunning, Phys. Rev. 71, 65 (1947).

[12] D. J. Hughes, J. A. Harvey, Neutron Cross Sections (McGraw-Hill, 1955).

[13] R. S. Carter, J. A. Harvey, D. J. Hughes, and V. E. Pilcher, Phys. Rev. 96, 113 (1954).

[14] J. A. Harvey, D. J. Hughes, R. S. Carter, and V. E. Pilcher, Phys. Rev. 99, 10 (1955).

[15] F. G. P. Seidl, D. J. Hughes, H. Palevsky, J. S. Levin, W. J. Kato, and N. G. Sjöstrand, Phys. Rev. 95, 476 (1954).

[16] R. Christensen, Phys. Rev. 92, 1509 (1953).

[17] V. V. Vladimirsky, Report, Stenographic transcription of the Conference. (Geneva, 1955).

[18] J. Heidmann, and H. A. Bethe, Phys. Rev. 84, 274 (1951).

NUCLEAR FISSION*

J. A. Wheeler

(Lorentz Institute, University of Leiden, Holland)

Nuclear fission is reviewed. The value of a channel analysis is noted in determining fission cross sections, fluctuations in fission widths and fission asymmetry. The importance of barrier height in any fission mode is emphasized. The difficulty of obtaining the mass distribution of fission fragments by a statistical theory is noted; this situation arises because the result is a strong function of the deformation factors of the fragments.

The physics of nuclear fission has seen an extremely rapid development in the recent past. The developments have been numerous and have encompassed a number of fields so that it is difficult to summarize them in this short report. However, two subjects are of paramount importance: fission widths and fission asymmetry. These two subjects have been the source of many new ideas and developments.

Research in nuclear fission is attended by one fortunate circumstance. In contrast with inelastic scattering of protons, for example, where the important question is whether the proton is scattered by the nuclear potential or whether a complex system is formed, in the fission case, we have a clear-cut example of the formation of a complex system. We are confident of this at least as a consequence of the large value of the characteristic time for collective oscillations ($\sim 5 \cdot 10^{-21}$ sec) as compared with the time required for a nucleon to traverse a distance of the order of nuclear dimensions ($\sim 0.3 \cdot 10^{-21}$ sec). It is also obvious that in considering fission we are dealing with a collective type of motion which is as far removed from a single-particle effect as is possible in nuclear physics.

It is hardly necessary to mention that the compound nucleus which is usually considered in fission may be produced in the bombardment of the nucleus by particles, the absorption of electromagnetic radiation or the absorption of a negatively charged meson; indeed, it may even be found in the ground state, as in the case of spontaneous fission. In the compound system there is a competition between the various decay modes of the compound nucleus: the emission of particles, γ-radiation and fission. The energy relations for these three processes are shown in Fig. 1.

The emission of γ-rays may occur either directly with a transition to the ground state of the compound nucleus and the emission of a γ-ray, γ_1, or to any of the excited states with the emission of γ-rays $\gamma_2, \ldots, \gamma_n$. The probability for a transition with the emission of a γ-ray to a given lower level fluctuates from level to level in the compound nucleus even for close-lying levels with the same spin and parity (Fig. 2). However, the total probability of a transition with the emission of γ-rays, taking into account transitions to all lower levels, is almost entirely free from these fluctuations and is usually of the order of magnitude $\Gamma_\gamma/\hbar \sim 0.040$ ev$/\hbar$ = $= 0.040$ ev$/0.6 \cdot 10^{-15}$ ev$\cdot$sec $= 0.7 \cdot 10^{14}$/sec for excitation by slow neutrons, which is the usual case.

---

* Expanded version of a report to the International Conference on Nuclear Reactions at Amsterdam, July, 1956.

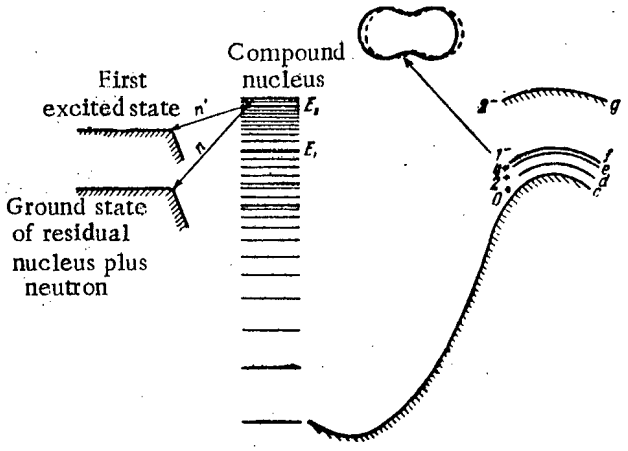

Fig. 1. Comparison of the energy levels for the compound nucleus (center) with the barriers for neutron emission (left) and fission (right). If the compound nucleus is in a state with energy E_1, emission of neutrons is possible only with a transition to the ground state of the compound nucleus a. If the compound nucleus is excited to a higher degree, say to the state E_2, then two channels become available for neutron emission, leaving the residual nucleus either in the ground state a or in the first excited state b. The probability for neutron emission varies with energy as shown in Fig. 2. The diagram presented here (Fig. 1) should be considered in connection with levels of a residual nucleus with specified spin and parity. For different spins and parities, the energy levels will be different for the compound nucleus but the same for the residual nucleus. The curve at the right showing the fission barrier as a function of the deformation parameter α refers to the case in which the compound nucleus is even-even and is in the state 0^+. The fission probability falls off smoothly if the excitation energy of the compound nucleus falls below the barrier height. It is 0.5 at the top of the barrier and approaches zero in the manner which is typical for barrier penetration where the energy falls considerably below the barrier height E_f. The curve of energy as a function of deformation, indicated on the diagram by c, corresponds to the ground state of the "intrinsic" or nucleonic motion of the system. Without changing this intrinsic state of motion, it is possible to excite collective rotation states for the system, corresponding to levels with angular momentum 2^+, or 4^+, or 6^+, etc. With a small additional expenditure of energy it is also possible to excite the lowest mode of the pear-shaped deformation (indicated in the upper part of the figure) which corresponds to the first vibrational state. In this case, the vibration wave function is antisymmetric with respect to rotation of the system through 180°. Consequently, the rotational state must also be antisymmetric and the system can only have the rotational states 1^-, 3^-, etc. The corresponding fission potential barriers, designated by the letters d, e, f actually should not appear on a diagram which is meant to show fission of a compound nucleus in a 0^+ state. However, the appropriate barrier (several tens of kev above 0^+) determines the fission rate in the case in which the compound nucleus is in one of the states of the 1^- type or in one of the states 2^+, 3^-, 4^+, etc. When, on the other hand, a residual nucleus is in an incompatible state, such as 2^-, fission through the lowest fission channel is not possible. However, a nucleus in a transition state can have some excited intrinsic state which is characterized by higher energy and a different angular momentum state. The letter g in the diagram indicates the fission barrier for an intrinsic excited state of the type 2^- (probably ~ 1 or 2 Mev above 0^+).

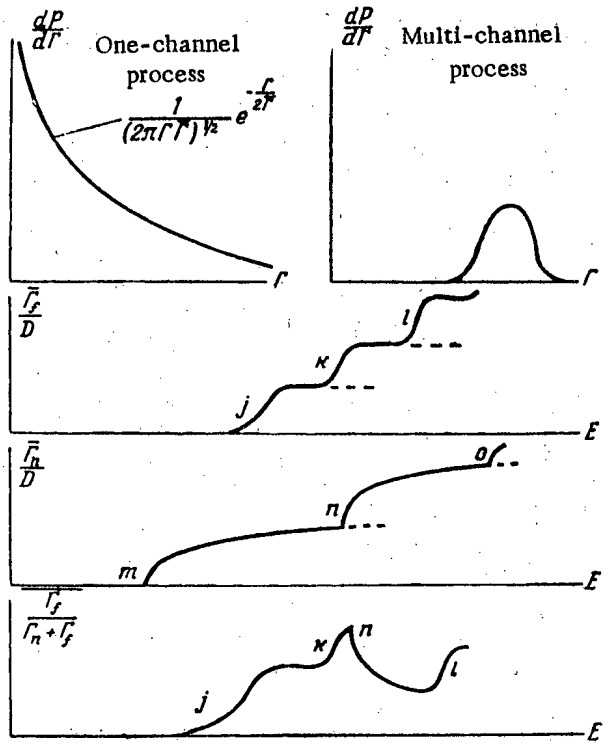

Fig. 2. Level widths, Γ. There are fluctuations in the widths from level to level even for levels with a given spin and parity, lying within a narrow energy interval ΔE. The fluctuation in level widths is greatest when the case being considered is a partial width for a single-channel process, for example, for a transition with the emission of γ-rays from the level being considered to one of the lower levels or for the emission of neutrons with a transition to a definite level of the residual nucleus, or for fission which takes place through a specified intrinsic state of the intermediate nucleus (Fig. 1). In all these single-channel processes the distribution of partial widths Γ about the mean value $\bar{\Gamma}$ have been considered by Porter and Thomas in accordance with the statistical law indicated in the upper left. The fluctuations of the partial widths are relatively smaller when the widths in question refer to a multi-channel process (Fig. 2, upper left). Hence, the partial width for γ-ray emission, averaged over transitions to all lower levels, is found to change only slightly in going from one slow-neutron resonance to another.

Nuclear theory cannot predict partial widths for any individual level for a given process. However, using statistical considerations it is frequently possible to predict the dependence of the average width on energy. For the ratio of the average fission width to the spacing between levels for a given parity and spin Bohr and Wheeler give the expression

$$\bar{\Gamma}_f/D=N/2\pi,$$

where N is the number of channels available.

Hill and Wheeler have shown that the value of this quantity does not increase by a unit when the energy E of the compound nucleus starts to exceed the barrier height E_f of a new fission channel but that this jump is given by the expression

$$N=\frac{1}{1+\exp 2\pi\ (E_f-E)/\hbar\omega}.$$

Here ω is a measure of barrier thickness (ω is the angular frequency which would be associated with the collective motion of the compound nucleus close to the transition point if the sign of the deformation potential were reversed). The quantity $\hbar\omega$ is probably considerably less than 1 Mev. This barrier penetration effect tends to join smoothly the steps in $\bar{\Gamma}_f$ and N which occur as the energy is increased. In contrast with this, the neutron widths have sharp breaks as each new channel becomes available (provided that the emission of s-neutrons is permitted by the conservation laws). In this case Γ_n increases as the first power of the velocity of the emitted neutron, as is indicated in the diagram. The emission of neutrons in p-states and in states with higher orbital momentum becomes significant only at energies well above the corresponding thresholds. The competition between fission and other energy dissipation modes in the compound nucleus is given by the ratio

$$\overline{\Gamma_f/(\Gamma_f+\Gamma_n+\Gamma_\gamma)}.$$

(Continued on following page)

(Fig. 2 caption, continued)

This ratio is plotted in the lower curve for an energy of the order of 1 Mev and higher. Here the radiation width is relatively small and has been neglected. The fission probability rises smoothly and quickly as each new fission channel becomes available but experiences a sudden drop when a neutron channel becomes available as is illustrated by the lowest curve in the diagram [see experimental curves for $\sigma(n, f)$ in Fig. 3].

When a neutron is emitted in an s-state and the residual nucleus remains in the ground state, the average width is of the order

$$\bar{\Gamma}_n = (E_n/1\text{ev})^{1/2} \cdot \overline{\Gamma_n^{(0)}} \sim 0.002\text{ev}\ (E_n/1\text{ev})^{1/2}.$$

Inasmuch as the emission of a slow neutron is a single-channel process, the individual neutron widths fluctuate strongly about this mean value. The measurements of individual widths (Geneva Conference, 1955) clearly indicate these fluctuations. Porter and Thomas found that, with reasonable accuracy, these widths follow a simple statistical law (Fig. 2, upper left). Below, in the same figure, is shown the expected dependence of $\bar{\Gamma}_n$ (or the ratio of $\bar{\Gamma}_n/D$) on energy, taking into account the new channels which become available in the cases in which the energy is sufficient to form a residual nucleus in one of the excited states.

It has been known for a long time that according to statistical analysis, the fission probability and the fission widths are given by the simple formula

$$\bar{\Gamma}_f/D = N/2\pi,$$

where N is the effective number of channels for fission which are available for a given excitation. Recently, an expression was obtained which took into account the effect of barrier penetration, which leads to a series of steps in N (E) which appear as new fission widths become available (Fig. 2).

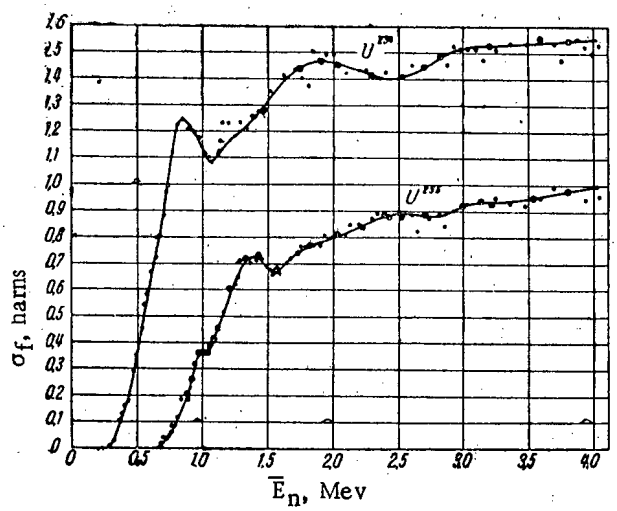

Fig. 3. Experimental results of Lamphere and Greene (Phys. Rev. 100, 763, 1955) for neutron-induced fission cross sections in U^{234} and U^{236} (see lowest curve in Fig. 2).

Until recently no one has considered seriously the "step" dependence on energy of the average neutron width and the fission widths as was predicted by simple statistical analysis, as indicated. However, measurements which have been carried out recently on fission cross section as a function of neutron energy in the region from several hundred kev to 3 Mev indicate a nonmonotonic behavior with a characteristic energy of the order of 50 to 200 kev, as is particularly well demonstrated by the measurements of Lamphere and Greene on U^{234} and U^{236} (Fig. 3). Several months ago A. Bohr presented a very reasonable explanation for the discontinuities which have been observed: the cross section is increased as each new fission channel becomes available and decreases as each new neutron channel becomes available (the lower curve in Fig. 2). In two cases there is a possible correlation between the energies for which there is a sharp drop in σ_f and the energy of a known excited level of the residual nucleus.

Now we have a substantial basis for considering the details of the fission picture shown in Figs. 1 and 2. Applying this analysis, it is possible to explain the angular distribution of neutrons and γ-rays in induced fission

and its dependence on energy, first considered by Bohr and Mottelson, and recently studied in detail by Chase and Wilets in interpreting the interesting observations of Henkel and Brolley (see the report by Wilets at this conference). A second application involves consideration of fission below threshold. It is usually assumed that Pu^{240} has a fission threshold at a neutron energy of several hundred kev. However, the formula for the barrier penetration effect (Fig. 2) indicates that there is no sharp fission threshold and that the average value of the fission width falls rapidly but smoothly, close to and below the peak of the fission barrier. The finite fission width at energies below the barrier is shown particularly well by the resonance at 1 ev in Pu^{240}. At exact resonance this level has a cross section of the order of 100,000 barns. Apparently, the absorption of neutrons at this level almost certainly leads to capture. However, Leonard has recently discovered a small resonance in the fission cross section at this same energy with a peak value of the order of 30 barns. Hence, the probability for fission is not negligibly small as compared with the probability for the emission of γ-rays. The observed width of the resonance, 30 mv, is almost completely due to the emission of γ-rays. Consequently, the fission width is of the order of: $\Gamma_f \sim 30$ mv (30 barns/100,000 barns) $\sim 10^{-5}$ ev.

The average spacing between levels in the compound nucleus Pu^{241} at the appropriate excitation is perhaps of the order of 50 ev, yielding a magnitude of the dimensionless ratio $N_{eff} = 2\pi\Gamma_f/D$ of the order of $10^{-6} = e^{-14} = e^{-2\pi \cdot 2}$. The statistical theory does not make any prediction as regards individual fission widths, but for the average value of a width considerably below the barrier, we have

$$N_{\text{eff}} = 2\pi\bar{\Gamma}_f/D = e^{-2\pi(E_f - E)/\hbar\omega}$$

for $(E_f - E)$ of the order of one, two or three hundred kev and $\hbar\omega$ of the order of 500 to 1,000 kev. If the exponential factor indicated is computed its value is found to be between $e^{-2\pi \cdot 0.1}$ and $e^{-2\pi \cdot 0.6}$. Consequently, it is to be expected that the characteristic fission widths in Pu^{240} will be considerably greater than the width of the individual level at which Leonard has found fission.

There are at least two ways of explaining this discrepancy: 1) the observed level is one of the class of levels with the expected mean width but accidentally (see the single-channel formula for width fluctuation, Fig. 2) has a width which is considerably smaller than the average width; 2) the observed level with an assumed assignment of $^1/_2{}^+$ belongs to a system of levels which are not connected with the lowest fission channels. The corresponding fission channel has an energy 1 or 2 Mev higher, hence the probability of barrier penetration is very small. A lower fission channel exists but it does not apply for a compound nucleus in the $^1/_2{}^+$ state. This lower channel may have, for example, a spin $^3/_2{}^-$. The collective motion of the nucleus is superimposed on this intrinsic state, resulting in a very small energy increase. Consequently, using this purely illustrative assumption, we have a group of close-lying fission barriers with energy several hundred kev above the neutron binding energy. Although these spin values are essentially inaccessible in bombardment by epithermal neutrons, they may be achieved in bombardment by neutrons with energies of several hundred kev. Thus, according to this picture, one would expect a rapid increase in the fission cross section at these energies, as is observed.

A third application of the analysis of fission by the decay-channel method is in the explanation of the fission of U^{235} by neutrons. Bohr and Mottelson have assigned a spin of $^7/_2{}^-$ to this nucleus on the basis of the curve plotted by Nilsson for the energy of individual particles as a function of deformation. In bombardment by slow neutrons the fissioning nucleus is found in one of the states 3^- or 4^-. The lowest fission channel of the even-even nucleus U^{236} has spin 0^+. At a somewhat higher energy the channels 2^+, 4^+, 1^-, 3^-, etc. are found. Of these channels, 3^- obviously should be close to or lower than the thermal energy because of the strong tendency for fission in U^{235}. On the other hand, when the compound nucleus is formed in the state 4^-, fission should occur via another channel, by virtue of an intrinsic state of the compound nucleus. This channel may be above the first-mentioned channel by 1 Mev or more. If the channel 4^- is sufficiently above thermal energy, the corresponding resonance for slow neutrons should have a highly reduced average fission width. However, a careful examination of the fifteen lowest resonances does not reveal any possible division of the fission widths according to two definite types of levels.

There are three possible explanations:

1) Levels of the 4^- class may be so rare at thermal energy, that, by chance, the first fifteen levels do not include such a state. A statistical analysis of the level density, carried out by Bloch, suggests that the density of levels with angular momentum 3 and 4 are comparable but this analysis does not cover the relative density of

levels of a more restricted type, for example, 3^- and 4^-. Thus, there is no convincing argument which excludes this reasonable explanation of the experiment (V. Sailor). In order to verify this explanation it will be necessary to determine the spins, either by a measurement of resonance scattering in polarized nuclei (V. Sailor) or, possibly, by a measurement of the difference between two types of levels according to the relative abundance of symmetric fission (see below).

2) The fission barriers for two different compound nuclei may differ by 1 Mev or more but both barriers, nevertheless, may be considerably below thermal energy. Thus, for each of the two nuclei the effective number of channels will be

$$N_{\text{eff}} = 2\pi\bar{\Gamma}_f/D = 1.$$

yet it is obvious that if the height above the barrier is higher in one case than in the other, this in no way presumes a difference in the average fission width for these two states. However, this explanation does encounter two difficulties: a) the observed mean value of the fission width, 0.75 ev, and the assumed average spacing between levels for one type of state $D = {}^1/_2 \cdot 1.3$ ev = 0.65 ev indicate an effective number of channels $N_{\text{eff}} = 2\pi \cdot 0.075/0.65 = 0.7$, which is somewhat less than one and contradicts the hypothesis; b) if the absolute value of the mean fission width is completely neglected and one considers instead only the relative fluctuations in the observed separation widths, in agreement with the arguments presented in the upper part of Fig. 2, then, following Porter and Thomas, we obtain for the effective number of channels a value of 2 or possibly more.

3) As a third attempt to explain these effects we will assume that the channel 3^- is below thermal energy by an amount which is somewhat less than 1 Mev. Then, for the state 3^-, produced by the capture of a slow neutron, the value of N will be close to unity; we assume, for example, that $N_3 = 0.9$. The barrier for 4^- will be connected with one or another of the excited intrinsic states of the compound nucleus. We will assume, once again only for an example, that there are three such intrinsic states, differing only slightly in energy, in which all three barriers, a, b, c, are slightly above thermal energy. Taking into account barrier penetration, one may assume for example that $N_{4a} = 0.4$, $N_{4b} = 0.3$, $N_{4c} = 0.2$. For simplicity we will neglect the energy differences between the three channels and write: $N_{4a} = N_{4b} = N_{4c} = 0.3$. Then the mean width of the 4^- channels will have the same value as the mean width for the 3^- channels,

$$\bar{\Gamma}_{f3} = \bar{\Gamma}_{f4} = N_{3\,(\text{or}\ 4)} \cdot D/2\pi,$$

which does not contradict the observed value $N_{\text{eff}} = 0.7$. To estimate the fluctuations in Γ_f we will assume that six of the observed levels are typical 3^- levels and nine are 4^- levels. Using the fluctuation function given by Porter and Thomas $F(\nu)$ [where $F(1) = -1.270$; $F(1.63) = -0.729$; $F(3) = -0.369$] for these characteristic width distributions, we have

$$\sum_{\substack{\text{six } 3^- \\ \text{levels}}} \ln \Gamma_3/\bar{\Gamma} = 6F(1) = -7.620,$$

$$\sum_{\substack{\text{nine } 4^- \\ \text{levels,}}} \ln \Gamma_4/\bar{\Gamma} = 9F(3) = -3.321,$$

whence:

$$\sum_{\text{all levels}} \ln \Gamma/\bar{\Gamma} = -10.941\ [= 15F(\nu_{\text{eff}}) = 15 \cdot (-0.729) = 15F(1{,}63)].$$

Thus, a purely illustrative analysis of the levels from the point of view of the phenomenological theory of Porter and Thomas leads to an "effective fluctuation channel number" $\nu_{eff} = 1.6$. This result is not in contradiction with the measurements. The well-known drop in the fission cross section in U^{235} in the region from 0 to 1 Mev may possibly be explained by this picture of the competition of a larger and larger number of channels for the emission of neutrons. Verification of this explanation will be forthcoming, obviously, after a determination of the spins (or fission asymmetry characteristics) of different levels.

As a fourth application of the analysis of fission by the channel method we consider the question of whether symmetric fission is possible for an even-even compound nucleus.

Let the excitation be rather small so that the important contribution to fission is due only to the lowest group of channels 0^+, 1^-, 2^+, 3^-, . . . with almost identical fission barriers. We will assume that the transition state of the nucleus is the 3^- state, formed 1) from the nucleon state 0^+, 2) from the state of collective motion corresponding to the first excited level of the pear-shaped type of vibration (Fig. 1 above), which is frequently designated by the deformation parameter α_3, and 3) from a third state due to the collective rotation. The wave function for the entire system is symmetric with respect to interchange of the two ends of the dumbbell shaped state of the nucleus so that the vibration and rotation wave functions are antisymmetric with respect to this interchange. This antisymmetry of the vibration wave function, recalling the well-known diagrams for the wave function of the first excited state of a harmonic oscillator, implies zero probability for a completely symmetric shape, $\alpha_3 = 0$. This situation would then lead one to expect in this state, zero or virtually zero, probability for symmetric fission. On the other hand, for the states 0^+, 2^+ . . . with a symmetric α_3 vibration wave function, the probability for symmetric fission may be small because of other circumstances but will not vanish by symmetry considerations. As a consequence one would expect a low relative abundance of products of symmetric fission products for the 3^- resonance in U^{235}.

Without additional information on the properties of the first intrinsic excited states of the compound nucleus it is impossible to make any simple prediction about symmetric fission from 4^- resonances of this same nucleus. If there is a sizable probability for symmetric fission from 4^- levels, then a simple means becomes available for distinguishing between the two kinds of levels. Present techniques (Auclair and Landon, Roeland and Rathenau, and Bollinger) are capable of detecting this difference if it exists.

A confirmation of certain channel features in asymmetric fission is found in the measurements by Duffield (reported at this same conference) on photofission in Th^{232}. For a description of the effects which have been observed we consider a highly simplified model, many features of which may possibly require subsequent modification in order to be brought into agreement with other properties of this nucleus.

We will assume that photo-absorption in the Th^{232} ground state in 0^+ occurs chiefly via the electric dipole component of the incident radiation, which leads to the excitation of the 1^- excited state, and secondarily by way of magnetic dipole absorption, which leads to the 1^+ excited state. We shall neglect quadrupole absorption and absorption by higher multi-poles for excitations in the range from 4 Mev to 10 Mev which pertains to these experiments. The 1^- channel will have essentially the same fission threshold as the 0^+ channel and corresponds to zero or almost zero probability for symmetric fission. The 1^+ channel will be associated with an intrinsic excited state the energy of which is greater by 1 or 2 Mev. We will assume that this channel leads to a small but appreciable percentage abundance of symmetric fission.

In considering competition between the fission process and the emission of neutrons, we assume that the residual nucleus, Th^{231}, in its ground state has a spin and parity such that in the 1^+ state of the compound nucleus neutron emission is easy above the neutron threshold $E_n = 6.3$ Mev, while it is difficult in the 1^- state. Thus, we would expect that normal asymmetric fission would increase approximately exponentially with the energy of the γ-rays. This increase will be noticeable in the vicinity of or at greater energies than E_n, partially as a consequence of the asymptotic approach of N_f to unity and partially as a result of the increasing probability for neutron emission from the 1^- state in the energy region 0.5 - 1 Mev above E_n.

We would expect that symmetric fission would have a very small probability, but would increase exponentially up to the energy E_n at which there will be a marked reduction as a consequence of the competition due to neutron emission; subsequently the exponential growth is repeated but at a much lower absolute level and over a region of 1 or 2 Mev up to the point at which it can no longer exceed the corresponding barrier, and Γ_f levels off. The ratio for the probabilities of symmetric and asymmetric fission derived from these considerations is found to be in qualitative agreement with the results reported by Duffield.

Turning now to another important topic of this report, namely, the mass distribution of fission fragments, it may be concluded from the existence of single-channel fission, that the old idea is valid that the mass distribution is determined not at the stage of penetration through the fission barrier, but considerably later, approximately at the moment of actual division. The only slightly deformed compound nucleus has no means of "foreseeing" the existence and energy distribution of the final fission products. In other words, the partial wave functions, which describe the outgoing fission products, should be understood as coherently connecting parts of a single wave function, which pertains to the single initial state of the compound nucleus, and a single channel in the intermediate state. In principle, it should be possible to delineate this connection by means of appropriate interference experiments. In practice, the number of outgoing partial waves is so large that such interference experiments become hopelessly complicated because of the great number of available excitation states for the fission fragments, even with the same mass.

Fong has related the number of possible states to the relative probability for a given type of fission. A calculation of the number of possible states at the moment of division is a more difficult problem. It requires a knowledge of 1) the shape of the two fragments at the moment of division and 2) the excitation energy available to the two fragments.

Fong used a model based on two deformed spheres which are in contact and has calculated the electric and surface energy of this configuration (see table) under the assumption that it is possible to neglect shell effects on the nuclear radii and nuclear deformations.

Estimate Given by Fong for Excitation Energy of Fragments at the Moment of Division in the Fission of U^{235} by Neutrons

Fission mode	Original nucleus – fission fragments mass difference ΔM, Mev	Energy of undeformed sphere in contact, Mev	Energy of deformation of fission fragments, Mev	Energy remaining for fragment excitation, Mev
Asymmetric	201	176	14	12
Symmetric	199	180	13	7

Additional excitation, which increases the probability for asymmetric fission, which is equal to 5 Mev.

This analysis predicts that the kinetic energy is greater for symmetric fission than for asymmetric fission, in contrast with ideas which have been presented but not completely verified (Brunton and Hanna, Stein). The energy balance is so complex that it is not really clear whether one may legitimately neglect shell effects in considering the energy in this case. Fong has paid considerable attention to shell effects in estimating ΔM (see table) and found that these removed any preference for symmetric fission which would be expected from a less sophisticated estimate of ΔM.

In Fong's instructive analysis it is implicitly assumed that the kinetic energy which corresponds to the fission degree of freedom and the energy of the internal excitation of the fragments contribute to the total energy in exactly the same degree. As Fong has shown, it follows that the kinetic energy is not 7-12 Mev as is indicated in the table, but is closer to $\frac{1}{2}$ (kT) ~ 0.5 Mev. In other words, the fragments divide more like a viscous drop than a drop of an ideal fluid.

The slow division associated with this "sticky fission model" leaves more than enough time for the development of various types of collective deformation of the fragments which are produced at the moment of fission. Consequently, one would expect a large variety of shapes at the moment of actual division, whereas the analysis given by Fong assumes a single shape. Along with this variety of shapes there would be a great variety of values of kinetic energy associated with the separation of the fragments, even for completely specified masses. On the other hand, the existence of a single shape in division would correspond to a relatively small spread in the kinetic energy. The experiments (Brunton and Hanna, Leachman, Cohen) indicate that the spread in kinetic energy is

approximately 11% of ~167 Mev. It may be concluded that the statistical theory for mass distribution in fission can give a consistent prediction only in those cases in which one allows a variety of shapes at division, and also multiple modes for the production of each shape.

At the present time attention is merited by the important regularities in fission barriers, spontaneous fission rates, and asymmetric fission noted recently by Swiatecki and the striking discovery made by Fairhall that bismuth exhibits a preference for symmetric fission.

The speaker wishes to express his gratitude to A. Bohr, D. Hughes, R. Leachman, A. Pappas, V. Sailor, W. Swiatecki and other colleagues for valuable discussions.

Received August 6, 1956.

INVESTIGATION OF FUSED SALT SYSTEMS BASED ON THORIUM FLUORIDE

V. S. Emelyanov and A. I. Evstyukhin

COMMUNICATION II*

Thermographic, x-ray, and other analytical methods have been used to plot phase diagrams for the system NaF – ThF_4 with four chemical compounds (Na_4ThF_8; α-Na_2ThF_6, β-Na_2ThF_6, $NaThF_5$, $NaTh_2F_9$) and KF – ThF_4 with six chemical compounds (K_5ThF_9, K_3ThF_7, $K_3Th_2F_{11}$, $KThF_5$, $KThF_9$, KTh_6F_{25}). X-ray investigation of melts of the system NaF – KF – Th_4 showed the existence of the compound $NaK(ThF_6)$ and its structure has been determined. Triangulation of the region NaF – Na_2ThF_6 – $KThF_5$ – KF was carried out and the polythermic section for NaF – $KThF_5$ has been plotted.

Investigation of the System NaF – KF – ThF_4

The system NaF – KF – ThF_4 and its constituent systems NaF – ThF_4, KF–ThF_4 were studied in the course of an investigation of the multicomponent electrolyte formed in the continuous electrolysis of the fused salt system NaCl – KCl – ThF_4 as the result of accumulation of the NaF and KF in it. Most attention in the investigation was devoted to the concentration region which is of interest from the aspects of the electrolytic production of thorium and of the determination of the composition and structure of the chemical compounds formed in the electrolyte.

The methods of thermal, phase x-ray, and chemical analysis described in Communication I were used in the study. The starting materials were chemically pure NaF, KF, and ThF_4, the preparation of which was described previously.*

The system NaF – Th_4 was investigated by the x-ray method [1], with the exception of the concentration region between 33 and 67 molar % ThF_4.

The phase diagram for the system KF – ThF_4 has been published [4]. According to these data it contains the chemical compounds K_3ThF_7, $KThF_5$ and KTh_3F_{13}, forming four simple eutectic systems. Thorium fluoride was fused in the air (when it readily decomposes to give thorium fluoride and oxide) and this diagram was held subject to doubt.

The system KF – ThF_4 has also been studied by the x-ray method [1]. It was shown that it contains six chemical compounds: K_5ThF_9, α-K_2ThF_6, β-K_2ThF_6, $KThF_5$, KTh_2F_9, KTh_6F_{25}, the structures of which were determined. No data have been published on investigations of the ternary system NaF – KF – ThF_4.

Investigation of the System NaF – ThF_4

More than 35 fused mixtures in the region from 0 to 35 molar % ThF_4 at 2-2.5 molar % intervals [2] and in the region from 35 to 100 molar % ThF_4 at 3.5 molar % intervals [3] were studied.

The results were used to construct the phase diagram for the system NaF – ThF_4, shown in Fig. 1. At 20 molar % ThF_4, a chemical compound with the composition Na_2ThF_8 is present. At 648° it decomposes by a

*Communication I (Consultants Bureau Translation page 561).

peritectic reaction. Melts containing 78% NaF and over undergo a transition at 648°, the heat effect of which has a maximum for the melt containing 20 molar % ThF_4, while the peritectic point on the liquidus curve lies at 27 molar % ThF_4. The endothermic effect at 606° also has a maximum at the point for 20 molar % ThF_4. This shows that at 606° the compound Na_2ThF_8 decomposes, forming NaF and the compound Na_2ThF_6. At 568° the polymorphic transition α- $-$ β-Na_2ThF_6 occurs. The compound Na_2ThF_6 (at the point with 33.3 molar % ThF_4) melts with an open maximum at 708°. The eutectic mixture of the compounds Na_4ThF_8 and Na_2ThF_6 melts at 620° and contains 24 molar % ThF_4.

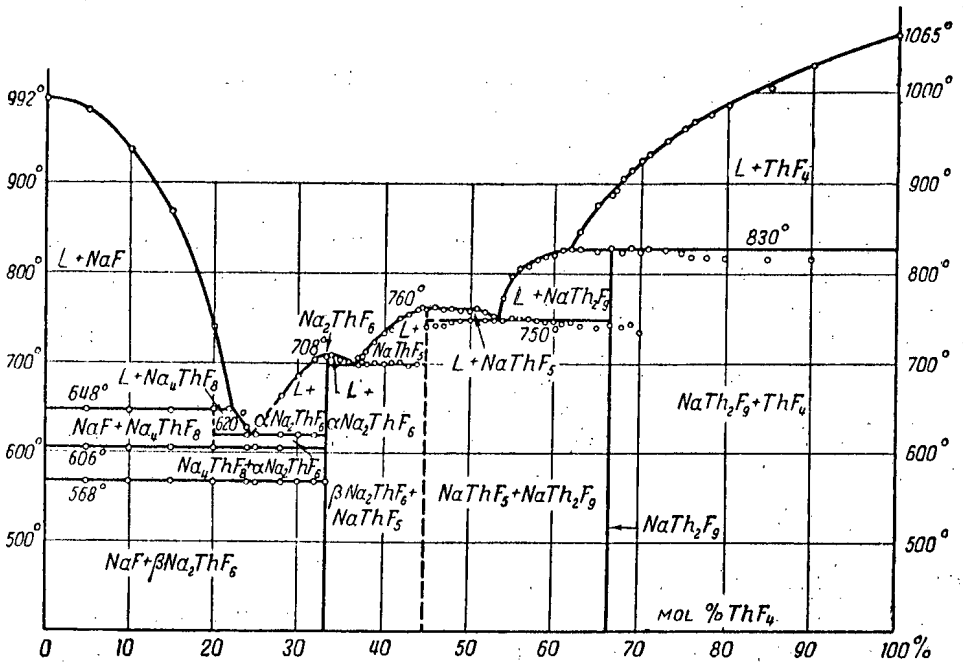

Fig. 1. The system NaF $-$ ThF_4.

The liquidus curve then gradually descends to the next eutectic point at 700° with 36-37 molar % ThF_4. From 36.5 molar % ThF_4 onward, the heat of fusion of the eutectic decreases, and vanishes at about 50 molar % ThF_4.

From thermal and microstructural analysis data it follows that in the region of about 50 molar % ThF_4 there is a chemical compound with the conjectural composition $NaThF_5$, with a very flat maximum. The liquidus curve from the $NaThF_5$ compound descends slightly to the eutectic at 750° and 53.5 molar % ThF_4, and then rises steeply with a break at 830° and 62 molar % ThF_4, after which it rises smoothly to 1065° (the melting point of pure ThF_4). At 830° peritectic decomposition of the chemical compound $NaTh_2F_9$ (66.7 molar % ThF_4) takes place; the composition of this compound is confirmed by the fact that the heat effect at 830° has a maximum at a point near 67 molar % ThF_4, and the heat effect of the fusion of the eutectic at 750° disappears near this composition.

Thus, the system NaF $-$ ThF_4 contains four chemical compounds: Na_4ThF_8, Na_2ThF_4, $NaThF_5$ and $NaTh_2F_9$. The compound Na_2ThF_6 exists in two modifications: α-Na_2ThF_6, β-Na_2ThF_6 and also probably in the fused state; the compounds Na_4ThF_8 and $NaTh_2F_9$ decompose by peritectic reactions. These results confirm Zachariasen's structural investigations [1]. The compound with the conjectural composition $NaThF_5$ has a very flat maximum on the liquidus curve in the region between 44 and 50 molar % ThF_4, and determination of the exact composition from this is very difficult.

Investigation of the System KF $-$ ThF_4

More than 40 fused mixtures at intervals of 2-3 molar % of ThF_4 have been prepared and studied [5, 6]. The results have been used to plot the phase diagram for the system KF $-$ ThF_4 (Fig. 2). It is seen that the system is highly complex, with six chemical compounds.

The chemical compound nearest to KF corresponds to the composition K_5ThF_9 (16.7 molar %). At 693° it decomposes by a peritectic reaction. The existence of this compound is confirmed by a maximum heat effect near 18 molar % ThF_4 on the phase transition at 693°. Another proof of the existence of the compound K_5ThF_9 is the sharp decrease of the exothermic effect as the result of solidification of the eutectic with the composition KF + K_5ThF_9 at 662° for mixtures containing over 18 molar % ThF_4.

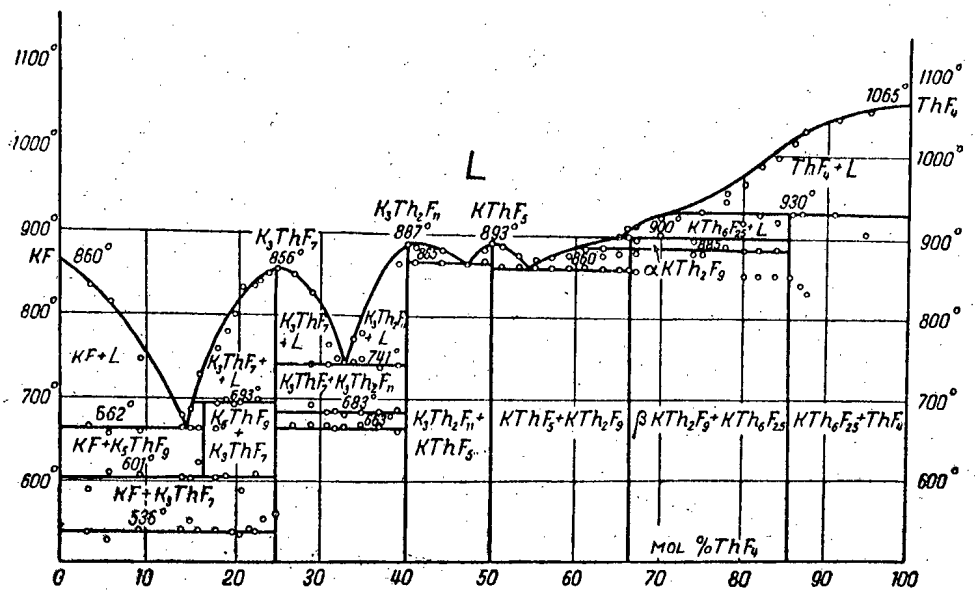

Fig. 2. The system $KF - ThF_4$.

The compound K_5ThF_9 is unstable and decomposes into KF and K_3ThF_7 when the temperature is lowered to 601°. This is confirmed by x-ray analysis of specimens annealed below 601°, which contain the K_3ThF_7 phase but not the K_5ThF_9 phase. Polymorphic transition of K_3ThF_7 apparently occurs at 536°.

The next compound, K_3ThF_7, corresponds to a content of 25 molar % ThF_4, and melts with an open maximum at 856°.

Near 40 molar % ThF_4 there is the chemical compound $K_3Th_2F_{11}$, which melts with an open maximum at about 887°. The K_3ThF_7 + $K_3Th_2F_{11}$ eutectic lies at 741° and 34 molar % ThF_4. The region of the diagram between 25 and 40 molar % ThF_4 shows solid state transitions at 683 and 663°. The nature of these transitions could not be established.

The fourth chemical compound is $KThF_5$ (containing 50 molar % ThF_4). It also melts with an open maximum at 893°, and the eutectic of the compounds $K_3Th_2F_{11}$ and $KThF_5$ lies at 47 molar % ThF_4 and 865°.

From 50 molar % ThF_4 the liquidus curve again descends to the eutectic at 860° and 54 molar % ThF_4, and then rises slowly. Mixtures containing over 63 molar % ThF_4, in addition to the effect corresponding to the liquidus point, show a new effect at 885° (accompanied by supercooling). Its value is at a maximum at 67 molar % ThF_4. The thermograms of melts containing over 66 molar % ThF_4 also show an effect at 900°, which also has a maximum in the region of 67 molar % ThF_4. These data indicate the existence of the compound KTh_2F_9 (66.7 molar % ThF_4). At 900° it decomposes by a peritectic reaction and undergoes a polymorphic transition at 885°.

At 85.7 molar % ThF_4 there is a chemical compound KTh_6F_{25}, which decomposes by a peritectic reaction at 930°. The existence of this compound was confirmed by x-ray analysis. The liquidus curve rapidly ascends with increasing ThF_4 content from 75 molar % to 100 molar % of ThF_4.

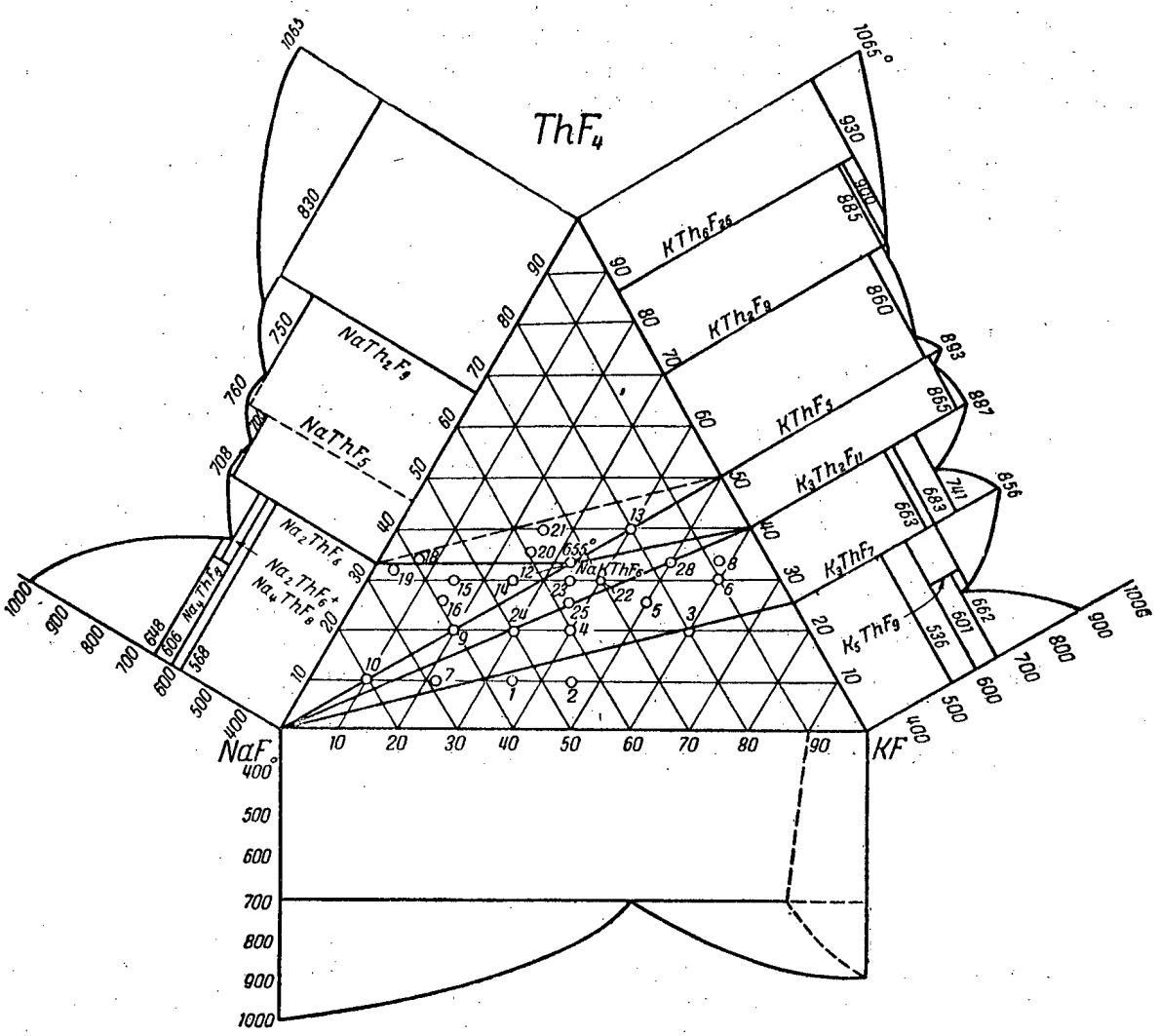

Fig. 3. The system NaF – KF – ThF_4.

These results differ significantly from the phase diagram for the system KF – ThF_4 obtained by E. P. Dergunov and A. G. Bergman.

A comparison of their results with those of W. Zachariasen [1] shows that the former authors:

a) confirmed the existence of the chemical compounds K_5ThF_9, $K_3Th_2F_{11}$, $KThF_5$, KTh_2F_9 and KTh_6F_{25}, found by W. Zachariasen [1, 10], but did not confirm the existence of the compounds with the theoretical composition α-K_2ThF_6 and β-K_2ThF_6 found by him;

b) discovered the compound K_3ThF_7, not detected by W. Zachariasen.

Investigation of the System NaF – KF – ThF_4

The region NaF – Na_2ThF_6 – $KThF_5$ – KF, which is of interest in the electrolytic production of thorium, has been studied. The phase composition has been determined by the x-ray method for 24 fused mixtures [7]. The mixtures are denoted by numerals in circles on the concentration triangle (Fig. 3) and the results of the investigation are summarized in Table 1. The data of Table 1 were used for triangulation of the NaF – Na_2ThF_6 – $KThF_5$ – KF region into the following ternary systems:

1) $NaF - K_3ThF_7 - KF$;
2) $NaF - K_3Th_2F_{11} - K_3ThF_7$;
3) $NaF - NaKThF_6 - K_3Th_2F_{11}$;
4) $NaF - Na_2ThF_6 - NaKThF_6$;
5) $Na_2ThF_6 - NaKThF_6 - KThF_5$;
6) $NaKThF_5 - KThF_5 - K_3Th_2F_{11}$.

TABLE 1

Phase Composition of Mixtures in the System NaF – KF – ThF_4

Specimen No.	Composition, M %			Phase composition
	ThF_4	KF	NaF	
1	10	35	55	$NaF+K_3ThF_7$
2	10	45	45	$NaF+K_3ThF_7$
3	20	60	20	A little $NaF+K_3ThF_7$
4	20	40	40	$NaF+K_3ThF_7$+weak lines
5	25	50	25	A little NaF+ $+K_3ThF_7+K_3Th_2F_{11}$
6	30	60	10	A little NaF+ $+K_3ThF_7+K_3Th_2F_{11}$
7	10	22.5	67.5	$NaF+K_3ThF_7$
8	33	62	5	A little $NaF+K_3ThF_7$ $+K_3Th_2F_{11}$
9	20	20	60	NaF+new phase X*
10	10	10	80	Ditto
12	33.33	33.33	33.3	Only phase X lines
13	40	40	20	Phase X and $KThF_5$
14	30	25	45	Phase X and weak lines
15	30	15	55	Na_2ThF_6+ Phase X
16	25	10	65	Na_2ThF_6+ Phase X $+Na_4ThF_8$(?)
18	33.5	11.5	55.0	Na_2ThF_6+ unidentified lines
19	32	5,0	63	Ditto
20	37	24	39	$KThF_5$**) +Phase X + + weak lines
21	40	25	35	Ditto
22	30	40	30	Phase similar to X, and unidentified lines
23	30	35	35	Ditto
24	20	30	50	Phase X absent, lines not identified
25	25	37.5	37.5	Ditto
28	33.3	50,0	16.7	Ditto

*Identified as $NaK(ThF_6)$.

**Cubic face centered structure with $a_1 = 5.94$ A.

TABLE 2

	Weight (%)				Density (g/cc)
	Na	K	Th	F	
Fused preparation	6.00	10.18	56.4	28.0	4.75
	6.44	10.88	56.03	27.44	4.8
Theoretical composition and density	5.57	9.55	56.95	27.93	5.0

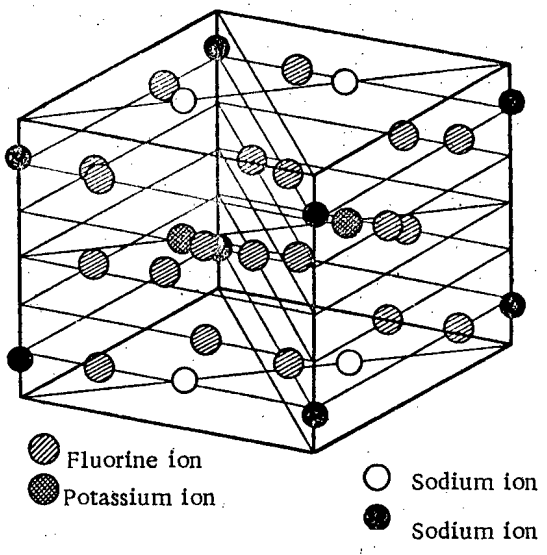

Fig. 4. Structure of the unit cell of the compound $NaK(ThF_6)$. Space group $D_{3h}^3 - \bar{C}6\,2m$. Hexagonal lattice. Dimensions: $a_1 = 6.30 \pm 0.01$ kX, $a_3 = 7.88 \pm 0.02$ kX. X-ray density $\rho = 5.00$ g/cm^3.

The investigation disclosed the existence of a new compound (phase X) with the composition $NaK(ThF_6)$ which had an appreciable homogeneity region. A particularly considerable region of solid solutions was found in the section $NaKThF_6 - K_3Th_2F_{11}$. An investigation of the structure [8] of specially prepared crystals of the compound $NaKThF_6$ of a composition close to the theoretical (Table 2) showed that it has a hexagonal lattice

with the periods $a_1 = 6.3 \pm 0.01$ kX; $a_3 = 7.88 \pm 0.02$ kX, and belongs to the space group $D_{3h}^3 - \bar{C}62m$. The unit cell contains two molecules. The structure of the compound (Fig. 4) is represented as the combined packing of figures formed by combinations of triangular prisms with distorted octahedra of ThF_6^{--} anions. It is a complex compound.

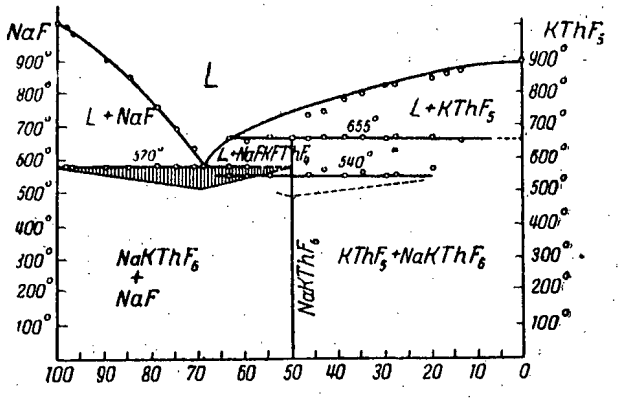

Fig. 5. Polythermic section of the system NaF – KF – ThF_4 along the line NaF – $KThF_5$.

The Polythermic Section NaF – $KThF_5$

For an additional investigation of the compound $KNaThF_6$, the polythermic section of the system along the line NaF – $KThF_5$ has been constructed [9].

The results are shown in Fig. 5. The compound $NaKThF_6$ (50 molar % NaF) decomposes at 665° by a peritectic reaction. At 540° it undergoes polymorphic transition. The peritectic point along the 655° horizontal lies at 63 molar % NaF. 570° and 31 molar % $KThF_5$ corresponds to the eutectic $NaKThF_6$ + NaF. Thus, the polythermic section confirms the existence of the complex compound $NaKThF_6$.

SUMMARY

1. The phase diagram for the system NaF – ThF_4 has been plotted. It contains the chemical compounds Na_4ThF_8 and Na_2ThF_6, and compounds with the supposed compositions $NaThF_5$ and $NaTh_2F_9$.

2. The phase diagram for the system KF – ThF_6 has been plotted, with six chemical compounds: K_3ThF_9, K_3ThF_7 (transition at 536°) $K_3Th_2F_{11}$, $KThF_5$, KTh_2F_9 (undergoes α- – β-transition at 885°) and KTh_6F_{25}.

3. A new compound $NaKThF_6$ has been found from x-ray phase analysis data, and the NaF – Na_2ThF_6 – $KThF_5$ – KF region of the NaF – KF – ThF_4 system has been triangulated into simple ternary systems. The compound $NaKThF_6$ belongs to space group $D_{3h}^3 - \bar{C}62m$ and has a hexagonal lattice with $a_1 = 6.3 \pm 0.01$ kX and $a_3 = 7.88 \pm 0.02$ kX. The theoretical density is 5.0 g/cc, and the experimental 4.75-4.8 g/cc.

4. The polythermic section of the ternary system NaF – KF – ThF_4 along the $KThF_5$ – NaF line has been constructed; this shows that the compound $NaKThF_6$ undergoes polymorphic transition at 540°, decomposes by a peritectic reaction at 665°, and forms a eutectic with NaF at 570° and 69 molar % NaF.

Received August 16, 1956.

LITERATURE CITED

[1] W. H. Zachariasen, J. Am. Chem. Soc. 70, 2147 (1948).

[2] A. I. Evstyukhin and P. D. Bystrov, Investigation of the Phase Diagram for the System NaF – ThF_4 in the Concentration Range 0 to 35 Molar % ThF_4, MIFI Report for 1949 (Unpublished).

[3] A. I. Evstyukhin and D. D. Abanin, Investigation of the Phase Diagram for the System NaF – ThF_4 in the Concentration Range 35 to 100 Molar % ThF_4, MIFI Report for 1950 (Unpublished).

[4] E. P. Dergunov and A. G. Bergman, Proc. Acad. Sci. USSR 60, 391 (1948).

[5] A. I. Evstyukhin and S. G. Malandin, Investigation of the Phase Diagram for the System KF – ThF_4 in the Concentration Range 0 to 37 Molar % ThF_4, MIFI Report for 1951 (Unpublished).

[6] A. I. Evstyukhin and Yu. G. Godin, Investigation of the Phase Diagram for the System KF – ThF_4 in the Concentration Range 35 to 100 Molar % ThF_4, MIFI Report for 1952 (Unpublished).

[7] A. I. Evstyukhin and P. D. Bystrov, Investigation of the System NaF – KF – ThF_4 and of the Electrolyte Composition in Electrolysis of the Chloride-Fluoride System NaCl – KCl – ThF_4, MIFI Report for 1953 (Unpublished).

[8] A. A. Rusakov, and Yudin, X-Ray Investigation of the Structure of the Compound NaK(ThF_6), MIFI Report for 1956 (Unpublished).

[9] A. I. Evstyukhin and V. N. Kokhanova, Investigation of the Polythermic Section of the System NaF – KF – ThF_4 Along the Line $KThF_5$ – NaF, MIFI Report for 1953 (unpublished).

[10] W. H. Zachariasen, Acta Cryst. 2, 388 (1949).

CALORIMETRIC MEASUREMENTS ON PREPARATIONS OF NATURALLY RADIOACTIVE FAMILIES OF ELEMENTS

G. V. Gorshkov and N. S. Shimanskaya

A method is described for calorimetric determinations of the activity of naturally radioactive families of elements. The ratios between the milligram-equivalents and millicuries for equilibrium RaTh and Ac sources have been determined. The half-life of Ra and the γ-radiation energy of Ra and Ac have been determined calorimetrically.

1. Despite the wide use of artificial radioactive isotopes, the elements of the naturally radioactive families are very important. Up to the present time, preparations of Ra, MsTh, RaTh, Ac, and others are irreplaceable as long-lived α-emitters, and are used for the production of neutron sources and in investigations of nuclear reactions. Radium preparations are used for medical purposes (internal and external radiotherapy), for flaw detection, and as standards in most ionization measurements.

Therefore, the development of exact and practically convenient methods for measurement of such sources is very important. At the present time the activity of powerful natural radioactive preparations is most commonly measured by the ionization method, by means of which relative measurements may be made on standard preparations to an accuracy of up to 0.2-0.5%.

However, in many cases it is more convenient to use a calorimetric method for determination of the activities of radium, thorium, and actinium sources. Indeed, the ionizing action of γ-radiation largely depends on the conditions of its absorption both in the preparation itself and in the walls of the apparatus, and in the recording instrument. Even when sources of the same nature are compared, ionization measurements can give inaccurate values for their relative activities, if these sources differ among each other in their contents of radioactive isotope and inactive constituents, the geometrical distribution of the activity within the container, and the thickness and material of the walls of the latter. For example, a change of one tenth of a millimeter in the thickness of the platinum tube walls containing a radium preparation changes its milligram equivalent by about 1.3%. Very much larger errors are introduced for similar reasons in measurements of preparations with softer γ-radiation, such as actinium preparations and the so-called nonstandard preparations, with activities differing appreciably from those of standard preparations. Such preparations may be kept in containers of much larger size than the ordinary standard tubes, and of different materials and different wall thickness. The preparations themselves may be liquid, or mixed with various inactive substances, some of which strongly absorb radiation. Exact evaluation of the absorption and self-absorption effects is generally almost impossible, and therefore the measurement accuracy usually does not exceed 2-3%. Even greater errors occur in determinations of the radioactivity of preparations by comparison with standards of different origin.

2. The calorimetric method for measurement of radioactive substances is based on the heat effects of radioactive radiations [1]. Its use requires a knowledge of the energy E_i of the α-, β-, and γ-radiation of the isotope to be measured, and the absorption of these radiations in the calorimeter. For preparations of natural radioactive substances the values of E_i can be calculated with adequate accuracy, as the α-ray spectra, the absorption of which produces a considerable proportion of the heat effect, are well known, while the γ-radiation

of Ra, MsTh, RaTh, and Ac preparations in which radioactive equilibrium has been established forms only a small part of the total energy balance (6-7 % for Ra and MsTh, ~ 5% for RaTh preparations, and ~1.5% for Ac sources). Therefore in calorimetric determinations of such preparations with a thin-walled β-calorimeter the errors in determinations of the self-absorption and absorption of the γ-radiation from the source has practically no effect on the accuracy of the result. For example, if the walls of the calorimeter, of the container, and the source itself absorb about 10% of the γ-radiation energy, and this absorption is determined to an accuracy of the order of 20 %, then the error due to this will not exceed 0.2% of the final result for a radium source. The accuracy of the ionization measurements cannot, of course, be higher than 2%. Fig. 1 shows graphs which illustrate the advantages of the calorimetric method for measurement of the activity of natural radioactive sources. Curve II shows the variation of the milligram equivalent of a Ra preparation with increase of the thickness of a lead filter from 0 to 10 mm, and Curve I represents the corresponding variation of the heat effect (Curve II was obtained with the aid of a standard SGM-1 ionization chamber, and Curve I with the calorimetric apparatus described in [2]). The advantages of the calorimetric method are particularly prominent in measurements of actinium preparations, the γ-radiation of which has low intensity and a soft spectrum. In addition, it must be stressed that the calorimetric method is an absolute method which does not require any comparison standards. The preparation of the latter by the ionization method is a very complex procedure. This is due to difficulties in determination of the ionization constants and the geometrical factors, calculation of the influence of scattered radiation, and to the impossibility of an exact determination of the absorption and self-absorption of the γ-radiation. The standardization is much more simply carried out by the calorimetric method. A brief account of some aspects of the calorimetric method for determination of naturally radioactive preparations is given below, and results of calorimetric measurements of Ra, RaTh, and Ac sources and mixed radium-mesothorium preparations are given.

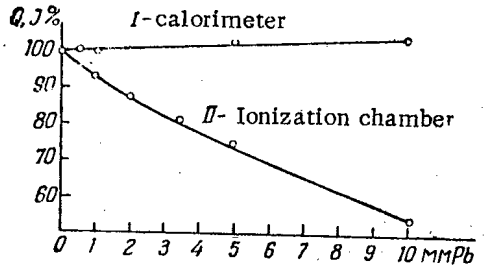

Fig. 1. Variation of the heat effect Q and of the milligram equivalent J with increase of the thickness of a lead filter from 0 to 10 mm.

3. In calorimetric measurements of naturally radioactive preparations we met the difficulty that modern tables of radioactive constants (for example, those of Hollander, Perlman, and Seaborg [3] for 1953) do not give exhaustive data on the radioactive radiations of the elements of these families. These tables, in particular, do not give exhaustive information on the γ-ray energies and their relative and absolute intensities; there are no data on the numbers of conversion electrons or on the values of the average energies of the β-spectra. This led us to carry out a thorough analysis of all available data on the energies and radiation yields of the elements of the three radioactive families. After a critical examination of a large number of experimental studies we were able to determine E_i for each element (see Tables I, II, and III in the Appendix) and to find the value of the total "thermal" energy E per single disintegration of equilibrium preparations of Ra, MsTh, RaTh, and Ac. These values of E are given in Table 1.

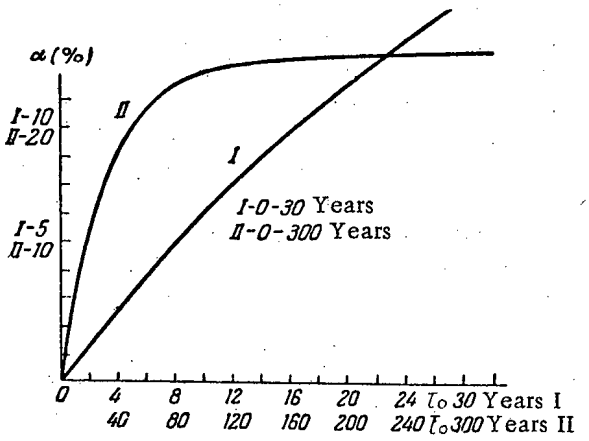

Fig. 2. Increase of the amount of heat emitted by radium preparations with time.

For radium sources, the corrections for their increased heat effects owing to accumulation of RaE and Po^{210} were also calculated (the results of these calculations are shown graphically in Fig. 2).

4. With a knowledge of these values it proved possible to carry out calorimetric determinations of the absolute activities of a large number of very different natural radioactive substances. Double calorimeters of the static type were used [2]. In most cases the measurements were carried out in thin-walled, so-called β-calorimeters, in which the absorption of the γ-radiation from the preparations was slight. The results of some of the determinations are shown in Table 2. The total heat effects of Ra and Ac preparations were deter-

mined in γ-calorimeters with thick walls of heavy metals (tungsten, lead). As the accuracy of the values for $E_{\alpha+\beta}$ and $q_{\alpha+\beta}$ given in Table 1 is probably not less than 0.5%, while the accuracy of the heat measurements themselves was of the same order, the error of the calorimetrically determined values for the activities of the sources usually did not exceed 1-1.5%.

TABLE 1

Average Radiation Energies E Emitted in Single Disintegrations by Equilibrium Preparations of Ra, MsTh, RaTh, and Ac, and the Heat Effects q of the Corresponding Sources With Activities of 1 Curie

Preparation	$E_{\alpha+\beta}$*)	$E_{\alpha+\beta+\gamma}$	$q_{\alpha+\beta}$	$q_{\alpha+\beta+\gamma}$
	Kev/disintegration		M cal/hr · curie	
Ra	25 350	27 140	129.3	138.4
MsTh	33 920	36 510	173.0	186.2
RaTh	33 390	35 060	170.3	178.8
Ac	33 690	34 210	172.0	174.4

*The value $E_{\alpha+\beta}$ includes the energy of the recoil atoms, the conversion electrons, and the x-radiation.

TABLE 2

Calorimetric Measurements of the Activity of Certain Preparations of Ra, RaTh, and Ac

Preparation	Ionization measurement of J, cal/hr	Calorimetric measurements	
		heat effect Q cal/hr	activity A, mcurie
Ra 5712*)	97.2±0,5	12.79±0.06	96.6
Ra 2792*)	101.6±0,5	13.43±0.07	102.3
Ra I	1490	199.8±1.0	1500±15
Ra II	2340	313.2±1.5	2350±25
RdTh I	226.1±2,0	42.6±0.2	247±2
Ac I	10.5±0,4	18.1±0.1	105±1
Ac II	—	1.93±0.03	11,2±0.2

*Standard Ra preparations, Rad. Inst. Acad. Sci. U. S. S. R.

Measurements of two standard Ra preparations, 5712 and 2792, were used to determine z (the number of disintegrations per second per 1 g Ra) and the half-life period of Ra ($T = 5.853 \cdot 10^{13} \cdot z^{-1}$ years). We had no pure preparation at our disposal in which the radium content could be determined by direct weighing. However, in view of the fact that the primary international Ra standards contain definite quantities of $RaCl_2$ by weight, ionization measurements of radium preparations should give their weight contents of radium fairly accurately (this is, of course, only true if the measured preparation and the standard are quite identical). Table 2 shows the results of Ra determinations by the ionization method in the two above-mentioned Ra standards, carried out at the All-Union Scientific Research Institute for Metrology. After appropriate corrections for accumulation of RaE and Po^{210} (1.2% and 0.3%), absorption of the γ-rays in the calorimeter walls, protective case of the preparation, and the salt itself (0.6%), and finally for the self-absorption and absorption difference for γ-radiation in the preparations used and the standards used in the Metrology Institute (0.6%), we obtained a value for the heat effect of 1 g Ra in equilibrium with its short-lived products, of $Q_{\alpha+\beta} = 130.0 \pm 1.5$ cal/hour. This gave for z and T the respective values of $(3.72 \pm 0.06) \cdot 10^{10}$ disintegr./sec/1 g Ra, and 1575 ± 25 years.

Great accuracy cannot be claimed for our estimate of the half-life of Ra, owing to the indirect determination of the radium in the preparations. Our value is close to the values of T = 1580-1590 years, which for a long time were considered to be the most reliable but it differs considerably from the value given in the recent paper by Kohman et al. [4] for the half-life of Ra (1622 ± 13 years). On the basis of this last result, the new value of $z = 3.61 \times 10^{10}$ instead of the formerly accepted value of 3.7×10^{10} has been used in a number of papers for the number of disintegrations in 1 g Ra per second. In the recent review by Hollander, Perlman and Seaborg [3] the value given for the half-life of Ra is 1631 years, which is the average from a number of results [5-9]. This value is in good agreement with Kohman's result, but such averaging is hardly legitimate, as the papers [5-7] give very similar values (1601, 1593, and 1600 years), while [8] and [9] constitute another group with sharply different results (1684 and 1691 years). It would be very interesting to carry out a second determination of the half-life of Ra by the method used by Kohman et al. (measurement of the number of α-particles from a known weight of Ra in an ionization impulse chamber) and also by other methods.

Table 2 also shows the result of a calorimetric activity determination of two strong Ra preparations (I and II). The salt ($RaBr_2$ + $BaBr_2$) in these sources was enclosed in a platinum tube which was in turn contained in an aluminum case with walls about 3 mm thick. The weight of the salt was 2.9087 g in the first preparation and 4.1795 g in the second. The value of the self-absorption in such preparations cannot be neglected. Calculations based on Dixon's approximate formulas [10] and Perry's experimental results [11] showed that the self-absorption was 7% for the first preparation and 8% for the second, giving 0.5 and 0.6% respectively as the corrections for the increased heat effect. The total correction for the γ-ray absorption in the platinum and aluminum containers and the millimeter copper calorimeter vessel was 1.4% for both sources. This value was found both by calculation and by direct measurements in the ionization chamber. These estimations enabled us to determine the activities of the preparations from the calorimetrically determined heat effects (199.8 and 313.2 cal/hour). The results were in good agreement with the results of ionization measurements on individual samples, the weight of which did not exceed 100 mg (see Table 2). The average results of ionization measurements carried out on separate samples were : 1490 mcurie for the first source, and 2340 for the second. An interesting fact is that ionization measurements on the preparations themselves, carried out in the usual chamber with a lead filter 6 cm thick, gave a value of 1.49 for the ratio of the γ-intensities of these preparations, which is rather below the value of 1.57 given by the ratio 2350/1500. This discrepancy ($\sim$ 5.5%) cannot be attributed to increased self-absorption in a more powerful source. It is probably due to different conditions of activity distribution within the preparations and of γ-ray absorption in the containers. This proves once again that the error of ionization measurements of even the relative activities of such nonstandard preparations is not less than 5%.

The calorimetric method was also used for measurement of the ratio between the milligram equivalent and millicurie values for equilibrium RaTh and Ac sources, important in ionization measurement practice. The ionization measurement conditions generally used in the USSR (lead filter 5 mm thick, and a standard thin-walled chamber SGM-1) gave:

1 mg-equiv. RaTh = 1.29 $\pm$ 0.02 mcurie RaTh, *

1 mg-equiv. Ac = 10.0 $\pm$ 0.5 mcurie Ac.

The γ-radiation energy of an equilibrium Ac source was estimated from calorimetric measurements of an actinium preparation of known activity in a β-calorimeter with and without a lead filter and from measurements in a γ-calorimeter. Our result (E_γ = 2.0 $\pm$ 0.5% of $E_{\alpha+\beta}$ = 3.4 $\pm$ 0.8 cal./hour curie Ac) is not in agreement with the result obtained by Sanielevici [13]. He measured the increased heat of an actinium preparation with increase of the thickness of the lead walls of the calorimeter, and found that E_γ(Ac) = 6 % of $E_{\alpha+\beta+\gamma}$(Ac). This result is probably erroneous, especially as his calorimetric absorption curve shows that the Ac preparation used contained considerable amounts of radioactive elements with an intense and relatively hard γ-radiation (5 mm of lead absorbed only 30% of the γ-ray radiation; in our ionization absorption curves this value reached 80%). Our estimate of the total γ-radiation energy of an equilibrium Ac preparation based on calorimetric measurements is in agreement with the value of E_γ which can be obtained by ionization measurements. Assuming for E_γ(Ra) a value of 9.1 cal./hour 1 g Ra [14], and the above value of 10.0 for the ratio between the milligram-equivalent and millicurie for Ac, we obtained for E_γ(Ac) the value of 3.9 cal./hour curie. Both experimental values are approximately 1.5 times as high as the value of 2.4 cal./hour curie Ac, calculated by us from α- and γ-spectroscopic data. It must be taken into account, however, that the results obtained by individual workers for the relative and still more the absolute, intensities of the γ-radiation of elements of the actinium series vary very greatly.

5. The calorimetric method was also used to determine the content of radioactive material in neutron sources of the type (X_α + Be). This, in conjunction with measurements of neutron intensities of these sources, made it possible to determine the neutron yield η, usually defined as the ratio of the total number of neutrons emitted by the source to the activity of the radioactive element present in it, measured in curies. The yield η was determined for the sources (Ra + Be), (Ac + Be), (Po + Be) and(RaTh + Be). The values of η so found were:

*Up to the present time this relationship has been determined only for equilibrium RaTh sources under the totally different geometrical conditions used abroad (a flat "Curie chamber" with a flat centimeter-thick lead filter situated in the immediate vicinity of the chamber itself). Winand [12] found the value of 1.08 (1 mg-equiv. RaTh = 1.08 mcurie RaTh) for the condition 1 mcurie = $3.7 \cdot 10^{10}$ disintegr./sec.

$0.95 \pm 0.08 \cdot 10^7$ neutrons/sec curie Ra;
$1.46 \pm 0.17 \cdot 10^7$ neutrons/sec curie Ac;
$1.58 \pm 0.16 \cdot 10^6$ neutrons/sec curie Po and
$1.38 \cdot 10^7$ neutrons/sec curie RaTh.*

The yield of the (Ac + Be) source, which we were apparently the first to study experimentally, is in good agreement with the value to be expected by calculation from the graphs given by Bjerge [15] and Stuhlinger [16] and from the known α-radiation energy spectrum for the elements of the actinium series. We must emphasize the great advantages of the calorimetric method of activity measurement of neutron sources, which as a rule require the calculation of corrections for γ-ray absorption in the source itself and in the containing metallic, often double, walls. This is especially evident in the case of the (Po + Be) source, which does not emit any appreciable γ-radiation, and the (Ac + Be) sources. Determinations of the amount of radioactive substance in a neutron source by α- or γ-determinations of its initial activity often lead to considerable errors owing to losses of substance during the preparation of the source itself.

6. The calorimetric method was also used for determination of the Ra and MsTh contents in radium–mesothorium preparations. In this case, the heat effect of the preparation is measured in parallel with the usual ionization measurements of the intensity i of the γ-radiation. The calorimetric method for determination of the composition of radium–mesothorium preparations, originally proposed by Curie [17], was studied in detail to evaluate its accuracy and to determine its applicability to determinations of the composition of preparations of different ages. Approximate equations were derived for "young" preparations, and also general formulas for determination of the percentage contents of Ra and MsTh, with some modifications of the calorimetric procedure and of the values of the numerical coefficients in Curie's formula [17]. The required original composition of a "young" radium–mesothorium preparation is given in general form by the equations

$$\left.\begin{aligned} x &= \frac{Q-\left(i-\frac{Q}{q_0}\right)h\frac{k_0}{k_1}q_2-\left(i-\frac{Q}{q_0}\right)\frac{k_0}{k_1}q_1}{q_0} \quad \text{for Ra,} \\ y &= \left\{i-x-\left(i-\frac{Q}{q_0}\right)h\frac{k_2}{k_1}\right\}\varkappa \quad \text{for MsTh;} \end{aligned}\right\} \tag{1}$$

where q_0, q_1, q_2 are the quantities of heat per millicurie emitted in the absorption of α- and β-radiations from Ra with its short-lived products, mesothorium MsTh (I + II) and radiothorium with its disintegration products (ThX, Tn, ThA, ThC, ThC'C'') respectively; k_0, k_1, k_2 are the ionization constants of the chamber used for Ra, MsTh, and RaTh. (In our case their respective values were 1; 0.524; and 0.775); h is the ratio of the number of atoms of RaTh disintegrating in unit time to the number of MsTh atoms disintegrating in unit time, at the instant of measurement; $\varkappa$ is a coefficient which allows for the decrease in the amount of MsThI (in %) in the time between the sealing of the preparation and the determination.

In the measurement of "old" (Ra + MsTh) preparations, the sealing date of which is not known, the following expression can be derived for R, the ratio of the milligram-equivalent to the so-called "thermal equivalent", equal to the ratio of the thermal powers of the standard and the measured preparations:

$$R=\frac{\frac{Q}{Q_0}}{\frac{J}{J_0}}=\frac{\frac{q_2\lambda_1N_1}{q_0\lambda_0N_0}e^{-\lambda_1t}\frac{\lambda_2}{\lambda_2-\lambda_1}\left(1-e^{-(\lambda_2-\lambda_1)t}\right)+\frac{q_1\lambda_1N_1}{q_0\lambda_0N_0}e^{-\lambda_1t}+1}{\frac{\lambda_1N_1}{\lambda_0N_0}e^{-\lambda_1t}\left(\frac{k_1}{k_0}+\frac{k_2\lambda_2}{k_0(\lambda_2-\lambda_1)}\left[1-e^{-(\lambda_2-\lambda_1)t}\right]\right)+1}, \tag{2}$$

*As the beryllium powder used in the sources was finely divided ($d \sim 5-50\mu$), it can be assumed that our values for the yield η (with allowance for the Be concentration coefficient) were in all cases close to the optimum values.

where N_0 and N_1 are the numbers of Ra and MsTh atoms initially present in the preparation; λ_0, λ_1, λ_2 are the decay constants for Ra, MsTh, and RaTh; t is the time from the sealing of the preparation to the measurement.

If we introduce the designations: $m = \frac{k_1}{k_0}$; $r = \frac{k_2}{k_0}$; $h = \frac{\lambda_2}{\lambda_2 - \lambda_1}\left[1 - e^{-(\lambda_2 - \lambda_1)t}\right]$; $\pi = \frac{m\lambda_1 N_1}{\lambda_0 N_0}$

and replace q_2/q_0 and q_1/q_0 by their respective numerical values 1.324 and 0.0201, which are easily found from the data in Table 1, then (2) can be written as:

$$R = \frac{\frac{\pi}{m} e^{-\lambda_1 t}(1.324h + 0.0201) + 1}{\left(1 + \frac{r}{m}\right) h\pi e^{-\lambda_1 t} + 1}. \qquad (3)$$

Numerical calculations based on Formula (3) and the results of prolonged ionization and calorimetric determinations of several radium–mesothorium preparations led to the conclusion that the calorimetric method is not suitable for practical determinations of the composition of this type of source, the "age" of which is not known, and which had been sealed for more than 2-3 years. For determination of the composition of "young" preparations, as in the rating of factory production, the calorimetric method is not inferior in accuracy to other methods for determination of Ra and MsTh in such preparations.

TABLE 3

Calorimetric Determination of Radium and Mesothorium in Mixed Preparations

Preparation No.	Sealing date	Calorimetric determinations		Ionization determinations		Calculated composition of the preparation			
						Ra.		MsTh	
		date	Q(cal/hr)	date	J mg-equiv	mcurie	%	mg-equiv	%
3137	17.4.52	4.6.52	11,43	29.5.52	128.0	80.5	64.0	45.3	36.0
3149	23.4.52	3—7.6.52	13,49	1.6.52	150.0	95.7	64.8	51.9	35.2
3360	21.9.52	25.10.52	14,12	28.10.52	164.8	100.6	62.0	61.7	38.0
3361	21.9.52	28.10.52	12,01	28.10.52	135.3	85.4	63.9	48.2	36.1

Table 3 shows the results of calorimetric and ionization measurements carried out with four mixed preparations of Ra + MsTh, and their calculated percentage compositions.

APPENDIX

Table 1 shows the values for the average energy E of radiations per disintegration of equilibrium preparations of Ra, MsTh, RaTh, and Ac. The values of E were calculated on the basis of an examination of much experimental data, mainly of recent years, on the α-, β-, and γ-spectra of the corresponding radioactive elements. Tables I, II, and III show average (or selected as the most probable and reliable) values for the average energies of the α-particles (E_α) and recoil nuclei (E_a), the average β-spectrum energies (E_β) and the sums of the energies of the conversion electrons and x-ray radiation $E_e + E_x$ and the γ-radiation E_γ.

Received March 29, 1956

TABLE I

Average Energies of Radioactive Radiations E_i Emitted in One Disintegration of Elements of the Ra Series

Element	Average energy per disintegration, Kev						
	α-particles E_α	recoil nuclei E_α	β-particles E_β	conversion electrons and x-ray quanta $E_{e^-} + E_x$	γ-quanta E_γ	$E_{\alpha+\beta} = E_\alpha + E_a + E_\beta + E_{e^-} + E_x$	$E_{\alpha+\beta+\gamma} = E_{\alpha+\beta} + E_\gamma$
Ra	4 766	86	—	5.6	5.1	4 858	4 863
Rn	5 482	101	—	—	—	5 583	5 583
RaA	5 996	112	—	—	—	6 108	6 108
RaB	—	—	225	54.3	208	279	487
RaC	1.8	—	680	11.7	1 572	694	2 266
RaC′—C″	7 683	146	—	—	—	7 829	7 829
ΣE_i	23 929	445	905	72	1 785	25 351	27 136

TABLE II

Average Energies of Radioactive Radiations E_i Emitted in One Disintegration of Elements of the Th Series

Element	Average energy per disintegration, Kev						
	α-particles E_α	recoil nuclei E_α	β-particles E_β	conversion electrons and x-ray quanta $E_{e^-} + E_x$	γ-quanta E_γ	$E_{\alpha+\beta} = E_\alpha + E_a + E_\beta + E_{e^-} + E_x$	$E_{\alpha+\beta+\gamma} = E_{\alpha+\beta} + E_\gamma$
MsThI	—	—	1	0.6	0.3	1.6	2
MsThII	—	—	430	91	932	521	1 453
RaTh	5 364	96	—	55	3	5 515	5 518
ThX	5 666	103	—	3	10	5 772	5 782
Th	6 278	116	—	—	—	6 394	6 394
ThA	6 774	128	—	—	—	6 902	6 902
ThB	—	—	120	97	119	217	336
ThC	2 100	40	384	7.6	419	2 532	2 951
ThC′	5 737	110	—	—	—	5 847	5 847
ThC″	—	—	201	13	1 111	214	1 325
ΣE_i MsTh	31 919	593	1 136	267	2 594	33 916	36 510
ΣE_i RaTh	31 919	593	705	175	1 662	33 393	35 055

TABLE III

Average Energies of Radioactive Radiations E_i Emitted in One Disintegration of Elements of the Ac Series

Element	Average energy per disintegration, Kev						
	α-particles E_α	recoil nuclei E_α	β-particles E_β	conversion electrons and x-ray quanta $E_{e^-} + E_x$	γ-quanta E_γ	$E_{\alpha+\beta} = E_\alpha + E_a + E_\beta + E_{e^-} + E_x$	$E_{\alpha+\beta+\gamma} = E_{\alpha+\beta} + E_\gamma$
Ac	59	1	—	5.5	—	65,5	65,5
AcK	—	—	5	—	—	5	5
RaAc	5 875	105	—	(10)	1 751	5 990	50
AcX	5 649	103	—	(10)	1 721	5 762	5 834
An	6 713	125	—	(20)	1 931	6 858	5 951
AcA	7 368	140	—	—	—	7 508	7 508
AcB	—	—	360	—	181	360	541
AcC	6 540	127	—	11	50	6 678	6 728
AcC′	24	—	—	—	—	24	24
AcC″	—	—	480	—	4	480	484
ΣE_i	32 228	601	845	56,5	475	33 730	34 206

LITERATURE CITED

[1] M. Popov, Thermometry and Calorimetry (Moscow State University, 1954).

[2] N. Shimanskaya, Calorimetric Method for Investigation of Radioactive Substances (in press).

[3] J. Hollander, J. Perlman and G. Seaborg, Rev. Mod. Phys. 25, 429 (1953).

[4] T. Kohman, D. Ames and J. Sedlet, Nat. Nuclear Energy Ser., Div. IV 14B, 1675 (1949).

[5] F. Ward, C. Wynn-Williams and M. Cave, Proc. Roy. Soc. (London) A 125, 713 (1929).

[6] H. Jedrzejowski, Ann. Physik. 9, 128 (1928).

[7] H. Braddick and H. Cave, Proc. Roy. Soc. (London) 121, 367 (1928).

[8] M. Gregoire, Ann. Phys. 2, 161 (1934).

[9] E. Gleditsch and E. Föyn, Am. J. Sci. 29, 253 (1935).

[10] W. Dixon, Nucleonics 8, 68 (1951).

[11] W. Perry, Proc. Phys. Soc. 57, 178 (1947).

[12] W. Winand, J. phys. radium 10, 361 (1939).

[13] A. Sanielevici, J. chim. phys. 33, 759 (1936).

[14] J. Zlotowski, J. phys. radium 6, 242 (1935).

[15] T. Bjerge, Proc. Roy. Soc. 164, 243 (1938).

[16] E. Stuhlinger, Z. Physik 114, 185 (1939).

[17] M. Curie, Compt. rend. 172, 1022 (1921); D. Jovanovitch, J. phys. radium 9, 297 (1928).

SYSTEMS FOR REMOVAL OF HEAT FROM NUCLEAR REACTORS (SURVEY OF THE LITERATURE)

V. S. Chirkin

A description is given of the differences in the arrangements for circulation of the heat-transfer medium and in the use of the main power equipment concerned in the removal of the heat developed in the active zone of a nuclear reactor. A classification is given of the existing systems of heat removal, in which the heat-transfer material is either water not allowed to boil, boiling water, an aqueous solution, a gas, or a liquid metal.

Special Features of the Removal of Heat from Nuclear Reactors [1,3,8]

The heterogeneous and homogeneous nuclear reactors for which the plans have been published are equipped with various systems for heat removal and differ from each other in the thermal parameters of the heat-transfer medium and the manner of its use.

Whatever its nature, the heat-transfer medium receives from the active zone of the reactor thermal energy which can then be used for industrial heat supply or converted into mechanical work.

The problems of heat transfer connected with the active zone of the reactor and with the choice of a heat-transfer agent will be taken to be known, since they relate not only to the heat removal system but to a number of interdependent parameters. Moreover, our considerations will not include such auxiliary equipment as purifiers, fittings, etc., which have no essential effect on the make-up of the heat removal system nor on the efficiency of the cycle.

Systems for removal of heat from nuclear reactors are distinguished by a number of special features which can be classified under the following main headings:

a) the heat-transfer medium may be one of a number of substances (helium, heavy water, liquid metals) rarely encountered in ordinary practice;

b) on leaving the reactor the heat-transfer agent is radioactive;

c) under the action of the radiation of the reactor, part of the heat-transfer material undergoes essential changes (for example, oxyhydrogen gas is produced from water, gases are ionized, and so on).

A survey of the systems for heat removal that are used can help to make clear the special features of these systems. Accordingly, we proceed to consider the various systems.

Heat Removal by Water Not Permitted to Boil [4,10,12]

System with open circuit. Water from a natural reservoir is taken into a purifying system, and then into the reactor (Fig. 1), in which it is heated to a temperature that ordinarily does not exceed 90°C; at this temperature the water is discharged back into the natural reservoir.

A major shortcoming of this system is the unproductive loss of heat.

Advantages include: first, the fact that the pressure of the heat-transfer medium is close to atmospheric. The low temperature of the heat carrier simplifies the operation of the system and permits the use in the active

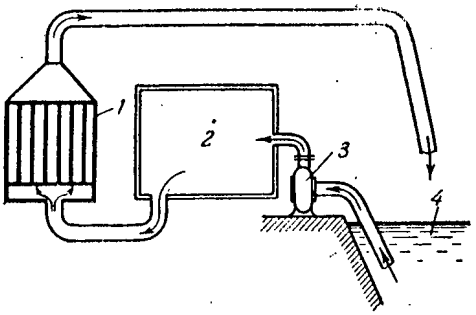

Fig. 1. Heat removal system using non-boiling water in an open circuit at low pressure.
1) Reactor; 2) water-purifying system; 3) pump; 4) natural reservoir.

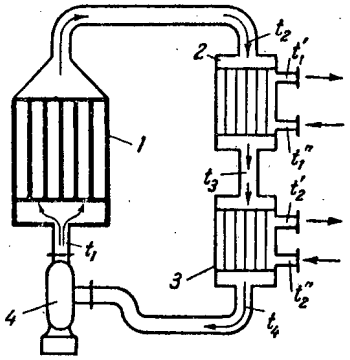

Fig. 2. Heat removal system with closed circuit.
1) Reactor; 2) high-temperature heat exchanger; 3) low-temperature heat exchanger; 4) pump.

zone of the reactor of cheap and relatively weak materials, such as aluminum and its alloys. A second point is that the low temperature and pressure simplify the construction of the reactor and the heat removal system.

System with closed circuit. This system is commonly used in power reactors (Fig. 2).

Water at temperature t_1 enters the reactor, where it is heated to temperature t_2, taking up the heat developed in the reactor, in amount

$$Q = g \cdot c_p (t_2 - t_1).$$

Since under ordinary conditions the temperature of the water on emergence from the reactor is fixed, in order to reduce the rate of expenditure of water (g, by weight) it is necessary to lower the temperature t_1. For this purpose it is convenient to install heat exchangers using high and low temperature ranges.

By giving up the heat

$$Q = q_1 + q_2,$$

where $q_1 = g \cdot c_p (t_2 - t_3)$ (for the first heat exchanger) and $q_2 = g \cdot c_p (t_3 - t_4)$ (for the second heat exchanger), the water is cooled to the temperature t_3, and then to the temperature t_4.

Advantages of this system include the possibility of using expensive heat-transfer materials, since the volume of the circuit is relatively small, and there is no danger of spreading radioactive contamination into the surrounding region, etc.

A disadvantage of such a system is the presence in the system of the high pressure necessary to raise the temperature of the water. For example, to produce water at a temperature of 300°C the pressure in the water circuit must be greater than 88 atm.

The quantity of steam formed in the second circuit is

$$G = \frac{g \cdot c_p (t_2 - t_3)}{c_p (t_1' - t_2'') + r} \text{ kg/hr}$$

Here t_1' is the temperature of the steam on leaving the heat exchanger, t_2'' is the temperature of the condensate fed into the heat exchanger, and r is the latent heat of vaporization in kcal/kg.

The efficiency of this system can be raised by using with it a steam superheater operated with ordinary fuel.

System with closed circuit and self-vaporization of the water (Fig. 3). In this system the heat-transfer material is at the same time the working substance [1,6]. Water at the temperature t_1 is sent into the reactor under pressure p_1, and there it is heated to the temperature t_2. In the self-vaporizer, where the pressure p_2 is less than p_1, partial vaporization of the water occurs with some drop of the temperature. The steam produced passes from the separator through a superheater and into the steam turbine. The exhaust steam from the turbine is condensed. The condensate again enters the reactor.

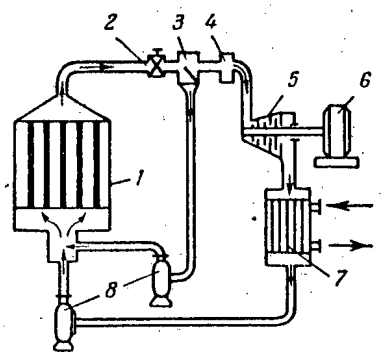

Fig. 3. System with closed circuit and self-vaporization of the water to produce steam.
1) Reactor; 2) self-vaporizer; 3) separator; 4) fire-heated superheater; 5) steam turbine; 6) generator; 7) condenser; 8) pumps.

If the enthalpy of the water entering the self-vaporizer is J_1, that of the water leaving the self-vaporizer is J_2, and the latent heat of vaporization is r (for the input pressure of the turbine), then from 1 kg of water circulating through the system the following quantity of steam can be obtained:

$$g = \frac{J_1 - J_2}{r} \frac{\text{kg steam}}{\text{kg water}}$$

By cooling the separated water the load of circulating water can be reduced. The water used to cool the circulating water can be used for space-heating purposes.

A disadvantage of this system is the radioactivity of the steam turbine and of the mains to the turbine, which comes about because of the presence in the water of activated impurities. To free the water from the latter it is proposed to include purifying devices in the system.

Systems of Heat Removal by Boiling Water or a Steam-Water Emulsion [1,10,12]

System with boiling of the water in the reactor (Fig. 4). Water at temperature t_1 is sent by a pump into the reactor, where it is heated to the boiling temperature t_b, vaporized and superheated to the temperature t_2. The steam produced is sent directly into the turbine. The condensate is sent back into the reactor.

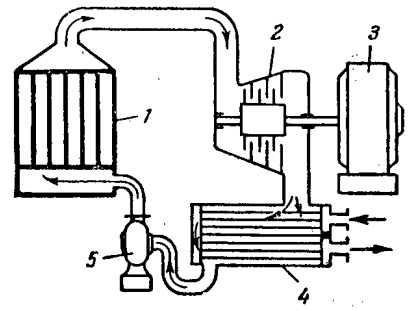

Fig. 4. System for boiling water in the reactor.
1) Reactor; 2) steam turbine; 3) generator; 4) condenser; 5) pump.

The quantity of heat removed from the reactor is

$$Q = g \cdot \underbrace{c_p^W (t_к - t_1)}_{\text{To heat water}} + \underbrace{g \cdot r}_{\text{To vaporize}} + \underbrace{g \cdot c_p^S (t_2 - t_1)}_{\text{To superheat steam}} \text{ kcal/hr}$$

Since the development of heat is nonuniform along the radius of the reactor and the thermal coefficients are not the same for the water, steam-water emulsion, and steam individually, the idea suggests itself of a reactor consisting of several zones. The water is fed into the central zone, where the energy release is greatest, so as to provide the most effective removal of heat. In this zone the water is partially converted into steam. From the succeeding annular zones with less rapid development of heat, it can be removed in a suitable way by the resulting steam-water emulsion and by the steam, which becomes superheated in the outermost channels (Fig. 5). The reactor consists of the economizer zone A and the steam generation zone B, in which the water is boiled and the steam is superheated. The superheated steam is sent into the turbine, and then condensed; the condensate goes back into the reactor.

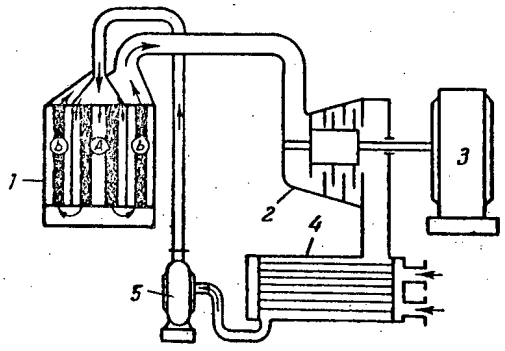

Fig. 5. System with zonal removal of heat from the reactor.
1) Zonal reactor; 2) steam turbine; 3) generator; 4) condenser; 5) pump.

One of the types of practical use of the system under consideration, as applied to an airplane propellor motor, is shown in Fig. 6. Here the cooling of the condensers is provided by the surrounding air.

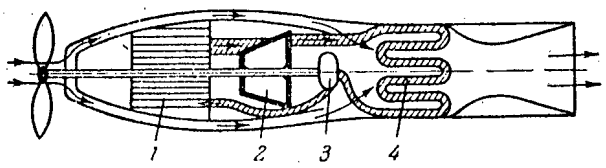

Fig. 6. Possible system for an airplane motor.
1) Reactor; 2) steam turbine; 3) pump; 4) condensers.

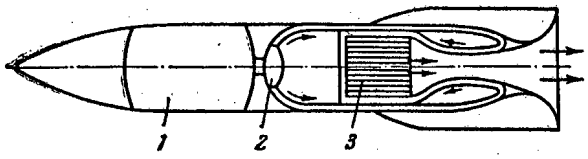

Fig. 7. Direct-flow open-circuit system.
1) Tank for liquid; 2) pump; 3) reactor.

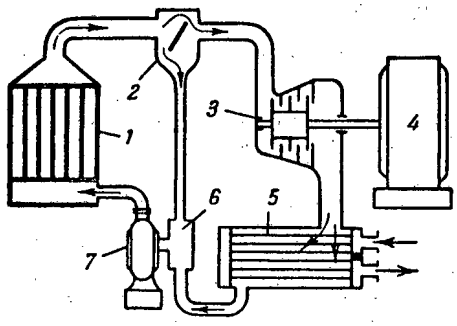

Fig. 8. Closed circuit with partial vaporization of the water and separation of the steam.
1) Reactor; 2) separator; 3) steam turbine; 4) generator; 5) condenser; 6) mixer; 7) pump.

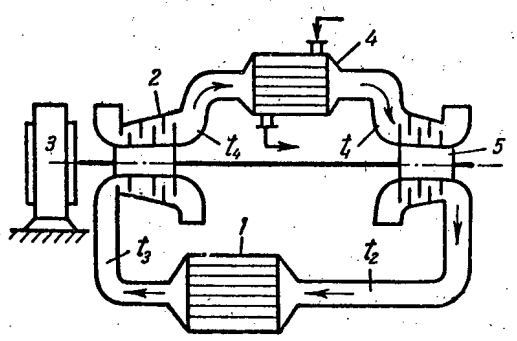

Fig. 9. Closed circuit with gas in reactor at constant pressure.
1) Reactor; 2) gas turbine; 3) generator; 4) heat exchanger; 5) turbocompressor.

Direct-flow system with open circuit. A liquid is forced by a pump into the reactor, where it is converted into superheated steam, which is ejected through a nozzle into the surrounding medium, producing a reaction thrust. Rocket motors can be devised on such a principle (Fig. 7).

Closed circuit with partial vaporization of the water and separation of the steam (Fig. 8). The water fed into the reactor is partly turned into steam. The steam-water emulsion thus formed is sent into a separator, where the steam is separated from the water. The wet steam is sent into the superheater, and then into the steam turbine. The condensate from the exhaust steam is then sent into a mixer, where it is combined with the water from the separator. The resulting mixture is forced by a pump into the reactor.

An advantage of such a system is the relatively low speed of the steam-water emulsion in the reactor channels in comparison with the speeds of the steam in steam heat-removal systems, as well as the smaller difference between the densities of the heat-transfer material entering and leaving the reactor. A disadvantage is the unproductive expenditure of energy by the circulation of the unvaporized part of the water.

Systems with Gaseous Heat-Transfer Medium

Closed circuit with constant gas pressure in the reactor [2,5,7]. The simplest heat removal system with the heat-transfer agent circulating in a closed circuit and with an auxiliary gas turbine is shown in Fig. 9.

Gas at pressure p and temperature t_2 is fed from the turbocompressor into the reactor, where it is heated to temperature t_3 and then goes to the gas turbine. In the turbine the gas expands, so that its temperature falls to t_4. The gas passes on through a heat exchanger, where it is cooled to the temperature t_1, i.e. it returns to its initial state, having completed the thermodynamic cycle shown in Fig. 10 on the p-v diagram and on the t-s diagram.

Closed circuit with regenerative heating of the gas in a heat exchanger and constant pressure in the reactor [11] (Fig. 11). This differs from the preceding system by the partial utilization of the heat from the exhaust gas to warm the gas entering the reactor. Gas from the compressor at temperature t_1 passes through the intermediate heat exchanger, where it is heated to the temperature t_2 by the gas coming from the gas turbine.

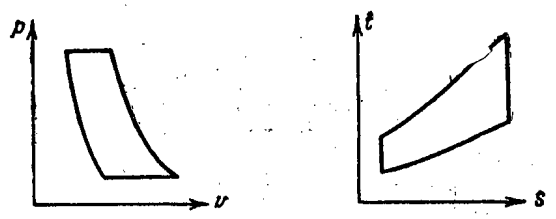

Fig. 10. P-v and t-s diagrams of the closed cycle for the heat remover.

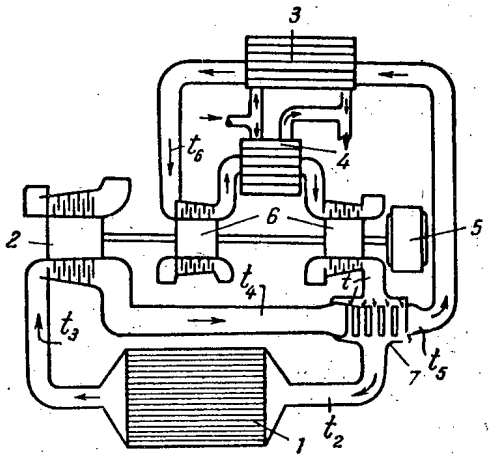

Fig. 11. Closed circuit with regenerative heating of the gas in a heat exchanger and constant pressure in the reactor.
1) Reactor; 2) gas turbine; 3) heat exchanger; 4) heat exchanger; 5) generator; 6) compressors; 7) heat exchanger.

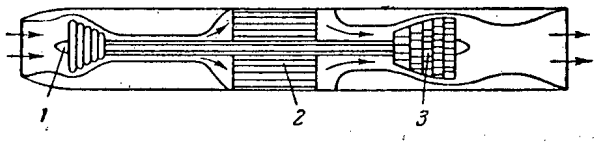

Fig. 12. Open circuit with constant gas pressure in the reactor (as applied to a turboreactive motor).
1) Turbocompressor; 2) reactor; 3) gas turbine.

Open circuit with constant gas pressure in the reactor [4,11]. A possible system for a turboreactive aircraft motor is shown in Fig. 12. Atmospheric air is compressed by the turbocompressor and heated in the reactor. The hot gas goes through the gas turbine and is ejected into the atmosphere.

It is possible to combine the use of nuclear and chemical fuels to intensify the heating of the gas. One type of this class of systems is shown in Fig. 13.

After passing through the compressor, the air from the atmosphere is used in two ways. Part of the air goes to a mixer, where it is mixed with fuel. The resulting mixture goes through the nuclear reactor, is heated, and passes into the combustion chamber. The products of combustion are ejected through the nozzle into the atmosphere. The other part of the air is used to cool the combustion chamber. The heated air drives a gas turbine and is exhausted into the atmosphere. The gas turbine serves to work the compressor.

As another example of a system with an open circuit we can consider that shown in Fig. 14. A turbocompressor mounted on the same shaft with the gas turbine can produce adiabatic compression of the air as well as isothermal compression. The compressed air fills the intake chamber and passes into the reactor space when the inlet valve opens. The air in the reactor chamber is heated (as a result of which its pressure rises), and is then released when the outlet valve opens. Both valves are operated by a special distributive mechanism.

Heat removal system with the gas heated without a compressor [9]. Systems of this type can be divided into continuous systems (P = const) and pulsed systems (v = const).

Fig. 15 shows the system of a reactive projectile driven by the passage of air through the diffuser into the reactor and the ejection of the hot air into the atmosphere through a nozzle. The means of removing heat from the reactor are chosen suitably for subsonic projectile speeds and for speeds exceeding that of sound.

Removal of Heat by Liquid Metals

The simplest two-circuit heat removal system [2,13]. The liquid metal circulates in the first circuit, which includes the reactor, the heat exchanger, and a pump. The second circuit uses water (Fig. 16). The quantity of heat removed from the reactor is given by the expression

$$Q = g_{\text{м}} c_p^{\text{м}} (t_2 - t_1),$$

where g is the rate of passage of the liquid metal (kg/hr), $c_p^{\text{м}}$ is the heat capacity of the liquid metal (kcal/kg °C), t_1 is the temperature of the liquid metal entering the reactor, and t_2 is the temperature of the liquid metal leaving the reactor.

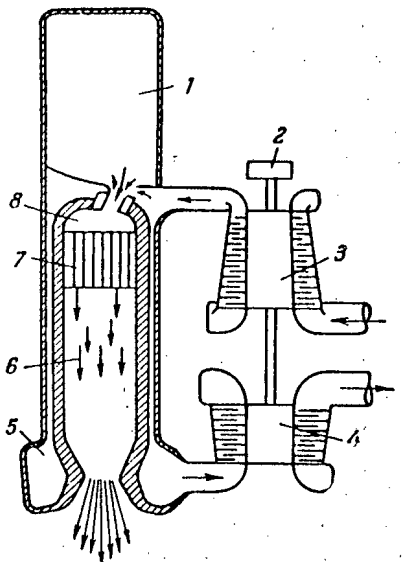

Fig. 13. One of the possible rocket systems with the chemical fuel first heated in the reactor and then burned in the combustion chamber.
1) Chemical fuel; 2) starting motor; 3) compressor; 4) gas turbine; 5) cooling jacket; 6) combustion chamber; 7) reactor; 8) mixer.

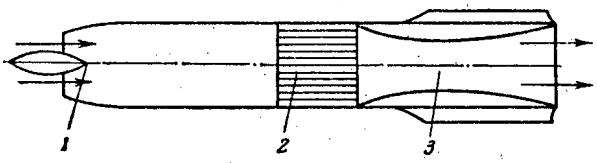

Fig. 15. System of a reactive projectile with the gas heated without a compressor.
1) Diffuser; 2) reactor; 3) exhaust nozzle.

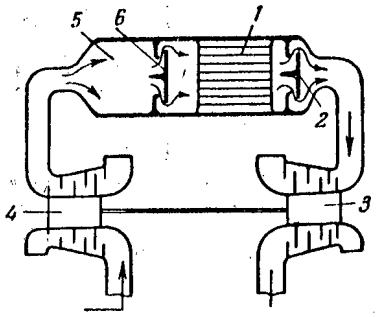

Fig. 14. Another possible type of open-circuit system.
1) Reactor; 2) outlet valve; 3) gas turbine; 4) compressor; 5) intake chamber; 6) inlet valve.

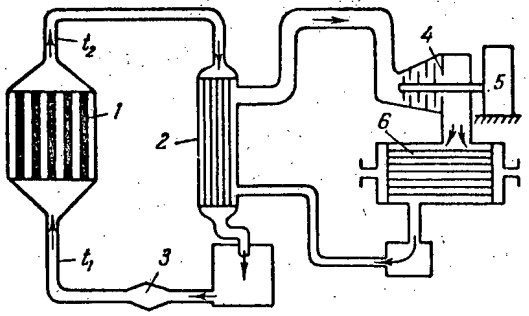

Fig. 16. Simplest system with liquid metal heat-transfer agent.
1) Reactor; 2) heat exchanger; 3) pump for liquid metal; 4) turbine; 5) generator; 6) condenser.

In the heat exchanger the heat is transferred to the water circuit. The water vapor formed is superheated and passes into the steam turbine.

The advantage of the use of liquid metals as heat-transfer agents consists in the fact that owing to the high boiling temperatures of liquid metals a high temperature of the heat-transfer agent leaving the reactor can be used without the application of pressure. The high temperatures of the liquid metals in turn make it possible to produce steam with high parameters.

Ordinarily the maximum temperature of the liquid metal is limited by the stability of the construction materials against corrosion. Examples of substances that can be used as liquid-metal heat-transfer agents are sodium, potassium, an alloy of sodium with potassium, lead, mercury, etc.

In the great majority of cases liquid-metal heat-transfer agents have high temperatures of solidification. This requires that there be provided a special system for heating the pipes and the various components of the system; this is turned on when the reactor is started, to prevent the formation of solid metal obstructions. Moreover, since the liquid metals are rapidly oxidized by air, arrangements are devised to provide buffer layers of inert gas over any open surfaces of the liquid metal.

High-pressure heat removal systems [11]. Heat removal from a reactor by means of boiling mercury as heat-transfer agent is accomplished at high pressure.

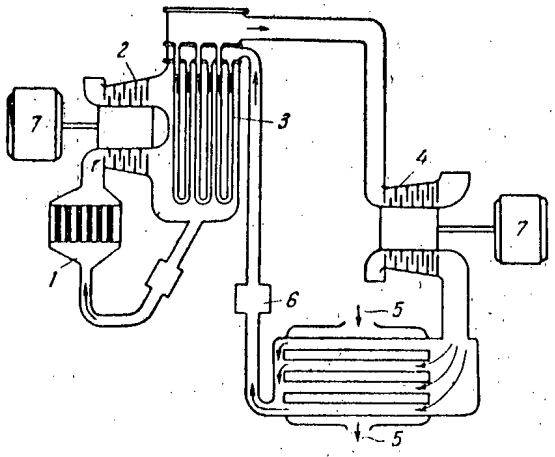

Fig. 17. Boiling-mercury heat-removal system with high-pressure circuit.
1) Reactor; 2) mercury-vapor turbine; 3) condenser for mercury and vaporizer for water; 4) steam turbine; 5) condenser; 6) pump; 7) generator.

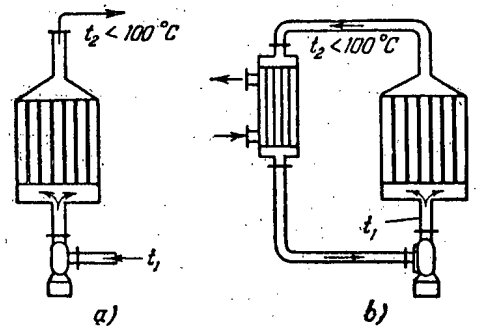

Fig. 18. Possible heat removal systems for nuclear reactors not used for power.

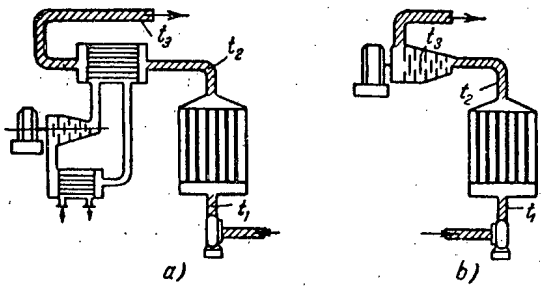

Fig. 19. Possible heat removal systems for nuclear reactors (open circuit).

The mercury vapor at somewhat elevated pressure passes through a mercury-vapor turbine (Fig. 17) and is then condensed; the mercury is then returned to the reactor by means of a pump.

The condenser for the mercury serves at the same time as a steam generator. A water pump sends water into the mercury condenser, where the water is converted into superheated steam. This steam, produced by the condensation of the mercury, is used in a steam turbine.

Such a system is called a binary-cycle system, and provides a high thermal efficiency, since in this case the total work includes the work from the mercury-vapor turbine and that from the steam turbine.

Classification of Heat Removal Systems

It is convenient to divide the systems that have been considered into two main groups.

To the first group belong systems in which the use of the heat to produce power is not intended; to the second, the heat removal systems of power reactors.

The first group in turn divides into two subgroups: systems with open and those with closed circuits for the circulation of the heat-transfer agent. In an open-circuit system (Fig. 18,a) a pump or compressor drives material at temperature t_1 into the reactor, from which the material emerges at temperature t_2 and is not reused. Such a system is used in cases in which ordinary water or air serves as heat-transfer material.

In a closed-circuit system (Fig. 18,b) the heat-transfer agent at the high temperature t_2 goes from the reactor into a heat exchanger, where it is cooled to the temperature t_1 and then is forced back into the reactor by a pump or compressor. The heat exchanger serves for the removal of heat from the heat-transfer agent by a secondary heat-transfer agent.

The main special feature of systems of the first group, in which no use of the heat for power is intended, is the relatively low temperature of the heat-transfer material leaving the reactor; ordinarily it is not over 100°C.

The second group of systems, like the first, can be divided into two subgroups: those with open and those with closed circuits for the heat-transfer material.

Possible heat removal systems for power reactors are shown in Fig. 19,a and b and Fig. 20,a and b.

Figure 19,a shows a system in which the heat-transfer agent is not the working substance. In this case the heat-transfer agent at temperature t_1 is driven by a compressor or pump into the reactor, where it is heated to the temperature t_2, after which it is cooled to temperature t_3 in the heat exchanger and ejected from the system.

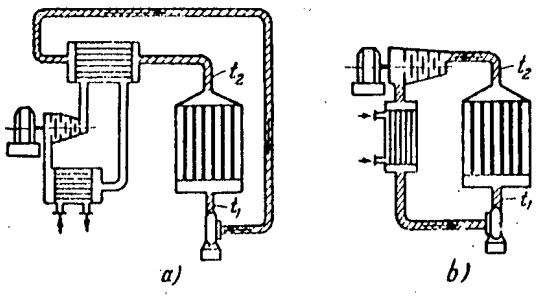

Fig. 20. Possible heat removal systems for nuclear power reactors (closed circuit).

The cooling of the heat-transfer agent from temperature t_2 to the temperature t_3 provides the necessary conditions for the operation of a turbine in the secondary circuit.

The distinctive characteristic of such a system is the possibility of removing heat from the reactor with a low pressure of the heat-transfer material in the primary circuit. For example, if atmospheric air going through the reactor is heated to the temperature t_2 = 500°C, and is then cooled in the heat exchanger to the temperature t_3 = 150°C, superheated steam at 20 atm. pressure can be produced in the second circuit for the operation of the turbine.

A system in which the heat-transfer agent is at the same time the working substance is shown in Fig. 19,b. Here the heat-transfer agent at temperature t_1 is driven by a compressor or pump into the reactor, where it is heated to the temperature t_2, and then passes into the turbine. After use in the turbine the heat-transfer agent is ejected at temperature t_3.

Such a heat removal system can be used in a turboreactive motor or a rocket motor. In the first case the air is compressed by a compressor, then heated in the reactor and sent through the gas turbine, from which it is ejected into the atmosphere through a nozzle.

In the second case the working liquid is forced into the reactor by a pump and vaporized; the vapor is sent either into a nozzle or into a turbine, and is ejected into the surrounding medium.

Power-reactor heat removal systems with the heat-transfer agent circulating in a closed circuit are shown in Fig. 20. In the first case (Fig. 20,a) the heat-transfer agent taking heat from the reactor goes into a heat exchanger. Here the heat is transferred to the secondary heat-transfer material, which drives the turbogenerator.

The advantage of the two-circuit system lies in the fact that the first, radioactive, heat-transfer material is separated from the second, which makes it possible to service the equipment in the power circuit, since it is not radioactive. In the second kind of system (Fig. 20,b) the circulating heat-transfer material is at the same time the working substance.

In this case the heat-transfer material goes directly to the turbogenerator, from which it is returned to the reactor by a pump or a compressor. In such a system the heat-transfer agent enters the turbine at an elevated pressure, and consequently the reactor is also at an elevated pressure. Moreover, the servicing of the turbines is rendered difficult because of the radioactivity of the heat-transfer material.

LITERATURE CITED

[1] Atomic Energy, Reports of foreign scientists at the International Conference on the Peaceful Uses of Atomic Energy (State Power Press, 1956).

[2] M. P. Vukalovich and I. I. Novikov, Technical Thermodynamics (State Power Press, 1952 and 1955).

[3] R. Murray, Introduction to Nuclear Technology (Foreign Lit. Press, 1955). (Translation).

[4] Atomic Energy (New Data), Translation, V. Ya. Fridman, editor (Foreign Lit. Press, 1954).

[5] W. Massey, Atoms and Energy (London, 1953).

[6] O. Condliffe, Chem. Eng. 53, 10 (1946).

[7] S. Glasstone and M. Edlund, Basic Theory of Nuclear Reactors (Foreign Lit. Press, 1954). (Translation.)

[8] C. Goodman (C. Goodman, editor), Scientific and Technical Foundations of Nuclear Power, vol. 1 (Foreign Lit. Press, 1949). (Translation).

[9] Ibid, vol. 2 (1950).

[10] V. P. Blyudov, D. N. Vyrubov, et al., General Thermal Technology (State Power Press, 1948).

[11] Applied Atomic Power, S. C. Smith, ed. (Prentice Hall, Inc., New York, 1946).

[12] Woodruff, Nucleonics 1953, No. 6, 7.

[13] Reports to the U.S. Atomic Energy Commission on Nuclear Power Reactor Technology (AEC, Washington, May, 1953).

Received April 20, 1956.

ON THE INFLUENCE OF ATOMIC EXPLOSIONS ON METEOROLOGICAL PROCESSES

E.K. Fedorov

We consider the influence of the physical processes arising as results of atomic explosions on the meteorological factors of the earth's atmosphere. Calculations based on an analysis of the existing data show that the thermodynamical effect of an explosion is insignificant and can have no important effect on meteorological processes. Some changes of weather can be caused indirectly by the considerable disturbance of the electrical properties of the atmosphere and the consequent intensification of processes of condensation. In order of magnitude these changes may be comparable with the changes of weather caused by the periodic variations of solar activity.

Atomic explosions release large quantities of energy, comparable with the energies of some meteorological processes, and produce changes in various physical properties of the atmosphere. Some of these changes are small in comparison with the natural variations of the state of the atmosphere; other changes are of significant size and can be detected at great distances.

Owing to this the question arises as to the possibility and nature of influences of atomic explosions on weather and climate. This has been the subject of a large number of papers that have appeared in recent years in foreign specialized and general literature [1-7], and a well known declaration of the Japanese Meteorological Society [8].

In considering this question it is necessary to define accurately what is meant by an influence on weather and climate, and what physical parameters or phenomena in the atmosphere are under discussion. We will include here those that have an important significance for present-day human activity, namely: the temperature of the air, the amount of precipitation, the degree of cloudiness, the winds.

It is well known that these features of the weather, like all others as well, are constantly changing over considerable ranges at any given point of the earth's surface. The changes noted include oscillations with daily and annual periods, and episodic changes connected with the development of synoptic processes.

Obviously the changes in the weather perhaps produced by atomic explosions can be of practical importance, if in order of magnitude and in the space they occupy, they are larger than or of the same size as those that occur daily in a natural way. This is true both for any given state of the weather and for changes in the sizes of the mean or most probable values of the meteorological quantities that characterize the climate of a region.

Finally, it must be taken into account that besides the immediate, direct effect of an explosion on atmospheric phenomena, an indirect effect is also to be expected.

The point is that the basic physical processes in the atmosphere – the motion of air masses, the evaporation and condensation of water, the exchange of heat between land and sea surfaces and the atmosphere – are in a state of dynamical equilibrium. In some cases this equilibrium is of an unstable type, and a disturbance that is relatively small as regards its energy can lead to a change in the character of the processes on an incomparably greater scale. Obviously an atomic explosion must also be considered from this point of view.

It is also necessary to specify somewhat more precisely the energy of the atomic explosion. We shall consider two types of explosions: the so-called nominal atomic bomb, which is equivalent in its destructive

power to 20,000 tons of TNT, and the large hydrogen bomb with an equivalent of 20 million tons of TNT. As is well known, the atomic bombs dropped by the Americans on the Japanese cities Hiroshima and Nagasaki were of power close to that of the nominal atomic bomb. The hydrogen bombs exploded in tests in the years 1954 and 1955 had equivalents of several millions of tons of TNT.

We consider below the physical changes occurring in the atmosphere as the result of an explosion, and also the possibility of an influence of these changes on the practically important features of the weather.

Heating

A considerable part of the energy of an explosion is dispersed in the form of thermal radiation, as a result of which the earth's surface and the atmosphere in the surrounding region are heated. The calculation of the thermal energy dispersed from the explosion and the accurate determination of its absorption in the atmosphere and at the surface of the earth are rather complicated tasks, but for our purposes only an extremely rough estimate is required.

The quantity of energy radiated in the explosion of a nominal atomic bomb is about $7 \cdot 10^{12}$ cal,* and in the explosion of a large hydrogen bomb about $7 \cdot 10^{15}$ cal. A considerable part of the energy of the shock wave from the explosion also results finally in the heating of the atmosphere and the surface of the earth in the surrounding region. Thus we may assume that approximately, but not more than, 10^{13} cal for a nominal bomb and 10^{16} cal for a large hydrogen bomb goes to heat the air and the surface of the earth in the region of the explosion.

This thermal energy is spread through the large volumes of air masses. We shall stipulate that the limits of the region in which appreciable heating of the atmosphere occurs are at such a distance from the place of the explosion that the magnitude of the integrated flux of radiant energy is 1 cal/cm^2. This corresponds to the integrated flux of radiant energy from the sun incident on the surface of the earth in one minute on a summer day of average brightness. We note that the energy of the explosion of an atomic bomb is almost completely transformed into thermal energy during the first minute after the explosion. Then the territory over which the air is heated to an appreciable degree is that of a circle of diameter 5 to 10 km for a nominal bomb and 50 to 100 km for a large hydrogen bomb. The areas of these territories will be about 50 sq km and 5000 sq km respectively. Calculations show that on the indicated areas the total quantity of heat expended in the heating of the surface of the earth and of the air by an atomic explosion corresponds to the heating by the sun during several hours on a summer day of average brightness.

It is known that a cloud layer reflects about 60% of the solar energy falling on it. During a total eclipse of the sun the incidence of direct solar radiation on the shadowed part of the surface of the earth is almost entirely cut off.** Thus the thermal action of an atomic explosion can be compared, in the degree of heating of the earth's surface and of the air above it, with the variations of the thermal balance that occur with changeable cloudiness or with a total solar eclipse.

One more example can be given of the disturbance of the thermal balance. In the seeding of undercooled clouds, of common occurrence in winter, by scattering solid carbon dioxide in the clouds, large volumes of the clouds, of the order of 10^4 km^3, are made to go over into the crystalline state. It is easy to calculate that with a water content in the clouds of about 0.3 gm/m^3 there is thus developed about $2 \cdot 10^{14}$ cal of heat from the liberation of the latent heat of crystallization, over an area of diameter about 70 km. In such cases no important changes in the weather are produced, and the cloud is dispersed as the result of other processes.

Here we have compared the effect of an atomic explosion with some processes in the atmosphere in terms of the total amount of thermal energy. But the energy of the explosion is produced in a short interval of time and is distributed extremely unevenly in space, while the variation in the thermal balance in the case of variable cloudiness or of the crystallization of clouds occurs tens of times more slowly and is uniform over a whole region. It must be supposed that this circumstance can only decrease the effectiveness of the action of the explosion on the atmospheric processes, since their characteristic time considerably exceeds the time during which the thermal energy of the explosion is produced.

*These and other data on the action of the explosions are taken from foreign published papers (references [1, 9,10] and others).

**Theoretical calculations and observations during total eclipses of the sun have shown that the temperature of the air falls by 2 to 3 degrees, and the temperature of the soil by 10 degrees [23].

Obviously the direct effect of the heating from an atomic explosion will be a small increase of the thermal convection in the lower layers of the atmosphere in the region surrounding the epicenter of the explosion.

It is possible that under some combination of conditions in the surrounding atmosphere that is particularly favorable for the production of such an effect, the explosion will stimulate small changes in the synoptic processes, which otherwise would occur somewhat later.

The Ascending Current

The fireball formed in the explosion begins to rise immediately after its formation, mainly owing to the force of bouyancy. The ascent of the fireball is accompanied by a strong rising air current, which draws with it the surrounding air. The water vapor drawn into the ascending current also rises, and owing to cooling condenses at a certain height. This leads to the formation of the mushroom-shaped cloud characteristic of an atomic explosion. The process of formation of this cloud resembles the development of an ordinary cumulus cloud, speeded up by a considerable factor.

If we calculate the energy expended in maintaining the ascending currents that feed a cumulus cloud, and compare it with the energy of atomic explosions, it turns out that a nominal atomic bomb and a small cumulus cloud on one hand, and a large hydrogen bomb and a rain or storm cloud on the other, have energies of about the same order.

But here it is necessary to point out one essential consideration. As is known from investigations carried out in recent years [11,12], cumulus clouds within air masses can develop not only owing to rising convective currents outside themselves, but also owing to the internal energy released in the condensation of water vapor. In this case each new quantity of water vapor drawn into the cumulus cloud and raised to high altitude releases energy by condensation, and perhaps more energy than was required to raise it. Thus a special sort of chain process is set up, which produces the development of cumulus clouds, at least beginning from a certain stage of their growth.

If one judges from the available data, such processes have not occurred in the case of atomic explosions. Here the formation of the cloud ends with the culmination of the ascending current. The energy released by the condensation of water vapor (the calculations show that this is several percent of the energy of the explosion), of course assist the development of the ascending current in this case too, but evidently not to such a degree as would lead to a chain process, i.e., to the prolonged existence of the ascending current.

Only in one case, namely that of the first explosion at Hiroshima, was there set up an ascending current lasting for several hours. It is quite possible that its cause was the fires in the city; this is the explanation given by all students of the case. It is known that in cases of large conflagrations, for example that following the earthquake at Yokohama, similar prolonged ascending currents have been established. In all the other atomic bomb explosions no prolonged ascending currents have been observed.

Accordingly the ascending current resulting from the dispersal of the fireball of a nominal atomic bomb leads to the formation of a cloud of the type of a small cumulus cloud, and that from the explosion of a large hydrogen bomb gives a large cloud, similar in size to a rain or storm cloud. Unlike those of natural occurrence, these clouds do not develop further, but disperse, since the original ascending current soon ceases, and the conditions favorable for a chain process of cloud formation are not established. It can be assumed that only in certain especially favorable conditions an atomic explosion can lead to the formation of a long-lasting and growing strong cumulus or cumulo-nimbus cloud.

Consequently, the thermodynamic action of an atomic explosion on the atmosphere, which involves almost all of its energy, is small in comparison with natural processes and does not have much effect, relative to the energy expended, in terms of either direct or indirect action.

A larger effect would be observed in the case of a less rapid expenditure of the same thermal energy.

Alteration of the Optical Properties of the Atmosphere

A ground explosion of an atomic bomb raises into the atmosphere a large amount of soil, broken up into small and very small particles, of sizes from millimeters to fractions of a micron. The largest fall to earth comparatively rapidly, but the smaller particles are in the atmosphere for a long time.

The presence of a large number of particles in the atmosphere leads to a change of its optical properties. Some part of the solar energy will be scattered from the particles and be reflected, in the same way as this

happens when this energy falls on the surface of clouds.

The screening effect of the dust cloud will be smaller in relation to the radiation of longer wavelengths emitted by the surface of the earth; therefore on the whole the dust in the atmosphere leads to a reduction of the amount of heat received from the sun.

As is well known, the explosion of the volcano Krakatoa at the end of the last century (1883) threw up into the air a large number of solid particles, which were carried about in the upper layers of the atmosphere for 2 to 3 years. Approximate calculations show that in the destruction of the volcano about 50 km^3 of ashes and lava were thrown out. Evidently about a third of this amount ($5 \cdot 10^{10}$ tons) remained in the atmosphere for a prolonged period in the form of particles of small size [13,14].

Observations at actinometric stations in Europe showed that the dust clouds carried in the atmosphere lowered the amount of direct solar radiation incident on the earth's surface in the northern hemisphere to a marked extent, by approximately 10 to 20%. This effect lasted for several months.

The majority of investigators believe that the volcanic dust did not bring about any essential changes in the weather or climate, but some ascribe a significant role to this dust, and also to micrometeorites – particles entering the atmosphere from cosmic space; for example, they explain the occurrence of ice ages in terms of an intensification of volcanic activity, relate the exceptional harvests in certain districts to volcanic activity, and correlate the amount of precipitation with the micrometeorites [15,26,27].

At the present time sufficiently precise quantitative data do not exist for an estimate of the changes in the weather produced by the occurrence of volcanic dust or micrometeorites in the atmosphere.

It is difficult to determine the amount of solid material thrown up into the atmosphere in the explosions of atomic bombs. We shall suppose, with a probable overestimate by a moderate factor, that in a ground explosion of a large hydrogen bomb there will be caught up into the ascending air current a layer of soil of thickness 10 cm from an area of 100 sq km, i.e., $4 \cdot 10^7$ tons of earth.

Thus we can expect effects at least hundreds or thousands of times weaker than from the explosion of Krakatoa. Therefore one can scarcely expect any important changes in the optical properties of the earth's atmosphere and in weather phenomena as a result of the throwing of soil into the air, even in the case of the ground explosion of a large hydrogen bomb.

Increase of the Radioactivity of the Atmosphere and of the Earth's Surface

In the explosion a large quantity of radioactive products is formed. One minute after the explosion of a nominal bomb this quantity is equal to 10^{12} curies, and for the explosion of a large hydrogen bomb it is 10^{15} curies.

Almost all of these products, just after the explosion, are concentrated in the fireball, are then deposited on the particles of the cloud, i.e., on droplets of water, ice crystals, and solid particles of earth, thrown into the air and carried up into the cloud by the ascending current. The percentage of these last particles in the total mass of the cloud, and their average size, depend most strongly on the height of the explosion above the ground.

For a ground explosion the solid particles make up a considerable fraction of the material in the cloud, but for an explosion in the air they are a negligible fraction of the cloud. The average size of the particles of earth drawn into the cloud is decidedly greater for a ground explosion than for an air explosion.

The spreading of the radioactive products of the explosion in the atmosphere is determined by the motion of the droplets, crystals, and particles of earth on which they have been deposited.

Owing to this a certain fraction of the radioactive products, having been adsorbed on relatively large particles of earth, fall out with them in the region immediately adjacent to the place of the explosion, forming a zone of radioactive contamination, and another fraction, having been deposited on small particles, or remaining in the form of extremely minute particles after the evaporation of water droplets, will be carried about in the atmosphere for a long time, settling very slowly to the ground.

As is shown by the results of observations [10,16], even in ground bursts a comparatively small fraction of the radioactive products falls out in the zone nearest to the epicenter, and in air bursts this fraction is entirely negligible.

The actual picture of the dispersal of the atomic cloud in the atmosphere is very complicated [17], but it can be approximately characterized by the numbers given in the table.

Dispersal of Radioactive Material in the Atmosphere *

Time after explosion	Distance of center of cloud from place of explosion, km	20,000 ton explosion			20 million ton explosion		
		total activity, curies	volume of cloud, km^3	concentration, curie/km^3	total activity, curies	volume of cloud, km^3	concentration, curie/km^3
1 minute	1	10^{12}	1	10^{12}	10^{15}	10	10^{14}
1 hour	50	$6 \cdot 10^9$	$3 \cdot 10^2$	10^7	$6 \cdot 10^{14}$	10^4	10^{10}
1 day	1000	$1.3 \cdot 10^8$	$2 \cdot 10^5$	10^3	$1.3 \cdot 10^{11}$	10^5-10^6	10^6-10^5
1 week	7000	$1.3 \cdot 10^7$	10^6-10^7	10^{-1}	$1.3 \cdot 10^{10}$	10^6-10^7	10^4-10^3
1 month	–	$2.3 \cdot 10^6$	10^8-10^9	10^{-2}-10^{-3}	$2.3 \cdot 10^9$	10^8-10^9	1-10
1 year	–	$1.1 \cdot 10^5$	$\sim 10^9$	10^{-4}	$1.1 \cdot 10^8$	$\sim 10^9$	10^{-1}

*The data on the total amount of the radioactive products and the character of the decay are taken from reference [10]; the estimate of mixing has been carried out by the author.

The data of the table are derived without taking into account gravitational settling of the particles to the ground, adsorption of the particles on cloud droplets, and fall-out of radioactive materials accompanying precipitation.

According to the observations of Japanese scientists [18], 6 months after the well-known hydrogen bomb explosion at Bikini on March 1, 1954, which was equivalent to about 15 million tons of TNT, the content of radioactive products in the atmosphere was from 10^{-3} to 10^{-1} curie per km^3, which confirms the correctness of the estimates given in the table; in this case the concentration in the upper layers of the atmosphere was larger.

It is known that radioactive materials of natural origin are always present in the atmosphere. For the most part these are products of the disintegration of the emanations of radium and thorium. In the layer near the earth their concentration in the atmosphere amounts to about 10^{-13} curie per liter, or about 10^{-1} curie per km^3, which for the entire atmosphere (in a layer up to 10 km high) amounts to about 10^8-10^9 curies of radioactive products.

Thus when a large hydrogen bomb is exploded the amount of radioactive material suspended in the air, even after a month, will be several times as large as the total amount of natural radioactive substances contained in the atmosphere. During this time the active products will be distributed, not through the whole atmosphere, but in 0,01 to 0.1 part of its volume.

An analogous effect of a marked increase of the concentration of radioactive substances will be observed for some time on the earth's surface as well. As is well known, radioactive elements are present in definite quantities in surface rocks. The total content of radioactive substances in a surface layer of the soil about a centimeter thick amounts on the average to 1 curie per sq km, or $2 \cdot 10^8$ curie for the whole surface of the earth; consequently, the radioactive products formed in the explosion of a large hydrogen bomb and settling during several months in a nonuniform layer on some part of the earth's surface decidedly increase the surface concentration of radioactive substances over wide areas for a period up to several weeks. *

Besides the shortlived radioactive products, the nuclear reaction gives rise to some small quantity of longlived products, for example Sr^{90}.

According to the American data [16] the explosion of a large hydrogen bomb produces about 10^6 curies of Sr^{90}. In the surface layers of the soil the content is about 10^{-3} curies of strontium per sq km, i.e., about 10^5 curies in the entire dry-land surface of the earth. Consequently, after the explosion of a large hydrogen bomb the total amount of strontium on the contaminated part of the dry-land surface is increased by more than

*Besides the decrease through decay, the surface concentration of the radioactive substances that have fallen on the ground will be rapidly reduced because of scattering by the wind, washing away by rain water, etc.

an order of magnitude, so that for a long period the effective surface concentration of all radioactive substances in these regions is increased by approximately 1 to 2%.

Thus, unlike the other changes in the physical conditions, the effects of the radioactive contamination of the atmosphere and the land surface decidedly change the corresponding parameters of the earth's atmosphere over an enormous area, clear up through the entire troposphere, and for a comparatively long time.

The variations of the atmospheric radioactivity of natural origin are not large; they are mainly due to processes of turbulent mixing and transport in the atmosphere, owing to which the approximately constant amount of radioactive material passing from the soil to the atmosphere in unit time is distributed in the atmosphere in different ways. Owing to this, the concentration of radioactive materials of natural origin varies over a fairly wide range.

The rather small number of investigations so far made of the nature and condition of the natural radioactivity of the atmosphere have for the most part been directed toward determining the influence of meteorological conditions on the distribution of radioactive substances in the air, and the influence of these radioactive products, present in the air, on the basic meteorological processes remains unclear. Because of this, a quantitative estimate of the influence of increased concentrations of radioactive products appears impossible at present. Here we can only make some qualitative observations.

Thus, it can be supposed that an increase of the radioactive materials in the atmosphere increases the concentration of atmospheric ions.

The increase of the concentration of heavy ions and the change in the entire ionic balance will depend not only on the amount of radioactive products, but also on the presence of aerosol impurities in the atmosphere (dust, smoke). Calculations and observations have confirmed the existence of an increase of the conductivity of the atmosphere at considerable distances from the place of an explosion [19].

There is reason to believe that a change in the ionic balance will have an influence on the processes of condensation. It is well known that condensation can begin on charged particles at lower pressures of water vapor, i.e., charged condensation nuclei are more effective. Now, an increase of the concentration of ions cannot fail to lead to an increase in the number of charged particles in the atmosphere.

If no natural nuclei for condensation existed in the atmosphere, the appearance of large numbers of charged aerosol particles would have an important influence on the formation of clouds. But, as is clear from all the observations, the atmosphere, or at any rate the troposphere, ordinarily contains an adequate number of condensation nuclei. Therefore the radioactive products cannot have a large influence on the formation of clouds.

A raising of the effectiveness of the condensation nuclei or an increase in their number can change the condensation process only to a certain degree. For example, an increase in the number of condensation nuclei can lead to condensation of the water vapor on a larger number of nuclei and to the formation of smaller droplets. This can somewhat accelerate the formation of clouds, but retard the occurrence of precipitation.

It must be noted, however, that other conditions may occur in the stratosphere. Here, as can be concluded from several phenomena, there is sometimes an insufficiency of natural nuclei for condensation, and thus the admixture of radioactive products of an explosion can facilitate the formation of clouds.

The amount of water vapor in the stratosphere is very small, so that the clouds formed there will have a negligible moisture content and will not give any precipitation. But they change to some extent the optical properties of the upper layers of the atmosphere, and this effect is probably greater than that of the addition of dust, which we considered earlier, since the droplets or crystals formed on the particles are of larger size than the particles themselves.

An important process in the development of precipitation is the coalescence of cloud droplets, which leads to the formation of large drops, which can fall to the ground.

The greatest part in the development of precipitation is played by gravitational coalescence of the droplets, i.e., their collision and mutual coherence because of their different speeds of fall. But this sort of coalescence can begin only when the droplets have reached a certain definite size. The nature of the process of the initial growth of small drops is still not entirely clear.

Calculations made very recently have shown [20] that the coalescence of small drops in clouds can take

place considerably more rapidly when the drops are electrically charged. An increase of the concentration of heavy ions in the atmosphere leads to an increase of the charges on the droplets of a cloud, although the growth of the conductivity of the air, i.e., the increase of the concentration of light ions, will have the reverse effect. When one takes into account the presence of various admixtures in the atmosphere, the conclusion is that on the whole, it is more probable that there will be an increase of the charges on the droplets, i.e., an acceleration of the coalescence, when radioactive products are added, and consequently an increase of precipitation from the same quantity of clouds.

An increase of the ionization leads to certain chemical reactions in the atmosphere: to the formation of ozone, nitric oxide, and oxygen peroxide. All of these substances will also act in the direction of facilitating the process of condensation. It must be noted, however, that an estimate of the total amount of the chemical products, for example nitric oxide, appearing in the atmosphere as the result of an explosion, gives values comparable with the discharge of these products into the atmosphere by industrial establishments in the course of three or four months.

After an explosion an increase of the content of radioactive products is observed in the precipitation falling in the region of motion and dispersal of the radioactive cloud. This is readily explained by the fact that the radioactive aerosols are taken up by the cloud droplets and raindrops and thus are "washed out" of the atmosphere. *

Thus the introduction of large quantities of radioactive products into the atmosphere should in general provide means for increased condensation of water vapor, and possibly for some increase in the amount of precipitation. Data are not available at present for a quantitative estimate of this effect.

Both in the troposphere and in the stratosphere, the condensation of water vapor leads to some fogging of the atmosphere and to a reduction in the amount of solar radiation reaching the surface of the earth. In this connection it is quite likely that the fogging caused by droplets formed on charged aerosol particles will be considerably greater than that caused by the particles themselves.

Changes in the State of Meteorological Factors

Besides looking for physical causal connections between the effects of explosions and meteorological phenomena, we can try to discover changes in the normal course of meteorological processes before and after atomic explosions.

This problem can be solved in two ways. One way is to analyze the state of the weather in the vicinity of the discharge and in the region of the initial spread of the radioactive cloud, at distances of hundreds and thousands of kilometers from the epicenter.

Here we can expect relatively short-time effects (of duration 1 to 2 days), caused by the passage of radioactive products and dust at high concentration.

It is not hard to record the state of the weather in this region, but it is very difficult to determine what would have been the weather here in the absence of the explosion.

So far as we know, such investigations have not been carried out, but from the published material one can get the impression that no special phenomena were observed in the region in question. Accordingly, if there were indeed any changes in the weather, then they did not go beyond the limits of the fluctuations usually found in the given region at the time in question.

The other procedure consists in looking for effects of great duration caused by the action of the radioactive products and dust that are spread (at low concentration) over a considerable part of the earth.

From the considerations given earlier about the spreading of radioactive products, we can expect the appearance of these effects at widely separated places over the earth 15 to 30 days after the explosion, and most of the effect during the next 2 to 3 months.

The duration of the action at any place will obviously not be short, since during this period the radioactive products and the dust are dispersed through a considerable part of the whole volume of the atmosphere. This gives us a basis for looking for changes in the trend of the monthly mean values of meteorological factors

*It has long been known that radioactive materials of natural origin are also readily adsorbed by the particles of clouds and of precipitation and fall with them out of the atmosphere.

at various points on the earth. Unlike the state of the weather on a given day, the monthly mean values are fairly stable characteristics of the climate.

The hydrogen explosion of several million tons of TNT equivalent at the Bikini test of March 1, 1954 is clearly the most suitable for such an analysis.

We have compared the monthly mean values of the air temperature, humidity, amount of cloudiness, and wind speed at several stations in the USSR (Leningrad, Moscow, Sverdlovsk, Tashkent, Vladivostok) in March, April, and May of 1954 with the analogous data for the period 1900-1955. It was found that at all the stations the values in 1954 do not go outside the range of the values previously observed for the period 1900-1955. In this connection it may be noted that the departure of the observed values from the averages for many years is not such as to contradict our considerations about the possibility of a small increase of cloudiness and precipitation and a lowering of the temperature.

Similar work has been carried out in the USA [1]. The average values of meteorological factors observed at stations located in the USA show variations in the years 1953-1955 that are not larger than those that have taken place over the past 50 years.

An increase in the number of recorded hurricanes and large tornadoes has been noted in recent years in the USA. No concrete connection has been found between any of them and the atomic explosions – neither with respect to the time of occurrence, nor with respect to the place of origin. The American investigators [1] explain this increase in terms of the improved quality of the weather service and the whole system of observations of natural phenomena, and the more so, since the increase is in the small and weak cases. Indeed the number of the larger hurricanes, noticeable even with imperfect methods of observation, did not increase appreciably.

Thus the existing preliminary and admittedly approximate data show that after the large explosions there were not observed any disturbances in the weather that would exceed the ordinary variations typical for the region and time in question. Whether or not some changes in the weather within the range of its usual fluctuations were brought about, it will be possible to ascertain only by further careful studies.

A Possible Analogy With the Effect of Solar Activity

For many decades astrophysicists and meteorologists have studied the question of the influence on the earth's atmosphere of certain special phenomena occurring on the sun [21].

As is well known, from time to time there appear on the sun spots or protuberances, and sharp increases of the intensity of the ultraviolet and corpuscular radiations are observed.

Prolonged observations have shown that there is a periodicity in the frequency and intensity of these phenomena. The most characteristic is the eleven-year period, besides which there can be detected a period of 80 to 90 years, and some others.

Once having appeared, the sun spots and some other formations maintain themselves for several months, i.e., for several times the period of rotation of the sun on its axis (28 days). Owing to this, there is naturally also a 28-day period in the appearance of the spots and other formations.

Numerous and detailed studies of the connection of the solar activity and geophysical phenomena have made it possible to give a satisfactory account of the influence of individual manifestations of solar activity and of the over-all activity on processes of electromagnetic nature occurring in the upper layers of the atmosphere at a height of tens to hundreds of kilometers. Examples are magnetic storms, changes in the behavior of the ionized layers, auroras, etc.

The rather definite character of the connections that have been found makes it possible, as is well known, to give predictions of the state of the ionosphere (for example, for proper choice of wavelengths for radio communication) on the basis of the periodic properties of the solar activity.

There have also been known for a very long time periodic changes in the most varied phenomena occurring in or associated with the lower layers of the atmosphere, for example, changes in cyclonic activity, variations of the levels of lakes and seas, speed of growth of trees, and many others [22, 24, 25].

If these small variations are considered for intervals of time amounting to hundreds of years, a correlation

is found between them and the variations of solar activity. But it has not been possible as yet to trace a definite effect of any single concrete manifestation of the solar activity on the meteorological processes in the lower layers of the atmosphere. This is explained by the fact that it is extraordinarily difficult to distinguish the effect sought for amid the background of the continual fluctuations of the meteorological factors that occur through the action of the most varied causes. On the other hand, the great relative stability of the mean values of the meteorological factors makes it possible to detect even small effects when systematically repeated. Up to now we also lack clear understanding with regard to the mechanism of such action, although many hypotheses have been put forward.

Since a large part of the radiations associated with the manifestations of solar activity do not reach the lower layers of the atmosphere, the action is primarily on the behavior of the stratosphere, with subsequent transmission of the effect to the lower layers. It may be supposed that in one way or another the manifestations of solar activity have a small but appreciable effect on the behavior of the lower layers of the atmosphere.

It is important to note that some effects produced by the corpuscular and ultraviolet radiations in the earth's atmosphere are comparable in their nature and scale with those that may occur from the dispersal in its upper layers of the radioactive products from atomic explosions. In one case,as in the other, the main point is evidently the considerable increase in the ionization.

As may be concluded from the peculiarities of magnetic storms and ionospheric disturbances, the variations in the flow of corpuscular and ultraviolet radiations from the sun owing to the different states of solar activity amount to tens or hundreds of percent.

The changes in the electrical state of considerable volumes of the atmosphere brought about by atomic explosions can, as we have seen above, be of the same order of magnitude over a period of several months.

On the basis of the indicated analogy it may be surmised that the ejection of radioactive products into the atmosphere by the explosions of large hydrogen bombs can in some indirect way bring about changes in meteorological processes. These changes can evidently be similar in nature and order of magnitude to those that are brought about by variations in solar activity.

SUMMARY

1. A consideration of the physical processes in the atmosphere that are developed as a result of an atomic explosion, and of the data from meteorological observations, provides a basis for the conclusion that an explosion (even in the case of a hydrogen bomb equivalent in power to several million tons of TNT) cannot lead to changes in the state of the practically important weather factors that would exceed their natural variations that are typical for a given region and period of time.

The thermodynamic effect of the explosion, in which almost all of its energy is expended, has the least (a negligible) effect on the state of the weather.

2. The question as to whether, as a result of an atomic explosion, there could occur changes in the weather which would be appreciable, though not exceeding its usual range of variation, must for the present be regarded as open.

There is reason to suppose that important disturbances in the state of the electrical properties, extending through considerable volumes of the atmosphere and over a long period of time (several weeks), could lead to changes in the weather in an indirect way (mainly through processes of condensation of moisture).

Further study of the role of electrical phenomena in the basic meteorological processes, investigation of the optical properties of atmospheric aerosols, elucidation of the physical mechanism of the effect of solar activity on the processes in the atmosphere, and careful study of the synoptic situation as related to the explosions that have taken place give promise of an answer to this question.

LITERATURE CITED

[1] L. Machta and D.L. Harris, Science 121, 3134, 75 (1955).

[2] Habert Garrigue, Comptes rend. 232, 10, 1003 (1951).

[3] B.J. Mason, Weather 5, 139 (1955).

[4] B. Holzman, Weatherwise 4, 1,3 (1951).

[5] J. Roy, Astr. Soc. Can. 47, 6, 253 (1953).

[6] Horst Teichmann, Naturwissenschaften 41, 21, 498 (1954).

[7] Charles-Noel Mortin, Compt. rend. 239, 20, 1287 (1954).

[8] Pravda, July 8, 1954.

[9] The Effect of Atomic Weapons, Atomic Energy Commission (Washington, 1950).

[10] Howard L. Andrews, Science 122, 3167, 453 (1955).

[11] R. Braham Roscoe, Jr., J. Meteorol. 9, 4, 227 (1952).

[12] N.I. Vulfson, Proc. Acad. Sci. USSR 97, 1, 77 (1954).

[13] H. Wexler, Bull. Am. Meteorol. Soc. 32, 1, 10 (1953).

[14] H. Wexler, Bull. Am. Meteorol. Soc. 32, 2, 48 (1951).

[15] W.J. Humphreys, Physics of the Air (New York, 1940).

[16] Willard F. Libby, Bull. Atomic Scientists XI, 7, 256 (1955).

[17] Neuwirth, Geofisica pura e applicata 32, 3, 147 (1955).

[18] Yasuchi Nishiwaki, Atom. Scient. J. 4, 5, 279 (1955).

[19] D. Lee Harris, J. Geophys. Research 60, 1 (1955).

[20] L.M. Levin, Proc. Acad. Sci. USSR 94, 3, 462 (1954).

[21] Eigenson, Gnevyshev, Ol and Rubashev, Solar Activity and Its Terrestrial Manifestations (Moscow-Leningrad, 1948).

[22] I.V. Maksimov, Bull. Acad. Sci. USSR, Geog. Ser. No. 1, 15 (1954).

[23] A.A. Dmitriev, G.V. Bonchkovskaia and G.A. Kalinina, Proc. Acad. Sci. USSR 103, 4, 597 (1955).

[24] A.A. Dmitriev, Meteorology and Hydrology 1949, 5.

[25] A.A. Dmitriev, "Consideration of some modes of action of solar activity on the circulation of the atmosphere," Bull. Acad. Sci. USSR, Geophys. Ser. (in press).

[26] Staff members of the Forecast Research Laboratory, Geophys. Mag. (Tokyo) 26, 3, 231 (1955).

[27] E.G. Bowly, J. Meteorol. 13, 2, 142 (1956).

Received July 5, 1956.

CONTRIBUTION TO THE PROBLEM OF THE FORM OF URANIUM IN PHOSPHORITES

I. G. Chentsov

Results of the investigation of apatite separated out of uranium-bearing phosphorites are presented. The entrance of uranium into the apatite (uranoapatite) crystal lattice is established, from which it follows that apatite is one of the bearers of uranium in phosphorites.

Phosphorites are often uranium ores. Some phosphatized fossils contain up to 0.5% and more uranium in the phosphatic material. Distinct uranium minerals are not always revealed in phosphorites and carbonaceous shales containing uranium. Most of the uranium in them is connected with organic and phosphatic material and occurs in a disseminated form. With solution of such phosphorites in weak acid, the uranium goes into solution and often appears in the tetravalent state. Uranium, together with calcium phosphate, is also extracted by acid from carbonaceous shales. The geochemical conditions in which formation of uranium-bearing phosphorites and carbonaceous shales occur are diverse. Some of them form in mildly aerating conditions; others form in strongly aerating conditions and, it follows, in a medium with a high oxidizing potential.

The primary taking-up of uranium from sea water and other natural solutions by phosphate material most probably occurred as a result of sorption and precipitation of uranium compounds and calcium phosphates. With formation of phosphorites rich in organic material and with formation of carbonaceous shales, the organic material which was the primary sorbent and concentrator of many elements, including uranium and phosphoric acid (phosphates of calcium), played an important part in the sorption and precipitation of uranium compounds. At the time of deposition of the muds of the majority of phosphorites and carbonaceous shales, the uranium was apparently in a hexavalent state, and its compounds – uranophosphates, urano-organic complexes, and others – precipitated with the phosphates and organic materials. Subsequently, when the mud formed into rock, reactions of reduction of hexavalent to tetravalent uranium occurred, and the possibility of isomorphous replacement of calcium in apatite by uranium arose. During transformation of the organic material, the urano-organic complexes freed the previously absorbed uranium compounds. Since phosphorites contain a low concentration of uranium and are often contaminated by impurities, it is difficult to establish the form of the connection of uranium with the phosphate substance.

During study of uranium-bearing phosphorites and carbonaceous shales of several deposits, we were able to separate pure crystalline apatitic material strongly enriched by uranium. Careful microscopic study showed the homogeneity of the crystals separated and the absence of mechanical admixtures in them. The crystals were determined as apatite. In association with the apatite were found calcium carbonate and pyrite, which were completely distinct from the apatite crystals. The samples were free from the organic material which often colors phosphorites. Uranium-bearing apatite was also separated out of fossil bone material. For separation of apatite from bone tissue, portions were selected which were not pigmented by organic substances. The apatite was separated from calcite and pyrite nearly pure, and contained only traces of impurities. Microscopic study of the apatite aggregates obtained showed their purity. The mineral was determined as apatite, with a lamellar-feathered structure and with a very low birefringence. The mineral was transparent, without inclusions.

The x-ray photographs of the uranium-bearing phosphates from the phosphorites and from fossil bone were identical to that of the apatite, without any additional lines (Table 1).

TABLE 1

Data from X-ray Investigation of Uranium-bearing Phosphates, $Fe_{emitter}$; 2R = 57.9; d = 0.6

№	1		2		3		4	
	I	dα	I	dα	I	dα	I	dα
1	4	3.40	4	3.40	5	3.40	4	3.42
2	3	3.14	3	3.14	4	3.12	3	3.14
3	4	3.05	3	3.05	4	3.04	4	3.05
4	10	2.78	10	2.77	10	2.76	0	2.77
5	7	2.7	6	2.70	7	2.71	8	2.70
6	5	2.00	4	2.62	5	2.62	7	2.62
7	4	2.27	3	2.23	3	2.23	5	2.25
8	5	1.937	6	1.936	4	1.935	7	1.934
9	—	—	—	—	—	1.882	5	1.880
10	3	1.832	5	1.834	4	1.836	3	1.835
11	3	1.798	3	1.800	3	1.802	5	1.800
12	—	—	—	—	3	1.760	5	1.761
13	—	—	—	—	3	1.736	5	1.738
14	7	1.716	5	1.716	2	1.718	5	1.718
15	1	1.636	—	—	—	—	2	1.631
16	—	—	—	—	—	—	1	1.523
17	—	—	—	—	—	—	1	1.497
18	—	—	3	1.463	2	1.465	1	1.465
19	3	1.449	—	—	—	—	4	1.448
20	3	1.423	—	—	—	—	4	1.420
21	—	—	—	—	—	—	1	1.398

1 - Uranoapatite from carbonaceous shales
2 - Uranoapatite from phosphorites
3 - Uranoapatite from bone tissue
4 - Kuamdespachn fluorapatite (calibration standard). Studies 1,2 and 3 were carried out in the laboratory of IGEM, Acad. Sci. USSR by N. N. Sludska.

TABLE 2

Chemical Analyses of Uranoapatite from (1) Carbonaceous Shales, (2) Phosphorites, and (3) Bone Tissue, in %

	1	2	3
CaO	54.61	54.11	53.37
UO_2	1.56	2.39	3.73
P_2O_5	41.79	41.56	41.46
F_2	3.51	3.37	2.10
H_2O	trace	trace	0.50
Cl	trace	—	—
Corr F_2	—1.47	—1.42	—0.88
Σ	100.01	100.00	100.28

The data of the chemical analyses (Table 2) fit well to the formula for apatite. In connection with entrance of uranium into the apatite, a deficit of fluorine and calcium in comparison with pure apatite is revealed. Calculation from the analyses allows us to hypothesize an equivalent substitution of the group $Ca(F, OH)_2$ by UO_2.

Thus, to the uranium-containing minerals and substances which were known earlier or hypothesized in phosphorites and carbonaceous shales, we should add uranoapatite (or uranous apatite) – $a\ Ca_9(PO_4)_6\ Ca(F,OH)_2 \cdot b\ Ca_9(PO_4)_6UO_2$.

Entrance of uranium into apatite may also, apparently, be carried out in the organic form by replacement of 3Ca by 2Na + U or by some other scheme. In natural phosphorites only uranium-poor apatites are usually found, in conjunction with disseminated uranium.

In the oxidation zone of phosphorite deposits and carbonaceous shales, during change-over of uranium from the tetravalent to hexavalent state, the uranium is freed from the apatite lattice and forms secondary minerals – autunite, zeunerite, and others.

LITERATURE CITED

[1] A. G. Betekhtin, Mineralogy (State Geologic Press, 1950).

[2] C. F. Davidson and D. Atkin, Compt. rend. 11, 13 (1953).

[3] Z. S. Altschuler, R. S. Clarke, Jr. and E. Y. Young, Bull. Geol. Soc. Amer. 65, 1225 (1954).

Received July 5, 1956

ISOTOPE COMPOSITION OF THE RARE EARTH ELEMENTS FORMED IN THE FISSION OF URANIUM, THORIUM, AND BISMUTH NUCLEI BY PROTONS WITH ENERGY OF 680 Mev

F. I. Pavlotskaya and A. K. Lavrukhina

The results are given of a radiochemical investigation, carried out in 1954, of the rare earth elements formed by the fission of uranium, thorium, and bismuth nuclei by 680 Mev protons, The main attention was devoted to methods of isolation and separation of these elements. In a search for the optimum conditions of separation by ion exchange chromatography, the effect of the nature of the complex former (ammonium acetate, nitrate, oxalate, and lactate), the pH of the eluant, and the concentration of the rare earth elements on the degree of separation was studied. A technique was evolved whereby it was possible to isolate the radioisotopes of almost all the rare earth elements and to determine the yields of some of them. In addition, the formation of a new samarium isotope with a half-life of about 20 days is presumed.

Determinations of the isotope composition of the rare earth elements formed in various nuclear reactions are of great interest in relation to the problem of the origin of the chemical elements. The choice of the rare earth elements for this purpose is not accidental, but is due to their conjoint migration in the earth's crust. Therefore a comparison of the distribution of the rare earth elements in various rocks and minerals with the probability of their formation and the isotope composition in nuclear processes will throw light on the role of such processes in the formation of these elements.

The yields of radioactive and stable isotopes of rare earth elements formed by the slow neutron fission of uranium are now well known. Hitherto it has not proved possible to determine similar data for the fission products of heavy element nuclei by the action of high-speed particles [1]. We therefore made an attempt in 1954 to determine the yields and isotope composition of the rare earth elements in the fission of uranium, thorium, and bismuth by 680 Mev protons. Ion exchange chromatography was used as the method of separation.

At the time this work began, numerous publications had appeared in the literature on the separation of the rare earth elements by ion exchange chromatography. However, the methods described proved unsuitable for our purpose, mainly because of the long time required for the experiments (30 hours and over). In addition, the separation efficiency is low for a number of elements: for example, europium and gadolinium [2], neodymium and promethium [3], samarium and gadolinium, and others, are eluted from the chromatographic column without separation.

Because of the absence of an exact theory of ion exchange chromatographic separation of the rare earth elements, empirical selection of eluants and experimental conditions is necessary.

The most important of the factors which influence ion exchange separation are the nature and the concentration of the complex former and the pH of the solution. Therefore the main attention in this work was devoted to a study of the influence of these factors on the efficiency of separation of the rare earth elements.

For separation of all the rare earth elements from the products of bombardment of uranium, thorium, and bismuth by 680 Mev protons, cerium was used as the carrier. This was based on the following considerations.

1) The behavior of various rare earth isotopes in the precipitation of cerium hydroxide, oxalate, and fluoride was found experimentally to be analogous to the behavior of cerium.

2) The main mass of the cerium can be easily separated from the other rare earths by oxidation to the quadrivalent state followed by extraction by diethyl ether [4].

METHOD

An ion exchange column 0.3 cm in diameter and 55 cm high was used for the separation. The column was filled with Dowex-50 or KU-2 cation exchange resins, previously ground to a particle size of ~ 0.25 mm and converted into the NH_4^+ form.

Ammonium citrate, acetate, lactate, and oxalate were used as complex formers.

In the selection of the separation conditions, use was made both of mixtures of rare earth oxides irradiated by slow neutrons, and of the mixture of radioisotopes isolated from the products of bombardment of uranium, thorium, and bismuth by 680 Mev protons. In the first case the mixture of oxides of the rare earth elements and yttrium was dissolved in concentrated hydrochloric or nitric acid. In the second case the radioisotopes of the rare earths were isolatedon cerium carrier. Plates of spectroscopically pure uranium, thorium, and bismuth, 25 x 7 x x 0.5 mm, were irradiated in the synchrocyclotron of the Institute of Nuclear Problems of the Academy of Sciences USSR, and then dissolved in the appropriate acids. A definite amount of cerium was added to the solution, and the separation from the main target substance was effected by precipitation of cerium fluoride from 0.4 N nitric acid solution (uranium), or extraction of thorium nitrate from 3 N nitric acid solution in presence of zinc nitrate (thorium), or precipitation of bismuth sulfide from 0.3 N nitric acid solution (bismuth). The radiochemical purification of the mixture of rare earths was effected by two- or therrfold repetition of precipitation of cerium hydroxide, oxalate, and fluoride from 0.3 N nitric or hydrochloric acid solution, and of thorium iodate and bismuth sulfide. To separate the main mass of the cerium from the radioisotopes ot the other rare earths, cerium (IV) was extracted by ether from 6N nitric acid solution in presence of sodium bismuthate. Further radiochemical purificationof the cerium was effected by precipitation of cerium (IV) iodate and repeated extraction. After extraction of cerium, bismuth sulfide (in 0.3 N nitric acid solution) was precipitated from the aqueous phase, followed by precipitation of cerium hydroxide, as part of the cerium had not reacted. The precipitate was dissolved in hydrochloric acid, and the solution, as in the case of the mixed oxides, was evaporated to dryness. The residue was dissolved in 5-10 ml of water, and from 30 to 200 mg of the cation exchange resin, according to the amount of mixture to be separated, was then added to the solution. The charge in all the experiments was less than 1% of the weight of resin in the column. The solution was stirred for 30 minutes, and the resin with the adsorbed rare earths was washed with water and transferred to the upper part of the column. It was found that 92-98% of the initial activity is adsorbed in these conditions. A narrow adsorption band was obtained if this method of transfer of the rare earth elements to the ion exchange column was used. The eluate was collected in separate fractions at definite time intervals, and aliquot portions were placed on targets for activity measurement on a counter. The fractions were taken at 10 minute intervals at an elution rate of 0.05-0.1 ml/minute.

The peaks on the elution curves were studied for isotope composition and radioactive purity. The products were identified by the half-life periods, β-radiation energy, and the nature of the radiation. The latter was determined with the aid of a magnetic analyzer.

The yields of the β-active isotopes were determined by the method described previously [1].

1. Study of the Influence of Various Factors on the Efficiency of Separation of Rare Earth Elements

Nature of the complex former. The results of experiments on the separation of rare earth elements with the aid of various complex formers: 4.75% ammonium citrate solution, 5% ammonium acetate solution, 0.1% ammonium oxalate solution, and 3.6% ammonium lactate solution, are shown in Figs. 1-5. The graphs show that the most efficient separation is obtained by elution with 3.6% ammonium lactate solution at pH = 3.4 (Fig. 5); all the elements are then obtained in a radioactively pure form. The use of 4.75% ammonium citrate solution (Fig. 1) did not give satisfactory results, as neighboring elements are eluted in the same peak; for example,

ytterbium and erbium; samarium, promethium and neodymium, etc. Elution with 5% ammonium acetate gives somewhat better separation, but satisfactory separation of these elements is again not obtained, as only ytterbium, samarium, and promethium are obtained in the radioactively pure state (Figs. 2 and 3).

To separate the heavy rare earths, we made use, for the first time, of ammonium oxalate, which forms soluble complex compounds with these elements. Elution with 0.1% ammonium oxalate solution (Fig. 4) resulted in separation of lutecium and erbium in the radioactively pure state; thulium and ytterbium were eluted together.

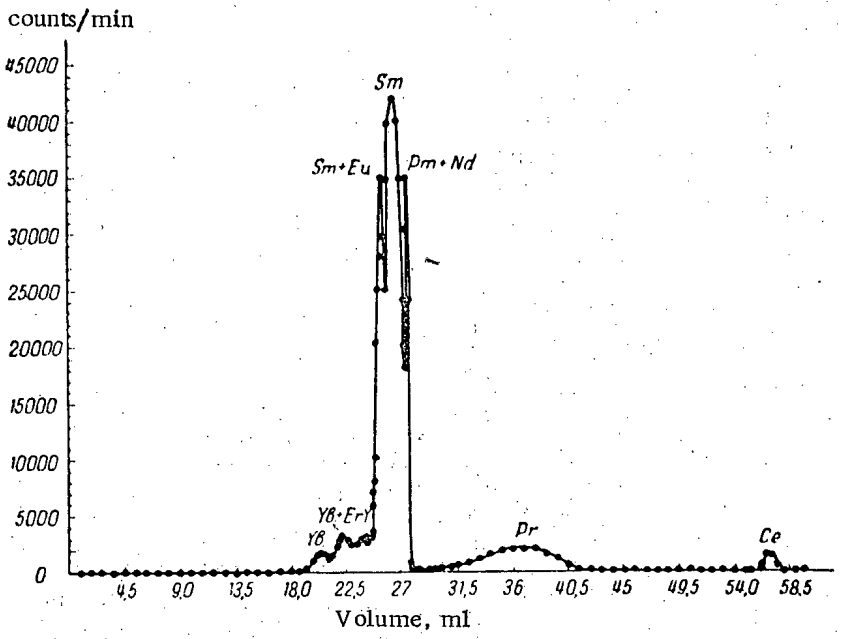

Fig. 1. Separation of a mixture of rare earth elements by 4.75% ammonium nitrate solution (pH = 3.25-3.4). Composition of mixture – oxides of cerium, praseodymium, neodymium, samarium, dysprosium, erbium, ytterbium, and yttrium, approximately 0.75 mg of each; Dowex-50 resin.

The solution pH. The influence of the pH of the eluant on the degree of separation of the rare earth elements is seen in the chromatograms in Figs. 2, 3, 5, and 6. A decrease of the pH of 5% ammonium acetate solution from 6 (Fig. 6) to 5 (Figs. 2 and 3) favors more efficient separation. A further decrease of pH to 4.5 did not give positive results; ytterbium, erbium, and thulium were eluted together in one peak, and samarium and europium in another. In addition, the elution time was much greater.

Increase of the pH of 3.6% ammonium lactate solution from 3 to 3.4 (Fig. 5) led to an increase of the elution rate of the individual elements and to a change in the form of the peaks from broad at pH = 3 to narrow and long at pH = 3.4.

It follows from these examples and extensive literature data that the efficiency of separation of the rare earth elements depends to a considerable extent on the pH of the eluant.

Concentration of the elements being separated. It has been shown by one of the present authors that elution of the elements is accelerated on decrease of their concentration [5]. The same conclusion follows from the data in Figs. 4 and 7, which show elution curves for imponderable amounts of rare earth elements and 3.7 mg of a mixture of the oxides of ytterbium, erbium, samarium, and europium by 0.1% ammonium oxalate solution. The graphs show that in the case of imponderable concentrations elution of ytterbium begins after the passage of 20 ml of solution; in the presence of weighable concentrations (0.3 mg Yb_2O_3) it commences after the passage of 100 ml of solution. This shift of the peaks at ultra-low concentrations of rare earth elements is important for their effective separation, and therefore it requires detailed study.

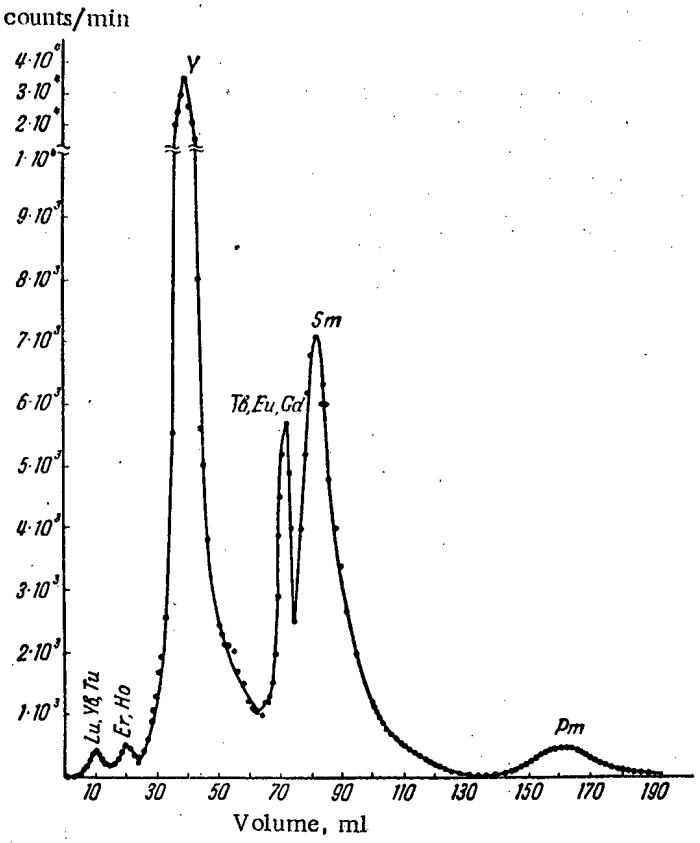

Fig. 2. Separation of radioisotopes of rare earth elements formed by the fission of uranium by 680 Mev protons, by means of 5% ammonium acetate solution (pH = 5.0). Composition of mixture – radioisotopes of all the rare earth elements without carriers; KU-2 resin.

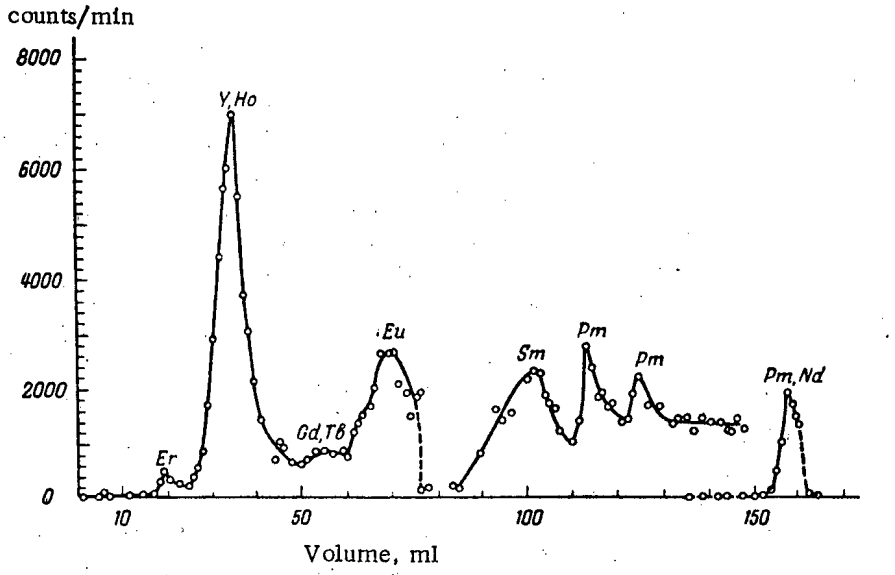

Fig. 3. Separation of radioisotopes of rare earth elements formed by the fission of thorium by 680 Mev protons, by means of 5% ammonium acetate solution (pH = 5.0). Composition of mixture – radioisotopes of all the rare earth elements without carriers; KU-2 resin.

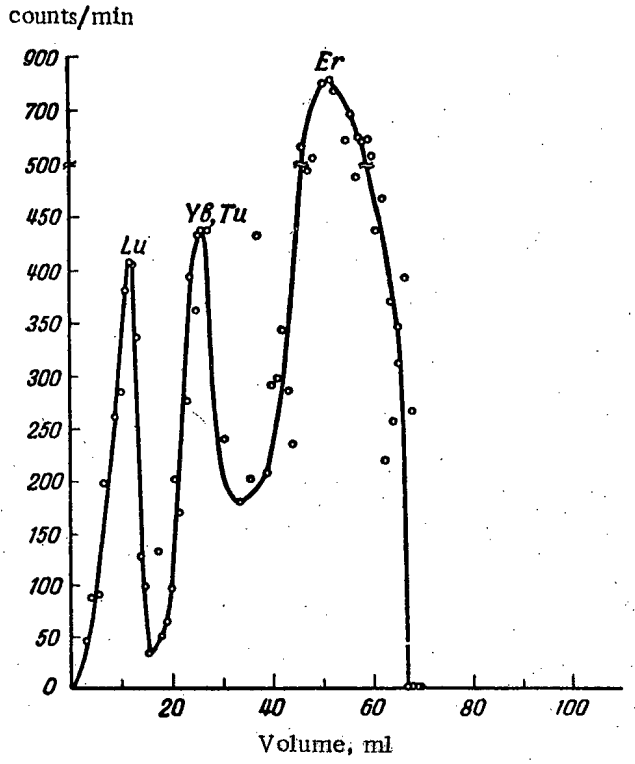

Fig. 4. Separation of radioisotopes of rare earth elements formed by the fission of bismuth by 680 Mev protons, by means of 0.1% ammonium oxalate solution. Composition of mixture – radioisotopes of all the rare earth elements without carriers; KU-2 resin.

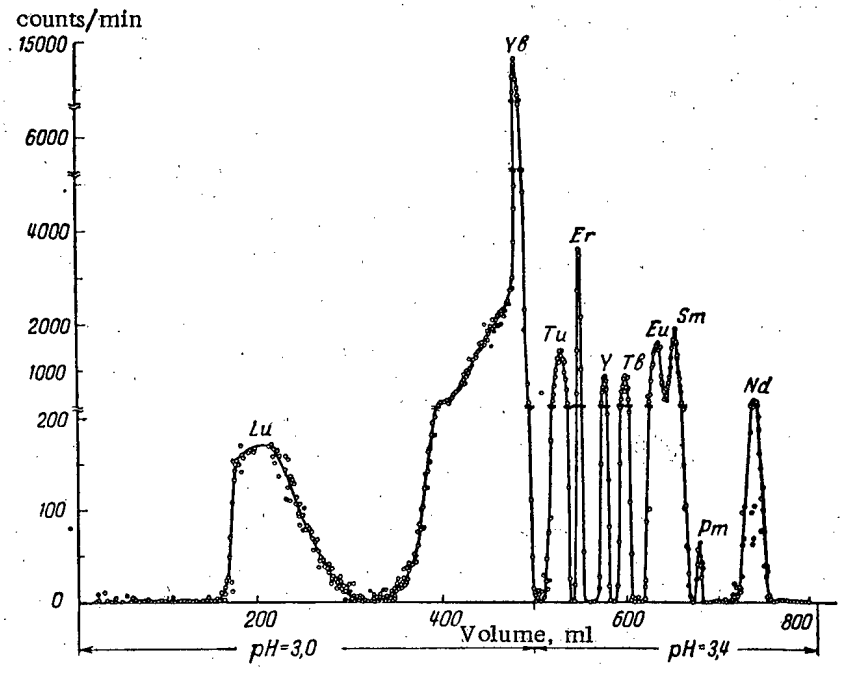

Fig. 5. Separation of a mixture of rare earth elements by means of 3.6% ammonium lactate solution (pH 3.0-3.4). Composition of mixture – oxides of lanthanum, cerium, praseodymium, neodymium, samarium, gadolinium, erbium, ytterbium, and yttrium, approximately 0.5 mg of each; europium and thulium as impurities; Dowex-50 resin.

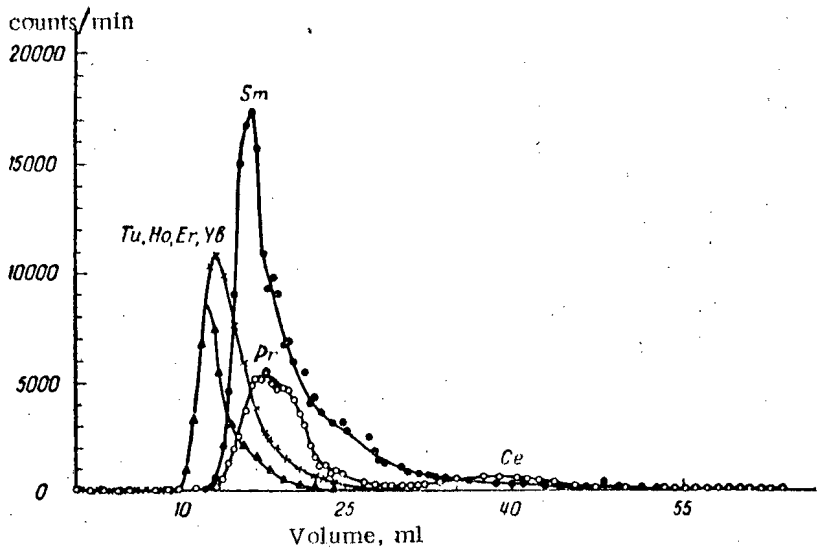

Fig. 6. Elution of rare earth elements by 5% ammonium acetate solution (pH = 6.0). KU-2 resin. ▲ – 0.65 mg erbium oxide; ● – 0.6 mg samarium oxide; O – 0.4 mg praseodymium oxide; X – 0.5 mg ytterbium oxide.

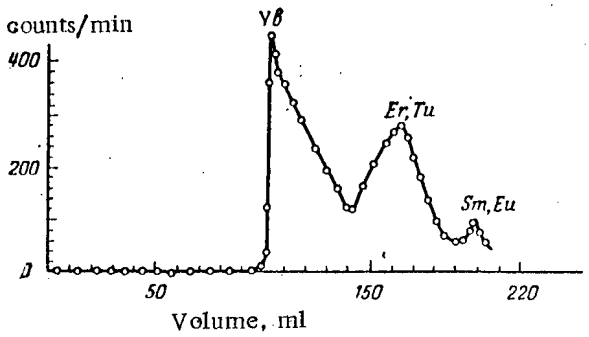

Fig. 7. Separation of a mixture of rare earth elements by means of 0.1% ammonium oxalate solution. Composition of mixture – oxides of ytterbium, erbium, and samarium, approximately 0.3 mg of each; thulium and europium as impurities; KU-2 resin.

2. Determination of the Isotope Composition and the Yields of Radioisotopes of Rare Earth Elements in the Fission of Uranium, Thorium, and Bismuth by 680 Mev Protons

The results of the chromatographic separation of rare earth radioisotopes formed in the fission of uranium, thorium, and bismuth by 680 Mev protons are shown in Figs. 2, 3, and 4.

The table, which summarizes all our results on the isotope composition and yields of certain radioisotopes of the rare earths, shows that in the fission of uranium, thorium, and bismuth by the action of 680 Mev protons radioisotopes of all the rare earth elements are formed, in contrast to the fission of uranium by slow neutrons, when isotopes of the heavy rare earth elements are not formed.

It must be pointed out that in view of the lack of a satisfactory method for determination of E-capture isotopes, only the yields of the β-active isotopes were estimated. Therefore these results do not give a complete picture of the yields of rare earths in the fission products; they only provide information on the isotope composition of the rare earth elements (especially in the case of the fission of bismuth).

Many of the identified radioisotopes distintegrate by positron emission or orbital electron capture, which indicates the formation of radioisotopes with a neutron deficiency, which were not found in the slow neutron fission of uranium.

The samarium fractions contained radioactivity with T = 17.5-22 days, which cannot be attributed to the presence of radioisotopes of neighboring elements, but is probably due to a new samarium isotope, Sm^{141}. From the short-lived activities of T = 40 minutes and 2.7 hours found in the fractions of the neighboring elements 30 hours after irradiation of the target, and from the value found for the β-radiation energy of samarium (2.4-2.8 Mev), we can write the following scheme for the disintegration of this isotope:

$$Sm^{141}\,(17.5-22d) \xrightarrow{\beta^+,\,E} Pm^{141}\,(38\,m) \xrightarrow[2.4-2.8\,Mev]{\beta^+} \rightarrow Nd^{141}\,(2.7hr) \xrightarrow{E,\,\beta^+} Pr^{141}\,(stable).$$

The data obtained for the yields of certain radioisotopes made it possible to plot distribution curves for the yields of β^--active isotopes of the radioactive elements according to their mass numbers. Such a curve for

Results of Radiochemical Investigation

No.	Identified radioisotope	Type of radiation (data from [6-8])	Half-life period		Formation cross-section 10^{-27} cm²		
			found	data of [6-8]	uranium	thorium	bismuth
1	$_{58}Ce$ 134	E, γ, e^-	68—95 hr	72 hr	+	+	+
2	139	E, γ, e^-	131—157 days	140 days	+	+	+
3	141	β^-, γ	26—36 days	30.6 days	+	+	+
4	143	β^-, γ	24.5—33 hr	33 hr	8.0	23.0	0,67
5	144	β^-, γ	274—281 days	275—290 days	—	+	+
6	145	β^-	1.75—2 hr	1.8 hr	+	—	+
7	$_{59}Pr$ 139	E, β^+	3.3 "	4.2 "	+	—	—
8	142	β^-, γ, e^-	18 "	19.34 "	+	—	—
9	143	β^-	10.75—13.5 days	13.5 days	4.9	11.2	+
10	$_{60}Nd$ 139	E, β^+	5 hr	5.5 hr	+	—	—
11	140	E, γ	2.8—3.3 days	3.3 days	+	+	—
12	141	E, β^+	2.7 hr	2.4 hr	—	+	—
13	$_{61}Pm$?	?	9.5—14 "	12.5 "	+	+	—
14	141 (?)	β^+	38—40 min	20 min	—	+	—
15	145	β^+	8.5—16 days	14—18 days	+	—	+
16	148	β^-, γ	47—48.5 "	42—48 "	+	—	+
17	149+151	β^-, γ	37—50 hr	27.5 hr 55 "	+	+	+
18	$_{62}Sm$ (141 ?)	?	17.5—22 days	?	+	+	+
19	145	E, γ	111—180 "	>72.150 days	+	+	+
20	153	β^-, γ	42—56 hr	47 hr	6.4	+	+
21	156	β^-	9.5 "	10 "	—	+	—
22	$_{63}Eu$ 152	β^-, γ, e^-	8.75—12 "	9.2 "	5.0	6.6	—
23	156	β^-, γ	13—16 days	15.4 days	5.3	2.7	+
24	$_{64}Cd$ 159	β^-, γ	16—19.5 hr	18 hr	0.1	0.3	+
25	$_{65}Tb$ 160	β^-, γ	68 days	73.5 days	—	0.07	—
26	161	β^-, γ	5.5—10.5 days	6.75 "	0.6	0.06	—
27	$_{66}Dy$ 166	β^-	60 hr	80 hr	—	—	+
28	$_{67}Ho$ 162	E, β^-	63.5—80 days	65 days	+	—	—
29	163	E, e^-	5.25—7 "	5.2—7 "	+	+	+
30	$_{68}Er$ 160	β^+ (?)	18.5—21 hr	~17 hr	0.02	0.009	+
31	163	β^+	40—60 "	~65 "		—	+
32	165	E		10 "			
	171	β^-, γ	10.25 "	7.5 "	0.05	—	—
33	$_{69}Tu$ 166	E, β^+, γ, e^-	7 "	7.7 "	+	—	—
34	170	β^-, γ	114—129 days	127 days	0.04	—	+
35	$_{70}Yb$ 166	E	36 hr	62 hrs	—	—	+
36	169	E, γ	22.5 days	33 days	+	—	—
37	175	β^-, γ	108—116 hr	99 hr	0.01	—	+
38	$_{71}Lu$ 172	E, γ, e^-	16—19.5 "	16.8 "	+	—	+
39	174	E, β^+	175 days	165 days	—	—	+
40	177	β^-, γ	7.6 "	6.8 "	—	—	+

Note. The sign + indicates that the radioisotope was identified but the yield was not determined. The sign − means that the radioisotope was not identified.

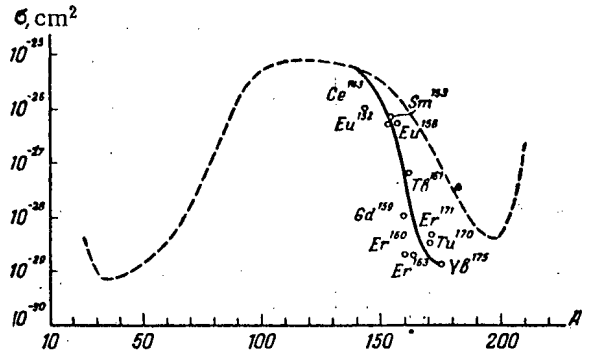

Fig. 8. Distribution curve for the yields of radioactive rare earth elements formed in the fission of uranium by 680 Mev protons, according to mass numbers.

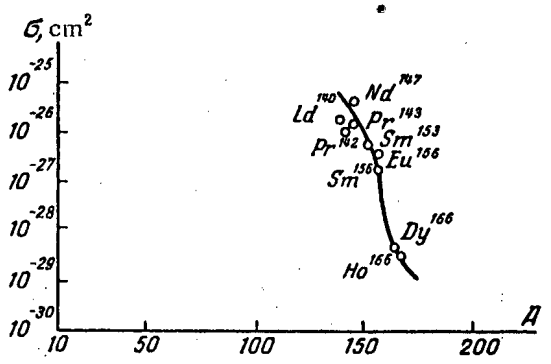

Fig. 9. Yields of β⁻-active isotopes of rare earth elements formed in the fission of uranium by 680 Mev protons (continuous line) and 340 Mev protons (O).

the fission of uranium is shown in Fig. 8. The broken line represents the distribution curve of the isotopes, by their mass numbers, for the bombardment of uranium by 480 Mev protons, carried out arbitrarily in the rare earth region.

A similar curve was obtained for the fission of thorium.

A comparison of the curve obtained for the fission of uranium with data for the fission of uranium by the action of 340 Mev protons for the yields of β-active isotopes are not changed by an increase in the energy of the bombarding protons from 340 to 680 Mev.

SUMMARY

1. The products of the fission of uranium, thorium, and bismuth by the action of 680 Mev protons, and mixtures of rare earth elements, were used to study the effect of the nature of the complex former (ammonium acetate, citrate, oxalate, and lactate), the pH of the eluant, and the concentration of the rare earth elements on the degree of separation. It was found that most efficient separation is obtained by elution with 3.6% ammonium lactate solution at pH = 3.4.

2. The isotope composition and the yields of β-active isotopes of the rare earth elements formed in the fission of uranium, thorium, and bismuth by 680 Mev protons have been determined.

3. From a comparison of the results obtained with the data of other workers it is concluded that the yield of β-active isotopes of the rare earth elements formed in uranium fission does not change if the proton energy is increased from 340 to 680 Mev.

4. The formation of a new samarium isotope, Sm^{141}, with T = 20 days, is presumed.

To obtain more complete data on the radioisotopes of the rare earth elements formed by fission of uranium, thorium, and bismuth nuclei by bombardment with 680 Mev protons, further research is necessary. Attention should be paid to an estimation of the yield of isotopes which disintegrate by electron capture.

Received May 29, 1956.

LITERATURE CITED

[1] A. Vinogradov, I. Alimarin, B. Baranov, A. Lavrukhina, T. Baranova, F. Pavlotskaya, A. Bragina, and Yu. Yakovlev, Session of the Academy of Sciences, USSR, on the Peaceful Uses of Atomic Energy, Div. Chem. Sci., p. 97 (1955).

[2] G. Higgins and K. Street, J. Am. Chem. Soc. 72, 5321 (1950).

[3] I. Marinsky, L. Glendenin and C. Gowell, J. Am. Chem. Soc. 69, 2781 (1947).

[4] M. Senyavin and V. Klinaev, Use of Labeled Atoms in Analytical Chemistry, Symposium (Acad. Sci. USSR Press, 1955), p. 118.

[5] A. Lavrukhina, Doctorate Dissertation, Institute of Geological Chemistry, Academy of Sciences USSR (Moscow, 1955).

[6] I. Semenov, Atomic Nuclei and Nuclear Transformations (State Tech. Press, Moscow-Leningrad, 1951).

[7] A. Nesmeyanov, A. Lapitsky, and N. Rudenko, Production of Radioactive Isotopes (State Tech. Press, Moscow, 1954).

[8] J. Hollander, I. Perlman and G. Seaborg, Rev. Modern Phys. 25, 469 (1953).

[9] R. Folger, P. Stevenson and G. Seaborg, Phys. Rev. 38, 107 (1955).

THE DEPENDENCE OF THE ACTIVITY OF SECRETIONS ON THE CONCENTRATION OF RADIOACTIVE MATTER WITHIN AN ORGANISM

Yu. M. Shtukkenberg

We present detailed calculations of the dependence of the activity of secretion on the amount of radioactive matter contained within an organism when the secretion of matter follows the exponential law.

INTRODUCTION

As has been shown by experiments on animals and by clinical observation, secretion of radioactive matter from the organism follows a law which is either exponential or a sum of exponentials.

Quantitative calculation with the results of this type of experiment makes possible the determination of the concentration of radioactive matter within the organism on the basis of the measured activity of the secretion; this is extremely valuable for the evaluation of the effect of incorporated matter on the human organism.

In the present article we establish some qualitative results and give a method of handling experimental data on the activity of secretion in order to determine the activity of matter within the human organism.

A sufficiently long time after a single or continued introduction of a radioactive isotope into the organism, the distribution of this isotope through the organs and tissue reaches equilibrium.

When the equilibrium distribution of radioactive matter has been achieved, its concentrations in the various organs and tissues are in definite ratios which do not change in time and are determined by transfer processes within the organism and the decay rate of the given radioactive substance. Before this equilibrium state has been achieved, the secretion of active matter takes place according to a rather complex law, which is the sum of a series of exponential functions with various time constants λ_i, i.e.,

$$A_1 e^{-\lambda_1 t} + A_2 e^{-\lambda_2 t} + \ldots,$$

where A_1, A_2, . . . are constant coefficients given by the radioactivity of the matter in the various organs at time $t = 0$. After some time t all the exponentials $e^{-\lambda_i t}$ with large values of λ_i practically vanish, and we are finally left only with the exponential with the smallest value of λ_i. This exponential law of secretion corresponds to the equilibrium distribution of the radioactive isotope in the organism.

All the above qualitative concepts are verified by experiment and can be obtained from theoretical considerations of the mechanics of the transfer of radioactive matter within the organism. The present work is concerned with the deduction of quantitative results for relating the radioactivity of the substances contained within the organism to the radioactivity of the secretion, for the case of the exponential secretion law.

It should be noted here that as a result of the dependence of the transfer processes on various physiological factors, the intensity of secretion of radioactive matter may be subject to fluctuations, and in various cases, it differs from the exponential law of radioactive decrease. Nevertheless, for average values this law is satisfied with sufficient accuracy, and therefore the calculations presented below can be applied in the overwhelming majority of cases as a most general method for solving the problem.

The relative decrease of radioactivity in the organism per day is called the effective secretion constant and is denoted by λ_{eff}. This quantity was introduced in order to calculate the maximum allowable dose of

incorporated radioactive matter. The quantity $\lambda_{eff} = \lambda_d + \lambda_b$, where λ_d is the decay constant of the given radioactive isotope, and λ_b is the biological secretion constant.

In the physical sense, the constant λ_b is the relative decrease of activity within the organism per day which is due only to biological secretion of radioactive matter from the organism, without taking account of the radioactive decay of this matter.

If the quantity λ_d is small in comparison with λ_b, then $\lambda_{eff} \approx \lambda_b$, i.e. the decrease of radioactivity within the organism takes place practically only because of the biological secretion as a result of the constant replacement processes going on within the organism.

If the quantity λ_d is large in comparison to λ_b, then $\lambda_{eff} \approx \lambda_d$, and in this case the decrease of radioactivity within the organism takes place almost entirely because of the radioactive decay of the matter.

In the literature dealing with the calculation of the maximum allowable doses, quantitative laws are given relating the doses for various substances to their effective secretion constants [1,2]; the question of quantitative laws, however, relating the activity of the matter within the organism to the activity of this matter in the secretions is not treated at all. Furthermore, this question is of much greater practical interest, since by knowing the above relationships, we can determine the amount of radioactive matter in an organism in terms of the radioactivity of its secretions.

The Relations Between the Radioactivity of an Isotope Within the Organism and Its Radioactivity in the Secretions

Let A_1 be the radioactivity of the isotope contained in the organism, and A_2 be the radioactivity of the isotope secreted by the organism in a time t.

Clearly, the total radioactivity of the given isotope is

$$A(t) = A_1(t) + A_2(t).$$

If the secretion law is exponential, then

$$\frac{dA_1}{dt} = -\lambda_{eff} A_1 \quad \text{or} \quad \frac{dA_1}{dt} = -(\lambda_d + \lambda_b) A_1 \tag{1}$$

The total radioactivity A of the isotope decreases according to the decay constant λ_d, and therefore

$$\frac{d}{dt}(A_1 + A_2) = -\lambda_d (A_1 + A_2). \tag{2}$$

Let us solve Equations (1) and (2), arriving at the desired conclusion.

Setting at $t = 0$, $A_1 = A_{10}$ and $A_2 = 0$, i.e. at $t = 0$ all the radioactivity A is contained within the organism, and the calculation of the radioactivity of the secretion is taken from time $t = 0$.

The solution of Equation (1) is of the form

$$A_1 = A_{10} e^{-\lambda t}, \tag{3}$$

where the effective secretion constant λ_{eff} is denoted by λ.

Equation (2) has the following solution:

$$A_1 + A_2 = A_{10} e^{-\lambda_d t}. \tag{4}$$

From Equation (2) we obtain

$$\frac{dA_2}{dt} = -\lambda_p (A_1 + A_2) - \frac{dA_1}{dt}. \tag{5}$$

Inserting the expression $\frac{dA_1}{dt}$ from Equation (1) into Equation (5), we obtain

$$\frac{dA_2}{dt} = -\lambda_d (A_1 + A_2) + \lambda A_1,$$

or, setting $\lambda = \lambda_d + \lambda_b$, finally

$$\boxed{\frac{dA_2}{dt} = -\lambda_d A_2 + \lambda_b A_1.} \tag{6}$$

It can be seen from Equation (6) that the change in radioactivity per day of the matter secreted by the organism takes place as a result of the biological secretion of radioactive matter from the organism as well as of radioactive decay of the secreted matter.

In order to relate the change in radioactivity of the secretion per day $\frac{dA_2}{dt}$ to the radioactivity of the matter contained within the organism A_1, we must express A_2 in terms of A_{10} and insert this into the right side of Equation (6).

Determining A_2 from Equation (4) and inserting the expression for A_1 from (3) into the expression so obtained, we arrive at

$$A_2 = A_{10} e^{-\lambda_d t} - A_{10} e^{-\lambda t} = A_{10} (e^{-\lambda_d t} - e^{-\lambda t}). \tag{7}$$

Introducing A_2 from (7) into (6), we obtain

$$\frac{dA_2}{dt} = -\lambda_d A_{10} (e^{-\lambda_p t} - e^{-\lambda t}) + \lambda_b A_{10} e^{-\lambda t} = A_{10} (\lambda e^{-\lambda t} - \lambda_d e^{-\lambda_d t}).$$

Therefore,

$$\boxed{\frac{dA_2}{dt} = A_{10} (\lambda e^{-\lambda t} - \lambda_d e^{-\lambda_d t}).} \tag{8}$$

Equation (8) can also be obtained by differentiating (4) and introducing A_1 from (3).

In order to obtain the dependence of the radioactivity of the daily secretions on the radioactivity of the matter contained within the organism, let us perform the following transformation.

We express A_2 and $\frac{dA_2}{dt}$ in terms of A_1.

From Equation (4)

$$A_2 = A_{10} e^{-\lambda_d t} - A_1. \tag{9}$$

Since

$$\lambda_d = \lambda - \lambda_d,$$

we have

$$A_{10}e^{-\lambda_d t} = A_{10}e^{-(\lambda-\lambda_b)t} = A_{10}e^{-\lambda t}e^{\lambda_b t}.$$

Replacing the term $A_{10}\,e^{-\lambda t}$ by A_1 according to (3) in this expression, we obtain

$$A_{10}e^{-\lambda_d t} = A_1 e^{\lambda_b t}. \tag{10}$$

Introducing $A_{10}\,e^{-\lambda_d t}$ from (10) into (9) we arrive at

$$\boxed{A_2 = A_1(e^{\lambda_b t} - 1).} \tag{11}$$

Replacing A_{10} in Equation (8) by A_1 from Equations (10) and (3), we obtain

$$\boxed{\frac{dA_2}{dt} = A_1(\lambda - \lambda_d e^{\lambda_b t}).} \tag{12}$$

This last expression can be obtained also by inserting A_2 from Equation (11) into (6).

From Equation (6) it follows that for $t = 0$

$$\left(\frac{dA_2}{dt}\right)_{t=0} = \lambda_b A_{10}, \qquad \text{since} \qquad A_{10} = 0.$$

The same dependence can be obtained from Equations (8) and (12), noting that

$$\lambda = \lambda_d + \lambda_b.$$

Thus, for $t = 0$

$$\left(\frac{dA_2}{dt}\right)_{t=0} = \lambda_b A_{10}. \tag{13}$$

Obviously, using $\left(\frac{dA_2}{dt}\right)_{sec}$ to denote the radioactivity of the secreted matter between the time t and a time Δt later, and using A_1 to denote the radioactivity of the matter within the organism at time t, at any instant t the following relations hold:

$$\boxed{\left(\frac{dA_2}{dt}\right)_{sec} = \lambda_b A_1.} \tag{13'}$$

If the radioactivity of the daily secretions changes insignificantly as a result of radioactive decay in one day, then it follows from (13') that this radioactivity is always equal to the biological secretion constant multiplied by the radioactivity of the matter within the organism.

If, on the other hand, a significant fraction of the matter decays each day, then Equation (13') is valid only for small time intervals Δt.

It must be emphasized that the radioactivity of the secretions is related to the radioactivity of the matter within the organism by the biological secretion constant λ_b, and not by the effective decay constant, and that the radioactive decay plays no role in this relation. This follows from the fact that A_1 and A_2 both decay at a rate determined by λ_d.

In order to find the relation between the radioactivity of the daily secretions and that of short lifetime matter within the organism, let us calculate more accurately how much of the activity is secreted by the organism in one day.

We have, from (7) and (11)

$$A_2 = A_{10}(e^{-\lambda_d t} - e^{-\lambda t}) \quad \text{or} \quad A_2 = A_1(e^{\lambda_b t} - 1).$$

The change in A_2 for an arbitrary time interval Δt is given by

$$\Delta A_2(\Delta t) = A_{10}(e^{-\lambda_d \Delta t} - e^{-\lambda \Delta t}).$$

The change in A_2 in one day is obtained by setting $\Delta t = 1$.

In this case

$$\Delta A_2(1) = A_{10}(e^{-\lambda_d} - e^{-\lambda}), \tag{14}$$

where $\Delta A_2(1)$ is the radioactivity of the secretions at the end of the day, and A_{10} is the radioactivity within the organism at the beginning of the day.

The change in A_2 in the second day can be expressed as

$$\Delta A_2(2) = A_1(1)(e^{-\lambda_d} - e^{-\lambda}),$$

where

$$A_1(1) = A_{10}\, e^{-\lambda}.$$

Obviously, $\Delta A_2(3) = A_1(2)(e^{-\lambda_d} - e^{-\lambda})$, where $A_1(2) = A_{10}e^{-\lambda t}$.

In general $\Delta A_2(n) = k_1 A_1(n-1) = k_1 A_{10}\, e^{-\lambda n}$, where $k_1 = (e^{-\lambda_d} - e^{-\lambda})$, and $\underline{n}$ is the number of days from the start of observation.

If the radioactive matter decays and is secreted rather slowly, that is if the magnitudes of λ_d and λ are sufficiently small, then

$$e^{-\lambda_d} \approx 1 - \lambda_p \text{ and } e^{-\lambda} \approx 1 - \lambda. \tag{15}$$

This last equation is sufficiently accurate if the decay half life T_d of the matter and the biological secretion half life T_b are greater than five days, or if the values of λ_d and λ_b are less than 0.14.

For this case $k_1 = \lambda - \lambda_d = \lambda_b$.

Similarly, from the expression $A_2 = A_1(e^{\lambda_b t} - 1)$ we arrive at the conclusion that the change in radioactivity of the secretions in one day is

$$\Delta A_2(1) = A_1(1)(e^{\lambda_b} - 1), \tag{16}$$

where $\Delta A_2(1)$ is the radioactivity of the daily amount of secretion at the end of the day, and $A_1(1)$ is the activity of the matter within the organism, also at the end of the day.

In general $\Delta A_2(n) = k_2 A_1(n)$, where $k_2 = (e^{\lambda_b} - 1)$, and n is the number of days from the start of observation.

Thus the radioactivity of the daily amount of secretion is given by

$$\boxed{\Delta A_2(1) = A_1(0)(e^{\lambda_d} - e^{-\lambda})} \tag{17}$$

or

$$\boxed{\Delta A_2(1) = A_1(1)(e^{\lambda_b} - 1).} \tag{17'}$$

This last expression depends only on the biological secretion constant λ_b and not on the radioactive decay constant λ_d.

For small values of λ_b we have $e^{\lambda_b} \approx 1 + \lambda_b$ and $e^{\lambda_b} - 1 \approx \lambda_b$.

Thus for small values of λ_d and λ_b, and therefore also of $\lambda = \lambda_d + \lambda_b$

$$\boxed{\Delta A_2(1) = A_1(0)\lambda_b} \tag{18}$$

and

$$\boxed{\Delta A_2(1) = A_1(1)\lambda_b.} \tag{18'}$$

This last equation is valid only for sufficiently small values of λ_b, independent of the magnitude of λ_d, since here the quantities ΔA_2 and A_1 refer to the same instant, namely to the end of the day.

Equation (18) is valid if the ratio

$$k_1 = \frac{e^{-\lambda_d} - e^{-\lambda}}{\lambda_b}$$

is not very different from unity.

Equation (18') is sufficiently accurate if the quantity $k_2 = \frac{e^{\lambda_b} - 1}{\lambda_b}$ is almost the same as unity.

As follows from (15), the magnitude of k_1 is close to unity if the decay half life of the matter is not less than five days; the quantity k_2 is close to unity if the biological secretion half life is greater than five days. Since the biological secretion half life of radioactive matter is usually greater than ten to fifteen days, for all radioactive substances the relation $\Delta A_2(1) = \lambda_b A_1$ is valid.

Let us investigate the time variation of the quantity $\Delta A_2(n)$, that is of the radioactivity of the daily amount of secretion.

Into the expression $\left(\frac{dA_2}{dt}\right)_{sec} = \lambda_b A_1$ we insert the relation $A_1 = A_{10} e^{-\lambda t}$, obtaining

$$\left(\frac{dA_2}{dt}\right)_t = \lambda_b A_{10} e^{-\lambda t}.$$

Since $\lambda_b A_{10} = \left(\frac{dA}{dt}\right)_{t=0}$, we have

$$\boxed{\left(\frac{dA_2}{dt}\right)_t = \left(\frac{dA_2}{dt}\right)_{t=0} e^{-\lambda t}.} \tag{19}$$

It follows, then, that the daily radioactivity of secretions measured on consecutive days also decreases exponentially, according to the effective secretion constant $\lambda = \lambda_d + \lambda_b$. Therefore, drawing a graph whose ordinate is the logarithm of the quantity $\left(\frac{dA_2}{dt}\right)_t$ at various times t, and whose abscissa is the time t, we obtain a straight line whose slope is determined by the magnitude of λ.

Thus in order to determine the radioactivity of the matter contained within the organism, the radioactivity of the daily amount of secretion must be divided by the biological secretion constant λ_b of the given substance from the organism.

If the magnitude of λ_b is unknown, then by use of the slope of $\log\left(\frac{dA_2}{dt}\right)_t$ as a function of t, we can determine λ or the effective secretion half life $T = \frac{0.693}{\lambda}$, and by use of the known decay constant λ_d, we can determine $\lambda_b = \lambda - \lambda_d$.

The Case of Two Substances

If the organism contains two radioactive substances A and B, then for them we can write a system of equations similar to (1) and (2):

$$\frac{dA_1}{dt} = -(\lambda_d^A + \lambda_b^A) A_1, \tag{20}$$

$$\frac{dB_1}{dt} = -(\lambda_d^B + \lambda_b^B) B_1, \tag{21}$$

$$\frac{d}{dt}(A_1 + A_2) = -\lambda_d^A (A_1 + A_2), \tag{22}$$

$$\frac{d}{dt}(B_1 + B_2) = -\lambda_d^B (B_1 + B_2). \tag{23}$$

Let us find the dependence of the radioactivity of the secretions $\frac{d}{dt}(A_2 + B_2)$ on the radioactivity of the substances A_1 and B_1 contained within the organism.

According to (6)

$$\frac{dA_2}{dt} = -\lambda_d^A A_2 + \lambda_b^A A_1, \tag{24}$$

$$\frac{dB_2}{dt} = -\lambda_d^B B_2 + \lambda_b^B B_2. \tag{25}$$

For $t = 0$, we have

$$\left(\frac{dA_2}{dt}\right)_t = \lambda_b^A A_1 \tag{26}$$

and

$$\left(\frac{dB_2}{dt}\right)_t = \lambda_b^B B_1. \tag{27}$$

If we can determine the radioactivity of substances A_2 and B_2 in the daily amount of secretion, then on the basis of Equations (26) and (27), for the case in which the quantities λ_b^A and λ_b^B are known, we can establish the radioactivities of the substances A_1 and B_1 within the organism, and therefore the total radioactivity of A_1 and B_1 within the organism.

If the magnitudes of λ_b^A and λ_b^B are unknown, then they can be determined on the basis of the following concepts.

Adding Equations (26) and (27), we obtain

$$\frac{d}{dt}(A_2 + B_2) = \lambda_b^A A_1 + \lambda_b^B B_1 \qquad (28)$$

or

$$\frac{d}{dt}(A_2 + B_2) = \lambda_b^A A_{10} e^{-\lambda^A t} + \lambda_b^B B_{10} e^{-\lambda^B t}. \qquad (29)$$

Thus for the case of two substances within the organism, the dependence of $\log \frac{d}{dt}(A_2 + B_2)$ on t will be a curve similar to the decay curve obtained from a mixture of two isotopes. From these curves, it is possible to determine the effective secretion constants λ^A and λ^B by ordinary methods, and then on the basis of the known decay constants λ_d^A and λ_d^B, to determine the biological secretion constants λ_b^A and λ_b^B of the two radioactive substances.

If only the total radioactivity of the daily amount of secretion is known, then it is also possible to determine the radioactivity contained within the organism. This is done by determining, from the dependence of $\log \frac{d}{dt}(A_2 + B_2)$ on t, the quantities $\left(\frac{dA_2}{dt}\right)_{t=0}$ and $\left(\frac{dB_2}{dt}\right)_{t=0}$ or the quantities $\left(\frac{dA_2}{dt}\right)_t$ and $\left(\frac{dB_2}{dt}\right)_t$ by ordinary methods, and from these to find the radioactivities A_1 and B_1 contained within the organism, or the total radioactivity $A_1 + B_1$. The method for determing the quantities λ_d, which in our case correspond to the quantities λ, as well as the magnitudes of the radioactivity of the isotopes, which in our case correspond to the quantities $\left(\frac{dA_2}{dt}\right)_t$ and $\left(\frac{dB_2}{dt}\right)_t$, from the decay curves, has been previously described by the author [3].

SUMMARY

1. It has been shown that if a radioactive isotope is secreted according to the exponential law and if the radioactivity within the organism A_1 decreases with an effective secretion constant λ, then the radioactivity A_1 and that of the daily amount of secretion $\left(\frac{dA_2}{dt}\right)_t$ are related by the expression $\left(\frac{dA_2}{dt}\right)_t = \lambda_b A_1(t)$, i.e. these quantities are related only by the biological secretion constant λ_b, and not at all by the decay constant λ_d.

2. If the magnitude of λ_b is known, then from the measured radioactivity $\left(\frac{dA_2}{dt}\right)_t$ of the daily secretions, it is possible to determine the radioactivity A_1 contained within the organism.

3. The radioactivities of the daily secretions, that is the quantities $\left(\frac{dA_2}{dt}\right)_t$ decreases exponentially in time but according to the effective secretion constant λ. At the same time, of course, the radioactivity of each sample of secretion decreases according to the decay constant λ_d.

4. If the magnitude of λ_d is not known, then from the slope of the graph of $\log \left(\frac{dA_2}{dt}\right)_t$ as a function of t the magnitude of λ can be determined, and from the known decay constant λ_d we can then find $\lambda_b = \lambda - \lambda_d$.

5. For the case of two radioactive isotopes A and B in the organism, the radioactivities A_1 and B_1 of the substances contained within the organism and therefore the total radioactivity can be found from known values of λ_b^A and λ_b^B as well as from the measured radioactivities of the first and second substances in the daily secretions, namely from $\left(\frac{dA_2}{dt}\right)_t$ and $\left(\frac{dB_2}{dt}\right)_t$.

6. If the magnitudes of λ_b^A and λ_b^B are not known, then from the curve of the logarithm of the total radioactivity of the daily secretions $\log \frac{d}{dt}(A_2 + B_2)$ as a function of t it is possible to determine λ^A and λ^B and to calculate the magnitudes of λ_b^A and λ_b^B, as well as of $\left(\frac{dA_2}{dt}\right)_t$ and $\left(\frac{dB_2}{dt}\right)$. From these quantities and from the known values of λ_b^A and λ_b^B, the radioactivities A_1 and B_1 of the substances within the organism, and therefore the total radioactivity, can be found.

LITERATURE CITED

[1] K. K. Aglintsev, Dosimetry of Ionizing Radiations (State Tech. Press, 1950), p. 339.

[2] Radiation Medicine, Edited by A. V. Lebedinsky (State Med. Press, 1955), pp. 61-72.

[3] I. I. Ivanov, V. K. Modestov, Yu. M. Shtukkenberg, E. F. Romantsev and E. I. Vorobev, Radiative Isotopes in Medicine and Biology (State Med. Press, 1955), Ch. I, § 19.

Received March 27, 1956

LETTERS TO THE EDITOR

ACTIVATION CROSS SECTION OF U^{236}

B. V. Efimov, Yu. I. Mityaev

The nuclear properties of U^{236} are of great interest for many questions of nuclear physics and engineering, especially due to the fact that U^{236} is produced in observable quantities in atomic reactors using U^{235} for fuel. Of particular importance, therefore, are the cross sections for radiative capture and thermal neutron fission.

In the present work the radiative capture cross section was measured from the β-activity of U^{237} produced in neutron capture by U^{236}. Samples of U^{236} were irradiated in the reflector of the RFT reactor. The neutron current was determined from the activity of a gold foil irradiated together with the sample. The absolute quantity of U^{237} produced (half-life 6.63 days [1]) was determined on the basis of β-γ-coincidence measurements. Since U^{237} has a complex decay scheme [1], it was necessary to take into account effects due to the thickness of the β-counter window [2]. This effect was calculated by extrapolating the absolute number of decays to zero thickness of the β-counter window. The uncertainty of the extrapolation is included in the probable error of the final value for σU^{236}_{rad}.

We have available two samples of uranium containing U^{236}. Sample No. 1 was obtained by chemical separation of uranium from aged plutonium, which contains Pu^{240}.

The uranium separated out consisted of U^{235} and U^{236}, which are produced by α-decay of Pu^{239} and Pu^{240}, as well as of U^{238} which is an impurity present in the plutonium.

Sample No. 2 was obtained by long-term irradiation of uranium in the reactor. The U^{236} was produced in the sample at hand as a consequence of radiative neutron capture by U^{235}. After irradiation the relative content of U^{236} was increased by means of isotope separation. The isotope content of the sample is given in the table.

TABLE*

	U^{232}	U^{234}	U^{235}	U^{236}	U^{238}
Sample No. 1	$2 \cdot 10^{-4}$ %	0.15%	9.4%	0.61%	89.8%
Sample No. 2	–	–	27%	0.7%	72.3%

* The relative contents of U^{235} and U^{236} in Sample No. 1 were determined by calculation on the basis of the isotope content of the initial sample of plutonium and the half-lives of Pu^{239} and Pu^{240}. The isotope content of Sample No. 2 was determined mass-spectroscopically.

When the samples containing U^{236} were irradiated in the reactor, in addition to fission and the reaction $U^{236}(n, \gamma)U^{237}$ which is of interest, the measured amount of U^{237} could be influenced by the following reactions: $U^{238}(n, 2n)U^{237}$; $U^{238}(n, \gamma)U^{239} \xrightarrow{\beta} Np^{239} \xrightarrow{\beta} Pu^{239}$. In order to take account of the first reaction, which is due to fast neutrons, a control sample of U^{238} was irradiated together with the U^{236} sample, and the amount of U^{237} produced in this sample was used to determine the contribution of the (n, 2n) reaction to the amount of U^{237} obtained (this contribution was of the order of 2%). The fission fragments of Pu^{239} and Np^{239} were separated in the chemical purification of the samples after their irradiation and before the measurements.

The fission fragments were separated by means of precipitation of uranium from a nitric acid solution in the form of $NaUO_2(CH_3COO)_3$. In addition the fragments were removed by sorption by solid manganese dioxide.

For removal of Np and Pu the precipitation was performed in a reducing agent with some SO_2 additive. The SO_2 transforms the Np and Pu into quadrivalent states, and in this form they precipitate out. After chemical purification the samples should contain only uranium isotopes. The β-half-life of Sample No. 1 was slightly greater than 6.63 days, which can presumably be explained by the presence of impurities with longer half-lives. The magnitude of $\sigma_{rad}^{U^{236}}$ for Sample No. 1 was measured as 26.4 ± 6 barns. Sample No. 2 gave a β-half-life close to 6.63 days and $\sigma_{rad}^{U^{236}} = 24.6 \pm 6$ barns. These values for the cross section are in good agreement within the limits of experimental error. Since, however, the amount of U^{236} in the first sample was not directly measured, and the presence of some β-active impurities could alter the result, we considered the first cross section value only approximate. Therefore we have taken the cross section for radiative capture as 24.6 ± 6 barns, as obtained with the second sample. This value was taken to the Geneva Conference on the Peaceful Uses of Atomic Energy [3]. It is in good agreement with the value of 24 ± 7 barns obtained by Auclair et al. [4].

In conclusion we consider it our duty to express our gratitude to M. I. Pevzner for interest in the work and for many valuable suggestions.

The chemical part of the work was carried out under the direction of G. N. Yakovlev, to whom the authors express their sincere gratitude.

Received May 17, 1956

LITERATURE CITED

[1] L. Melander, H. Slätis, Phys. Rev. 74, 709 (1948); S. A. Baranov and E. P. Shlyagin, . Proceedings of the Conference of the Academy of Sciences USSR on the Peaceful Uses of Atomic Energy, July 1-5, 1955 (Meeting of the Division of Phys.-Math. Sciences) (Acad. Sci. USSR Press, 1955), p. 251.

[2] M. Wiedenbeck, Phys. Rev. 72, 974 (1947).

[3] I. K. Shvetsov and A. M. Vorovyev, "Investigation in the field of geology, chemistry, and metallurgy," Reports of the Soviet Delegation to the International Conference on the Peaceful Uses of Atomic Energy. (Acad. Sci. USSR Press, 1955), p. 225.

[4] J. Auclair et al., "Mesure de sections efficaces de noixaux fissiles pour les neutrons lents, Report No. 354 to the International Conference on the Peaceful Uses of Atomic Energy, 1955.

PRODUCTION OF THIN LAYERS OF PLUTONIUM, AMERICIUM, AND CURIUM BY ELECTRODEPOSITION

G. N. Yakovlev, P. M. Chulkov, V. B. Dedov, V. N. Kosyakov, and Yu. P. Sobolev

For studies of the nuclear properties of transuranic elements, it is often necessary to have thin layers of isotopes of these elements applied to metal surfaces of various configurations. In accordance with such requirements the authors have developed a technique for quantitative electrodeposition of plutonium, americium, and curium on metal surfaces. The elements were deposited in the form of hydroxides from neutral and weakly acidic alcoholic acetone solutions of the chlorides. The results of an electrochemical investigation of this process were published earlier [1].

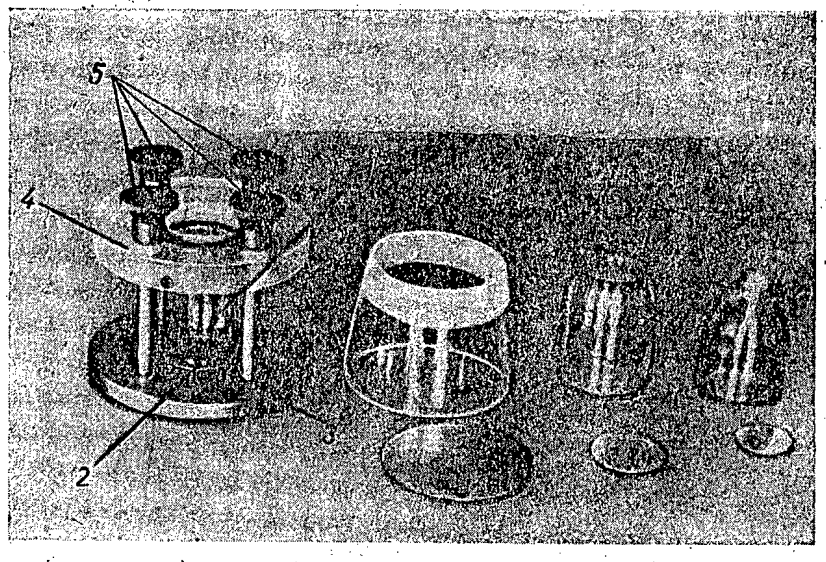

Fig. 1. Electrolytic cell for application of layers to flat surfaces. 1) Glass vessel; 2) cathode; 3) metal support; 4) clamping ring of organic glass; 5) assembly nuts.

Apparatus

Several types of electrolytic cells were used in the work. Cells of the type shown in Fig. 1 were used for application of layers to flat surfaces. The carefully ground edge of the glass casing is pressed flush with the cathode. The platinum anode is arranged to be strictly parallel with the cathode. With a selection of glass vessels it is possible to obtain layers of varying area and shape.

Figure 2 shows a cell for application of layers to the inner surfaces of cylinders. The lower end of the cylindrical cathode is pressed against a special base with an interlayer; the electrolyte is poured inside; the

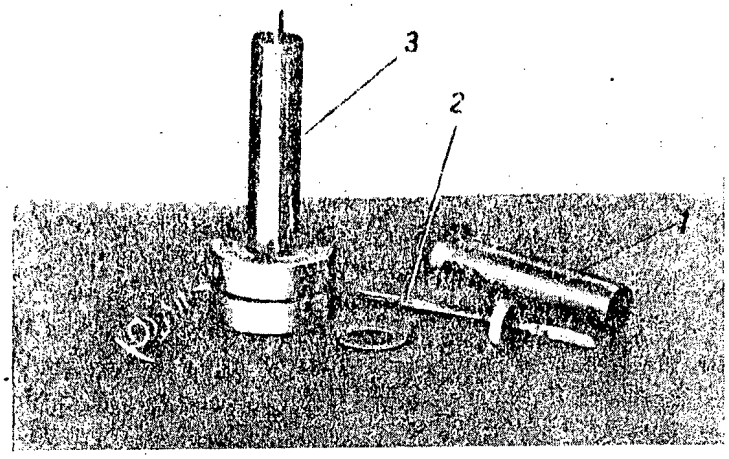

anode (a platinum wire or a cylinder of smaller diameter) is accurately centered. Layers on spherical surfaces are obtained in a special cell, in which the anode is a spherical platinum grid or basin; in this case the cathode must also be accurately centered. The design of the cells may be modified according to the experimental requirements.

Apart from platinum, the cathode may also be made of nickel, aluminum, and other metals. The cathode surface is polished and degreased before the experiment.

The electrolyte is stirred by rotation of one of the electrodes, but if gas evolution is abundant stirring is not essential.

Experimental Methods

Electrolysis of neutral solutions of amercium, curium, and plutonium (III). The best results, from the point of view of complete deposition and of the required quality of the layers, were obtained by electrolysis of neutral solutions of trivalent chlorides. The solvent was a mixture of 50% ethyl alcohol, 45% acetone, and 5% water. The current density for the electrodeposition was 0.2 m a/cm^2.

Aqueous solutions of plutonium trichloride were obtained by reduction of the tetrachloride by hydroxylamine or hydrogen in presence of platinized platinum. Excess acid must subsequently be carefully removed.

The best method for obtaining plutonium in the trivalent state is chlorination of plutonium dioxide by carbon tetrachloride in an inert gas atmosphere at 625-650°C.

For the electrolysis, the anhydrous plutonium trichloride was dissolved in the minimum volume of water and diluted with alcoholic acetone.

The preparation of neutral solutions of americium and curium chlorides presents no difficulties.

The electrolytic procedure described resulted in quantitative deposition of the elements and yielded layers of quite satisfactory quality, the maximum thickness in the case of plutonium approaching 0.5 mg/cm^2.

Electrolysis of acid solutions of americium, curium, and plutonium (III). Weakly acidic electrolytes can also be used for the deposition. This appreciably simplifies the preparation of the starting materials, but the deposition is accompanied by evolution of hydrogen, which rather worsens the quality of the deposits. The electrolysis conditions must be strictly adhered to in such cases, as the current densities and electrolyte acidities required to give satisfactory layers are found to be interdependent.

Electrodeposition of plutonium was effected from hydrochloric acid – alcoholic acetone solutions of the composition indicated above, at pH 1.5 to 2 and current density 5-10 m a/cm^2. Plutonium was deposited in usable amounts and layers of satisfactory quality up to 0.3 mg/cm^2 thick were obtained.

Electrodeposition of americium and curium was carried out at a current density of 10 m a/cm^2 and electrolyte pH 2 to 2.5. However, the acidity should always be kept as low as possible, as this makes it possible to lower the current density, diminish gas evolution, and improve the quality of the deposits.

The choice of the electrode (cathode) material for an acid medium is in practice confined to the noble metals.

To avoid desolving the cathode deposit formed, the electrolyte must be removed without interruption of the current.

As the electrodeposition conditions for all three elements are essentially the same both in neutral and in weakly acidic media, these elements may be deposited simultaneously if necessary.

Electrodeposition of plutonium from tetrachloride solutions. Plutonium (IV) solutions are hydrolytically stable only in fairly acid media. Therefore in this case the electrolytic deposition of plutonium was effected from an alcoholic acetone solution of the tetrachloride at pH 1, with a current density of 40 m a/cm^2. In some instances up to 97% of the plutonium was deposited in the form of layers of satisfactory quality up to 0.3 mg/cm^2 thick. In these conditions the electrolysis was accompanied by considerable evolution of gas and heat, and it was necessary to cool the electrolyte continuously.

The foregoing methods have been used repeatedly by the authors in the laboratory. The results are reproducible and reliable, and these methods can therefore be recommended for the production of thin layers of transuranic elements, suitable for nuclear investigations and other experiments.

Received May 4, 1956

LITERATURE CITED

[1] V. B. Debov and V. N. Kosyakov, Investigations in the Fields of Geology, Chemistry and Metallurgy, Papers of the Soviet Delegation at the International Conference on the Peaceful Uses of Atomic Energy (Acad. Sci. USSR Press, 1955), p. 250.

DETERMINATION OF THE HALF-LIFE OF Ac^{227} BY A CALORIMETRIC METHOD

N. S. Shimanskaya and E. A. Yashugina

Recent determinations of the half-life of Ac^{227} have not been very reliable. The published values of this quantity range from 10 to 30 years [1]. For a long time, the most accurate value was taken to be T = 13.5 years, obtained in 1928 by Meyer [2] from detailed measurements of the decay curve of an actinium preparation.

F. Curie and G. Bouissieres [3] found that the half-life of Ac^{227} was 21.7 years. This value was verified by Hollander and Leininger [4] who found the half-life of Ac^{227} to be 22 ± 0.3 years from a measurement with a differential ionization chamber.

Having available a suitable amount of pure Ac^{227} we have attempted to determine the half-life of this isotope by a calorimetric method. As is known, the calorimetric method of measuring the half-life of long-lived isotopes entails a determination of the heating produced in a calorimeter of known weight by an amount of radioactive material. If p is the weight of radioactive material in the sample being investigated (in grams) and Q is the amount of heat generated per unit time, then from the fundamental formula for radioactive decay we have:

$$T = \frac{N \cdot \ln 2}{dN/dt} = \frac{p \cdot \frac{N_0}{A} \cdot \ln 2}{Q/\epsilon},$$

where N_0 is Avogadro's number ($6.025 \cdot 10^{23}$), A is the atomic weight of the radioactive isotope and ϵ is the energy produced in the calorimeter per decay event. The last quantity is easily calculated if one knows the decay scheme.

The sample with which this study was carried out was first cleaned chemically. The final weight of the sample compound ($Ac_2^{227}O_3$) was 2.01 ± 0.02 mg. Spectral analysis of the source indicated that it contained (as compared with the weight of actinium) the following: Fe (3%), Pb (3%), Ba (2%), Na (~ 1.5%), Si (~ 0.5%) and some insignificant amounts of Al, Mg and Ca. There were no radioactive impurities.

In one stage of the cleaning process both Th and the isotope RdAc were precipitated, both being daughter products of Ac^{227}. For this reason, all the main calorimetric measurements were carried out after 6 months, that is, after radioactive equilibrium was established in the sample. The measurements were performed in the double static calorimeter used at the Radiation Institute, Academy of Sciences USSR for such measurements of radioactive materials [5]. The heating capacity of the sample was found to be 23.7 mw (± 0.5 %). In determining the activity it was assumed that in the total decay energy of the sample at equilibrium ϵ = 33.69 $\frac{\text{Mev}}{\text{decay } Ac^{227}}$. This value of ϵ was computed on the basis of the most recent experimental data on the energies and yields of radioactive emanations for all elements of the actinium series. Taking into account the corrections for the decays which occurred in the time following weighing and the absorption of γ-rays in the walls of the calorimeter cylinder, the activity of the sample was found to be 120.1 ± 1.2 mC. Calculations using the formula given above indicate that the half-life of Ac^{227} is 21.2 ± 0.8 years.

The present value of T, taking into account the error limits, is in agreement with the results obtained in [3 and 4].

It should be noted that the spectral analysis which was performed on the source was not comprehensive and does not rule out the presence of insignificant amounts of other elements aside from those indicated above. In particular, no attempt was made to control the content of arsenic, sulfur and certain other elements; it is not likely, however, that these are present. If these elements are present, then the value of T obtained in the present work would be somewhat high.

In conclusion the authors wish to express their gratitude to their collaborators at the A. A. Zhdanov Leningrad State University, N. I. Kaliteevsky and A. N. Razumovsky, for carrying out spectral analysis of the sample.

LITERATURE CITED

[1] I. Hollander, I. Perlman, and G. Seaborg, Rev. Mod. Phys. 25, 469 (1953).

[2] S. Meyer, Wien. Ber. 137, 235 (1928).

[3] F. Curie and G. Bouissieres, Cahier phys. 26, 1 (1944).

[4] I. Hollander and R. Leininger, Phys. Rev. 80, 915 (1950).

[5] N. Shimaskaya, Works Rad. Inst. Acad. Sci. USSR 7, 1, 216 (1956).

Received March 29, 1956.

ALCOHOL AND IONIZING RADIATION

N. V. Luchnik

In recent years the attention of numerous workers has been directed to studies of means of reducing the harmful biological effects of radiation. The interest in such means is due, first, to the fact that their study will provide a basis for the development of methods of prevention and cure of radiation damage, and second, to the fact that such experiments help to give a deeper insight into the mechanism of the biological action of radiation.

The literature contains a number of references to the protective action of ethyl alcohol. The use of ethyl alcohol before irradiation decreases damage to bacteria [1], infusoria [2], frogs [3], and mice [3 - 5]; it is ineffective for rats [5] and dogs [6].

These results are not only of theoretical but also of considerable practical interest, as alcohol is a product of low toxicity which has long been used in medicine. Some authors have suggested the use of alcohol for the treatment of radiation sickness [7]. However, in view of the general availability of alcohol this could lead to abuse of alcohol, which is undesirable not only because of the harmful effects of alcohol in general, but because its protective action is not sufficiently well understood.

TABLE 1

Protective Action of Ethyl Alcohol, Introduced Into the Abdominal Cavity in Doses of 50 mg per Animal Immediately Before Irradiation, on Different Strains of Mice

Strain of experimental mice	Radiation dose, r	Control mice			Mice with ethyl alcohol			P
		number of mice	died by the 30th day		number of mice	died by the 30th day		
			number	%		number	%	
Females, M	500	12	8	66.7	12	5	41.7	0.207
Females, X	600	12	9	75.0	12	3	25.0	0.019
Females, H	700	30	20	66.7	30	18	60.0	0.590
Males, H	700	24	17	70.8	24	9	37.5	0.020

A number of experiments have been carried out in our laboratory on the use of alcohol in irradiation, and the results suggest that in these conditions alcohol is harmful rather than useful.

White mice were used for the experiments. Co^{60} γ-radiation at a dose rate of 42 r/minute was used. Since some protective substances have different effects on different animals [8], mice of three different strains and of different sexes, with different radiation sensitivities [9] were used. For females of M, X, and H strains the 50/30 lethal dose* is 460, 560, and 590 r respectively, and for H males it is 530 r. The experimental animals, of 20 g average weight, were each injected with 50 mg ethyl alcohol in the form of 25% aqueous solution into the abdominal cavity. The results of these experiments, shown in Table 1, confirmed the existing data on the protective action of alcohol. It is also seen that alcohol has different effects on different mice. Statistical treatment (by means of the χ^2 criterion [10]) shows that a real decrease of mortality occurred only in strain

* Dose which leads to death of 50% of the animals in 30 days.

TABLE 2

Effect of Ethyl Alcohol (150-200 mg per Animal), Administered in Irradiation by 700 r Doses, on the Mortality of White Mice (Strain H Males)

Experimental group	Number of mice	Died in 2 days			Died in 20 days		
		number	%	P	number	%	P
Irradiation only	20	0	0	—	18	90.0	—
Alcohol only	18	1	5.6	0.500	2	11.1	—
Alcohol before irradiation	20	6	30.0	0.010	12	60.0	0.032
Alcohol after irradiation	17	11	64.8	0.000	14	82.4	0.500

X females and strain H males. Experiments with the H mice were especially illuminating; the male mortality decreased by 35% and the female mortality by only 7%. On the average, however, the protective action of ethyl alcohol was fairly pronounced. The figure shows mortality curves based on combined data on all the strains. The curves show that a difference in mortality between the control and experimental mice existed throughout the experiment. By the end of a month 43 of 78 experimental animals survived, and only 21 of the same number of controls. Thus, ethyl alcohol on the average doubled the survival rate. The protective action of alcohol is restricted by the radiation dose. When it was introduced before irradiation with 100 r doses, all the animals died, and their survival period was no longer than that of the controls. Alcohol has no curative properties; that is, it does not decrease mortality when introduced after irradiation. In several experiments alcohol was introduced after irradiation, but in no case was there a real decrease of mortality.

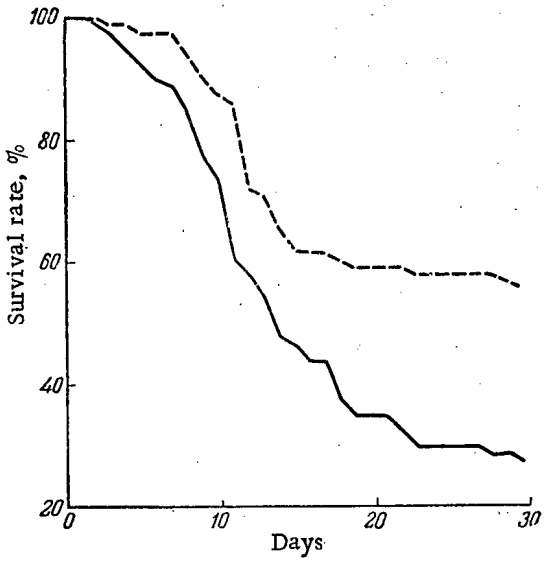

Mortality curves for mice in all the experiments, with 50 mg doses of alcohol. The continuous line represents the survival of the control mice in the course of the experiment, the broken line, the same for the protected mice. Each group contained 78 animals.

The most interesting results were obtained with large doses of alcohol. It was found that large but not lethal doses of alcohol, administered against a background of irradiation, caused death. This effect was especially pronounced when alcohol was administered after irradiation. Table 2 shows the results of one such experiment. In this experiment strain H males received 150-200 mg doses of alcohol and irradiation at a dose of 700 r. At this dosage the mice began to die not earlier than the third or fourth day; on the other hand, toxic doses of alcohol caused death of nonirradiated mice within the first two days. Therefore the mortality during the first two days must be attributed to alcohol, and the later mortality to irradiation. Table 2 shows a quite real and considerable increase of the toxicity of alcohol, although in the final analysis its administration before irradiation has a protective effect in this case also.

In view of the fact that ethyl alcohol does not have the same protective effects on different mice exposed to radiation, there is no reason to believe that it alters the course of the primary physico-chemical processes, as is highly probable in the case of other protective agents such as anaerobiase or cysteine [11]. The fact that alcohol, while decreasing the mortality of irradiated animals, is nevertheless toxic, suggests that its protective action is effected through metabolic changes.

The actual biochemical mechanisms by which the effect is brought about require special investigation.

It may be concluded from these results that the use of alcohol after irradiation is ineffective. The data on the increased toxicity of alcohol to irradiated animals provide a warning against the use of alcohol in work in which irradiation is possible.

Received March 14, 1956

LITERATURE CITED

[1] A. Hollaender, T. Stapleton, and W. Burnett, "Variations of sensitivity to x-rays under the action of chemical substances," in Isotopes in Biochemistry (Foreign Lit. Press, 1953) p. 96.

[2] R. F. Kimball, N. Gaither, Genetics 36, 558 (1951).

[3] E. I. Bakin, I. P. Dolgachev, and O. S. Ilyina, cited by M. N. Pobedinsky, Radiation Complications on X-Ray Radiotherapy (State Medical Press, 1954).

[4] E. Paterson, and J. J. Matthews, Nature 168, 1126 (1951).

[5] L. J. Cole, and M. E. Ellis, J. Physiol. 170, 724 (1952).

[6] P. I. Lomonos, Summaries of Reports at the Administrative Plenum of the All-Union Society of Roentgenologists and Radiologists, June, 1952.

[7] H. Nevermann, Klin. Wochenschr. 2, 1747 (1923).

[8] H. S. Kaplan and J. Paull, Proc. Soc. Exper. Biol. Med. 79, 670 (1952).

[9] N. V. Luchnik "Dependence of the mortality of irradiated mice and rats on the radiation dose, sex, weight, and strain of the animals, and the time distribution of this mortality," Reports of the Biophysical Laboratory, Ural Branch, Academy of Sciences USSR 1956, No. 1.

[10] B. I. Romanovsky, Use of Mathematical Statistics in Experimentation (State Tech. Press, 1947).

[11] H. M. Patt, Phys. Rev. 33, 35 (1953).

INVESTIGATION OF THE PROTECTIVE PROPERTIES OF CONCRETE

V. S. Dikarev, M. B. Egiazarov, E. N. Korolev, and V. G. Madeev

The protection around nuclear reactors should be effective enough to weaken both γ-radiation and neutrons of various energies emitted from the active zone of the reactor. Materials consisting of combinations of heavy and light elements provide the most effective protection against radiations from nuclear reactors.

Substances containing hydrogen are most commonly used for the light components, but this only has an appreciably retarding effect on neutrons with energies not exceeding a few Mev. Retardation of neutrons of higher energy by hydrogen is slight because of the small scattering cross section. Heavy elements ensure effective retardation of high-speed neutrons as the result of inelastic scattering and theyalso effectively absorb γ-radiation emitted from the nuclear installation or formed in the protective screen in the course of neutron retardation and absorption.

Concrete is the most convenient and cheapest protective material. The protective properties of concrete are determined by the composition of the aggregate used in it. By suitable choice of aggregate it is possible to obtain optimum protective properties with respect to various types of radiation [1 - 3].

This communication presents the results of an investigation of the space distribution of neutron and γ-ray streams in two grades of concrete: ordinary (PSh grade) and limonite (LL grade). The protective properties of these concretes were studied with the use of radiation from the active zone of an experimental nuclear reactor with ordinary water. The purpose of the investigations was to obtain experimental data for calculation and design of concrete shields for a proposed nuclear reactor intended for investigations in the fields of nuclear physics, radiochemistry and biology.

Chemical Composition of Concretes in %

Chemical compounds	Ordinary concrete (PSh grade)	Limonite concrete (LL grade)
SiO_2	68.3	8.0
Al_2O_3	9.2	2.1
Fe_2O_3	3.3	61.7
CaO	7.4	8.2
MnO	1.2	0.6
SO_3	0.6	0.6
Moisture	7.6	10.8
Impurities	2.4	8.0

The materials studied were ordinary concrete , average density 2.4 g/cc, containing 30% sand (by weight), 52.4% gravel, 9.7% cement, and 7.3% water; and limonite cement, average density 2.7 g/cc, containing 33.7% limonite sand, 44.6% limonite gravel, 12% cement, and 9.7% water. The chemical compositions of these two concretes are shown in the table.

Blocks 750 × 750 × 105 mm in size were made from the concrete. The concrete blocks, placed in an experimental recess in the reactor, formed a prism 750 × 750 mm in section and 1260 mm long. Measures were taken to prevent direct passage of radiation from the reactor along the side faces of the prism. The distance from the front edge of the prism to the center of the active zone of the reactor was 860 mm.

Gamma-radiation was detected by means of a small graphite ionization chamber. The high-speed neutron flux was measured by means of a threshold phosphorus indicator by the reaction $P^{31}(n, p)Si^{31}$ ($E_{eff} \approx 1.5$ Mev). Resonance neutrons were detected by an iodine indicator ($E_0 \approx 20$-50 ev) surrounded by cadmium, and thermal neutrons by a dysprosium indicator and a counter filled with BF_3 gas. The total neutron flux was measured by means of an "all-wave" counter.

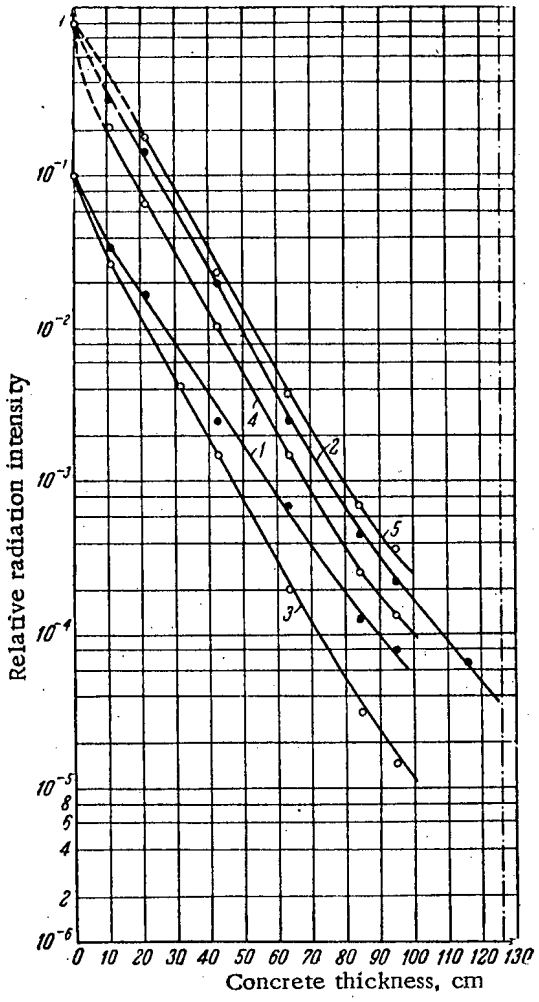

Fig. 1. Curve for the attenuation of γ-radiation intensity and neutron flux in ordinary concrete. 1) γ-rays; 2) high-speed neutrons; 3) total neutron flux; 4) resonance neutrons; 5) thermal neutrons.

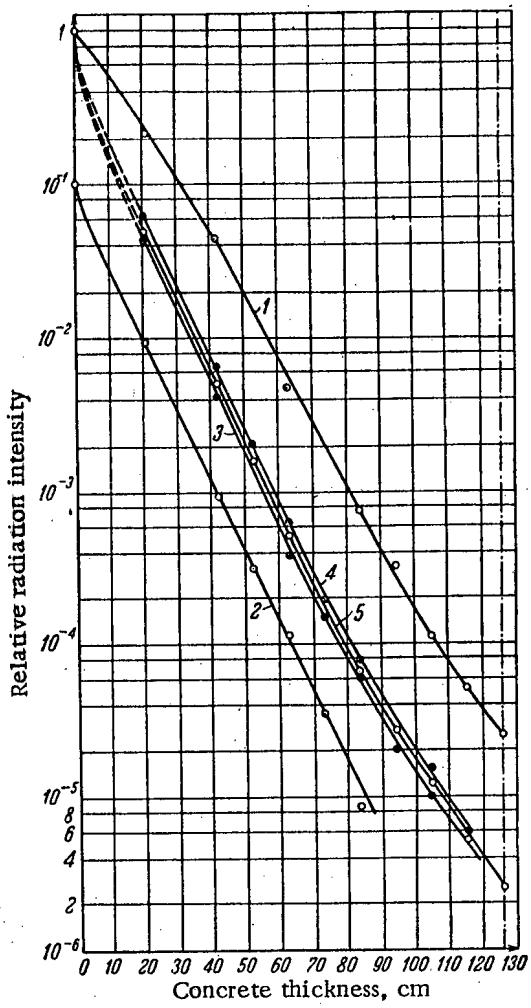

Fig. 2. Curve for the attenuation of γ-radiation intensity and neutron flux in limonite concrete. 1) γ-rays; 2) high-speed neutrons; 3) total neutron flux; 4) resonance neutrons; 5) thermal neutrons.

For measurements of the γ-radiation intensity and the flux of high-speed, resonance, and thermal neutrons the detectors were placed in the concrete at various distances from the source. With this method of measurement it is necessary to take into account not only weakening of the radiation in the protective screen, but also weakening due to the distance from the active zone of the reactor.

For measurement of the attenuation of the total neutron flux the "all-wave" counter was placed behind the concrete prism at a definite distance from the center of the active zone. The thickness of the concrete was varied by consecutive removal of the concrete blocks, starting with the one farthest from the active zone of the reactor. The space distribution of the total neutron flux measured in this way depends only on the thickness of the concrete.

Figures 1 and 2 show, in semilogarithmic coordinates, curves for attenuation of γ-radiation and neutron flux in ordinary and limonite concretes. The results of measurements within the concrete were multiplied by the square of the distance between the point of measurement and the center of the active zone, so as to exclude attenuation due to the geometrical factor. The root mean square error is 8%.

The graphs show that in the range of distances between 20 and 80 cm the space distribution of neutrons of different energy groups in the concretes studied is determined by the space distribution of the high-speed neutrons. Attenuation of the neutron flux in this region approximately follows an exponential law with relaxation lengths of about 11 cm and 9 cm for ordinary and limonite concrete respectively.

At high thicknesses of concrete (> 80 cm) the curves for attenuation of neutron flux become flatter, and the relaxation lengths increase to approximately 16 cm for ordinary and 13 cm for limonite concrete. It seems that the more penetrating component of the high-speed neutrons begins to take effect here, and this determines the space distribution of neutrons at large thicknesses of concrete.

The γ-ray flux in concrete is the sum of the primary γ-ray flux from the active zone of the reactor, and the secondary γ-quanta generated in the concrete by the interaction of neutrons with nuclei of substances forming part of the concrete.

Attenuation of the γ-radiation intensity in the concretes studied to a depth of 80 cm is determined largely by primary hard γ-quanta from the reactor. In this region the decrease of the γ-radiation intensity is characterized by relaxation lengths of $\approx$ 13 cm and 11 cm for ordinary and limonite concrete respectively.

The relaxation length of γ-radiation in concrete more than 80 cm thick corresponds to the relaxation length of the leading component of the high-speed neutrons. This type of curve for the decrease of γ-radiation intensity at high shield thicknesses is probably the result of a decrease in the fraction of primary hard γ-radiation from the reactor relative to the secondary γ-radiation, while the relaxation length of the latter is less than the relaxation length of slowed-down neutrons.

The results of this investigation show that limonite concrete has more effective protective properties than ordinary concrete against the neutron and γ-ray spectra studied.

Received May 17, 1956

LITERATURE CITED

[1] P. Jensen and O. Ritter, Z. Naturforsch. 2a, 376-384 (1947).

[2] P. C. Gugelot and H. G. White, J. Appl. Phys. 21, 369-374 (1950).

[3] V. Delano and C. Goodman, J. Appl. Phys. 21, 1040-1047 (1950).

[4] Yu. G. Nikolaev, Reactor Construction and Reactor Theory, Papers of the Soviet Delegation at the International Conference on the Peaceful Uses of Atomic Energy (Acad. Sci. USSR Press, 1955), pp. 91, 119.

SCIENCE NEWS FEATURES

DISCUSSION OF QUESTIONS OF THE DEVELOPMENT AND USE OF HIGH-ENERGY ELEMENTARY-PARTICLE ACCELERATORS AT THE SYMPOSIUM OF THE EUROPEAN CENTER FOR NUCLEAR RESEARCH (CERN) IN GENEVA

From June 11 to June 23, 1956 there took place in Geneva an International Conference on High-Energy Accelerators and Meson Physics*, called by CERN. About three hundred physicists and engineers from twenty countries took part in the conference, among them about forty Soviet specialists. The first week of the conference was devoted to questions of the development and use of high-energy accelerators.

The foreign scientists gave their main attention to new types of accelerators with magnetic fields constant in time. Of primary interest among these are the ring-shaped strong focussing constant-field accelerators. Besides simplification of the technical problems of construction, this type of accelerator has the advantage of a considerable increase of the intensity of the accelerated beam.

The first accelerator of such a type (the ring phasotron) was proposed by the Soviet scientists A. A. Kolomensky, V. A. Petukhov, and M. S. Rabinovich as early as 1953. A characteristic property of the ring phasotron is the presence of sections with reversed direction of the magnetic field. Subsequently an analogous accelerator was also proposed by K. R. Symon (USA), who presented a report at the conference (on behalf of himself and Laslett) on theoretical studies of the motion of particles in constant-field accelerators. In a report by Jones and others (USA) data were presented on a small working model of a ring phasotron in which electrons are accelerated from 20 to 400 kev by a revolving electric field.

Another variety of constant-field ring accelerator has the distinguishing feature that the pole faces consist of several spiral ridges to produce a magnetic field of the necessary form. The possibilities of these accelerators were considered in the report of Pickavance, who spoke for the Harwell group of scientists (England), and in the report of D. W. Kerst, representing the MURA group (USA). The reports of A. Roberts and R. Saltzman (USA), and E. M. Moroz and M. S. Rabinovich (USSR) were devoted to the development of the theory of the cyclotron with azimuthal variation of the magnetic field (Thomas type), the use of which may perhaps make it possible to extend the cyclotron mode of acceleration right up to several hundred million electron volts.

Recently the attention of specialists has been drawn to systems in which it might be possible to produce collisions between intense beams of relativistic particles. If in the laboratory system of coordinates the energy of the particles in each beam is E, then in the collision of such particles the effect is essentially that of a greater energy, of the order of $2\gamma^2 E$, where $\gamma = E/m_0c^2$. But in order for such collisions to occur in numbers sufficient for physical experiments, the current of the accelerated particles must attain enormous magnitudes, at least of the order of some tens of amperes. Problems of developing systems with colliding beams of great intensity were considered in reports by D. W. Kerst and G. K. O'Neill (USA).

Great interest and lively discussion were aroused by the reports of the Soviet scientists V. I. Veksler and Ya. B. Fainberg on new methods of acceleration.

---

*See also the report by Ya. A. Smorodinsky, p. 832.

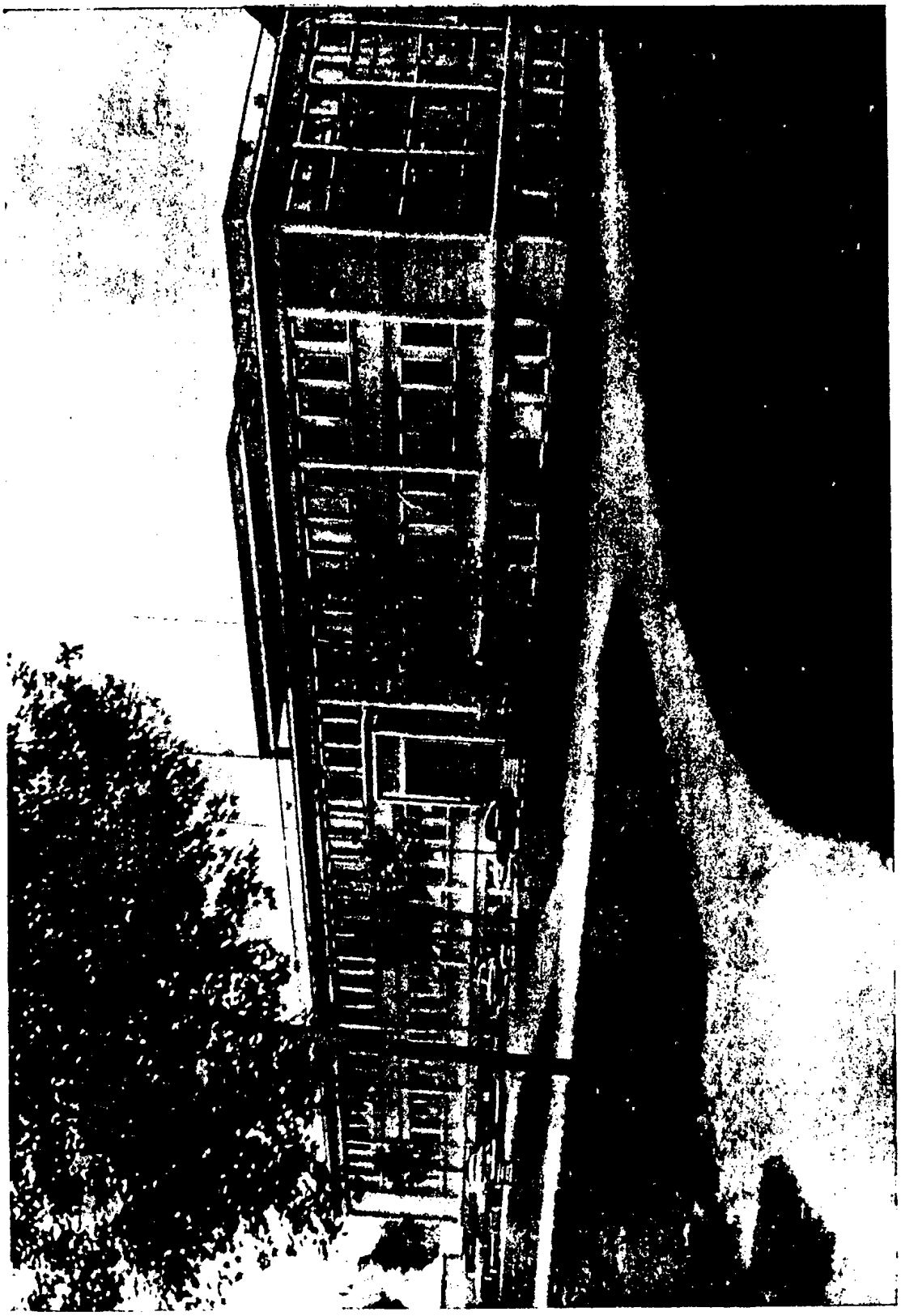

Building of the Physical Institute in Geneva, where the CERN symposium on high-energy particle physics was held (June, 1956).
Photograph by V. Parkhitko

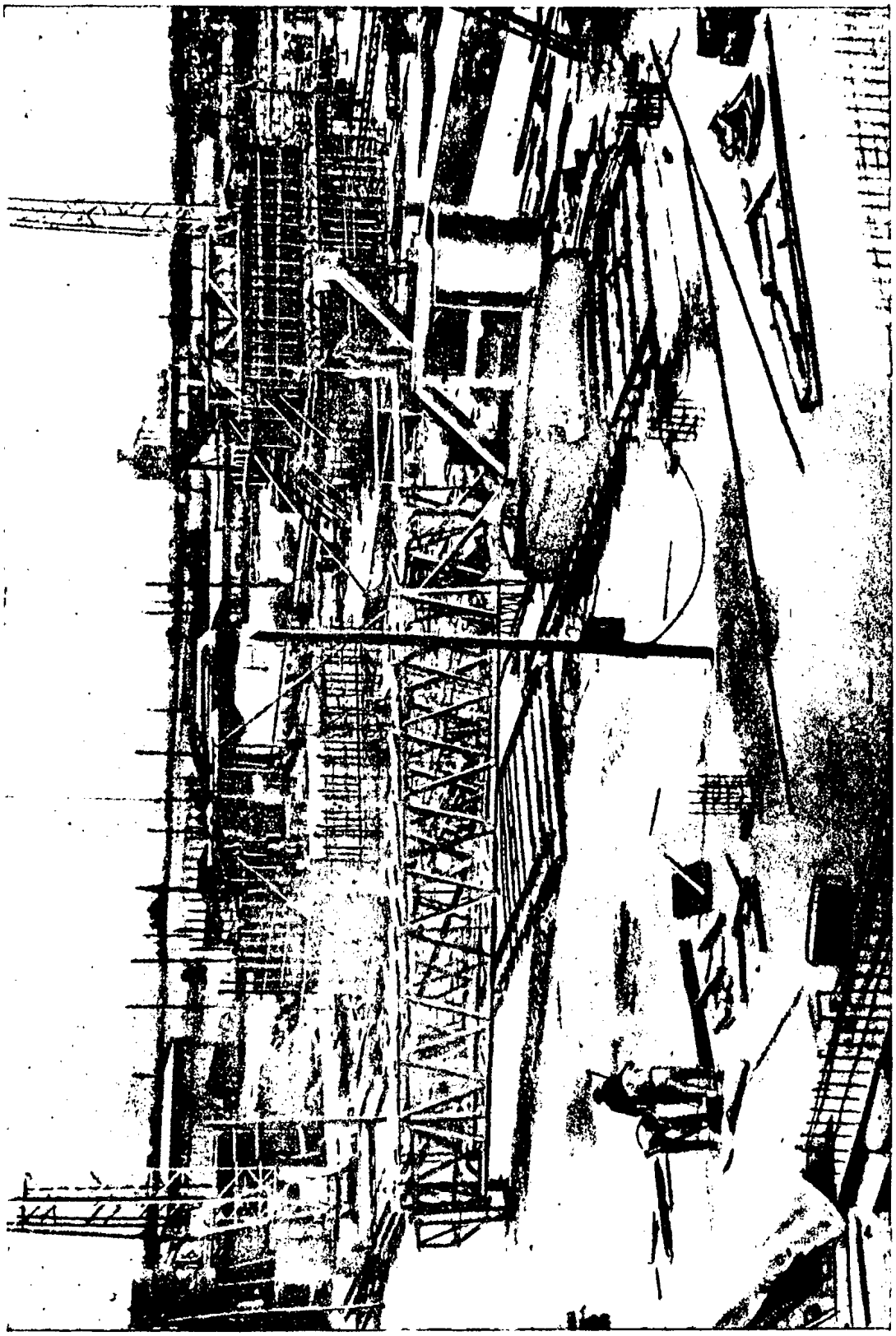

Construction of the largest synchrophasotron in Western Europe, 9 km north of Geneva, on the Swiss-French frontier.
Photograph by V. Parkhitko

A. A. Naumov gave a report on behalf of G. I. Budker on the physical properties of the electron beam and the theory of its relativistic stabilization, and about the experimental researches carried out by himself and G. I. Budker*. By a stabilized beam is meant an intense beam of relativistic electrons revolving in a magnetic field, with the charge of the electrons compensated to a certain extent by ions. The accelerated ions moving in such a beam must be subject to deflecting and focussing forces greater by two or three orders of magnitude than in ordinary cyclic accelerators. The main difficulty is evidently that the required current of relativistic electrons in the beam has to reach very large values (of the order of 20,000 amp).

V. I. Veksler told about his proposed "coherent" method for accelerating particles. If a cluster of particles is sufficiently small, then in its interaction with an electron beam or an electromagnetic wave the size of the accelerating field proves proportional to the number of particles in the cluster, i. e., the interaction occurs in a coherent manner. In other words, the accelerating field can be multiplied by an enormous factor. The difficulty of carrying out this method is due to the problem of producing sufficiently compact clusters of protons with the number of particles between 10^{11} and 10^{13}.

The report of Ya. B. Fainberg was devoted to a new modification of linear accelerators. He considered the possibilities of using as the accelerating system in linear accelerators plasma waveguides and beams of charged particles, and pointed out definite advantages of such systems. Besides this, he proposed and developed a method of variable-phase focussing in linear accelerators, analogous to strong focussing in cyclic accelerators, which makes it possible to achieve simultaneous radial and phase stability.

Problems of the passage through the critical energy in strong-focussing accelerators were dealt with in reports by G. K. Green (USA), K. Johnsen (CERN), A. A. Kolomensky, and L. L. Sabsovich (USSR). G. K. Green reported, in particular, that the passage through the critical energy was first accomplished experimentally at the Brookhaven Laboratory with a special electron synchrotron with variable-gradient electrostatic fields. The frequency of the accelerating field was controlled by means of the accelerated beam itself.

V. V. Vladimirsky (USSR) told about the main parameter values of the strong-focussing 7 Bev synchrotron built in our country, and about the projected large synchrotron of the same type for energies 50-60 Bev (authors of report V. V. Vladimirsky, E. G. Komar, A. L. Mints, et al.**). A characteristic feature of these synchrotrons is the elimination of the critical energy by the introduction of special compensating magnets. Such a system was suggested in the USSR by V. V. Vladimirsky and E. K. Tarasov.

In a number of reports – those of J. J. Livingood (USA), G. Salvini (Italy, and M. G. White (USA) – accounts were given of proposals and plans for lessening the expense and reducing the weight of high-energy accelerators.

In the use of cyclic accelerators it is necessary to devise effective means for bringing out the accelerated particles. Among a number of communications on this subject, note must be taken of the report of G. B. Collins (USA) about the method of removal and the characteristics of the proton beam of the 3 Bev Brookhaven cosmotron, and the report of V. P. Dmitrievsky (USSR) on the effective removal of the proton beam from the 680 Mev synchrocyclotron.***

In reports by A. Citron (CERN) and V. V. Vladimirsky (USSR), who represented a group of authors, accounts were given of proposed arrangements for beam removal from strong-focussing accelerators.

In the development of present strong-focussing accelerators requiring very strict tolerances for various specifications, it is not permissible to rely on the linear theory, and it is necessary to use a nonlinear treatment of the motion of the particles. Various problems of this theory were considered in reports by M. G. Hine, R. Hagedorn, and A. Schoch (CERN), E. D. Courant (USA), A. A. Kolomensky (USSR), K. R. Symon (USA), and others.

Problems of designing electromagnets for cyclic accelerators and methods for measuring and correcting the magnetic field were subjects of reports by C. A. Ramm (CERN), H. Bruck (France), H. E. Blewett (USA), E. G. Komar (USSR), and J. W. Blamey (Australia).

---

*The report of G. I. Budker is published in this issue of this journal, page 673.

**See Atomic Energy, No. 4, page 479.

***See Atomic Energy, Nos. 4 and 5, page 459.

The radio-frequency systems of various accelerators were discussed in reports by C. Schmelzer and K. Johnsen (CERN), S. M. Rubchinsky and others (USSR), R. L. Thornton (USA), and I. Kh. Nebiazhky, A. L. Mints, and B. I. Poliakov (USSR). In the report of C. Schmelzer and K. Johnsen, a study was made of the important problem of controlling the frequency of the accelerating voltage in the strong-focussing synchrophasotron by means of signals obtained from the beam.

Lively discussion among the participants in the conference was aroused by reports devoted to the problems of developing high-energy electron synchrotrons. M. S. Livingston (USA) gave the basic data on the plan developed under his direction for a 6 to 7 Bev strong-focussing synchrotron. An important property of large electron synchrotrons is the presence of intense electromagnetic radiation from the electrons. A. A. Kolomensky (USSR) reported on a theory developed by himself and A. N. Lebedev of the influence of this radiation on the motion of the electrons in the synchrotron. It was shown that, depending on the type of magnetic system used, the radiation can lead either to strong damping or to divergence of the oscillations of the particles.

Several reports were devoted to the planning and implementing of linear accelerators for high energies and large currents, in particular linear accelerator injectors for large installations. B. K. Shembel' (USSR) gave a report on behalf of a number of authors on several problems of the operation of linear accelerators at large currents. In the report of K. D. Sinelnikov, Ya. B. Fainberg, and P. M. Zeidlits (USSR) the possibility was indicated of a modification of the linear accelerator, in which the focussing is accomplished by means of a magnetic field, and the accelerator itself is bent into an open ring.

Experience in the operation and use of large accelerators, which is of great practical interest, was described in reports by L. W. Smith (USA), E. J. Lofgren (USA), and V. P. Dzhelepov (USSR), who represented a group of authors.

On the whole it must be said that "accelerator week" at the Geneva conference provided much new and valuable material, which will aid greatly in the further development of the physics and technology of accelerators.

K. A.

DISCUSSION OF PROBLEMS OF HIGH-ENERGY PARTICLE PHYSICS AT THE SYMPOSIUM OF THE EUROPEAN CENTER FOR NUCLEAR RESEARCH (CERN) IN GENEVA

(Impressions of a Soviet delegate)

During the second week in Geneva* we heard reports on work carried out with accelerators and about new apparatus constructed for this work. The program was very diversified and the days were quite full. As during the first week, there were two sessions every day at 9:00 A. M. and 2:30 P. M. with the traditional breaks for coffee at 10:00 A. M. and for afternoon tea at 4:00 P. M. As at all of the recent conferences, these intervals and the dinner in one of the innumerable restaurants of Geneva were an essential part of the conference. The meetings and conversations at the tables led to new friendships, and the discussions begun here will probably lead to new researches.

The sessions of the conference brought forth much that was unexpected. We cannot even attempt a description of all the reports (there were about 80); all that can be done is to indicate the general directions of work and to tell in more detail about those researches which revealed new physical phenomena.

Two days were spent in discussions of experimental methods: bubble chambers ane other types of chambers, Cherenkov counters. During these days reports were given on English, American, Italian, Soviet, and French work. It was pointed out that the new devices, such as the hydrogen bubble chamber, will be uneconomical unless automatic methods of scanning and analysis are developed, since already it is becoming impossible to examine under the microscope with the human eye the enormous quantity of photographs that have accumulated in the laboratories.

If an attempt is to be made to evaluate the results presented at the conference, then we must distinguish four directions in which outstanding successes have been achieved. These are the following:

a) the discovery of the antiproton and the study of its properties,

b) scattering of electrons by protons and the structure of the proton,

c) scattering of photons by protons, and

d) π-mesonic atoms.

We must go into a fair amount of detail about each of these effects.

The antiproton. By now it is well known both from journals and from the report by Segre at the Moscow Conference in May 1956 that the antiproton exists. It was discovered in Berkeley in November, 1955 by four physicists: Wiegand, Ypsilantis, Segre, and Chamberlain [1]. The properties of the new particle were also studied by a group of Italian physicists headed by Amaldi [2]. The search for the antiproton had gone on for many years. But not one of the photographs obtained from cosmic rays had given convincing evidence of its existence. The 6.5 Bev accelerator constructed in Berkeley was to a considerable extent intended just for this experiment. The result was that the efforts of the physicists were rewarded by the proof of the existence of the antiproton.

---

*With regard to the work of the first week, see page 827.

This discovery confirmed the charge symmetry of the elementary particles. Up to this time it had been known that electrons and all the light mesons π, μ, and K exist with both signs of the charge, positive and negative. Now we know that the same is true of the heavy particles as well. Next comes the search for the antineutron, already begun in Berkeley in September 1956 *, and for the antihyperons, the neutral anti-Λ and the two (positive and neutral) anti-Σ hyperons. An interesting problem arises in connection with the Σ hyperons. According to present ideas the three particles Σ^+, Σ^0, and Σ^- are not like the triad π^+, π^0, and π^-. Whereas π^+ is the antiparticle of π^- (and, conversely, π^- is the antiparticle of π^+), Σ^+ and Σ^- are not antiparticles. If the scheme now accepted is correct (the scheme of Gell-Mann and Pais, which assigns to Σ the "strangeness" $=1$, while the "strangness" of the π meson is 0), there must exist a whole family of antiparticles: a negative antiparticle to the Σ^+, a neutral anti-Σ^0; and a positive antiparticle to Σ^-, whose basic property is that the anti Σ particles can annihilate with the emission of π mesons, while two Σ particles cannot annihilate each other in this way. The search for anti-Σ is one of the most attractive problems.

The discovery of the antiproton unexpectedly presented another problem: the first measurements of its interaction with nuclei of beryllium and lithium [3] (and also in lead glasses [4]) showed that this cross section is twice as large as the interaction cross section of protons with these same nuclei. This effect was observed at antiproton energies of 400 Mev: it may possibly increase with decreasing energy.

This paradoxical result demands further study, which began in Berkeley in June of this year.

Scattering of electrons by protons. (Hofstadter and Chambers, Stanford University, USA). The idea of observing the scattering of electrons by protons is not new. But the experimental difficulties of obtaining an external beam of high-energy electrons and of working with them have been overcome only with the linear accelerator at Stanford, which gives electrons with energies up to 1000 Mev. The first results for electrons with energies 188 and 236 Mev were published by Hofstadter in 1955 [5]. Experiments have now been completed in the energy range from 200 to 550 Mev. The results proved to be very interesting and important.

Right down to distances ("impact parameters") of the order of 1 fermi ** the scattering of electrons by protons is described by the ordinary formulas for the scattering of point particles. But at smaller distances these formulas do not give agreement with experiment. The proton acts like a particle having dimensions. These dimensions are somewhat smaller than the range of nuclear forces or the Compton wavelength of the π meson (1.4 fermi); for the mean square radius Hofstadter finds the value 0.7 to 0.8 fermi.*** The analysis of the experimental results requires the elucidation of the role of the interaction of the electron with the magnetic moment of the proton and of the space distribution of this moment.

The first theoretical analysis was given by Levy, Jenny, and Rosenbluth.

The distributions of the charge and magnetic moment, considered as static, have the same radius.

The results of these experiments, and also of the experiments on the scattering of electrons by deuterons, evidently indicate that the radius of charge and magnetic moment of the neutron are decidedly smaller, i. e., that the meson cloud surrounding the neutron is neutral for the greater part of the time. These results are, however, preliminary, and call for more careful theorectical analysis.

The researches of Hofstadter and his collaborators open up a new and fruitful development in contemporary physics. (It is interesting to note that with this same accelerator there was also carried out a brilliant series of researches by Panofsky, part of which were reported in Moscow.)

Scattering of photons by protons [Auerbach, Bernardini, Filosofo, Hanson, Odian, and Yamagata, Urbana (USA)].

The report of Bernardini was not on the program and was not expected by the parcipitants. Bernardini told about the first results of experiments in which a study was made of the scattering of high-energy photons by protons.

---

*The antineutron has actually been discovered in Berkeley.

**1 fermi = 10^{-13} cm.

***We recall that the scattering of protons by protons also indicates the existence of a "proton radius" of the order of 0.5 fermi (the two values should not agree exactly, since they relate to different phenomena).

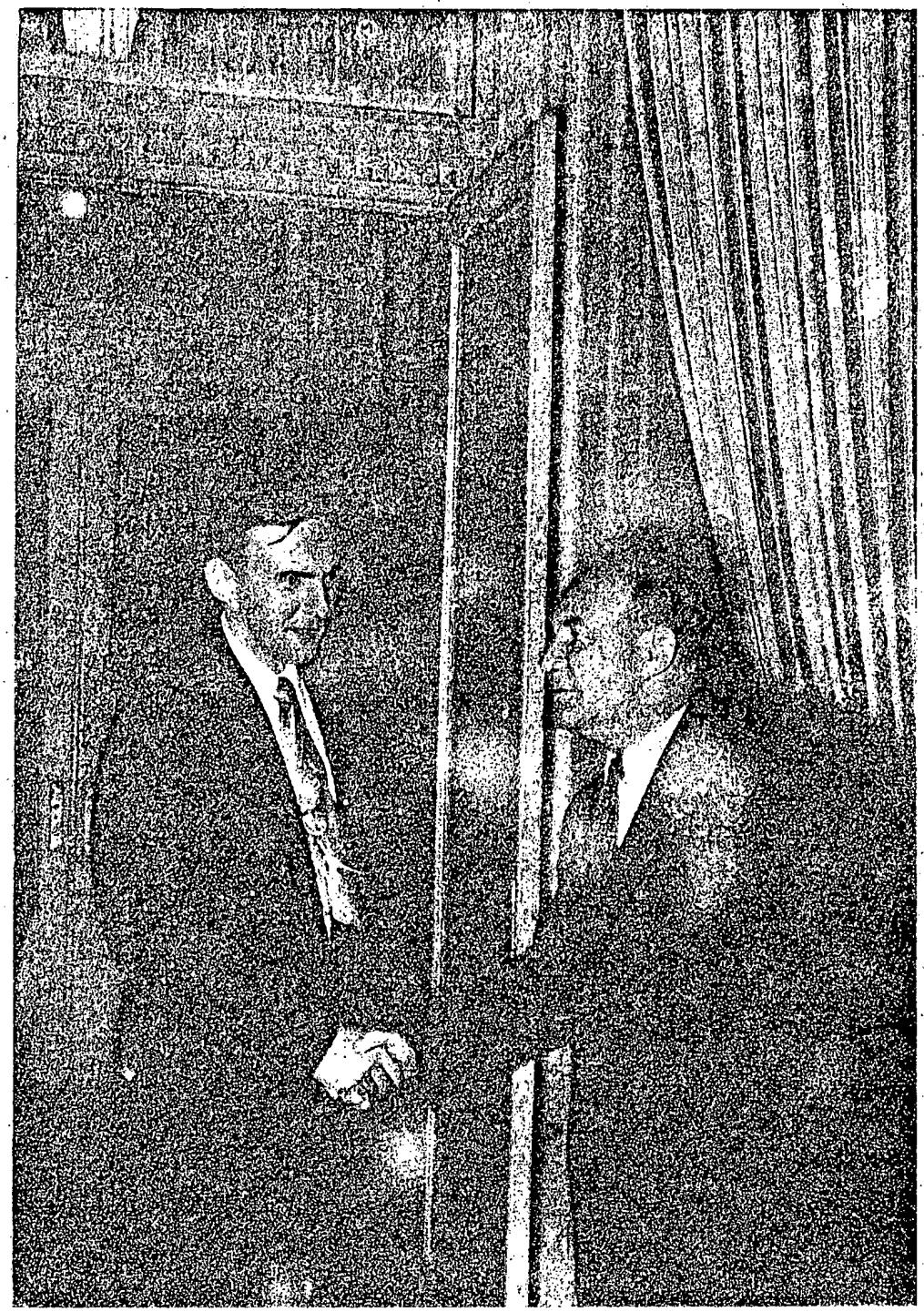

The head of the Soviet delegation at the CERN symposium on high-energy particle physics (Geneva, June, 1956), D. I. Blokhintsev, arranged a reception in honor of the participants in the symposium. Photograph: Before the beginning of the reception, D. I. Blokhintsev meets the American physicist Matthew Sands, representative at the seminar from the California Institute of Technology in Pasadena (USA).

Photograph by V. Parkhitko

Attempts to carry out such measurements have been made in many of the world's laboratories (here in the Soviet Union, in particular Goldansky recently obtained the first results on the scattering of γ-rays with energy about 140 Mev), but the results led only to some qualitative conclusions. Bernardini described all of the details of this research in an unofficial seminar. Since the work is not finished and the results are not published, the responsibility for the numbers given below is with the writer of these lines.* Measurements of the flux were carried out only in a relatively narrow range of energies of the photons (three energy values, 200, 240, and 270 Mev), and only for two angles (90° and 130° in the center-of-mass system). At these points the cross section for the Compton effect with the proton is found to be considerably greater than the cross section for scattering by a point charge (calculated from the Thomson formula), and increases with the energy. For example, for the angle 90° and the three energy values the following values of the cross section were obtained : 1.2; 5.4; 10.1 (in units $\frac{2}{3}\left(\frac{e^2}{mc^2}\right)^2 = 1.57 \cdot 10^{-32}$ cm^2 · steradian^{-1}; we recall that the total scattering cross section in these units is 4π). For the angle 130° the cross section at 200 Mev is 1.8, and for 240 Mev it is 6.9.

At the same seminar Osborne told about work by a group of physicists at the Massachusetts Institute of Technology (Rugh, Jones, Frisch, and Comer) who obtained results on the Compton effect with the proton in the energy range 40 to 130 Mev (for the angle 45°). In these experiments the cross section for energy less than 90 Mev was larger than the cross section for a point charge (by a factor of 4 at 50 Mev), and at higher energies it was less.

These results also indicate an extension of the proton, and their theoretical analysis ought to give evidence about the spatial distribution of charge and current at small distances.

An interesting addition to these experiments would evidently be a study of the polarization of the electrons and photons by the scattering. The possibility of such very difficult work was considered in the discussion.

π-Mesonic atoms. The study of mesonic atoms began several years ago. They were the subject of the last sessions of the conference in Geneva. Of greatest interest were the results presented by Stern (Pittsburgh, USA), who has carried out very careful measurements of the energies of "x-rays" arising in transitions of π-mesons from one orbit to another. In these amazingly precise experiments the error was a fraction of a percent. The K and L lines were measured in the following elements: Li, Be, B^{10} and B^{11}, C, N, O, and F. Roughly speaking, the energies of the lines (for a point nucleus and purely Coulomb interaction) should be 272.8 times those of the corresponding electronic lines (the ratio of the mass of the π meson to that of the electron).** The departures from this value are due to the size of the nuclei and to the specifically nuclear reaction of the π meson with the nuclei. The results of these measurements are not yet published and the theoretical analysis is not finished.

Besides these fundamental researches, there was discussion at the conference on a large number of new experimental facts on the scattering and production of mesons. The Soviet physicists presented the rich supply of material obtained with the synchrocyclotron at the Physical Institute of the Academy of Sciences of the USSR (all of these data will be discussed more than once in what follows).

Interesting discussions arose in connection with the problem of the scattering of nucleons by nucleons. New results were presented from the experiments of English, American, and Soviet scientists, and problems of phase-shift analysis were also discussed.

Interest was also shown in the report of Landau and Pomeranchuk on the possibility of studying the size of π mesons by examining the formation of π meson pairs by high-energy photons.

Besides the discussion of questions directly related to experiment, several theoretical seminars were conducted at the conference. Kallen (Denmark) told about a new type of proof of the inconsistency of quantum electrodynamics. An interesting survey of the application of the dispersion relations to the scattering of π mesons by nucleons was given by Salam (England and Pakistan). He also told about his attempt (together with Gilbert) to fit all the decay schemes of mesons into the form of a universal interaction.

*I take occasion to thank Prof. Bernardini for private information.

**Since relativistic effects must be taken into account, the theoretical value differs somewhat from that stated because of the difference of spin between the π meson and the electron.

There was also a discussion of the new work of Schwinger on the K mesons, in which he tried to formulate the laws of interaction of π and K mesons with hyperons and to obtain a qualitative explanation of the mass spectrum of hyperons. This work is closely related with that of the CERN physicists d'Espagnat and Prentki, which was also presented at a special seminar.

There is one more event that occurred at the conference about which we must tell: during the conference W. Pauli received a telegram from Reines and Cowan in Los Alamos (USA) about the measurement of the cross section for the reaction $p + \nu \rightarrow n + e^+$. This reaction was observed near a pile and is the inverse of ordinary β-decay. The measured cross section of $6 \cdot 10^{-44}$ cm^2 is in agreement with theory. This is the smallest cross section that has been measured experimentally. If the data are confirmed that indicate that the reaction $Cl^{37} + \nu \rightarrow Ar^{37} + e^-$ is not observed (as surmised by Alvarez in Moscow), then it must be concluded that the difference between neutrino and antineutrino has been shown by direct experiments. This same conclusion was reached recently by Awschalom [6] from a research on double β-decay, and is confirmed by experiments by Dobrokhotov, Lazarenko, and Lukyanov.

There are probably other researches about which we should tell, since it is clear that the choice of the most important work made for this survey is subjective to a high degree. We would just like to emphasize again that the Geneva conference was very useful and valuable for its participants, and this was largely made so by its excellent organization. The scientific relationships that have come from this conference will undoubtedly serve to advance our common task, the development of physics.

Ya. A. Smorodinsky

LITERATURE CITED

[1] Chamberlain, Segre, Wiegand, Ypsilantis, Phys. Rev. 100, 947 (1955); Brabant, Core, Horwitz, Moyer, Murrey, Wallace, Wentzel, Phys. Rev. 101, 498 (1956).

[2] Chamberlain, Chupp, Goldhaber, Segre, Wiegand, Amaldi, Baroni, Caltagnoli, Fransinetti, Manfredini, Phys. Rev. 101, 909 (1956).

[3] Chamberlain, Keller, Segre, Steiner, Wiegand, Ypsilantis, Phys. Rev. 102, 1637 (1956).

[4] Brabant, Core, Horwitz, Moyer, Murrey, Wallace, Wentzel, Phys. Rev. 102, 1622 (1956).

[5] Hofstadter, McAllister, Phys. Rev. 98, 217 (1955).

[6] Awschalom, Phys. Rev. 101, 1041 (1956).

THE INTERNATIONAL CONFERENCE ON NUCLEAR REACTIONS IN AMSTERDAM

From July 2 to July 7 of the current year there was held in Amsterdam an international conference devoted to nuclear reactions in the middle range of energies. Over 500 delegates from 25 countries took part in the conference, among whom were 24 Soviet scientists, who gave 35 communications. The program of the conference included 16 survey and original reports on the fundamental problems of the physics of nuclear reactions and about 150 prepared remarks on the reports and brief communications.

I. Nuclear Reactions and Models of Atomic Nuclei

In an introductory report on the development of the physics of nuclear reactions in recent years H. Bethe (USA) remarked that the most important achievement in this field was the development by Weisskopf and others of the quasioptical theory of nuclear reactions, which was based on the experiments of Barschall and his collaborators. The results of measurements of neutron cross sections, which in recent times have become extremely accurate, agree well with this theory. Bethe believes that a good foundation for the quasioptical theory of nuclear reactions, as well as for the single-particle model of nuclear structure is provided by the theory of Brueckner, developed in the years 1954-1956.

In the last few years surface phenomena have been widely investigated, in particular the stripping reaction, and this has been important for the understanding of many nuclear processes.

Much evidence has been accumulated on the dimensions of the nuclear surface, i. e., the radial distance in which the potential changes appreciably. This distance is approximately the same according to all the data, and lies between the limits 1.2 to $1.5 \cdot 10^{-13}$ cm.

A theory of collective states of the nucleus has been developed by A. Bohr, Mottelson, and others. Many researches have been devoted to the observation of these states, mainly by means of Coulomb excitation, and good agreement has been found between the predictions of the theory and the experimental results.

The emergence of new ideas led to a weakening of the role of the statistical theory and even to a certain distrust of it. But it must be noted that the statistical theory still gives the best qualtitative description of nuclear reactions in the energy range from 1 to 50 Mev and stands in need of only a certain amount of modification to take into account new mechanisms of nuclear processes. At the present time nuclear temperatures are well known. It has turned out that the nuclear temperature varies rather rapidly with the energy of the particle exciting the nucleus. From experiments on the bombardment of nuclei with 2.5 Mev neutrons the value $T \sim 0.3$ Mev is found, while for energies of the incident neutrons in excess of 10 Mev one has $T \sim 1$ Mev.

In experiments with slow neutrons many new data have been obtained about the parameters of nuclear levels, making it possible to establish certain regularities in the location of the levels and in their distribution with regard to the values of their partial widths.

Great advances have been made in experiments on the scattering of high-energy particles by nuclei. Here the main attention has been given to the study of the polarization of the particles, since at high energies it is only from data on the polarization that one can obtain full information about the interaction of the nucleons in the nucleus.

The questions touched upon in the report by Bethe were then discussed in detail in the separate sessions of the conference.

In a report by R. Christy (USA) methods were explained for analyzing the experimental data on elastic scattering of protons of energies up to several million electron-volts by light nuclei. Owing to the interference between the nuclear scattering and the Coulomb scattering, whose characteristics are known, the elastic scattering of charged particles provides considerably more information about nuclear forces than do other reactions.

In the discussion on Christy's report R. Jastrow (USA) read a communication from J. Butler and H. Holmgren about the search for an excited state with T = 3/2 in a nucleus with T = 1/2 in the ground state, to show the existence of a quartet isobaric state. Indications have been found that the nucleus F^{19} is formed in such a state when O^{18} is bombarded with 1.169 Mev protons.

The report of P. Gugelot (Holland) discussed the scattering of protons in the middle range of energies. From an analysis of the experimental data on the elastic scattering of protons it is found that the size of the mean free path of the nucleon in nuclear matter is of the same order as the dimensions of the nucleus. Such a result requires the rejection of the usual picture of the formation of an intermediate nucleus in reactions with protons and neutrons. One must take into account not only the direct interaction at the surface of the nucleus but also the fact that owing to the great transparency of the nucleus the formation of the final nucleus from the (p, p') reaction in a state near the initial state becomes especially likely, and, for example, in the reaction (p, α), where the final state of the nucleus is entirely unlike the initial state, an entirely different shape of the spectrum of emitted articles is to be expected.

The experiments (unpublished data of Brady, Princeton, USA) show that actually the probability for the emission of a fast proton can be larger by several orders of magnitude than that for the emission of a fast α-particle. For low energies of the emitted particles the ratio of the probabilities decreases to unity.

Gugelot also remarked that considerations of the great transparency of the nucleus for protons can evidently eliminate the difficulties that arise in comparing the reactions (p, p') and (α, α') from the point of view of the surface reaction.

In the discussion that arose after the report B. Cohen (USA) told about experiments on the reactions of 22 Mev protons with elements of intermediate atomic weight. The charged particles formed in these reactions were registered by means of a scintillation spectrometer and coincidences with a proportional counter. The angular distributions of the protons and α-particles are strongly peaked in the forward direction. From them it follows that only 75 percent of all the reactions go through an intermediate nucleus. The analysis of the energy distrbution of the protons on the assumption that the departures from the Weisskopf distribution are due to direct interaction indicates that only 50 percent of all the reactions go through an intermediate nucleus. At large angles the protons have an energy distribution that is approximately Maxwellian, corresponding to nuclear temperatures $\sim$ 1.2 Mev for E_p = 6 Mev and $\sim$ 2.7 Mev for E_p = 12 Mev.

E. Bleuler (USA) told about work on the scattering of 19 Mev α-particles from Ne, Al, A and Cu, which he had carried out together with O. Gailor, L. Seidlitz, and D. Tendam. The cross section for elastic and inelastic scattering of the α-particles was measured at angles from 12 to 170° by means of photographic plates. The interaction radii found from the angular distributions on the basis of the surface interaction model for the elastic scattering and for scattering with excitation of the first level of Ne^{20} are equal to 5.8 and $6.6 \cdot 10^{-13}$ cm, respectively. In the case of A the interaction radius for elastic scattering is $6.9 \cdot 10^{-13}$ cm, and for scattering from the 1.46 Mev level it is $7.1 \cdot 10^{-13}$ cm. The elastic scattering from Al at angles smaller than 90° corresponds to a radius of $6.4 \cdot 10^{-13}$ cm, i. e., somewhat larger than had been found for E_p = 40 Mev. For Cu the similar estimates could not be made.

T. Huus (Denmark) gave a survey report on Coulomb excitation, in which he showed that the experimental data in this field are in good agreement with the predictions of the collective model of the nucleus.

V. Weisskopf (USA), in his report on the "Formation of the Intermediate Nucleus", remarked on the great advances that have been made in recent years in the understanding of the mechanism of the formation of the intermediate nucleus, owing to the use of the optical model with a complex potential, which makes it possible to distinguish between the processes that go through the intermediate nucleus and the potential scattering. The question of the decay of the intermediate nucleus appears more difficult, since a detailed consideration shows that

the conditions under which the decay of the intermediate nucleus does not depend on the manner of its formation are fulfilled only in rare cases. Discrepancies with Bohr's hypothesis of independence are caused not only by direct interaction of the primary particle with the emerging nucleon, but also by a lack of "thermal" equilibrium in the intermediate nucleus.

In the discussion on Weisskopf's report an interesting remark was made by R. Eisberg (USA). The angular distribution of inelastically scattered protons will be symmetrical with respect to 90° under the following conditions: 1) the reaction goes through the intermediate nucleus; 2) many overlapping levels in the intermediate nucleus are excited; and 3) the phases of these levels are statistically distributed. In cases in which the second condition is known to be fulfilled, an asymmetry in the angular distribution is usually ascribed to direct interaction (violation of the first conditions). But it can also be regarded as a result of the nonfulfillment of the third condition, while in some cases only this explanation is possible. R. Eisberg and N. Hints have measured the angular distributions of protons from the reaction $A^{40}(p, p')\ A^{40*}$ for primary proton energies 9.8, 9.0, and 8.5 Mev. It is found that the angular asymmetry of the distribution changes strongly with change of the primary proton energy, which would not be the case if it were a result of direct interaction.

The report of A. Bohr (Denmark) was devoted to collective excited states of the nucleus. In the opinion of the speaker, inelastic scattering is most effective in the excitation of collective states when it occurs through direct interaction. At present the most precise data on collective levels are obtained from the study of Coulomb excitation of nuclei. A. Bohr discussed the available experimental data and showed that for even-even nuclei several of the lower excited states can be well described by the collective model. In nuclei with uneven A, besides the collective degrees of freedom, those of the last nucleon also play an important part. The collective excited states correspond to oscillations of the nuclear surface, and the shell structure of the nucleus has an important influence on them. In nuclei with a relatively small number of particles in unfilled shells the oscillations of the surface take place around the spherical shape. If there are enough nucleons in unfilled shells, the equilibrium shape is ellipsoidal, and in this case the collective motion can be resolved into oscillations of the surface and rotation with unchanged shape. Ordinarily the excitation of collective levels does not involve change of the parity of the state, which means that the deformation in the surface oscillations is of quadrupole type. Recently data have been obtained on the existence of collective states with negative parity.

Many communciations were devoted to the collective model of the nucleus.

S. Yoshida (England) told about an attempt to treat the inelastic scattering of nucleons as a result of surface interaction. The theory he developed was compared with the experimental data on the scattering of 10 Mev protons from Mg^{29}. For inelastic scattering with the final nucleus in the first excited state, good agreement was obtained in the size of the cross section. But the theory was unable to explain the change of the cross section that resulted from reduction of the energy of the primary protons to 9 Mev.

S. I. Drozdov (USSR) told about a quasiclassical treatment he has carried out on the scattering of fast neutrons ($E \gtrsim 5$ Mev) and protons ($E \gtrsim 20$ Mev) by nonspherical nuclei. The model used was a "black" nucleus having the shape of an ellipsoid of revolution. It was found that the angular distributions for elastic scattering by spherical and nonspherical nuclei are qualitatively not unlike. But for considerable deformations of the nucleus the angular distribution of nucleons that are scattered with excitation of rotational states differs decidedly from the distribution for elastic scattering.

L. A. Sliv (USSR) delivered a communication on the subject "Alpha Decay and the Shell Model". He made a calculation of the probability of α-decay for a nucleus executing surface oscillations with amplitude depending on the number of nucleons outside closed shells and with a distribution function for α-particles on the surface that had a maximum where there was deformation. It was shown that such a scheme provides an explanation of many features of the α-decay of nuclei that do not have stationary deformations.

A. S. Davidov (USSR) told about an investigation he made with G. F. Filipov on the problem of separating the collective degrees of freedom in a system consisting of N spinless particles interacting with central forces. It turned out that for some particular states of motion the energy of such a system can be represented as the sum of the energy of internal motion and a rotational energy determined by the angular momentum of the system.

V. M. Strutinsky (USSR) told about a calculation of the probability of excitation of rotational states in the α-decay of even-even nuclei in the case of small deformation. Another communication by Strutinsky dealt with asymmetrically deformed nuclei. He showed that the interaction of two-nucleon states with an asymmetrical deformation of the nuclear surface can lead to a stable asymmetrical deformation playing an important part in the asymmetry of nuclear fission. A calculation was made of the collective dipole moment of the asymmetrically deformed nucleus. For nuclei of the uranium group the dipole moment is found to be of the order of 1/10 to 1/20 R. Strutinsky pointed out the great importance of measuring the probabilities of dipole and octupole transitions, since such data would make it possible to determine whether the 1^- states of even-even nuclei are of collective or single-particle nature.

A report by H. Bethe was devoted to the Brueckner theory, in the development of which Bethe has recently been engaged. The shell model and the model of the semitransparent nucleus have led to great progress in the explanation of experimental data. But until very recently there was no possibility of deriving these models from the known forces acting between two nucleons. Contrary to the opinions of some other theorists, Bethe believes that the Breckner theory makes it possible in a certain sense to place a foundation under the shell model and the quasioptical theory of nuclear reactions. This theory amounts to a self-consistent-field method, with the potential originally taken to depend in a general way on the velocities and positions of the nucleons. The wave functions of the individual nucleons are calculated in this potential. The Slater determinant Φ of these functions is called a "model" of the wave function of the nucleus. The actual wave function ψ of the nucleus can be obtained from Φ by taking into account the interactions of the nucleons by pairs. This requires the exact solution of an integral equation that describes the interaction of pairs of nucleons in the average field produced by the other nucleons. In the whole calculation the most important role is played by the Pauli principle, which leads to the absence of interaction between identical particles. It has been shown that in this way one can construct an approximate solution of the Schrödinger equation for the nucleus as a whole that satisfies the equation with high precision. This theory leads to a method of calculating the nuclear levels that, with small exceptions, is analogous to the method used in the usual shell theory.

In the report by D. Hughes (USA), "Neutrons and Nuclear Structure",* an analysis was carried through of the experimental data obtained in work with slow neutrons. In the discussion on the report by Hughes and in a section meeting of the conference devoted to the interaction of neutrons with nuclei, many communications were presented on the latest work in this field.

Ya. A. Smorodinsky told about the work of I. I. Gurevich and M. I. Pevzner (USSR) on the phenomenon of "repulsion" of nuclear levels, which had been considered in the report by Hughes. Hughes showed from a large amount of experimental data on even-even nuclei that the relative number of closely spaced levels is significantly smaller than should occur in a random distribution. In the even-even nuclei only one spin state is realized and the "repulsion" effect appears in its pure form. Gurevich and Pevzner carried out an analysis of the data for nuclei with odd mass number, i. e., for levels characterized by two spin values ($I + 1/2$ and $I - 1/2$). They showed that in this case also a "repulsion" of the levels occurs and brings the distribution closer to an equidistant one.

I. A. Radkevich (USSR) reported the results of work on "Measurement of the Total Effective Cross Sections of Pd, Os, Ir, Mo, In, Ta, Th, and U^{238} for Resonance Neutrons", which he had carried out together with V. V. Vladimirsky and V. V. Sokolovsky.** In particular he noted that for a number of substances (Ta, U^{238}) the distribution of neutron widths is markedly different from exponential, while in the opinion of Hughes, expressed in his report, the distribution of neutron widths has approximately exponential shape.

II. Capture Reactions and Photonuclear Reactions

The report of P. M. Endt (Holland) contained an analysis of the experimental data on reactions of the type (x, γ), where x is a neutron, proton, or α-particle. These reactions are very convenient for purposes of

*The full text of the report is published on page 715 of this issue.

**The work of I. A. Radkevich, V. V. Vladimirsky, and V. V. Sokolovsky is published on page 727 of this issue.

nuclear spectroscopy, since a study of the spectrum, angular distribution, and angular correlation of the γ-rays gives complete information about the excited states of the nucleus formed as the result of the capture of the particle. Referring to the well known work of Kinsey and others (Canada) and of Groshev and others (USSR) on the (n, γ) reactions, Endt devoted his report mainly to the (p, γ) reactions of light elements. These reactions provide an almost ideal way of measuring the spins and parities of nuclear levels. The data on the intensities make it possible to verify the selection rule for isotopic spin for electric dipole radiation, or, conversely, to determine the isotopic spins of nuclear states. Of greatest interest are the results of a study of the reaction (p, γ) for the light nuclei near Al, which, in the opinion of the speaker, provide evidence of the existence of rotational levels in these nuclei. The existence of rotational levels in light nuclei is now regarded as quite possible (especially by A. Bohr and his group).

In the discussion on Endt's report H. Gove (Canada) presented experimental evidence of the existence of rotational levels in light nuclei. Together with A. Litherland, E. Paul, and others he has measured the energies, spins, and parities of the low-lying levels of several nuclei with mass numbers near 25, and also the ratios of intensities of γ-transitions for these levels. The most complete data have been obtained for the nucleus Al^{25}, for which studies of the reactions Mg^{24} (p, γ) and Mg^{24} (p, p', γ) gave the characteristics of 18 levels. The collective model provides an unexpectedly good interpretation of the results. Measurements were also carried out for the nuclei Mg^{25}, P^{31}, Si^{29}, Al^{27} and Na^{23}. In the case of P^{31} and Si^{29} calculations on the basis of the collective model give somewhat worse agreement with the experimental data than for Al^{25}, but in general it is clear that the collective model is extremely useful for the description of the lower excited levels of light nuclei.

E. Paul (England) then gave a survey of the data on other light nuclei with odd mass numbers to determine to what extent the strong-interaction model can be used for the description of the known properties of these nuclei. The parameters for the levels that can be regarded as of rotational type were compared with the theoretical predictions made on the basis of the Nilsson model (Dan. Mat. Fys. Medd. 29, No. 16, 1955). Excellent agreement was found for the distribution of the levels, and fairly good agreement for the intensities of the γ-transitions. The analysis of the experimental data indicates that the nuclei at the beginning of the d-shell have a prolate shape, and those at the end, oblate.

The report of D. Wilkinson (USA) was devoted to the theory of photonuclear reactions. He considered the various mechanisms of absorption of electromagnetic radiation by a nucleus. It was pointed out that the shell model and the collective model can be applied only in the region of relatively low energies, since a calculation of photonuclear processes at high energies requires a detailed knowledge of the wave function of the nucleus. An analysis of the experimental data at low energies shows that there is good agreement with the independent-particle model; in particular, the behavior of the cross sections for photonuclear reactions in the region of the so-called "giant resonances" can be explained if the process of interaction of the γ-quantum with the nucleus is regarded as a process of direct interaction of the electromagnetic wave with one of the nucleons in the nucleus. Wilkinson remarked that the independent-particle model and the statistical model sometimes give very similar results. Thus the observation of a "Maxwell distribution" of the products of photonuclear reactions does not make possible a choice between these two models.

A large number of communications were devoted to problems of photonuclear reactions, both in the discussion on Wilkinson's report and in a supplementary section meeting.

In a research by V. I. Goldansky (USSR) reported by I. S. Shapiro cross sections of (γ, p) reactions with the final nucleus formed in the ground state were calculated for several light atoms by application of the principle of detailed balancing to data on the radiative capture of protons. It was shown that these reactions make an appreciable contribution to the total cross sections in the "giant resonance" region. For example, in the range of γ-ray energies up to 21 Mev the integrated cross section for the reaction C^{12} (γ, p) B^{11} with formation of the B^{11} in the ground state amounts to about 10 percent of the integrated cross section for the entire "giant resonance" peak (20-24 Mev).

V. Stevens (USA) used the photographic emulsion method to study yields and energy distributions of the photo-protons from Be, C, and O for bremsstrahlung of maximum energy 25 Mev. The excitation curves of the (γ, p) reactions calculated from these data show a fine structure in the "giant resonance" region, in approximate agreement with the structure of the excitation curves of (γ, n) reactions with these nuclei.

L. E. Lazareva presented several communications about researches on photonuclear reactions carried out at the Lebedev Physical Institute of the Academy of Sciences of the USSR. G. K. Kliger, V. I. Riabinsky, and others used the photographic plate method to study the angular and energy distributions of the protons emitted from C^{12}, Be^{9} and Li^{6} under the action of bremsstrahlung with $E\gamma_{max}$ = 30, 42, 60 and 80 Mev. The angular distributions are well approximated by curves $a + b \sin^2\theta(1 + \gamma \cos\theta)^2$, and can be explained by direct interaction of the γ-quantum with an individual nucleon in the nucleus. The fraction of electric quadrupole absorption increases with increasing energy from 5 to 11% for C^{12} and from 15 to 20% for Be^{9}. The data obtained at energies 60 and 80 Mev indicate the existence of a two-nucleon mechanism of absorption of γ-quanta by nuclei.

In a research by G. N. Zatsepina, L. E. Lazareva, and A. N. Pospelov thick emulsion photographic plates were used to measure the angular and energy distribution of neutrons emitted from Bi under the action of bremsstrahlung with maximum energy 18.9 Mev. A considerable part of the energy distribution found consists of energetic neutrons whose emission cannot be accounted for within the framework of the statistical theory. The angular distribution of the neutrons is anisotropic, with a maximum between 45° and 90° relative to the direction of the γ-rays, with the degree of anisotropy increasing with increasing energy of the photoneutrons.

A study of the photoneutrons from Bi was also the subject of the communciation by F. Ferrero (Italy). The excitation curve and the angular distribution of the neutron were measured by means of the activation of Si and Al by (n, p) reactions. The maximum energy of the bremsstrahlung varied from 10 to 31 Mev. It was found that from 5 to 10% of the neutrons are fast neutrons. Their angular distribution has the form $1 + 0.8 \sin^2\theta$. The excitation curves indicate that the "giant resonance" regions for fast and slow neutrons coincide. This confirms Wilkinson's hypothesis that from the point of view of the shell model the "giant resonance" can be explained by single-particle transitions from the ground states.

H. Wäffler (Switzerland) told about observations of photonuclear reactions of the (γ, T) type in Al, Co, and Cu with maximum bremsstrahlung energy 31 Mev. The results obtained agree well with calculations based on the model of the intermediate nucleus. The conclusion is drawn that the statistical theory is correct for photonuclear processes with emission of heavy particles such as α-particles and tritons.

A communication by I. S. Shapiro (USSR) ("Photonuclear Reactions and the Scattering of Nucleons by Light Nuclei") took up the question of the connection between the processes (γ, p), (γ, n), and (N, N'), where N and N' are nucleons. On the assumption that the cross sections for photonuclear processes are small in comparison with those for the scattering of nucleons, general formulas are obtained giving a connection between transmutation processes and dipole transitions for nuclei with arbitrary isotopic spin.

III. Stripping and "Pick-Up" Reactions

J. R. Holt (England) presented a survey report on experimental work on reactions of stripping and "pick-up".

In the last two or three years there has been much study of the reactions (d, p) and (d, n) for deuteron energies up to 20 Mev. Analysis of the angular distributions and total cross sections on the basis of simple theories of the type of the Butler theory has given much information about the constants for excited states of nuclei. In particular a great many researches have been concerned with (d, p) reactions, which present less experimental difficulties. Many methods have been developed for separating the groups of protons of various energies that are formed in these reactions.

Recently there have come into use scintillation counters with inorganic crystals, which have high efficiency with good resolving power, and a method of magnetic analysis that makes it possible to separate groups of protons with energies differing by 60 to 100 kev. The (d, n) reactions, on the other hand, have mostly been studied by means of nuclear emulsions, which are very laborious and do not give good results because of the large background produced by the continuous part of the neutron spectrum. Only very recently have scintillation spectrometers been used for the study of (d, n) reactions. There are still many valuable data to be obtained in this way.

Least work of all has been devoted to the study of "pick-up" reactions, (p, d) and (n, d), although they are as easily susceptible to analysis by Butler's theory as the stripping reactions. This is accounted for by the great experimental difficulties brought about by the fact that the energy Q of "pick-up" reactions is uaually negative and amounts to 5 to 10 Mev, so that the deuterons formed in the reaction have low energies.

Analyzing the available data on the (d, p) and (p, d) reactions, Holt stated that for the light nuclei up to calcium good agreement between the distribution curves calculated from the Butler theory and the experimental data is obtained for $r_0 = (4.37 + 0.042A) \cdot 10^{-13}$ cm.

Holt remarked that the wealth of experimental material obtained in the study of stripping and "pick-up" reactions is not fully utilized because of the lack of a good theory of these processes. It has now become clear that the cross section of the stripping reaction is still relatively large even at low energies of the deuterons (down to 1 Mev). But the experimental data obtained at low energies cannot be interpreted by the present theory, which does not take into account Coulomb interactions. The excitation curves of the stripping reactions and the variation of the angular distributions with change of the deuteron energy indicate that a large part is played by interference between stripping processes and resonance phenomena, which is not taken into account in the existing theory. Much new information about the nucleus can be obtained from measurements of the polarization of the protons and neutrons from stripping reactions and their angular correlation with γ-rays, if the theory of these phenomena is worked out.

In the discussion ot stripping reactions N. A. Vlasov (USSR) told about a study made together with G. F. Bogdanov, S. P. Kalinin, B. V. Rybakov, and V. A. Sidorov of the spectra of neutrons from the bombardment of light nuclei with 14 Mev deuterons. The neutron spectra were measured by a time-of-flight method. The "natural" pulsed deuteron source was a 150-cm cyclotron. Comparison of the neutron spectra from the reactions T + d and He^3 + d gives indications of the influence of an excited state of He^4 with excitation energy about 22 Mev and of the absence of such a state in Li^4. In the neutron spectrum of the reaction He^4 + d a group has been found corresponding to the ground state of the final nucleus Li^5, but there is no group from an excited state. In the other spectra the maximum intensity occurs at a neutron energy somewhat more than half the energy of the deuteron.

The differential cross section for neutron production at angle 0° from the light nuclei up to and including boron is approximately proportional to the number of nucleons in the nucleus and is about 50 millibarns per steradian for each nucleon.

Yu.A. Nemilov (USSR) told about an investigation of the relative probabilities of the stripping process and the formation of a compound nucleus.

It was found that the ratio of the stripping cross section for the reaction Mg^{26}(d, p) Mg^{27} (together with a correction term for the interference between the processes of stripping and formation of the compound nucleus) to the cross section for the formation of the compound nucleus has its largest value of 8 to 9 at deuteron energies of 1 to 2 Mev and decreases both with decrease and with increase of the deuteron energy.

R. Jastrow (USA) told about a study made by H. Holmgren and others of the angular distributions and yields in the reactions $Be^9(He^3, p)B^{11}$, $C^{12}(He^3, p)N^{14}$, $C^{13}(He^3, p)N^{15}$, and $C^{13}(He^3, \alpha)C^{12}$ produced by He^3 nuclei of energies 2 Mev and 4.6 Mev. The angular distributions obtained are asymmetrical around 90°, which indicates that a large contribution is made to these reactions by processes that occur without the formation of an intermediate nucleus. It is possible that these mechanisms are similar to the stripping and "pick-up" reactions in deuteron bombardment.

J. Horowits (France), in his report "Theory of Direct Interaction", gave a survey of the known methods of calculating stripping reactions and other direct processes.

In the discussion that followed, J. Dabrowski (Poland) told about his work "Direct Interaction and the Formation of the Compound Nucleus in Nuclear Reactions", which is in press. In this work an attempt is made to find a formula for the effective cross section of a nuclear reaction, taking into account direct interaction and the formation of the compound nucleus:

$$\sigma = \sigma_{dir.} + \sigma_{comp.} + \sigma_{interference}.$$

The comparison of the results with the experimental data is being prepared for publication.

The interaction of fast deuterons with nuclei was discussed in a communication by A. I. Akhiezer and A. G. Sitenko (USSR). It was shown that a diffractive stripping must occur along with the elastic scattering, and that the expression for the total cross section published recently by R. Glauber is incorrect.

A survey report by E. Segre (USA) was devoted to the present status of the problem of n, p and p, p scattering, in particular for an energy of the incident nucleon of about 300 Mev, for which the most complete data have been compiled. He remarked that experiments to measure the polarization in double and triple p, p scattering can in principle give sufficient information for the determination of the complete set of phase shifts in p, p scattering. But experimental errors still do not allow the choice of the correct set of phases from among four sets that satisfy the data obtained within the limits of accuracy of the measurements. Segre presented the values of the phases that look best at present and pointed out that for their final determination it is important to relate the data obtained at 300 Mev with data for lower energies. Segre also analyzed the data on elastic scattering of protons by the nuclei from He to Ta, in particular those obtained in experiments on the polarization, from the point of view of the complex potential model with inclusion of spin-orbit interaction.

In the discussion on Segre's report Ya. A. Smorodinsky (USSR) pointed out that for the final determination of the phases for the p, p scattering it would be sufficient to measure the correlation of the proton polarizations in this scattering.

R. Hofstadter (USA) told about a study of the scattering of electrons of energy 188 Mev from the nuclei of C^{12}, Mg^{24}, Si^{28}, S^{32}, and Sr^{88}. Analysis of the data shows that the "skin thickness" of these nuclei is $2.4 \cdot 10^{-13}$ cm, i. e., approximately the same as for the heavy nuclei (Ca – Au). The distance to the half-density point varies with the atomic weight approximately according to the law C $1.08 \cdot A^{1/3} \cdot 10^{-13}$ cm, which holds both for light and for heavy elements.

The communication of A. I. Baz' (USSR) dealt with the scattering of 1 to 5 Mev neutrons by lead. Comparison of the angular distributions and cross sections calculated on the basis of the model of the semitransparent nucleus with the experimental data indicates that the true value of the nuclear radius lies between 7.5 and $8 \cdot 10^{-13}$ cm, and the radial thickness of the diffuse region at the edge of the nucleus is close to $1 \cdot 10^{-13}$ cm. The polarization of the neutrons, calculated from the interaction of the neutron magnetic moment with the electric field of the nucleus, reaches values of $P \sim 50\%$ for $\theta = 1°$, $P \sim 40\%$ for $\theta = 2°$, and $P \sim 30\%$ for $\theta = 3°$, which is in decided disagreement with the results of Schwinger, which were obtained from cruder assumptions.

IV. Reactions Produced by Heavy Ions, and Fission Processes

In a report on "Reactions Produced by Heavy Ions", J. Fremlin (England) told about the results of a study of reactions with accelerated ions of C and N, carried out by radiochemical methods. The nature of these reactions shows a decided change with change of the atomic number of the target nucleus. With the light elements, besides processes involving formation of an intermediate nucleus, an important role is played by direct processes of disintegration of the incident particle in the field of the target nucleus and by breaking up of the whole system into several compound particles (principally α-particles). For the middle elements the main process is the formation of the intermediate nucleus, accompanied by evaporation of particles, with the relative probability of evaporation of neutrons increasing with the atomic number. For the elements at the end of the periodic system the most probable process is fission.

A. Zucker (USA) told about research on reactions with heavy ions in Oak Ridge. From the differential cross section for elastic scattering of N^{+++} ions in nitrogen at energy 26 Mev the radius of the nitrogen nucleus was found to be $4 \cdot 10^{-13}$ cm.

An analysis of the experimental data on fission of nuclei was presented in the report of J. Wheeler (USA).*

In the discussion of this report L. Wilets (USA) told about theoretical work on nuclear fission carried out in Los Alamos. Wilets and Chase showed that the angular distributions of fragments from the fission of Th^{232} by neutrons near threshold are in agreement with the model of A. Bohr. A statistical analysis of the observed fission widths for the fission of U^{235} by slow neutrons, carried out by Porter and Thomas, indicates that the fission occurs through a small number of "fission channels", although the probability that only one channel occurs is small.

---

*The full text of the report is published on page 743 of this issue.

Interesting data were presented by R. Duffield (USA). He and R. Smith have measured the excitation curve of symmetrical and asymmetrical photofission of U^{238} and Th^{232}. For Th^{232} the probability of symmetrical photofission increases monotonically as the maximum energy of the bremsstrahlung is raised from 6.5 to 10 Mev. For U^{238} the probability of symmetrical photofission first rises to a maximum at 6 Mev, then falls to a minimum at 8 Mev, after which it rises monotonically up to 20 Mev. The first measurements have been obtained of yields below the fission threshold (fission through the barrier).

S. I. Drozdov (USSR) told about work of V. G. Nosov dealing with the energy dependence of the fission width. Nosov points out that the estimates of the fission width put forward by various authors can be written in the form

$$\Gamma_f \sim \frac{\hbar\omega}{2\pi} \cdot \frac{N^*(E - E_f)}{N^*(E)},$$

where ω is the frequency of the oscillations in the shape of the nucleus that are related to fission. The exponential formula for the number of levels, $N^*(E) \sim e^{S(E)}$, is valid only at sufficiently large excitation energies E. Near the fission threshold the function $\Gamma_f(E)$ is not monotonic, since $N^*(E - E_f)$ is step-shaped owing to the relatively large separations between the first excited levels of the nucleus. The formula proposed by Nosov gives a qualitative explanation of the observed discontinuities of the fission cross section near the threshold.

The concluding remarks were made by L. Rosenfeld (England). Noting that the main question at the conference was that of nuclear models, Rosenfeld gave a short survey of the development of the various models. He expressed confidence that the conference will have great significance for the further development of the theory of the nucleus.

The Amsterdam Conference, organized by the Netherlands Physical Society, took place in a friendly and businesslike atmosphere. It will undoubtedly contribute greatly to the development of international scientific relations and the cooperation of scientists of different countries.

B. Rybakov

ATOMIC POWER PROBLEMS AT THE FIFTH WORLD POWER CONFERENCE IN VIENNA

The Fifth World Power Conference was held in Vienna from June 17 to June 23, 1956. About 2000 engineers and scientists from 52 countries were present at the conference. The Soviet delegation was led by Deputy Minister of Electric Power Stations, A. S. Pavlenko.

Two sectional meetings were devoted to atomic power problems.

Most of the papers at these sections dealt with descriptions of atomic power stations being planned or built; the rest consisted of general descriptions of atomic power development in various countries, evaluations of the efficiency of atomic power stations and comparisons with other sources of power, and problems of radioactive waste disposal.

The paper presented by the Soviet delegation described the prolonged experience in operating the first atomic power station for a period of two years, and outlined prospects of atomic power development in the USSR. The principal attention was devoted to the program of construction of industrial atomic power stations. In their contributions to the sectional discussions the Soviet delegates considered certain questions of the economics and technology of atomic power.

Nearly all the foreign papers (with two exceptions) dealt with projects which had already been described in various degrees of detail at the Geneva Conference or in the journals. However, as a rule these papers contained amplifications and modifications of the previously published texts. The exceptions were two new projects described by the US delegation. Reports on one of these, namely the project for the construction of an atomic power station with an oil-fired steam superheater, "Indian Point" (authors R. Milne and W. Moore), had been published earlier, but a detailed description of the project was given for the first time. The station will be built on the Hudson river 40 km to the north of New York by the Consolidated Edison company. Construction of the station is to begin in the spring of 1957, so that startup could take place by the end of 1959 and full power would be developed by the middle of 1960.

The main feature of the station is that the reactor is used only for the production of saturated steam, which is superheated by means of ordinary organic liquid fuel (oil). Ordinary water under pressure is used as the moderator and heat transfer medium in the reactor. The maximum thermal power of the reactor is 500,000 kw.

The core of the reactor is a cylinder 1.8 m high and 1.8 m in diameter. It is assembled from more than a hundred similar elements of square cross section. Each element consists of alternating plates, containing either an alloy of highly enriched uranium with Zircaloy or thorium. The plates are separated from each other by gaps for the heat transfer medium and enclosed in a Zircaloy case. The thickness of the alloy plates is 1.5 mm, and of the thorium plates, 2 mm. The gap width is 2.5 mm. Such a construction as a whole, in the opinion of the authors, should increase the life of the whole element. Thorium was chosen for its good structural properties, compatibility with Zircaloy, radiation resistance, and fuel-breeding power. The thorium charge is 8100 kg, and that of U^{235} about 275 kg. Water occupies 70% of the core volume.

The core is surrounded by a side water reflector 15 cm thick. The whole reactor is contained in a thick-walled cylindrical tank of carbon steel 3 m in diameter and 7 m high. To prevent corrosion, the inner surface of the tank is faced with stainless steel. The core and reflector are surrounded by a steel shield which protects the tank walls against neutron and γ-radiation.

The primary circuit of the heat transfer system which carries heat from the reactor to the steam generators consists of four parallel loops. The water temperature is 250°C at the entry to the reactor and 267°C at the exit. The average heat flow through the surface of the fuel element is approximately 0.5 million kcal./m^2/hour. The water pressure in the circuit is 100 atm. The primary circuit is enclosed in two steel spheres (two

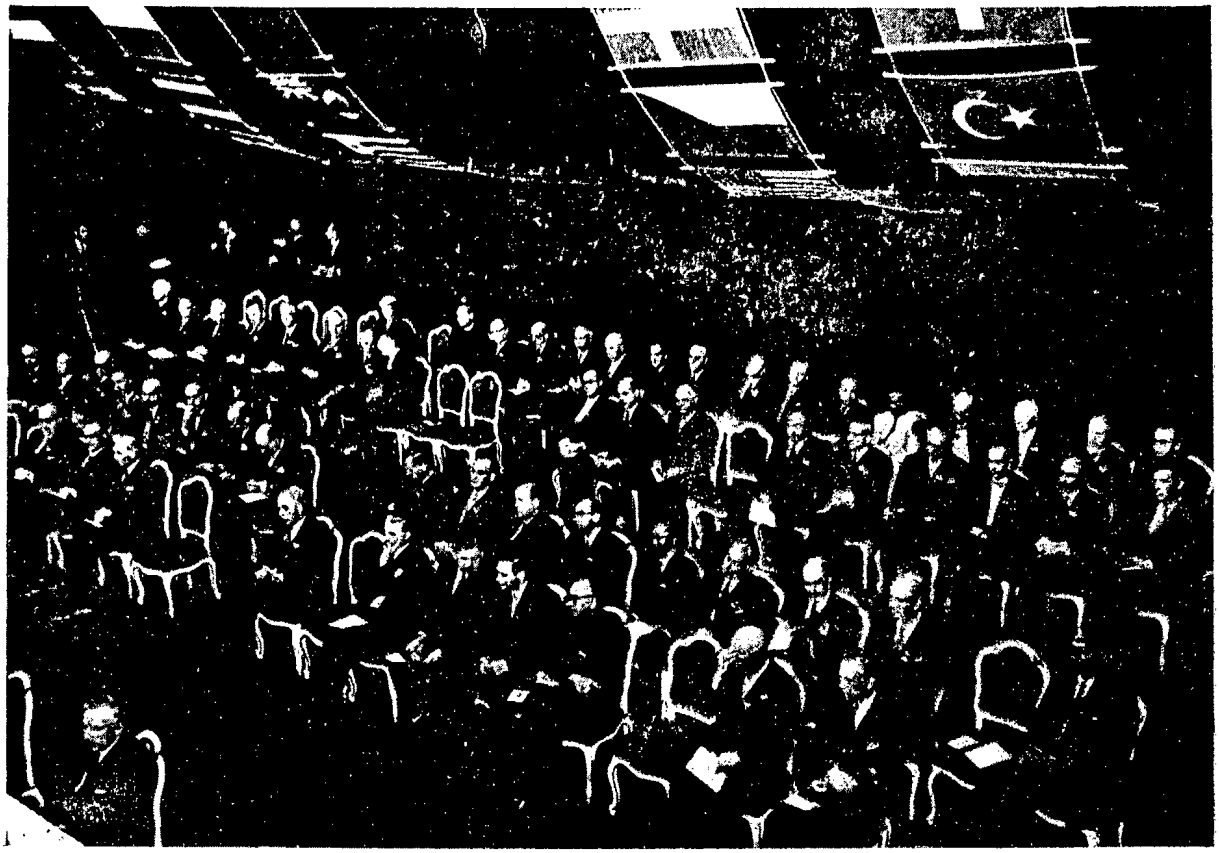

Opening of the Fifth World Power Conference in the Vienna Opera House, June 17, 1956.

loops in each sphere) 21 m in diameter, which prevent escape of radioactive contamination in the event of an accident.

The charging scheme is intended to allow one-third of the fuel elements to be changed in 36 hours (including cooling-down and startup of the reactor). The capacity of the steam generator is 860 tons of saturated steam per hour at a pressure of 29.5 atm. The steam is heated to 538°C in an oil-fired superheater. To illustrate the advantages of this system, Table 1 shows data for the proposed station and a station with a similar reactor but without oil-combustion superheating.

The table shows that the cost per power unit is much lower for the combined installation than for a pure nuclear plant. It must be remembered, however, that the fuel costs are higher in the combined plant. A clearer picture is obtained by a comparison of data for a "combustion annex" to an atomic power station with data for ordinary power stations using organic fuel. The relevant data are shown in Table 2.

Table 2 shows that the use of a combustion superheater is highly advantageous.

A report on an atomic power station with an organic moderator (OMR) was presented by the North American Aviation Company; its subject-matter was as follows.

With the use of organic liquids as moderators it is possible, while retaining all the main advantages of water – water reactors (small dimensions, good nuclear characteristics), to avoid many defects inherent in such systems. A reactor with an organic moderator does not require the use of high pressures and eliminates or appreciably diminishes the risk of corrosion by the heat transfer medium. However, the use of organic liquids encounters difficulties because of the instability of organic liquids under the action of radiation and high temperatures.

Studies of the stability of organic liquids in conditions similar to those in reactors have been carried out for a number of years. The best results have been obtained with polyphenyls. Table 3 shows data on the polyphenyls investigated.

TABLE 1

Comparative Data for Power Stations With Superheating and Without Steam Superheating

Parameters	Saturated steam	Superheated steam
Pressure in steam generator, abs atm	29.5	29.5
Steam pressure before turbine, abs atm	28.5	26.0
Temperature, °C	230	538
Electric power, kw	140,000	236,000
Heat consumption, kcal/kw-hr	3,270	2,700
Cost of 1 kw of installed power, dollars	322	233

TABLE 2

Characteristics of a Combustion Superheating and Without Steam Superheating

Additional power obtained by superheating, kw	96,000
Additional cost of superheating installation, millions of dollars	10
Cost of additional power, dollar/kw	104
Heat consumption, kcal/kw-hr	1,940
Cost of additional power with allowance for the lower heat consumption in comparison with the most modern power station, dollar /kw	74
Cost of installed power at modern power stations in the New York district, dollar /kw	200

TABLE 3

Comparative Characteristics of the Polyphenyls Studied

	Diphenyl	Mixture of terphenyl isomers	o-Terphenyl	m-Terphenyl	p-Terphenyl
Melting point, °C	69	60-145	50-55	75-85	200-215
Boiling point, °C	255	364-418	330-341	368-378	381-388
Vapor pressure at 325°C, atm	3.7	0.4	0.8	0.4	0.3
Vapor pressure at 425°C, atm	15	2	3.4	2.0	1.5
Hydrogen atom density, 10^{22} atoms/cc	3.035	3.18	3.16	3.25	3.275
Approximate cost, dollar /kg	0.33	0.37	1.98	3.06	1.98
Polymerization rate at 325°C, kg/1000 kw-hr (on heat consumption)	0.27	0.23	0.27	0.23	0.16
Feed costs in plant operation, cent /kw-hr	0.036	0.034	0.216	0.278	0.125

The relatively cheap mixture of terphenyls is the most suitable in properties.

The authors of the report consider that organic moderators are the most promising for low-power reactors. A description of an atomic station with an electrical power of 12,500 kw (thermal power 45,000 kw) with a reactor of this type (OMR) is given in the report.

The core of the reactor, in the form of a cylinder 1.4 m in diameter and 2 m high, consists of 138 elements of square cross section contained in a thin-walled tank filled with the organic liquid. Each element contains 10 heat-emitting units in the form of aluminum-coated uranium plates. Uranium 1.8% enriched is used. The reactor is regulated by means of 10 control rods. The core is surrounded by a shield against thermal neutrons, consisting of iron 15 cm thick.

The maximum temperature of the fuel elements is 339°C on the surface and 482°C in the center. It is intended to reach rates of fuel consumption corresponding to total power of 3000-4000 megawatts/day per ton of fuel.

The heat transfer system of the reactor consists of two parallel loops in separate shielded chambers. The heat transfer medium moves downward in the core. The maximum temperature of the heat transfer medium is 325°C, the pressure is 2.5 atm. (On increase of pressure from 1 to 2.5 atm the boiling point of the liquid rises from 365°C to 454°C.) The flow rate of the transfer medium is 3000 tons/hour. The steam generators (one in each loop) are designed to produce 37 tons of steam each at 280°C at a pressure of 29 abs atm.

Special attention is devoted to removal of polymerization products from the heat transfer medium. As can be easily calculated from the data cited, the polymerization rate is 250 kg per day. The primary circuit includes an appropriate purification system with a special device for continuous feeding of additional heat transfer medium. The purification method is based on the use of a compact fractionating column. The possibility of using other methods (cold traps, filtration, centrifugation) for this purpose is to be investigated.

According to the authors' estimates, the power plant should be economically competitive with ordinary electric power plants of the same power. In order to carry out all the necessary trials, it is intended to build an experimental organic moderator reactor (OMRE)*; to be started up early in 1957.

With regard to the other atomic power stations plans for which were discussed at the Conference, we will confine ourselves to a few comments and notes on the differences between the information given and data published previously.

Unit with a sodium–graphite reactor (SGR). The diameter of the core has been decreased from 5.27 to 3.66 m, the height from 4.27 to 3.05 m. The enrichment of the uranium has been raised from 1.8 to 2.3% and the U^{235} charge has been increased from 443 to 518 kg. Three instead of four parallel loops have been left in the process system.

Experimental sodium reactor (SRE). The reactor is constructed in a unit with a turbo-generator. The station will be connected to the general network. The electrical power of the station is 7,500 kw.

Station with a fast-neutron reactor in Detroit. The whole process system, including the turbo-generator, is designed for a maximum electrical power of 150,000 kw although the nominal electrical power is 100,000 kw as before. The fuel elements will consist of rods and not plates. The diameter and height of the core have been decreased from 90 to 77.5 cm.

The report by J. West (Netherlands) contains a discussion of stations with homogeneous reactors, which it is intended to develop in that country. Most attention is devoted to a reactor containing a suspension of uranium oxide and thorium in heavy water. The dimensions of the fuel particles are chosen to be smaller than the range of the fragments which considerably facilitates the removal of fission products.

In many of the reports and statements attempts were made to carry out economic calculations and to estimate the energy costs at future atomic power stations. However, great importance should not be attached to the figures obtained. First, it is evident that many of the component terms of these values, namely those directly relating to the reactor sections of the power stations, are largely arbitrary because of the lack of the necessary experience. In addition, there is no definite established criterion as to what should be included in power costs. Some include research and development charges, others do not. The minimum quantity of fissionable material required for operation of a plant (including the charge required to reach critical conditions and all the fuel undergoing regeneration) is generally not included in calculations of capital costs, while these factors may influence the energy cost. Therefore the figures cited in the reports cannot be used even for approximate comparison of the relative economics of different types of power stations. The only conclusion which can be drawn is that the cost of energy from atomic power stations does not differ greatly from that obtained from ordinary power stations, and consequently atomic energy will compete with ordinary power sources even in the nearest future, at least in some parts of the world.

Many of the delegates at the Conference stressed that at the present time it is impossible to speak of any optimum or most profitable atomic power station. Work must be continued in all directions, and atomic power plants of different types must be built. Only after enough experience has been gained will it be possible to select a small number of main types of atomic power stations. It was generally acknowledged that this tendency toward all-round development of work in the field of atomic power has been most pronounced in the programs of the USSR and USA.

The work of the atomic power section, as of all the other sections, proceeded in an atmosphere of friendship and mutual understanding. It helped to establish working contacts between engineers and scientists of different countries working on the peaceful uses of atomic energy.

O. Kazachkovsky

* Atomic Energy, No. 3, 143 (1956).

QUESTIONS RELATING TO THE APPLICATION OF RADIOACTIVE ISOTOPES IN METALLURGY

(From the Moscow Conference on Experimental Techniques and Methods of High-Temperature Research)

A conference was held from the 26th to the 30th of June 1956 in the A. A. Baikov Institute of Metallurgy of the Academy of Sciences U.S.S.R. on the techniques and methods of high-temperature research.

An important feature of the work of the Conference was the contributions on the application of tracer atoms – radioactive isotopes – in metallurgy.

V. Shikhov and O. Esin have employed P^{32} and S^{35} in investigating the kinetics of dephosphorization and desulfurization of metal by slag, demonstrating the advantages of this method over other methods, including high sensitivity, high level of accuracy and relatively high speed of the analysis. The radioactive additions in the metal were: 1) ferrophosphorus, obtained by dissolving active and inactive phosphorus in nitric acid and mixing this solution with iron oxalate followed by drying, calcination and reduction with hydrogen; 2) iron sulfide powder, obtained by mixing solutions of active and inactive Na_2S with a given quantity of $FeCl_2$ followed by filtration and drying.

The reaction between the metal and slag was carried out in a special crucible of fused magnesite in a hermetically sealed electric resistance furnace with graphite heating element in an atmosphere of pure nitrogen. The radioactivity of samples of both phases was measured mainly on specimens of the powders.

N. Bogdanova, P. Gruzin, G. Ermolaev and I. Mikulinsky (Kuznetsk metallurgical combine) reported on the results of a study of the movement of metal and distribution of the alloying elements in open-hearth furnaces of various capacities by means of radioactive isotopes (Co^{60}, Cr^{51}).

By means of this method it was possible to establish that blending of the metal occurs as a result of movement of the metal in turbulent and convectional flows, the speed of which attains 1-5 m/min. The flow of metal in the top layers of the bath travels along the furnace from the middle to the edges, where scattering occurs of the smoothly travelling streams with conversion of the motion to turbulent motion, involving the entire mass of metal. The time for equalization of the composition of the metal bath was determined for dephosphorization, boiling and reduction with ferrosilicon and manganese-silicon. It was recommended that the boiling period for 370-ton furnaces should be limited to 45 minutes. A study has been made of the process of solution of ferrochrome in the steel bath and it was found that final equalization of the composition occurs only on discharging the steel into the ladle. It was recommended that the time-lag in the bath after introducing the ferrochrome should be reduced almost to half.

A. Kolesnik and V. Maslova (Kuznetsk metallurgical combine) reported on a study of the penetration of feeder-head fluxes into the body of the ingot by means of radio-active isotopes P^{32}, Co^{60}, Fe^{59}, Ca^{45} and S^{35}. The feeder-head flux was moistened with a solution of one of the isotopes, mixed, placed in paper packets and after drying was introduced into the feeder-head on to the surface of the metal. After the ingot was rolled samples were taken from the finished rail and low-carbon steel type 10T for testing by radiometric, radiographic and other methods.

Investigation of the macrostructure of the metal and segregation of the carbon, sulfur and phosphorus depending on the feeder-head flux material showed that it was advantageous to employ fire-clay powder for the feeder-head flux on low-carbon steel and carbon black for high-carbon steel.

L. Karagintseva (Kuznetsk metallurgical combine) has investigated sources of contamination of ball-bearing steel by means of radioactive isotopes. It has been established as the result of experiments carried out in industrial furnaces with a capacity of 30-40 t, that the fraction of nonmetallic inclusions formed as a result of a disintegration of the lining of the ladle does not exceed 1.6% (of all the nonmetallic inclusions) and as the result of disintegration of the refractories of the syphon notch still less. This was confirmed by the investigations of E. Kalinnikov and A. Samarin (Moscow Steel Institute), demonstrating with the aid of radioactive isotope Ca^{45} that contamination of ball-bearing steel through the syphon notch comprises on the average 0.13% of the total nonmetallic inclusions.

M. Goldshtein, I. Bolotov and P. Sklyuev (Ural Iron and Steel Institute) have investigated segregation processes in a steel ingot by means of radioactive isotopes C^{14}, P^{32}, S^{35}.

A medium carbon alloy steel was melted in a 40 kg induction furnace, and at the end of smelting the radioactive isotope was introduced. Samples were cut out from the investigated zones of crystallization of the ingot for autoradiography. The autoradiogram negatives obtained were examined photometrically for quantitative evaluation of dendrite disuniformity. By this method a study was made of dendrite segregation of phosphorus and sulfur on industrial ingots weighing 7.4 t.

V. Borisov, V. Golikov and B. Lyubov (Central Iron and Steel Technical Research Institute) have made a study with the aid of the radioactive isotope Fe^{59} of the self-diffusion of iron in the alloy with 3% Si and have constructed a quantitative theory of diffusion along the grain boundaries.

E. Belyakova

INTERNATIONAL SCIENTIFIC-TECHNICAL EXHIBITION ON THE PEACEFUL USES OF ATOMIC ENERGY AT GÖTEBORG

In May of this year, at the annual Swedish Industrial Fair in Göteborg for the first time there was an exhibition on the peaceful uses of atomic energy. In addition to Sweden, the USSR, USA, France, England and Denmark were represented.

At the Soviet pavilion of the exhibition there were working models of atomic electric-power stations and reactors, in particular a model of the 200,000 kw electric-power station, various devices for measuring radiation and for control of manufacturing processes, collections of minerals and uranium-bearing ores, as well as equipment used in medicine. There were exhibits with charts and posters and other demonstrations showing the results of research in radiochemistry, application of radioactive isotopes in agriculture, biology, geology and engineering. Many new models of devices issued in 1956 were shown here for the first time.*

The most prominent exhibit at the Swedish pavilion was the one showing the harnessing of the Karolinska waterfalls in which there were models of two atomic power stations being built in Sweden.

One of these power stations, "Adam", is designed for heating purposes (in the city of Vesteros). The capacity of the station is 75,000 kw and the reactor operates with natural uranium using heavy water at a pressure of 8 atm in the primary cooling circuit as a moderating element and heat transfer material. Following heat exchange the ordinary water of the second circuit moves into the heating system. The station should be in operation in 1960. The second atomic electric power station "Eve" is designed to have a capacity of 100,000 kw and should be in operation in 1963. The reactor is similar to that of the first station. The only difference is that the pressure in the primary circuit is 60 atm, while in the second circuit it is 20 atm at the output to the turbine.

There were also a small collection of uranium ores and a map of the uranium deposits in Sweden. Although the amount of rich ore in Sweden is small there is a large deposit of shale with a radium content of 0.03-0.3%. In 1953 in Quantorn an experimental refining plant for the extraction of uranium from the shale was set in operation. Leaching with H_2SO_4 is followed by precipitation of the uranium phosphate. Phosphates containing uranium up to 30% are precipitated from the solution and dried, and then undergo further processing to become uranium metal.

There was a great deal of interest in a model of an experimental reactor which has been operating since 1954 at the Karolinska Institute in Stockholm (this was built by a private company "A.B. Atomic Energy"). The reactor operates with natural uranium and heavy water is used as a moderator element and coolant. The charge consists of three tons of uranium and five tons of heavy water and the capacity is 300 kw. The heavy water is cooled by heat exchange with air which is blown through it. Its primary function is the production of isotopes.

The exhibition of the physical chemistry division of the Karolinska Institute in Stockholm was devoted primarily to the use of radioactive isotopes in manufacturing: investigation of various technological processes in the manufacture of soap, wear studies of machine parts, metal cutting and the study of defects in metals.

The exhibits set up by the Institutes of Physics and Nuclear Chemistry of the Halmerk Technical Institute in Göteborg were very interesting.

There were diagrams and photographs of a 4.5 mev Van de Graaff generator and a mass spectrometer.

*A more detailed description of a number of the exhibits in the Soviet pavilion is given in Atomic Energy 1956, No. 1 p. 102 [T.p. 105] [T.p. = C.B. Translation pagination].

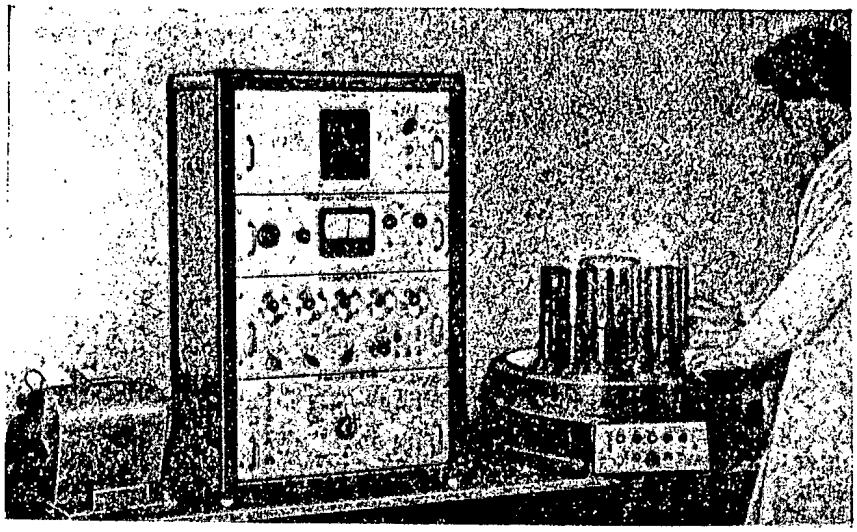

Fig. 1. General view of the Robot Scaler machine.

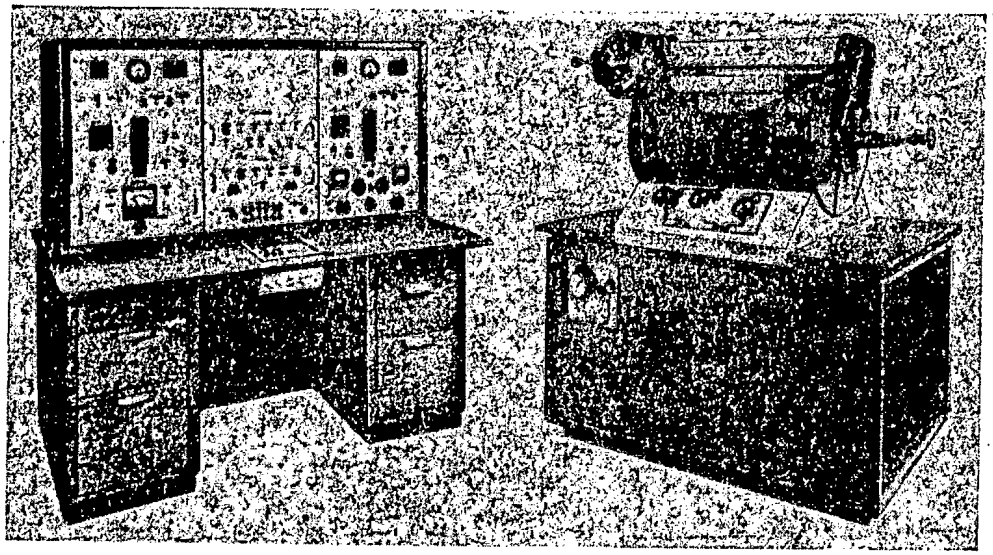

Fig. 2. β-Spectrometer.

There was a novel instrument for the measurement of very small quantities of C^{14}. The carbon in the sample being studied is converted in methane and the gas is passed through a system of channels in which Geiger counters are mounted. At the demonstration on uranium research there was shown a method for determining the uranium content in shale and shist as well as a diagram of a uranium-bearing shale. The results of studies of uranium corrosion in heavy and ordinary water and the diffusion of xenon in different metals were presented. An apparatus for examining diffusion in solid bodies, which makes it possible to detect automatically the exchange of atoms between solutions and solid bodies was of great interest. The counter in this instrument makes use of a new vacuum tube called the trochotron.

A number of instruments were exhibited by the Swedish scientific-research defense laboratory. One of these devices, which was rather interesting, was an 80-channel spectrometer for β and γ rays. The sample of of radioactive material being studied is placed in a chamber with two scintillation counters disposed at an angle of 90°. The pulse height analyzer and the channel sorter make use of a "magnetic memory" of nickel wire which operates as a binary storage counter. The results of the measurements are displayed on a cathode-ray oscilloscope in which the 80 channels are plotted along the horizontal axis while the vertical signal indi-

cates the number of pulses in each channel in the binary system. The spectra are photographed. There were two interesting radiation-level meters: one, a "self-starting" device, had an ionization chamber in which the wire was charged by friction between mercury and the walls of the chamber; the other was a radiation meter with phosphate walls. There was a special booth devoted to the use of γ defectoscopy in the manufacturing control of cast parts and welded pieces.

Fig. 3. Thickness and weight gauge manufactured by "LKB".

The radiology section of the Karolinska Institute in Stockholm presented diagrams and graphs showing the use of radioactive emanations for medical purposes and instruments for analyzing the radioactive content of air which can operate automatically. The exhibit of instruments of the Swedish firm "L.K.B. Products, Inc." was especially interesting. For example, an automatic device for measuring the radioactivity of samples called the Robot Scaler (Fig. 1) allows one to carry out measurements of the activity of 500 samples for γ and β radiation in 1.5 hours. The device makes use of trochotrons having a resolving time of 2.5 μsec.

Fig. 4. Prospecting instrument for radioactive ores – depthmeter.

The counter device has 5 trochotrons used in one unit in conjunction with a control tube. After the scaler there is a "memory unit" which stores the number of pulses accumulated during the counting time. The "memory" group consists of a system of relays which provide a light signal and simultaneously, (by means of a collection of cams) a current to the solenoid coils which operates the printing mechanism of a standard machine register. Six quantities which are of interest in the counting operation can be shown on the "register" tape: the number of pulses and the counting time, the number of pulses and the difference of the number of pulses as compared with an earlier test and so on. The results of the test are stored serially in a magazine which automatically sets up the samples in front of the detector and removes them after the measurement.

Another interesting device made by this firm is a β-spectrometer which is based on a design given by Siegbahn* (Fig. 2). The resolving power of the device is 1.5%.

*Phys. Rev. 75 (1955).

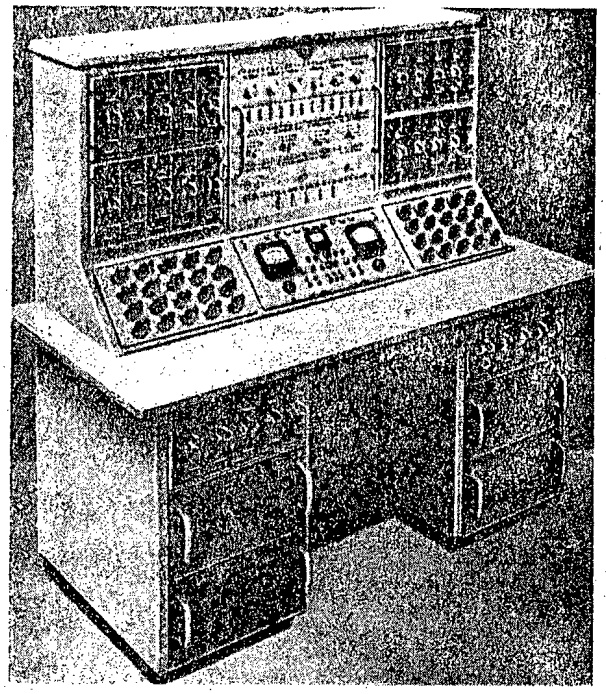

There was also an interesting weight and thickness gauge which makes it possible to determine the weight of paper (from 10 to 6000 g/cm^2) and the thickness of a tape (from 0.003 to 5 mm) of plastic, aluminum, steel or copper. The detection device in the instrument consists of two differentially-connected ionization chambers with variable calibrating units. The radiation source was Sr^{90} or Tl^{204}.

This instrument (Fig. 3) is built in two units (a measuring unit and a detection unit) with automatic recording of the results of the measurements; provision is made for connecting the control instrument to a rolling mill.

The Falliko firm exhibited several devices for radioactive-ore prospecting at depths varying from 30 to 100 m. One of these devices, a depth meter using scintillation counters made by the Detectron Company (USA), is shown in Fig. 4.

At the pavilion operated by the USA there were models of electric power stations and multicolor charts explaining prospecting and extraction of atomic fuels, the behavior of a chain reaction, the mechanism of nuclear fusion, the nuclear reactor, the procurement and application of isotopes in biology, agriculture, medicine and technology and the construction of atomic power stations in the USA.

One of the most interesting exhibits in the French pavilion was the one set up by the large metallurgical firm Pechiney which fabricates materials for reactors. This firm exhibited samples of aluminum, magnesium, perborate, titanium, beryllium, zircon, graphite and uranium.

The Dervenx firm showed an instrument for process control in reactors. Another interesting device exhibited by this firm was an analog computer, which reproduces the kinetics of an operating reactor (Fig. 5, top) used in conjunction with an electronic counter (Fig. 5, bottom). The use of the analog machine makes it possible to carry out calculations in connection with processes in reactors which relate to time-dependent neutron fluxes.

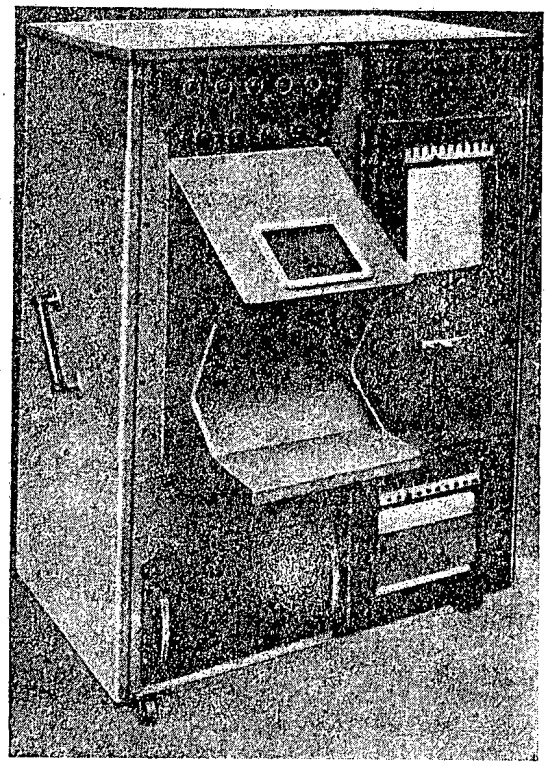

Fig. 5. Computer part of analog machine.

An interesting exhibit by the Gachot firm showed products made from teflon tetrafluoroethylene) in the form of tubes, slabs, gaskets, balls etc. This plastic is not affected by acids or alkalis, is not etched, and remains stable at temperatures ranging from −80 to +350°C.

On the basis of the charts and tables which were shown it would appear that in 1956 or 1957 four reactors should be put in operation in France: the research reactor at Sacle EL3 (third since 1948) and three reactors G-1, G-2 and G-3 at Marcul. The latter reactors are graphite with gas cooling. Reactor G-1 (started in operation in

January of 1956) provides an electric power of 8,000 kw with air-cooling and operates with natural uranium. Reactors G-2 and G-3 will be cooled by carbon dioxide and have an electrical power capacity of 60,000 kw. The last three reactors whould yield 100 kg of plutonium per year. The total capacity of the atomic power stations in France in 1958 should be 350,000 kw. The English pavilion contained exhibits of several firms which showed various stages in the construction of atomic electric-power stations.

In the Danish pavilion there were models of a Van de Graaff generator and a Wilson cloud chamber. There are also photographs and diagrams of an atomic power station.

S.T. Nazarov

NEWS OF FOREIGN SCIENCE AND TECHNOLOGY

WORK ON THE DEVELOPMENT OF AN AIRPLANE WITH AN ATOMIC MOTOR

At the present time intensive studies are being carried on in the USA, directed toward the development of an airplane with atomic propulsion. The operations headed by the Air Force of the USA are being conducted in four directions:

1) at the National Station for Reactor Testing (State of Idaho) an airstrip about 5 kilometers long is being constructed;

2) a new contract has been concluded with the company "General Dynamics, Convair Division", which will carry on work at its research center on the development of an atomic aircraft;

3) a contract has also been concluded with the company "Lockheed Aircraft", which will build a research laboratory for this purpose near Dawsonville (60 miles north of Atlanta, Georgia), to employ several hundred scientists and engineers;

4) the Air Force will begin construction in the very near future, in Dayton, Ohio, on a reactor of power about 10 megawatts, designed for testing airplane materials and proposed construction features and units. It is announced that this reactor is similar to the well-known American reactor for testing materials (MTR); it uses ordinary water as moderator and heat-transfer material. It is planned to have two large compartments in the reactor for radiation testing of materials. The equipment will be mostly of the standard sort used at the present time in reactors of the "basin" type and in other American reactors. Along with the reactor there will be built a complex of auxiliary equipment – cooling towers, "hot" laboratory, storage for radioactive materials, water purifier, etc. It is planned that the construction of this reactor will be completed at the beginning of 1958.

The problems arising in the construction of an airplane with an atomic motor are regarded as the most difficult in the whole history of airplane construction. The main difficulties are connected with the removal of heat from the reactor and its effective use in a motor of the turbopropellor, turboreactive, or even rocket type, together with the necessity of reducing the weight and providing shielding. Instead of a common shield for the reactor and the motor, it is proposed to use separate shielding.

At the present time the USA has an experimental airplane (a B-36), in the nose part of which an experimental nuclear reactor is mounted.

To assure the safety of the population the reactor is operated only at times when the airplane is in flight over a special reserved territory (in the State of Texas). The take-off and landing of the airplane are performed with the reactor stopped. Besides this, precautionary measures are taken to preclude the possibility of the dispersal or explosion of the reactor even in case the airplane is wrecked.

There has also been almost completed in the USA the development of an experimental aircraft reactor for stationary testing. The fuel elements of the reactor are plates of UO_2 coated with stainless steel. The temperature of the fuel reaches 1000°C. The moderator is ordinary water, and the heat-transfer material is air, which is fed directly into a gas turbine.

Advantages of the reactor are its small weight, the high temperature, and the relatively low pressure of the heat transfer material.

Its shortcomings include: low thermal efficiency, the radioactivity of the air, which makes the turbine inaccessible for servicing, and the large amount of air passed through the reactor. It is admitted that there is not full confidence in the successful operation of the reactor.

The expenses connected with this work in the USA have now amounted to many millions of dollars.

Similar studies, though on a smaller scale, are also being carried out by several British aviation companies, in particular by the firm of Rolls-Royce, which is completing the fitting-out of a special laboratory, and by several French companies.

Yu. K.

LITERATURE CITED

[1] Atomics 7, 3, 77 (1956).

[2] Atomics 7, 5, 173 (1956).

[3] Aeroplane 1956, 2321, 37.

[4] Nucleonics 14, 3, 94 (1956).

[5] Nucleonics 14, 5, 22 (1956).

A REACTOR WITH A GASEOUS HEAT-TRANSFER MEDIUM*

A plan for a nuclear power reactor with a gaseous heat-transfer medium was worked out at the University of Chicago in 1944. But the construction of the reactor, begun in 1947 at Oak Ridge, was discontinued. At the present time the project is being reconsidered in the light of available experience in the operation of reactors.

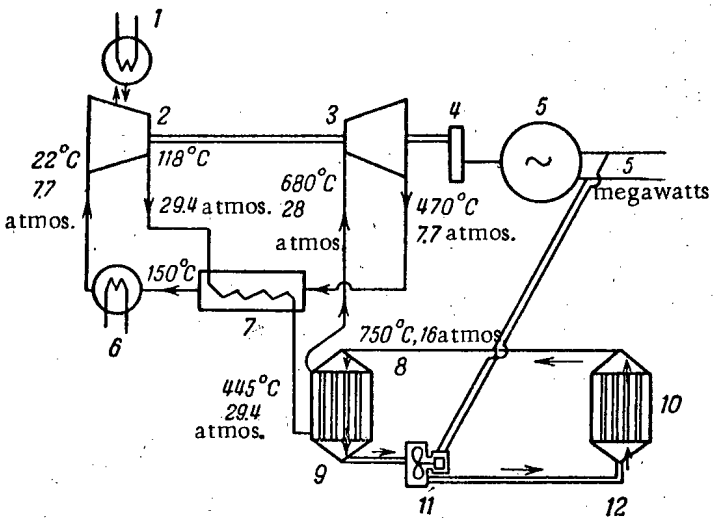

Fig. 1. Thermal block diagram of reactor with gaseous heat-transfer medium (power 5 megawatts, efficiency 25%). 1) Internal cooling; 2) compressor; 3) gas turbine; 4) reducing gear; 5) generator, 5.4 megawatts; 6) preliminary cooling; 7) heat exchanger; 8) helium; 9) heat exchanger, helium to air; 10) reactor; 11) hermetically sealed gas blower for helium, power 400 kw; 12) helium at 450°C, 16 atmos.

The type of reactor in question, with helium as heat-transfer agent, is designed for small power stations producing 5 to 10 megawatts.

Figure 1 shows the general plan of the reactor. The reactor is inclosed in a thick-walled steel case, cooled by air from the outside. Tubes for the motion of the regulating rods are brought out through the top of the case. The shielding of the reactor consists of concrete, lined on the inside with stainless steel. The heat exchanger is also surrounded by a concrete shield. The turbine room with concrete walls is directly joined to the heat exchanger.

The active zone of the reactor is made up of graphite blocks forming a cylinder of diameter 1.8 m, height 1.7 m, and total weight 9 tons. The blocks are held in a molybdenum network and supported by molybdenum columns. The reflector is of graphite 0.5 m thick. Channels 1.27 cm in diameter, forming the square lattice of the reactor, go through the active zone and the end reflectors. A breeding zone is included, cooled by channels through the side reflector. Between the reflector and the case there is an insulating graphite lining 15 cm thick.

The fuel elements contain uranium carbide (UC_2) and withstand temperatures up to 2000°C in an atmosphere of helium. The blocks are pressed from a mixture of uranium carbide and powdered graphite and are loaded into a graphite tube closed by a graphite plug. The fuel elements prepared in this way are placed in 4 of the 16 channels of each graphite block (Fig. 2). There are in all 1000 channels in the reactor, into which there is loaded about 150 kg of uranium carbide with 10% enrichment, i.e., 13.7 kg U^{235} in all. The critical mass for the reactor is 10 kg of U^{235}; the remaining 3.7 kg are intended to compensate for contamination, waste formation, and consumption of the uranium. The term of service of the reactor is 6 months at thermal power 20 megawatts; the electrical power is 5 megawatts.

The regulating and emergency rods consist of molybdenum tubes filled with boron or boron carbide. The use of molybdenum is explained by its high melting point and relatively low cost; it is adequately stable at

*Nucleonics, No. 3, pages 34 and 42 (1956).

high temperatures in an atmosphere of helium; in the presence of nitrogen or oxygen the molybdenum is rapidly corroded.

The helium used as heat-transfer medium is pumped at pressure 15.7 atmos. through 3000 channels in the reactor. The temperature of the helium is 440°C when entering the reactor, and 800-1000°C when it leaves the reactor. The temperature at the surfaces of the fuel elements can reach 2000°C.

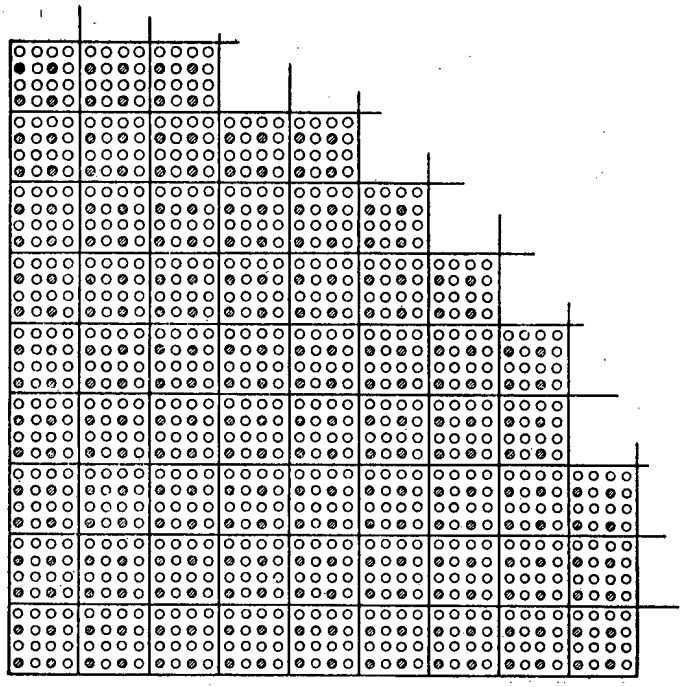

Fig. 2. Part of the active zone of the reactor with gaseous heat-transfer medium (shaded circles are fuel elements).

The heat exchanger, 1.5 m in diameter and 7.6 m high, is of standard type. Since the construction of the heat exchanger does not permit extreme overheating, a mixing chamber is provided, to which cold gas can be supplied. The gas blowers are located in a special building, separate from the reactor. The working gas in the turbine is air under pressure 30 atmos, and at input temperature 680°C. The air leaving the turbine is at temperature 400°C.

The gas turbine used is similar to the 2 megawatt turbine put out by the Swiss firm "Escher-Wyss Company". The weight of the turbine and compressor is 31 tons. The heat exchanger in the secondary circuit weighs 52 tons, and the electric generator weighs 23 tons.

To free the helium of impurities (moisture, air, hydrocarbons, carbon dioxide, fission products) there is a special filter of activated charcoal, cooled with liquid air. To check the oxygen content in the helium use is made of thin molybdenum or titanium wires, through which a current is passed. The change of the electrical resistance of such a wire gives evidence of the amount of oxygen in the reactor.

The greater part of the buildings for the reactor are buried in the ground. The total volume of the building is about 1700 cubic meters. The semicylindrical metal roof of the building is sealed against leakage of radioactive gases and as a precaution against emergencies.

The total cost of the equipment (including fuel) of a station to produce 5 megawatts is about 2 million dollars. The cost of the power can be reduced if there is supplementary production of U^{233} or P^{239} in the breeding zone of the reactor.

Besides the reactor project that has been described, others have also been worked out, in which nitrogen or air serves as heat exchange medium.

The use of gas-cooled reactors makes it possible to reduce the dimensions and weight of the turbine and

to raise the efficiency of the installation. But the construction materials for gas-cooled reactors must withstand temperatures of the order of 2000 to 2500°C. The most promising materials for this purpose are ceramics and metallized ceramics.

I. S.

AN ANGLO-AMERICAN REACTOR*

An Anglo-American company, formed from the English company "Mitchell Engineering Ltd. of England" and the American company "Atomics Incorporated of New York" has announced that after studying the various types of reactors designed for small power stations it has been decided to build a reactor with boiling of water in the active zone, as the most economical and safest type.

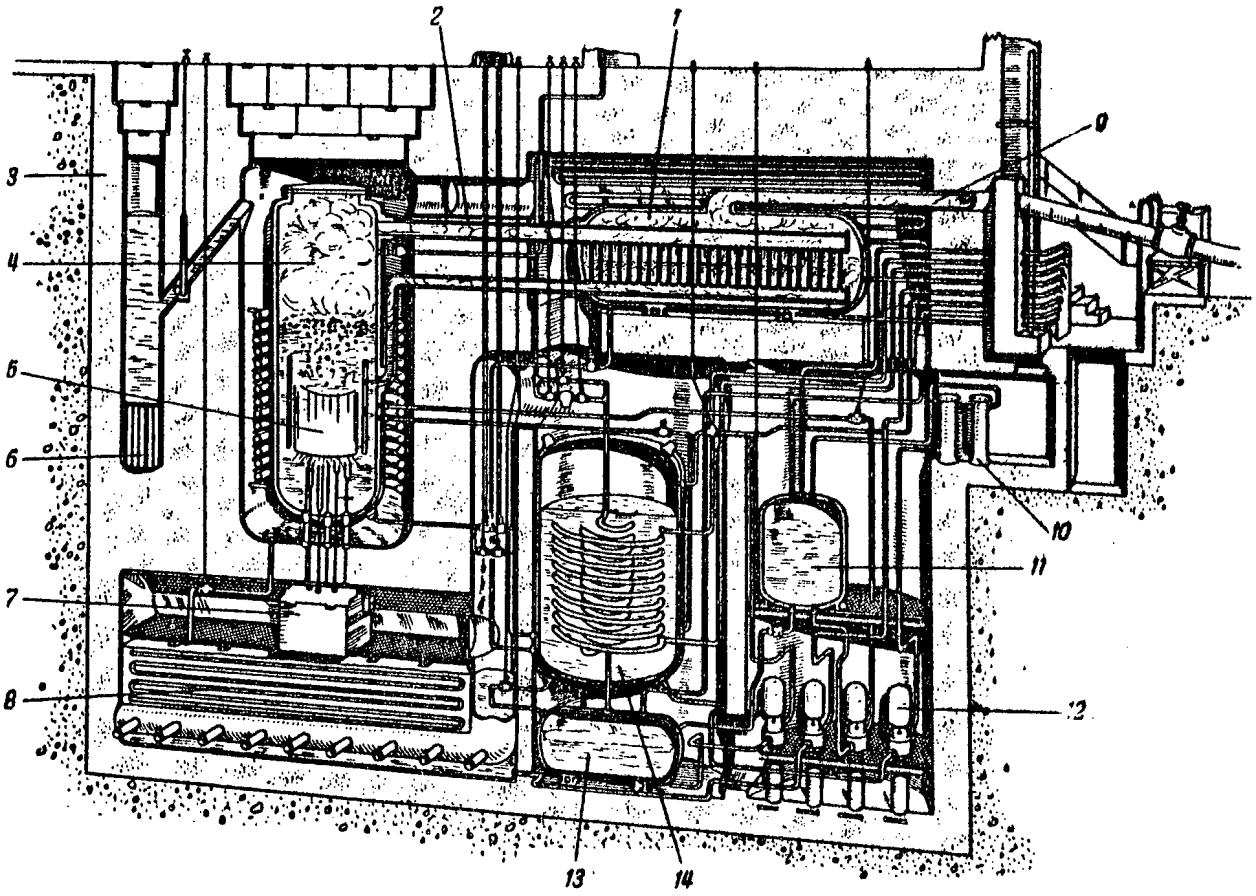

Plan of the installation.

1) Heat exchanger; 2) steam main of primary circuit; 3) concrete shaft lined inside with stainless steel; 4) reactor tank; 5) active zone of reactor; 6) storage for used fuel elements; 7) reactor control mechanism; 8) emergency condenser; 9) steam main of secondary circuit; 10) filters; 11) water storage tank; 12) pumps; 13) sump tank; 14) overflow tank.

*Nuclear Eng. 1, 3, 123 (1956).

The reactor consists of a thick-walled steel tank, the lower part containing the active zone. The upper part of the tank serves as the separator for the steam.

The majority of the fuel elements are made of thin sheets of natural uranium covered with a zirconium alloy. Some of the plates contain enriched uranium, and form the "kindling" zone. The protective and control system consists of eleven rods.

The removal of heat is accomplished by natural convection of the steam-water mixture in the active zone. From the separator the steam goes to a heat exchanger. The temperature of the steam leaving the reactor is 280°C, and the pressure is 63 atmos. The flow of water through the active zone is 6000 tons per hour, and the flow of steam is about 150 tons per hour. The heat exchanger produces steam at pressure 45.7 atmos and temperature about 260°C.

If necessary, the steam can be superheated in a special superheater. The steam pressure can be varied to suit the requirements of the user.

The regulating system for the steam pressure in the turbine is connected to the protective and control system of the reactor, so that the pressure of the steam in the reactor is always adjusted to the steam pressure in the turbine.

In case the steam pressure in the reactor goes up by 5%, the emergency protective system goes into operation; if the pressure continues to rise, that is, if the fission chain reaction has not been stopped, a solution of boric acid is sprayed into the reactor, or the valve is opened to release the steam.

In case of explosion the concrete shield can withstand an instantaneous rise of pressure to 3.5-4 atmos. A special receiver is provided to condense the steam in case of emergency.

To purify the water of radioactive matter, part of it is constantly circulated through a filter and an ion-exchange column.

During changing of the channels the space around the reactor is flooded with water. The concrete plugs over the reactor are removed, and the space so cleared is also flooded with water. The reloading of the channels is done by means of a manipulator. Worked-out elements are thrown into a storage space, where they are retained for a period of a year.

Before the reactor is set in operation all parts of the installation will be heated by special equipment to the working temperature. A cross-section of the reactor is shown in the diagram.

I.S.

WAYS OF PRODUCING FISSIONABLE MATERIALS

The production of enriched uranium or pure U^{235} is of enormous practical importance [1].

Of the numerous methods for separating the uranium isotopes – U^{235} and U^{238} – there are three that are evidently the most practical and that are in competition with each other: gaseous diffusion, separation in a gas centrifuge, and separation in Laval nozzles.

Separation by means of gaseous diffusion was carried out in the USA during the Second World War, at Plant K-26 in Oak Ridge. At present the process has been developed to the point where several kilograms of U^{235} can be produced per day [1].

The practical utilization of gaseous diffusion requires high technical development and is very expensive. Gaseous diffusion plants cost some thousands of millions of dollars. In Europe there is naturally a search for more economical methods of separation.

Separation of the isotopes of heavy elements by means of gas centrifuges, proposed by Groth, Beyerle, and others [2], has the advantage that in this method the separation factor is determined, not by the ratio of the masses, as in all other methods, but by the difference of the masses of the isotopes, and for uranium amounts to almost 5% with a simple centrifuge [3].

By use of thermal convection cycling [4] inside the centrifuge drum, a separation factor amounting to 20% can be obtained, whereas the ideal separation factor for uranium isotopes in the gaseous diffusion process comes to only 0.4%.

The separation of the uranium isotopes requires a continuously operating gas centrifuge, the development of which involves a number of technical difficulties. They are due to the fact that the centrifuge drum must rotate with extremely high angular velocity, and have not been completely solved, although the method of centrifuging has been known for about 40 years [2]. Despite these difficulties, Beyerle, Groth, and others have developed considerably more effective apparatus, which makes it possible to produce 2% U^{235} by joining in succession 6 centrifuges in all, while by using 20 stages in succession an output containing 20% U^{235} is obtained.

The apparatus including 20 centrifuges with all the auxiliary devices is estimated [1] to cost approximately 0.8 to 1.0 million German marks.

The separation by means of Laval nozzles [5] is a new and relatively little developed method. It is based on the fact that in the passage of a gas mixture through a Laval nozzle it is enriched in the light components around the edge, and in the heavy components in the center. By arranging suitable separating diaphragms in the form of cones inserted into the flow in the nozzle, one can secure a separation of the components. Using a nozzle with a very small aperture (0.5 mm), a study was made of the factors affecting the separation.

In order to effect savings in the total pumping power, the ratio of the amount of gas removed at the periphery to the total flow of gas is kept considerably smaller than 0.5. A detailed study was made of the separation of the seven xenon isotopes (with atomic weights from 128 to 135). On the basis of the data obtained with the noble gases, preparations are being made for experiments with the uranium isotopes.

An increase in yield can be achieved by replacing nozzles with cylindrical openings by nozzles with slots. The practical application of this method of separation, like that of separation by centrifuges, requires pumps that are stable under exposure to UF_6.

By the nozzle method enormous yields can be obtained at small separation factors, in contrast with the centrifuge method, which gives large separation factors (for uranium) with small yields. An advantage of the

nozzle method is the fact that the most critical parts of the apparatus remain at rest. This apparatus does not require as careful handling as centrifuges, and the replacement of worn out parts can be accomplished more rapidly.

L.M.

LITERATURE CITED

[1] K. Reger, Atomwirtschaft 1, 2, 61 (1956).

[2] K. Beyerle and W. Groth, Uber Gasenzentrifugen (Frankfurt a/M 1950).

[3] K. Cohen, "The theory of isotope separation," Nat. Nuclear Energy Ser, Div. 3, BI, 104 (1951).

[4] H. Martin and W. Kuhn, Z. phys. chem. A 189, 219 (1940).

[5] Becker et al., Z. Naturforschung 10A, 7 (1955).

DISTRIBUTION OF FISSION WIDTHS FOR Pu^{239}

In a paper by Farley [1] a distribution in sizes of fission widths is given for 25 resonance levels of Pu^{239} (see diagram). This distribution is of exponential character, which is in agreement with the data given by Hughes for U^{235} [2]. The average value of the fission width for Pu^{239} is 46 ± 12 mv.

P.K.

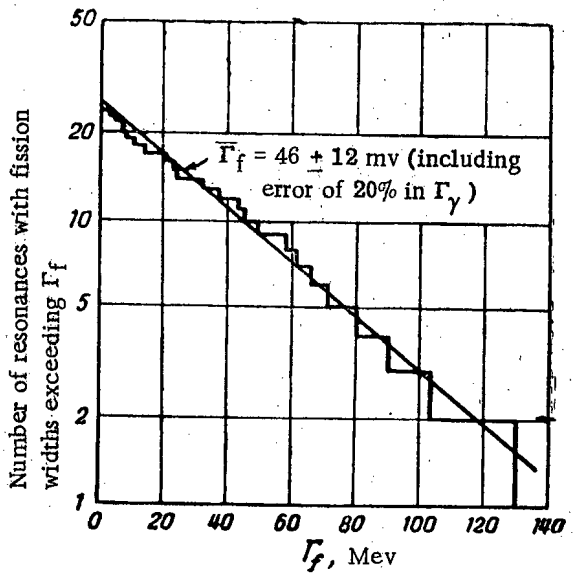

LITERATURE CITED

[1] F.J.M. Farley, J. Nucl. Energy 3, 1/2, 33 (1956).

[2] D. Hughes, J. Atomic Energy (USSR) 5, 42 (1956) (T.p. 715). *

*T.p. = C.B. Translation pagination.

PARTIAL SEPARATION OF Na^{22} AND Na^{24} BY THE METHOD OF ION-EXCHANGE CHROMATOGRAPHY *

Experiments on the separation of Na^{22} and Na^{24} have been carried out with a column of length about 1 m; the adsorbent used was the cation-exchange resin Dowex-50 in hydrogenous form with average grain size ~ 25μ.

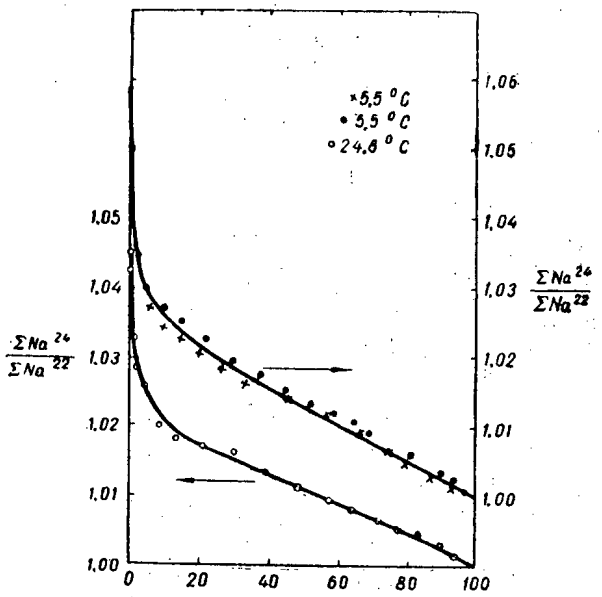

Enrichment of filtrate in Na^{24} isotope.

Solutions of radioactive isotopes $Na^{22}Cl$ and $Na^{24}Cl$** were first mixed together in definite proportions and adsorbed on 0.2 gm of the resin, which was deposited in a thin layer on the upper part of the column. The adsorbent was washed through with 0.7 M hydrochloric acid sent through at an extremely slow rate, which was kept constant to an accuracy of ±5%. The filtrate was collected in separate fractions, in which the ratios of the relative activities of the isotopes were measured by a radiometric method. Here it was necessary to introduce a correction for the decay of the short-lived Na^{24} during the experiment.

The calculation of the ratio of the isotopes was carried out by means of the formula

$$\frac{N_1^{22}}{N_1^{24}} = \frac{N_1 - N_2 + [\Delta N/(f-1)]}{N_2 - [\Delta N/(f-1)]},$$

where N_1^{22}, N_1^{24} and N_2^{24} are the relative activities of the isotopes Na^{22} and Na^{24} in counts per minute at the initial time (T_1) and at the end of the experiment (T_2); N_1 and N_2 are the total activities of the specimens, referred to the times T_1 and T_2; $\Delta N = N_1 - N_2$; $\Delta T = T_1 - T_2$; and

$$f = N_2^{24}\,[\exp(0{,}693\,\Delta T/15{,}04) - 1].$$

Curves giving the variation of the isotopic ratios in the eluted solution for various temperatures of the column are shown in the diagram. The initial Na^{24}/Na^{22} ratio is taken to be unity. The highest enrichment of the solution in Na^{24} isotope occurs in the first portions of the filtrate.

V.P.

*Can. J. Chem. 34, 1, 65 (1956).

**The half-value periods of Na^{22} and Na^{24} are 2.7 years and 15.0 hours respectively.

SUBLIMATION OF PLUTONIUM FROM IRRADIATED URANIUM*

The apparatus in which the experiments on sublimation of plutonium were carried out is shown in the diagram.

The specimen of irradiated uranium was placed in a crucible of beryllium oxide and heated by a tungsten spiral. The crucible was surrounded on the outside with thermal insulation, and also with a molybdenum radiation shield. This assembly was mounted in a glass bulb, which was then evacuated and placed in a sealed box behind a lead shield.

TABLE

Data on Distillation of Plutonium

Run No.	Weight of U, gm	Time, hours	Area of specimen	Distribution of Pu, %		
				specimen	crucible	condenser
		Temperature	1540° C			
92	3.972	2.75	0.581	65.7	7.0	27.3
101	2.464	3.61	0.441	56.5	16.3	27.2
103	2.022	7.31	0.490	31.0	33.8	35.2
104	2.362	9.00	0.528	8.4	54.2	37.4
109	2.044	10.00	0.441	23.0	33.9	43.1
102	1.446	7.50	0.478	4.8	42.2	53.0
110	2.183	14.00	0.540	4.4	42.4	53.2
117	1.442	10.68	0.554	4.3	50.8	44.9
		Temperature	1650° C			
81	3.460	0.82	0.581	67.1	7.7	25.2
85	4.229	2.00	0.528	38.0	25.2	36.8
82	4.017	1.75	0.581	32.6	33.6	33.8
83	4.307	3.67	0.515	25.8	35.8	38.4
84	4.027	4.27	0.586	13.4	37.4	49.2
107	1.841	3.58	0.430	3.9	40.0	56.1
106	3.393	10.37	0.407	4.3	34.7	61.0
108	3.157	7.62	0.515	1.9	40.2	57.9
116	5.487	13.58	0.502	2.0	25.5	72.5
		Temperature	1769° C			
89	3.454	0.40	0.465	35.7	24.8	39.5
90	3.723	0.75	0.609	24.2	28.1	47.7
119	2.179	0.61	0.708	4.1	46.4	49.5
120	2.005	0.85	0.650	1.5	51.5	47.0
121	1.838	1.07	0.622	2.1	64.4	33.5

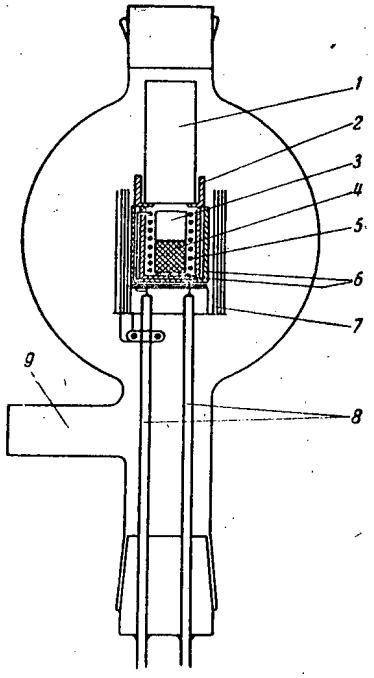

Diagram of apparatus for evaporation of Pu. 1) Corundum condenser; 2) condenser holder (BeO); 3) crucible made of BeO (diameter 1 cm); 4) crucible support of BeO; 5) tungsten spiral; 6) thermal insulation (BeO); 7) molybdenum shield against radiation loss; 8) copper leads; 9) to vacuum pump.

The distillation was carried out at temperatures of 1540°, 1650°, and 1769°C, which were controlled by means of a radiation pyrometer to an accuracy of ± 15°C. The plutonium vapor was cooled in a condenser placed above the crucible. The amount of plutonium sublimated was determined radiochemically from the difference of the plutonium content of the

*D.E. McKenzie, Can. J. Chem. 34, 4, 515 (1956).

specimens before and after a run.

The results of a number of experiments are given in the table.

The observed rates of evaporation of plutonium were compared with calculated values found from Langmuir's equation and Raoult's law.

There was agreement within the accuracy of the experimental measurements. This indicates that the plutonium contained in irradiated uranium obeys the laws of ideal solutions.

V.P.

GAS SCINTILLATION COUNTERS

At the present time, in addition to liquid and plastic scintillators for the detection of elementary particles, counters are used in which various noble gases serve as the scintillating substance. The main advantages of the devices to be described below are the speed of production of the pulses from light and the almost complete insensitivity to γ-rays.

The first paper [1] describes a gas chamber consisting of an aluminum hemisphere 5 cm in diameter with an α-particle source placed inside. The chamber is filled with argon to a pressure of 5 atmos. At one end of the chamber there are a pyrex window and a photomultiplier. The inner surface of the window and the walls of the chamber are covered with a thin layer of tetraphenyl butadiene in polystyrene, to convert ultraviolet to visible light.

The resolving power of the chamber just described, in counting the 5.47 Mev α-particles from Pu^{239}, is 15%. The rise time of the light pulse is 10^{-8} sec. The counter is not sensitive to γ-rays.

The mechanism of production of the light pulse can be conceived as follows. First the heavy charged particle loses energy by exciting and ionizing atoms of the stopping gas. Each excited atom returns to its initial state, emitting one or several photons in the course of 10^{-9} sec, and thus the light pulse is produced.

A difficulty in working with gas scintillators that is hard to overcome is the low intensity of the light pulses, since in the process of converting the energy of the particle into energy of electrons at the cathode of the photomultiplier losses occur, owing to geometrical factors, reflection, transformation of energy, change of wavelength, and efficiency of the photomultiplier cathode.

The total number of photons produced is about 10^5 per Mev. But, owing to the indicated losses, α-particles of energy 5 Mev give in practice only about 500 photoelectrons from the cathode of the photomultiplier.

Another difficulty is a quenching, consisting in a decrease of the height of the light pulse with time. This effect is evidently due to the accumulation of harmful gases and vapors evolved from the surface of the material used for the conversion of ultraviolet into visible light.

One of the ways to combat the quenching is to use a material for shifting the wavelength of the light that does not give out harmful gases. Such a material was found in nitrogen, which changes the ultraviolet radiation of helium or argon into visible light, if mixed with the noble gas in a certain proportion.

Quenching can also be avoided by doing without a material to alter the light. It is then necessary to use a photomultiplier with a quartz bulb (EMI), and also to make the window of the chamber of quartz or of LiF. This increases the resolving power of the counter for 5 Mev α-particles to 30%.

At the Los Alamos Laboratory a careful study [2] has been made of the dependence of the properties of scintillation counters on the composition of the filler and other variables.

To free the gas from contaminations a special chamber was built, in which the gas is continuously circulated through a section filled with purifiers, which consist of uranium shavings heated to 800°C, or of cold uranium (to adsorb hydrogen).

To find the effect of impurities in a quantitative way, measurements were made of the variation of the pulse heights with several mixtures of xenon with contaminating substances. The most harmful contaminations were found to be oxygen and methane: admixture of 2 to 4 percent of these gases reduces the pulse height by a factor of 6. Circulation of the gas mixture through the purifier restores the pulse height to that characteristic for pure xenon.

The material used to shift the wavelength of the light was tetraphenyl butadiene or quaterphenyl. Evaporation in vacuum was used to produce a uniform coating of the surface of the counter with these substances. It was found by experiment that although tetraphenyl butadiene is roughly $\frac{1}{3}$ more effective, quaterphenyl is more stable.

To increase the yield of light, a reflecting system was developed: a layer of MgO was deposited on the surface of the counter, which was made of unpolished duraluminum, and then the coating of quaterphenyl was added. Such a reflecting system increases the light yield by a factor of five.

Using this reflecting system, these writers compared the various noble gases and a NaI crystal scintillator. The relative light yields of these substances were as follows:

$$NaI : Xe : Kr : A : Ne : He = 72 : 32 : 16 : 5 : 1 : 10$$

A study of the linearity of the dependence of counter output on particle energy showed a strict proportionality, with the different charged particles (protons, deuterons, helium ions) of a given energy producing almost identical light yields.

Besides the gases, the writers also used liquid and solid xenon, krypton, and argon. Preliminary tests showed that liquid or solid xenon gives roughly twice the light yield of the gas, and is thus comparable with NaI. Liquid and solid krypton and argon are comparable with xenon in light yields.

All of the substances studied in the liquid and solid states gave a higher counting speed, with resolving times below 10 mμ sec. This distinguishes them from the gases, for which the resolving time depends on the pressure and amounts to (approximately) 75 mμ sec at 25 cm, 30 at 50, and 14 at 100 cm.

The third paper [3] presents considerations on the possibility of using gaseous scintillators, in particular hydrogen, for neutron dosimetry.

S. L.

LITERATURE CITED

[1] C. Eggler and C.M. Huddleston, Nucleonics 14, 4, 34 (1956).

[2] J.A. Northrop and R. Nobles, Nucleonics 14, 4, 36 (1956).

[3] C.O. Muehlhause, Nucleonics 14, 4, 38 (1956).

DETERMINATION OF RADIATION DOSAGES FOR THE ATOMIC BOMB EXPLOSIONS AT HIROSHIMA AND NAGASAKI*

Most of the data on dosimetry that might have been obtained immediately after the atomic explosions at Hiroshima and Nagasaki are by this time unavailable. The author attempts a restoration of the dosimetric picture for these explosions by combining data from later explosions with known data about the bombs used in Japan in 1945. A difficulty of this procedure lies in the fact that the power of the bombs exploded over Japan is not well enough known. For calculation of dosages at Nagasaki use can be made of data from the test atomic explosions in New Mexico and at Bikini, since similar bombs of about the same power were used there.

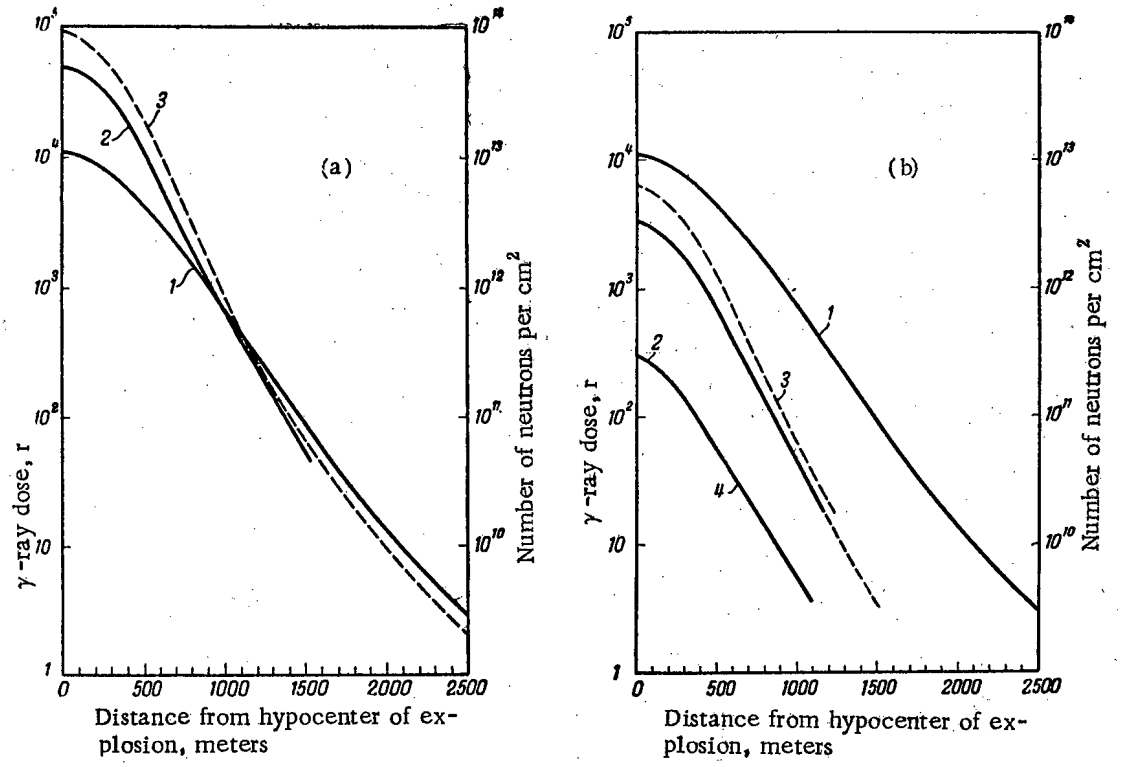

Fig. 1. Dose of γ-radiation as function of distance from the ground center of the explosion. a) Hiroshima; b) Nagasaki. 1) γ-radiation; 2) slow neutrons; 3) fast neutrons (0.1-3 Mev); 4) neutrons over 3 Mev.

The γ-radiation resulting from an explosion can be divided into three categories:

– instantaneous radiation, occurring at the moment of the explosion because of the disintegration and activation by neutrons of the outer parts of the bomb,

– delayed radiation, coming from fission products in the fireball and from the activation of the air by delayed neutrons, and

*R. Wilson, Rad. Res. 4, No. 5, 349 (1956).

– residual radiation, coming from induced activity of the soil and from fission products falling out from the radioactive cloud in one form or another.

A large part of the dosage produced was due to delayed radiation and can be expressed by the formula

$$D = \frac{Se^{-R/\lambda}}{R^2}, \qquad (1)$$

where λ is the mean free path of a neutron, amounting to 0.32 km in air, and S is a constant depending on the power of the bomb. The correctness of this formula has been verified for the Nagasaki type bomb by measurements at various tests.

The bomb dropped at Hiroshima was of entirely different construction; in particular the fissionable material used was uranium instead of plutonium. In the past it has been customary to estimate the power (S) of this bomb on the basis of a study of exposed photographic plates found in a Red Cross hospital. But the specimens found in the first and in subsequent searches gave extremely contradictory results.

Since the γ-rays came mainly from the fireball, their intensity was relatively independent of the construction of the bomb. Moreover, since the disintegration products of plutonium and uranium are almost the same, it can be concluded that the intensity of γ-radiation was roughly the same at Hiroshima and Nagasaki, and the differences depended only on the relative powers of the bombs. Therefore it can be assumed that the total dose in roentgens, both at Hiroshima and at Nagasaki, can be expressed by the formula

$$D = \frac{3{,}5 \cdot 10^4 e^{-2R/\lambda}}{R}, \qquad (2)$$

with $S = 3.5 \cdot 10^4$, which corresponds to a "nominal" bomb of explosive power equivalent to 20,000 tons of TNT.

These data are shown graphically in Figure 1a and b.

The indicated dose was not instantaneous, but was released in a time of several seconds: about 15% in the first 0.1 sec, about 50% in the first second, about 80% in the first 10 sec, and the whole dose in roughly a minute.

In the residual γ-radiation two components can be distinguished: one, caused by the radioactivity produced by neutrons, must be distributed more or less uniformly with respect to the center of the explosion; the other, caused by the dispersion of the fission fragments, depended to a considerable extent on the weather at the time of the explosion. The amount of residual γ-radiation was measured after the explosions and is at present well known. The activity decreases with the time approximately as $1/t^{1.2}$ during the first two days, and thereafter as $1/t^{1.5}$. Figures 2 and 3 show curves of the distribution of the residual activity according to the data of Thibault (AEC WO-170, 1946). For distances beyond 300 m the residual radiation dose was less than 10 r, except at Nagasaki, where the cloud containing the fission products and moving toward the east gave fall-out of radioactivity on hills a mile from the place of the explosion. Here the total dose due to residual activity can have amounted to 100 r.

Owing to the differences in bomb construction and fissionable material, the ratio of neutrons to γ-rays was evidently different at Hiroshima and at Nagasaki. Therefore by a comparative study of the effects in these two cities one can separate the effect caused by neutrons from the effect of γ-rays.

The neutrons may be divided into two different classes: the instantaneous neutrons from fission and the delayed neutrons. The delayed neutrons amount to only 1% of the instantaneous neutrons from the fission of uranium, and about 0.5% in the case of plutonium fission. But an experiment conducted in New Mexico showed that at a height of 600 m the fission neutrons make up only 20% of the total dose of neutrons, and the other 80% follow the critical decay law of the delayed neutrons. These considerations apply to the plutonium type of bomb used at Nagasaki.

On the assumption that the neutron dose at Nagasaki depended mainly on the delayed neutrons, important conclusions can be drawn about the neutron dose at Hiroshima. As was pointed out above, in uranium fission the fraction of delayed neutrons is twice as great as in plutonium fission. Thus it can be expected that the ratio of the neutron dose to the γ-ray dose must be at least twice as large at Hiroshima as at Nagasaki. The difference in the construction of the bomb may increase this ratio by a factor of ten or more because of the greater "transparency" of the uranium bomb for fast neutrons in comparison with the plutonium bomb.

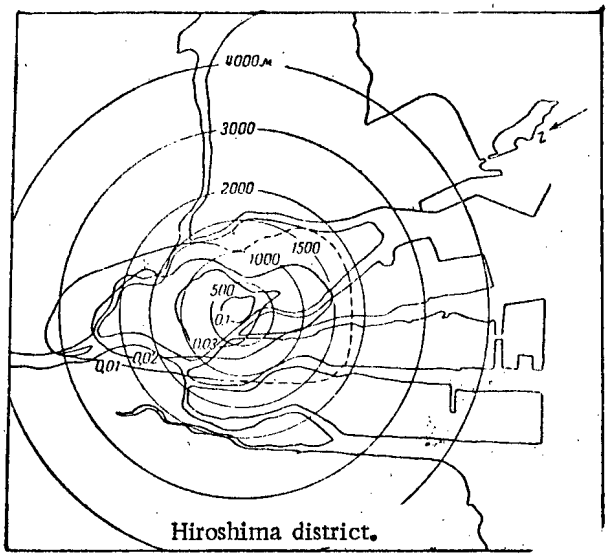

Fig. 2. Hiroshima. Curves of equal dosage on October 3 to 7, 1945, in mr/hour.

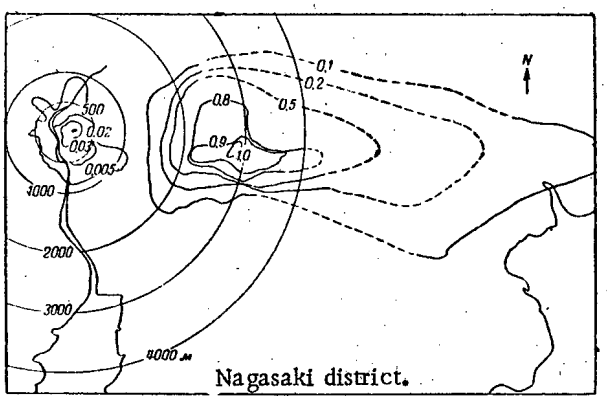

Fig. 3. Nagasaki. Curves of equal dosage on October 3 to 7, 1945, in mr/hour.

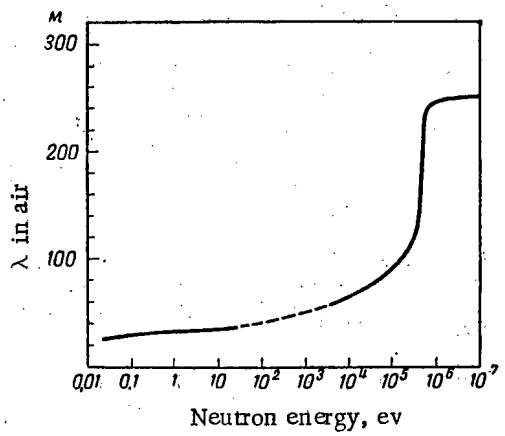

Fig. 4. Mean free path of neutrons in air as function of energy.

The energy spectrum of the instantaneous fission neutrons emitted at the time of the explosion is very broad, with a large fraction of the neutrons having energies of several million electron-volts. The delayed neutrons are also fast, but their average energy is lower than the energy of the instantaneous fission neutrons. Most of the delayed neutrons have energies of about 0.9 Mev or less.

Slow neutrons can easily be measured by the induced radioactivity of silver, arsenic, or phosphorus. Such measurements were made at the experimental explosions; the results can be compared with measurements in Hiroshima and Nagasaki. Two specimens of bone were studied by Warren's group: one found in Hiroshima at a distance of 200 m from the center of the explosion, the other in Nagasaki at a distance of 800 m. It is known that between the center of the explosion and its victims there was not more than 1.25 cm of wood. The induced radioactivity of phosphorus was measured in the specimens found. Since both measurements were made by the same persons and with the same equipment, the relative numbers of slow neutrons at Hiroshima and Nagasaki must be well known. Comparing the slow neutron dose found at a distance of 200 m in Nagasaki with the dose found at the same distance at Hiroshima, one can conclude that there were about 30 times as many slow neutrons at Hiroshima. Japanese physicists made measurements at Hiroshima on the activity of phosphorus at various distances, and the data they obtained also provide evidence that there were at least 10 times as many neutrons at Hiroshima as at Nagasaki.

Since the slow neutrons are formed from fast ones, an idea of the number of the latter can be obtained on the basis of measurement of the slow neutron dose. The number of neutrons with energies above 3 Mev can be judged from measurement of the induced activity of sulfur. Experiments at the test explosions show that the neutrons with energies above 3 Mev follow almost the same curve as the thermal neutrons, but are fewer by about a factor of 20. In Fig. 1b are shown the results of measurements carried out at the Los Alamos Laboratory, which can be applied directly to calculate the number of neutrons at Nagasaki. Here the fast neutrons are evidently instantaneous neutrons from fission that have passed through the bomb casing. It can be expected that in the case of Hiroshima there would be more of them because of the greater "transparency" of a bomb of that type. The measurements of Japanese physicists (Nakaidzumi) show that at Hiroshima the neutrons with energies above 3 Mev were about 3 times as numerous as at Nagasaki, and that they penetrated to great distances.

The magnitude of the neutron flux F in an energy range from E_1 to E_2 in which λ does not change very much can be expressed approximately by the following equation:

$$F = 2 \cdot 10^{-2} F_S \lambda \log \frac{E_2}{E_1} ,$$

where F_S is the slow neutron flux shown in Fig. 1,a and b and λ is shown in Fig. 4, in meters. Thus, according to this expression, the number of fast neutrons per cm^2 with energies between 0.1 and 0.5 Mev, at a distance of 1000 m from the ground center of the explosion in Nagasaki was $1.3 \cdot 10^{11}$. The author used these considerations in constructing the curves of Fig. 1,a and b.

If we assume as the lethal dose $5 \cdot 10^{11}$ slow neutrons per cm^2 and 10^{11} fast neutrons per cm^2, and suppose that radiation injury is produced by 0.1 of this dose, then effects of neutrons could occur at a distance of 1500 m in Hiroshima and about 1000 m in Nagasaki. It is possible that at Hiroshima the neutron effects were greater than the γ-ray effects.

S. L.

BIBLIOGRAPHY

RECENT LITERATURE ON THE PEACEFUL USES OF ATOMIC ENERGY, BOOKS AND COLLECTIONS OF ARTICLES

Beryllium, Collection of Articles Translated from Foreign Periodical Literature, M. B. Reifman, Editor, Foreign Lit. Press, 1956, 178 pp.,9 rubles 80 kopecks.

Problems of Radiobiology, Collection, M. N. Pobedinsky and P. N. Kiselev,Editors, State Medical Press, Leningrad Div., 1956, 430 pp., 14 rubles 20 kopecks.

Gorshkov, G. V., Gamma Radiation of Radioactive Bodies, Leningrad Univ. Press, 1956, 139 pp., 4 rubles, 50 kopecks.

Radiation Effects and the Use of Isotopes in Biology, Collection of Translations, Reviews and Abstracts of Foreign Periodical Literature, 1956, No. 2, 146 pp., 8 rubles, 40 kopecks.

Von Laue, M., History of Physics, Translation from German by T. N. Gornshtein, with article by I. V. Kuznetsov, Editor, State Tech. Press, 1956, 230 pp., 7 rubles, 35 kopecks.

Nesmenyanov, A. N.,et al., Practical Guide to Radiochemistry (Textbook for Chemistry Departments of Institutes and Universities), State Tech. Press, 1956, 398 pp., 10 rubles, 70 kopecks.

New Methods of Treating Food Products (Irradiation), Ministry of the Meat and Dairy Products Industry USSR, Dept. Tech. Inform., Abstracts and Reviews of Foreign Technical Literature, No. 32, 1956, 34 pp., gratis.

Tarasenko, D. M., Determination of Wear of Automatic Machines by the Use of Radioactive Isotopes (All-Union Org. for Dissemination of Political and Scientific Information, Leningrad House of Scientific and Technical Propaganda), 1956, 12 pp., 40 kopecks.

ARTICLES IN JOURNALS

Averkiev, M. S., "Scattering of Radiation Without Clouds," Meterorology and Hydrology (USSR) 1956, No. 5.

Alimarin, I. P.,et al., "Quantitative Separation of Zirconium from Iron and Nickel by Ion Exchange Chromatography," Bull. Moscow Univ. 1956, No. 3.

Antonov, Yu. A., "Radio Waves from the Sun and Galaxy, Collection of Papers of the Scientific Students' Organization of the Moscow Inst. of Power Eng." 1956, No. 9.

Astreeva, O., "Radioactive Isotopes in the Control of Cement Production," Structural Materials, Products and Structures (USSR) 1956, No. 5.

Afrikyan, L. M., "On the Theory of the Production and Annihilation of Antiprotons," J. Exptl.-Theoret. Phys. (USSR) 30, 4 (1956).

Akhiezer, A. I. and Polovin, R. V., "On the Theory of Wave Motion in an Electron Plasma," J. Exptl.-Theoret. Phys. (USSR) 30, 5 (1956).

Berestetsky, V. B. et al., On the Radiative Correction to the Muon Magnetic Moment, Letter to Editor, J. Exptl.-Theoret. Phys. (USSR) 30, 4 (1956).

Born, G. I. et al., "On the Solution of Some Analytic Problems concerning the Rare Earths by Radioactive Analysis," Trans. Commission on Analytic Chemistry, Acad. Sci. USSR, 7, (1956).

Buberman, G. S., "The Use of Radioactive Isotopes in Textile Industry (From Foreign Literature)," Textile Industry (USSR) 1956, No. 4.

Burkser, E. S. and Eliseeva, G. D., "The Use of Radioactive Isotopes in Paper Chromatography of Inorganic Compounds," Trans. Commission on Analytic Chemistry, Acad. Sci. USSR Vol. 7 (1956).

Vdovin, Yu. A., "Production of a Nuclear Star and Pion by a Gamma Quantum," Letter to the Editor, J. Exptl. Theoret. Phys. (USSR) 30, 4 (1956).

Vizbaraite, Ya. I. et al., "Self-Consistent Fok Field of an Excited Helium Atom," Optics and Spectroscopy (USSR) 1, 1 (1956).

Volovik, G. A., "Investigation of Blast-Furnance Smelting and Cast Iron Production with the Aid of Radioactive Isotopes (From Foreign Literature)," Steel (USSR) 1956, No. 6.

Gavrilov, B. I. and Lazarev, L. E., "Photoneutron Yields from Medium Heavy and Heavy Nuclei," J. Exptl. Theoret. Phys. (USSR) 30, 5 (1956).

"Gamma-Ray Apparatus for Industrial Irradiation (Type GUP-Co-0.5-1)," Electrical Industry 1956, No. 5.

Glazov, A. N., The Use of Radioactive Isotopes in Hydrogeological and Engineering-Geological Studies Abroad, Exploration and Conservation of Mineral Resources (USSR) 1956, No. 4.

Gragerov, I. P., "Microflotation Method for Analyzing Heavy Water," J. Analyt. Chem. (USSR) 11, 3 (1956).

Granilshchikov, V. P. and Parkhomenko, G. M., "Sanitary and Hygienic Requirements in the Planning and Equipping of Laboratories Using Radioactive Materials," Medical Radiology 1, 3 (1956).

Grigorov, N. L., "Average Characteristics of Interactions between Primary Cosmic Rays from 2 to 1000 Bev with Light Nuclei," Progr. Phys. Sci. (USSR) 58, 4 (1956).

Phase Diagrams of Some Plutonium Systems, Referat A. G., Metallography and Metal Processing (USSR) 1956, No. 5.

Dukelsky, V. M. et al., "Conversion of Positive Helium Ions into Negative Ions through Collisions with Inert Gas Atoms," Letter to the Editor, J. Exptl. Theoret. Phys. (USSR) 30, 4 (1956).

Elovich, S. Yu. and Kuzmina, L. G., "Investigation of Inversion of Adsorbed Series in Ultrasmall Concentrations Using Tracers," Colloid J. (USSR) 18, 3 (1956).

Eselson, B. N. and Bereznyak, N. G., "Liquid-Vapor Phase Diagram of $He^3 - He^4$ System," J. Exptl.-Theoret. Phys. (USSR) 30, 4 (1956).

Ivonina, T. F. and Funtikova, V. I., "The Use of Tracers to Determine the Solubility of Tin in Milk and Dairy Products," Collection of Student Researches, Moscow Tech. Inst. of the Meat and Dairy Industries, 1956, No. 4.

"A Study of the Character and Rate of Heat Erosion of Blast Furnaces Using Radioactive Isotopes," Information and News Section, Steel (USSR) 1956, No. 6.

Karalnik, S., et al., "Radiographic Study of X-Ray Photoelectric Emission," Letter to the Editor, J. Exptl.-Theoret. Phys. (USSR) 30, 4 (1956).

Karpman, V. I., "The θ Meson and the Fermi-Yang Hypothesis" Letter to Editor, J. Exptl.-Theoret. Phys. (USSR) 30, 4 (1956).

Kolesnikov, N. N., "Characteristics of the Energy Surface of Heavy Nuclei," J. Exptl.-Theoret. Phys. (USSR) 30, 5 (1956).

"Conference at the Gorky State University on the Use of Tracers in Chemistry," Chronicle, J. Analyt. Chem. (USSR) 11, 3 (1956).

Kopylova, V. D., "The Radiochromatographic Method in the Study of Chromatogram Precipitates," Trans. Moscow Tech. Inst. of Meat and Dairy Industries, 1956, No. 6.

Kudryavtsev, R. V., et al., "Determination of the Isotope Ratio of Oxygen in Organic Compounds," J. Gen. Chem. (USSR) 26, 4 (1956).

Kurnosova, L. V., et al., "Scattering of 250 Mev Photons by Free Electrons," J. Exptl.-Theoret. Phys. (USSR) 30, 4 (1956).

Kursanov, D. N., and Kudryavtsev, R. V., "A Study of the Mechanism of Hydrolysis Using the Heavy Isotope of Oxygen," J. Gen. Chem. (USSR) 26, 4 (1956).

Liberberg-Kucher, T. I., "Interaction Energy of Point Charges in an Ionic Crystal," J. Exptl.-Theoret. Phys. (USSR) 30, 4 (1956).

Logunov, A. A. and Terletsky, Ya. P., "On the Acceleration of Charged Particles by a Moving Magnetic Medium," Bull. Moscow Univ. 1956, No. 3.

Marei, A. N., "On the Sanitary Protection of Open Water Reservoirs from Radioisotope Contamination," Byelorussian Sanitation (USSR) 1956, No. 4.

Matveev, A. N., "Radiation Resonance in Synchrotrons, Letter to the Editor, J. Exptl.-Theoret. Phys. (USSR) 30, 4 (1956).

Mukhtarov, A. I. and Chernogorodova, V. A., "Photoproduction of Neutral Mesons Taking Account of Nucleon Spin States," Proc. Acad. Sci. Azerbaid SSR 12, 1956, No. 2.

Neiman, M. B. and Feklisov, G. I., "The Kinetic Method of Utilizing Tracers to Investigate the Mechanism of Complex Chemical and Biological Processes," J. Phys. Chem. (USSR) 30, 5 (1956).

Nemilov, Yu. A. and Litvin, V. F., "The Use of Magnetic Analysis of Products of (d, p) Reactions to Study the Quantum Characteristics of Resultant Nuclear Levels," J. Exptl.- Theoret. Phys. (USSR) 30, 4 (1956).

Novik, G. Kh., "Prospects for the Utilization of Radioactive Isotopes for Automatization in the Mining Industry," Mining J. (USSR) 1956, No. 6.

Novoselova, A. V. et al., "On Beryllium Oxyacetate 2," Bull. Moscow Univ. 1956, No. 3.

Olshanova, K. M., "The Use of Radioactive Isotopes for the Study of Adsorption and Desorption of Inorganic Ions in the Chromatography of Aluminum Oxide," Trans. Moscow Tech. Inst. of the Meat and Dairy Industries 1956, No. 6.

Ostankovich, V. E., "Changes in the Upper Respiratory Passages Produced by Small Doses of Ionizing Radiation in Industry," Bull. Otorino-Laring. (USSR) 1956, No. 3.

Panchenkov, G. M. and Moiseev, V. D., "Mass-Spectroscopic Isotope Analysis of Boron Fluoride," J. Phys. Chem. (USSR) 30, 5 (1956).

Peshkov, V. P., "Experiments on the Enrichment of Helium with He^3," J. Exptl.-Theoret. Phys. (USSR) 30, 5 (1956).

Ratner, A. P., "On Methods of Establishing the Mechanism of Coprecipitation of Radioactive Elements with Precipitates of Slightly Soluble Salts," J. Gen. Chem. (USSR) 26, 4 (1956).

Rudenko, N. P., "Methods of Separating Radioactive Isotopes Through Complexing," J. Inorg. Chem. (USSR) 1, 5 (1956).

Sondak, V. A., "Injury to the Organism through the Introduction of Small Doses of Radioactive Phosphorus," Biophysics (USSR) 1, 3 (1956).

Strelkov, S. A., "On the Utilization of Radioactivity in Structural and Road Engineering," Structural and Road Engineering (USSR) 1956, No. 5.

Stroganov, A. I., "Conference on the Use of Radioactive Isotopes in Ferrous Metallurgy, Magnitogorsk, January 1956," Steel (USSR) 1956, No. 6.

Timan, B. L., "The Influence of Noncentral Forces on Bremsstrahlung in Neutron-Proton Collisions," J. Exptl.-Theoret. Phys. (USSR) 30, 5 (1956).

Khromchenko, L. M., "Investigation of the Energy Levels of S^{33} by Magnetic Analysis," J. Exptl.-Theoret. Phys. (USSR) 30, 4 (1956).

Chamberlain, O., et al., "The Detection of Antiprotons" (From the Radiation Laboratory of the Physics Dept. of the University of California), with Translator's comments; Progr. Phys. Sci. (USSR) 58, 4 (1956).

Shekhtman, Ya. L., "The Effect of Drying on the Radiobiological Effect in Wheat Seed," Biophysics (USSR) 1, 5 (1956).

Shekhtman, Ya. L. and Radzhevsky, G. B., "The Reproduction of a Roentgen Unit for Gamma Rays with the Aid of an Extrapolation Ionization Chamber," Biophysics (USSR) 1, 3 (1956).

Shur, I., "The Use of Radioactivity to Sterilize Meat and Meat Products" (From information in American literature), with remarks by the editor; Meat Industry (USSR) 1956, No. 2.

Shliagin, K. N., "The Electronic Spectra of Pu^{239}, Pu^{240} and Pu^{241}," J. Exptl.-Theoret. Phys. (USSR) 30, 5 (1956).

CONTENTS (continued)

Price per article: $ 12.50.
Address orders to: CONSULTANTS BUREAU, INC., 227 West 17th Street, New York 11, N. Y.